AD-A062 703 RCA LTD STE ANNE DE BELLEVUE (QUEBEC) RESEARCH AND D--ETC F/G 20/9
STUDY OF ELECTROSTATIC PROBES IN NONEQUILIBRIUM PLASMAS.(U)
JUN 75 I P SHKAROFSKY, A BONNIER F33615-73-C-4123
UNCLASSIFIED MNLD-75-TR-002 ARL-75-0228 NL

1 OF 3
AD
A062703

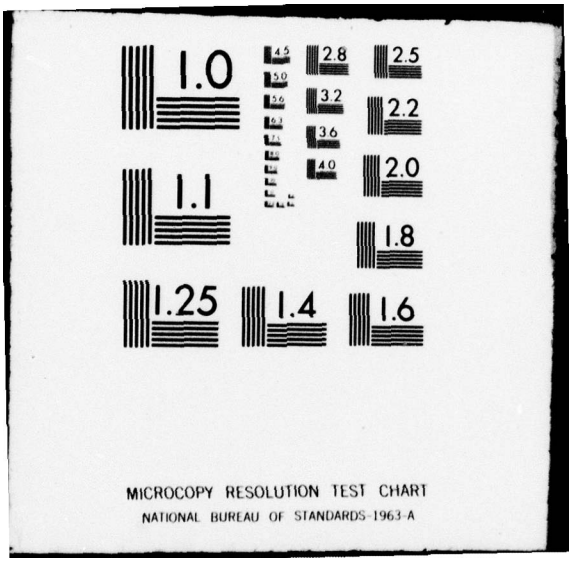
1.0
1.1
1.25
1.4
1.6
1.8
2.0
2.2
2.5
2.8
3.2
3.6
4.0
4.5
5.0
5.6
MICROCOPY RESOLUTION TEST CHART
NATIONAL BUREAU OF STANDARDS-1963-A

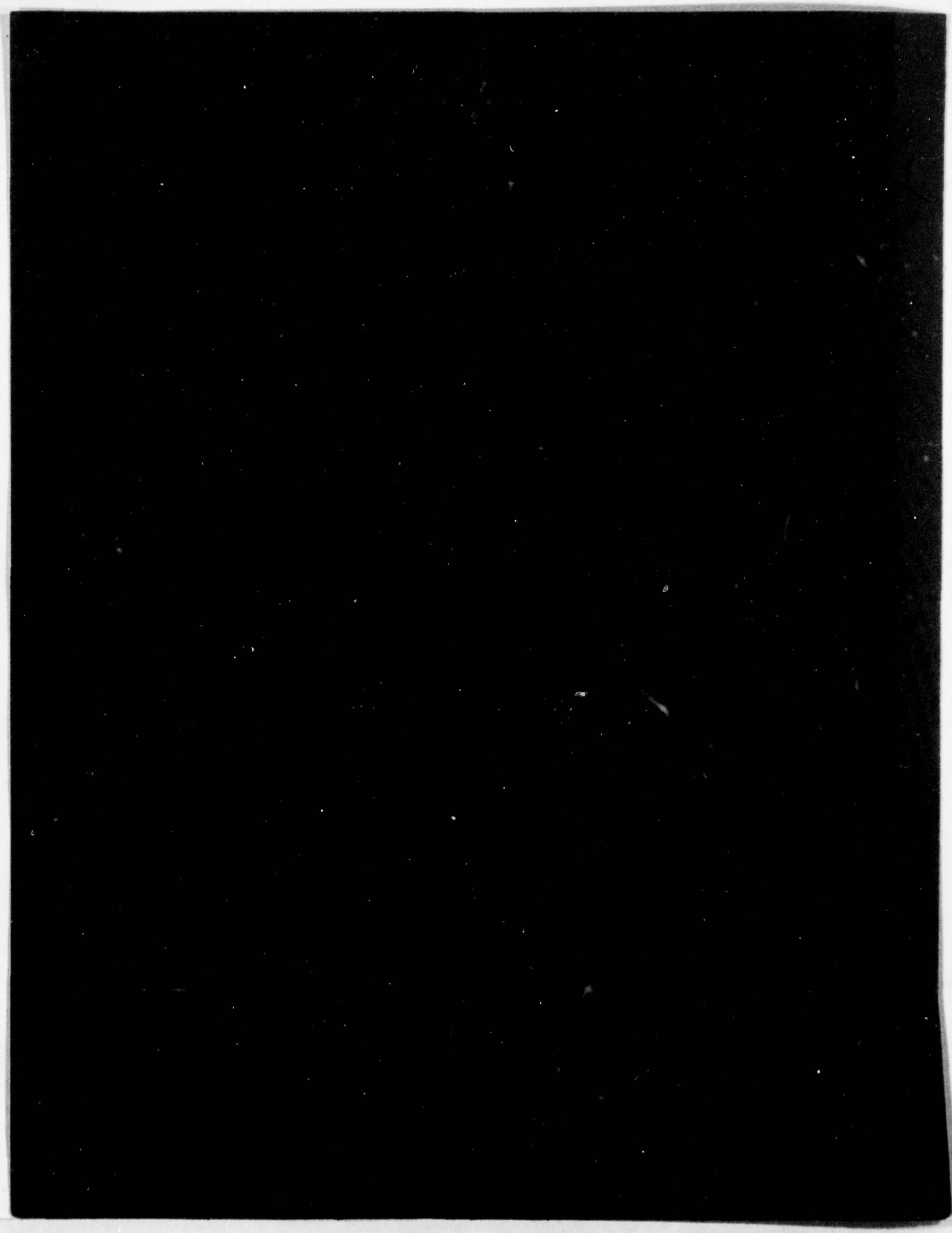

LEVEL II

UNCLASSIFIED
SECURITY CLASSIFICATION OF THIS PAGE (When Data Entered)

REPORT DOCUMENTATION PAGE

READ INSTRUCTIONS BEFORE COMPLETING FORM

(18) 1. REPORT NUMBER: ARL 75-0228 ✓ (19) 75-0228 | 2. GOVT ACCESSION NO. | 3. RECIPIENT'S CATALOG NUMBER (9)

(6) 4. TITLE (and Subtitle): STUDY OF ELECTROSTATIC PROBES IN NONEQUILIBRIUM PLASMAS,

5. TYPE OF REPORT & PERIOD COVERED: Technical - Final Rept. 1 Sep 73 - 31 Mar 75

6. PERFORMING ORG. REPORT NUMBER: MNLD-75-TR-002 PSP-113, FXC667

(10) 7. AUTHOR(s): I. P. Shkarofsky, A. Bonnier (15)

8. CONTRACT OR GRANT NUMBER(s): F33615-73-C-4123 ✓, Can. Grant DIR.NO. XE-501 (DRB-5502-06)

9. PERFORMING ORGANIZATION NAME AND ADDRESS: RCA Limited, R&D Laboratories ✓, Ste. Anne de Bellevue, Quebec, Canada, H9X3L3

(16) 10. PROGRAM ELEMENT, PROJECT, TASK AREA & WORK UNIT NUMBERS: 7073, 61102F

11. CONTROLLING OFFICE NAME AND ADDRESS: Plasma Physics Research Laboratory, LU, Aerospace Research Laboratories (AFSC), Wright-Patterson AFB, OH 45433

(11) 12. REPORT DATE: June 1975

13. NUMBER OF PAGES: 224

14. MONITORING AGENCY NAME & ADDRESS (if different from Controlling Office): Canada: Director General, DREV, Valcartier, P.Q.

(12) 228 p.

15. SECURITY CLASS. (of this report): Unclassified

15a. DECLASSIFICATION/DOWNGRADING SCHEDULE

16. DISTRIBUTION STATEMENT (of this Report)

Approved for public release; distribution unlimited.

DDC RECEIVED DEC 21 1978 A

17. DISTRIBUTION STATEMENT (of the abstract entered in Block 20, if different from Report)

(14) MNLD-75-TR-002, PSP-113

18. SUPPLEMENTARY NOTES

19. KEY WORDS (Continue on reverse side if necessary and identify by block number)

electrostatic langmuir probes
media suitable for lasing
collisionless sheath analysis
quasicollisional sheath analysis
diagnostics of nonequilibrium plasmas
anisotropic distribution functions
determination of distribution function components
hybrid sheath analysis

20. ABSTRACT (Continue on reverse side if necessary and identify by block number)

The response of electrostatic probes (plane, sphere, and cylinder) in a nonequilibrium plasma, whose electron energy distribution function is neither Maxwellian nor isotropic, is studied with application to diagnostics of a lasing medium. First, the situation of a collisionless sheath is considered. The current-voltage characteristics of probes are derived, for given arbitrary variations for the first three Cartesian tensor components of the distribution function. The inverse problem is then solved, and analytical and numerical

→ next Page (cont'd)

DD FORM 1 JAN 73 1473 EDITION OF 1 NOV 65 IS OBSOLETE UNCLASSIFIED
SECURITY CLASSIFICATION OF THIS PAGE (When Data Entered)

78 12 20 001

407 176

Block 20, cont'd

means to deduce these details of the distribution function from the currents are provided, based on using a plane probe whose orientation is varied. Next, the quasicollisional sheath is analyzed. We generalize the works of Swift and Lukovnikov and Novgorodov to include the anisotropic contribution from the distribution function. Finally, we use a hybrid moment approach to analyze the continuum regime. This approach uses our previous results to match properly (including anisotropic terms) at the boundary between the colisionless and collisional parts of the sheath and improves the works of Waymouth and Wilkins and Katra.

PREFACE

This final report was prepared by RCA Limited, Research Laboratories, Ste. Anne de Bellevue, Quebec, Canada. The program was cost-shared between two agencies. The first is the Director General, Defence Research Establishment Valcartier, Valcartier, Quebec, and the work was done under Project No. XE-501. The second is the Plasma Physics Research Laboratory of the Aerospace Research Laboratories, Wright-Patterson Air Force Base, Ohio, and the work was done under the technical cognizances of Capt. William F. Bailey and Lt. William H. Long under Contract No. F-33615-73-C-4123. The research was conducted from September 1, 1973 to March 31, 1975.

Part of the work reported here in Sections II and III and in the appendices is a joint effort of Drs. A. Bonnier and I.P. Shkarofsky of RCA Limited, and it was previously issued as the separate Research Report FXC66-3, MNLD-74-TR-003 (Lab Report No. PSP-110), dated April 1974. Besides thanking Dr. A. Bonnier for his important contributions, the author wishes to acknowledge helpful discussions with Drs. S.Y.K. Tam and A.K. Ghosh of RCA Limited. He greatly appreciates as well the efforts of Dr. A.K. Ghosh in the design of the plane probe and of Mr. M. Fossiez in its actual construction. Finally, the author is grateful for the joint collaborations with Lt. W.H. Long and Capt. W.F. Bailey of ARL.

The originator's report numbers for this report are FXC66-7, PSP-113 and MNLD-75-TR-002.

TABLE OF CONTENTS

LIST OF ILLUSTRATIONS

SECTION I

INTRODUCTION

One of the most useful diagnostic tools for studying a plasma medium is a Langmuir probe, which consists of a small electrode immersed in the medium and biased to collect the charged particles. Although the principle is simple conceptually, the theory for its operation can become quite complicated, especially in nonequilibrium plasmas.

With a Langmuir probe, we can determine the plasma parameters from the current-voltage (I-V) characteristic of the probe. These parameters are usually the local charged particle density and temperature and the plasma potential. A more ambitious aim is to derive the form of the electron velocity distribution function. Thus far nearly all such measurements were concerned with the isotropic component of the distribution function. However, in an active discharge with a sufficiently strong electric field, the distribution function is anisotropic, and both the directional and tensor components of the distribution function are nonnegligible. Moreover, at higher pressures, gradients, which exist in the collisional part of the sheath, also induce a directional component to the distribution function with associated diffusion effects. In this report, our basic aim is to study the behaviour of electrostatic probes in a nonequilibrium plasma, by which is meant one in which the electron distribution function is neither Maxwellian nor isotropic. Pursuant to this goal, relations are derived for the I-V characteristics and probe response to a calculated distribution function given by the solution of the collisional Boltzmann equation.

The electron energy distribution function is of fundamental importance in determining the operating characteristics of gas discharges. Numerical

solutions of the Boltzmann equation including inelastic collisions have yielded great insight to laser discharge operation. Certain features in the calculated distribution functions can be associated with energy regimes where electrons strongly excite the gas molecules, which is important to know for laser operation. However experimental confirmation of the forms of the distribution function and its components is lacking. Thus a major objective of this research is to develop an accurate method of determining the details of the electron energy distribution function in molecular gases from appropriate electrostatic probe measurements.

The approach that is used depends on the pressure regime. At very low pressures, collisionless probe theory is suitable. The sheath as a whole can be considered to be collisionless when the sheath thickness is greater than both the probe radius and collisional mean free path. Sections II and III are concerned with such a situation. The electric field in the discharge induces first and second order anisotropic parts to the distribution function, in addition to the isotropic part which exists in any case. We calculate new results for the responses of probes in terms of arbitrary forms for the three components of the distribution function. In Section III, the change in potential across the sheath due to the discharge electric field is accounted for, whereas in Section II, the voltage drop across the sheath is associated only with the potential applied to the probe. The results in Section II are thus much simpler. Various geometries are investigated, such as the one-sided plane probe, the spherical probe, the cylindrical probe, and a spherical grid system. Both electron retarding and accelerating regions are analyzed.

We find that, by combining several probes of various geometries or orienting a one-sided plane probe at several angles, one can separate the

three individual current contributions to the probe associated with the three terms in the distribution function. After this is done, we deduce relations which give each part of the distribution function in terms of its respective current contribution. This generalizes previous works which were restricted to the isotropic part of the distribution function.

We recommend the geometry of a one-sided plane probe for use in the collisionless regime. In conjunction with this, in Appendix A, we provide a parameter map delineating the regimes of operation for a plane probe in a nitrogen plasma,and, in Appendix B, we specify the construction details of such a probe. Computer programs are listed and explained in Appendix C. These programs provide numerical means for calculating I-V characteristics from the distribution function and vice versa. In Section IV, results based on sample calculations using the computer programs in Appendix C are plotted.

As the pressure is raised, the quasicollisional regime is encountered where the probe radius becomes comparable to or larger than the mean free path, with the mean free path still larger than the sheath thickness. This situation is analyzed in Section V. The presence of the probe is felt by the external plasma, since charged particles have to diffuse from the undisturbed plasma up to one mean free path from the probe surface. Diffusion through the quasicollisional part of the sheath implies that it creates a directional part to the distribution function in addition to a change in the isotropic part. Macroscopically, the plasma density in the quasicollisional sheath near the probe can differ substantially from that in the undisturbed plasma. To simplify matters, we omit in this section the anisotropic effects associated with the external electric field and include only the new directional contribution and change in the isotropic distribution. We provide

relations for the I-V characteristics in this regime which include these effects, generalizing the works of other authors who included only the change in the isotropic part of the distribution function. Our results reduce to the collisionless limit as the mean free path becomes very large. In the quasicollisional regime, the isotropic part of the distribution function can still be derived by iteration from the probe response. However, the analysis, based on free electron diffusion, omits ambipolar effects and is valid only when the ion temperature is very much less than the electron temperature.

At still higher pressures, corresponding to the continuum limit where the mean free path is less than the sheath thickness, we are able to derive I-V characteristics, given the isotropic part of the distribution function, but not to accomplish to inverse. We provide in Section VI a hybrid theory, modelled on a double layered sheath which consists of an inner collisionless layer and an outer collisional layer. Our theory can be applied to any given form of the isotropic part of the distribution function, any mean free path variation with electron energy, and any of three geometries, namely, plane, sphere, or cylinder. It incorporates flow effects associated with ambipolar diffusion and electrostatic space charge fields, both of which cause the distribution function to acquire a directional component within the collisional part of the sheath. Using our formulation in Section II, which allows for anisotropic effects in the distribution function, we can match properly at the boundary between the collisionless and collisional parts of the sheath. Thereby, we provide proper moment relations, or averages over the distribution function, which include these flow effects. Our relations generalize other hybrid theories which did not have available our present results in Section II.

Finally, in Section VII, we discuss our results, and give our conclusions.

SECTION II

COLLISIONLESS PROBE THEORY FOR AN ANISOTROPIC DISTRIBUTION FUNCTION

1. INTRODUCTION

Due to the strong electric field within the active discharge, the electrons acquire an anisotropic energy distribution function. Our prime interest lies in the electron retardation region from which the details of the electron distribution functions are obtainable. The anisotropy is written in terms of spherical harmonic components, and the analysis is performed by including f_o, $\underset{\sim}{f}_1$ and $\underset{\approx}{f}_2$, viz., up to second order tensor terms. For the plane probe, we can generalize the calculation of the electron current density to include all parts of the spherical harmonic expansion of the distribution function. We find that all parts contribute to the current at a plane probe. Consequently, the isotropic part of the distribution function cannot be derived by the usual method of taking the second derivative of the current with respect to potential. Nonetheless, $\underset{\sim}{f}_1$ can be deduced from the difference of the currents intercepted by the probe facing forward from that facing backward.

Next we analyze the response of a spherical probe and find that the $\underset{\sim}{f}_1$ and $\underset{\approx}{f}_2$ parts of the distribution function do not contribute. This suggests using a spherical probe to deduce f_o from the current in the retardation region.

The response of a cylindrical probe is also investigated. In this case, $\underset{\sim}{f}_1$ doesn't contribute. If the isotropic currents in a retarding potential are eliminated between a spherical and cylindrical probe, the net current at the cylinder is due to the $\underset{\approx}{f}_2$ contribution. Thus, $\underset{\approx}{f}_2$

can be deduced by using two probes, the sphere and the cylinder. A sphere and a plane probe will do as well.

In a retarding potential, the current intercepted is found to be independent of the sheath radius even with the $\underset{\approx}{f}_2$ anisotropic term which appears in the cylindrical case. However, in an accelerating potential, the current intercepted depends on the ratio of sheath to probe radius for a sphere or a cylinder. The results become independent of this ratio in the limits of thin or large sheaths. For a thin sheath, the results for a cylinder and sphere are derivable from the plane probe results.

An alternative electrostatic analyzer, namely, a spherical grid system, is then investigated. Finally, the analytical results are summarized.

A few basic assumptions are made. First, we assume that the external electric field in the discharge is sufficiently weak that the particle drift velocity is less than the thermal velocity. Furthermore, we assume that the electric field variation multiplied by the collecting probe plus sheath dimension (actually the part with normal projected parallel to the electric field) is negligible compared to the probe potential. The following Section III redoes the analysis, including correction terms due to this last effect. We also assume that the sheath is concentric or parallel to the probe. In this section, we adopt a collisionless sheath model which requires a sufficiently low pressure that the mean free path is greater than the sheath width and probe dimension. We also assume that the electric field at the sheath edge is predominantly due to the external electric field rather than to the potential decrease associated with the potential on the probe. These assumptions are more thoroughly discussed in Appendix A, which also provides a parameter map. Appendix B gives the design and construction of a plane probe.

2. THE PLANE PROBE

a. Retarding Region. Calculation of Electron Current Density from the Electron Distribution Function

Let the one-sided plane probe be oriented with the normal along the Z-axis (see Figure 1). Then each electron whose minus Z-velocity component, $-v_Z$, is smaller than $-v_o = -(2V_p/m)^{\frac{1}{2}}$ will reach the probe. Here, V_p/e is the magnitude of the probe retarding potential with respect to the potential at the sheath edge, and e and m are the magnitudes of the electron charge and mass. The magnitude of the electron current density at the probe surface is

$$j_Z = e \int_{-\infty}^{-v_o} \int_{-\infty}^{\infty} \int_{-\infty}^{\infty} v_Z f^* dv_Z dv_Y dv_X \qquad (1)$$

where f^* is the electron distribution function just outside of the collisionless sheath. The star signifies that f^* is expressed in the XYZ coordinate system attached to the probe. Transforming to spherical coordinates (v, θ, Φ) in the velocity space, we write

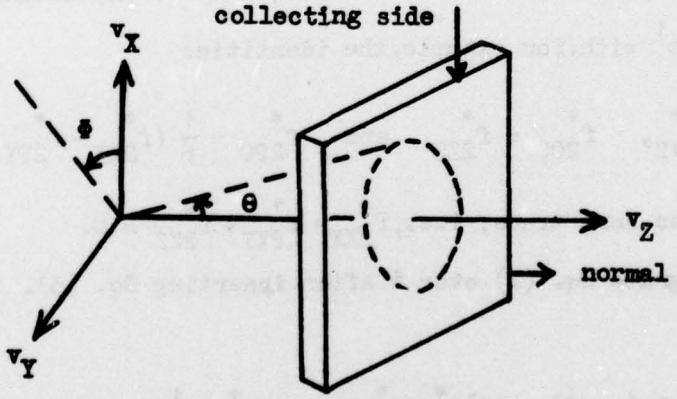

Figure 1. Coordinate System for the One-Sided Plane Probe, with the Outer Side Collecting Charge

$$j_Z = e \int_{v_o}^{\infty} \int_{\pi}^{\pi-\theta_1(v)} \int_{o}^{2\pi} (v\cos\theta) f^* v^2 \sin\theta \, dv \, d\theta \, d\Phi$$

where

$$\theta_1(v) = \cos^{-1}(v_o/v) \tag{2}$$

The electron distribution function is expanded in terms of Cartesian tensors or, equivalently, in terms of spherical harmonics[1]; thus

$$f^* = f_o^*(v) + \underset{\sim}{f}_1^*(v) \cdot \underset{\sim}{v}/v + \underset{\approx}{f}_2^*(v) : \underset{\sim}{vv}/v^2 + \ldots$$

$$= \sum_{l,m,s} f_{lms}^*(v) P_l^m(\cos\theta) [\delta_{os} \cos m\Phi + \delta_{1s} \sin m\Phi] \tag{3}$$

where P_l^m is an associated Legendre polynominal and δ_{ab} is the Kronecker function equal to 1 or 0 depending on whether its subscripts are equal or not. Since θ is the angle of $\underset{\sim}{v}$ with respect to the Z axis, and Φ is the angle in the XY plane of $\underset{\sim}{v}$ with respect to the X axis, the two expansions in Eq. (3) are equivalent[1] with, for example, the identities

$$f_{100}^* = f_{1Z}^*, \quad f_{200}^* = f_{2ZZ}^* \quad \text{and} \quad f_{220}^* = \frac{1}{6}(f_{2XX}^* - f_{2YY}^*) \tag{4}$$

The tensor $\underset{\approx}{f}_2^*$ also has zero trace, i.e., $f_{2XX}^* + f_{2YY}^* + f_{2ZZ}^* = 0$.

We first integrate Eq. (1) over Φ after inserting Eq. (3). This yields

$$\int_o^{2\pi} f^* \, d\Phi = 2\pi \sum_l f_{loo}^* P_l(\cos\theta) = 2\pi[f_o^* + f_{1Z}^* \cos\theta + f_{2ZZ}^* \tfrac{1}{2}(3\cos^2\theta - 1)] + \ldots \tag{5}$$

Further integration of Eq. (1) over θ up to $l = 2$ yields

$$j_Z = j_{0Z} - j_{1Z} + j_{2Z} \tag{6}$$

with

$$j_{0Z} = \pi e \int_{v_o}^{\infty} v^3 f_o^*(v) \sin^2\theta_1(v)\,dv = \pi e \int_{v_o}^{\infty} v^3 [1 - (v_o/v)^2] f_o^*(v)\,dv \tag{7}$$

$$j_{1Z} = \frac{2}{3} \pi e \int_{v_o}^{\infty} v^3 [1 - (v_o/v)^3] f_{1Z}^*(v)\,dv \tag{8}$$

and

$$j_{2Z} = \frac{1}{4} \pi e \int_{v_o}^{\infty} v^3 [1 + 2(v_o/v)^2 - 3(v_o/v)^4] f_{2ZZ}^*(v)\,dv \tag{9}$$

Defining

$$U = \frac{1}{2} mv^2, \quad K_o = 2\pi e/m^2 \quad \text{and since} \quad V_p = \frac{1}{2} mv_o^2 \tag{10}$$

with U and V_p in MKS units (i.e. in joules), one can express Eqs. (7) to (9) as

$$j_{0Z} = K_o \int_{V_p}^{\infty} (U - V_p) f_o^*(U)\,dU \tag{11}$$

$$j_{1Z} = \frac{2}{3} K_o \int_{V_p}^{\infty} U[1 - (V_p/U)^{3/2}] f_{1Z}^*(U)\,dU \tag{12}$$

$$j_{2Z} = \frac{1}{4} K_o \int_{V_p}^{\infty} [U + 2V_p - 3V_p^2/U] f_{2ZZ}^*(U)\,dU \tag{13}$$

The above results can be generalized to include higher order terms. Substitution of Eq. (3) into (1) gives

$$j_Z = 2\pi e \sum_1^{\infty} \int_{v_o}^{\infty} dv\, v^3 f_{loo}^*(v) \int_{\pi-\theta_1}^{\pi} P_l(\cos\theta)\cos\theta \sin\theta\, d\theta = 2\pi e \sum_1^{\infty} \int_{v_o}^{\infty} dv\, v^3 f_{loo}^*(v) \int_{x_o}^{1} P_l(-x)x\,dx \tag{14}$$

where $x_o \equiv \cos\theta_1(v) = v_o/v$. We use the relations

$$P_l(-x) = (-1)^l P_l(x) \tag{15}$$

and

$$\int_{x_o}^{1} P_n(x)\, x\, dx = \frac{1}{(2n+1)}\left[\left(\frac{n+1}{2n+3}\right)(P_n - P_{n+2}) + \left(\frac{n}{2n-1}\right)(P_{n-2} - P_n)\right] \tag{16}$$

and obtain $j_Z = \sum_l (-1)^l j_{lZ}$ with

$$j_{lZ} = \frac{2\pi e}{(2l+1)} \int_{v_o}^{\infty} dv\, v^3 f^*_{loo}(v) \left[\left(\frac{l+1}{2l+3}\right)(P_l - P_{l+2}) + \left(\frac{l}{2l-1}\right)(P_{l-2} - P_l)\right] \tag{17}$$

where the argument of the P's is v_o/v or $(V_p/U)^{\frac{1}{2}}$. In terms of U,

$$j_{lZ} = \frac{2K_o}{(2l+1)} \int_{V_p}^{\infty} dU\, U\, f^*_{loo}(U) \left[\left(\frac{l+1}{2l+3}\right)(P_l - P_{l+2}) + \left(\frac{l}{2l-1}\right)(P_{l-2} - P_l)\right] \tag{18}$$

Equations (17) and (18) reduce to Eqs. (6) to (13) when $l = 0$, 1 and 2, upon using

$$P_o = P_{-1} = 1, \quad P_1 = (V_p/U)^{\frac{1}{2}}, \quad P_2 = \tfrac{1}{2}(3V_p/U - 1), \quad P_3 = \tfrac{1}{2}(V_p/U)^{\frac{1}{2}}(5V_p/U - 3)$$

and

$$P_4 = \frac{1}{8}\left[35(V_p/U)^2 - 30V_p/U + 3\right] \tag{19}$$

b. Accelerating Region

In the case of an accelerating voltage, the upper limit on v_Z is zero. For generality, we investigate as well the particle accelerating region and the effect of its anisotropic distribution function. Thus

$$j_Z = e\int_0^{\infty}\int_{\pi}^{\pi/2}\int_0^{2\pi} v\cos\theta f^* v^2 \sin\theta \, d\theta d\Phi$$

$$= 2\pi e\int_0^{\infty}\int_0^{\pi/2} v^3 \sin\theta\cos\theta \sum_1 (-1)^l f^*_{loo} P_l(\cos\theta) dv d\theta$$

$$= \Sigma(-1)^l j_{lz} \tag{20}$$

To perform the θ integration, we use the following equality for $n = 0$, 1 and n even,

$$\int_0^1 P_n(x)x\,dx = \frac{\pi^{\frac{1}{2}}}{4\Gamma\left(\frac{n+4}{2}\right)\Gamma\left(\frac{3-n}{2}\right)} \tag{21}$$

where Γ is a Gamma function. If n is odd and greater than one, the answer is zero. We thus obtain (except for $l = 3,5,7$ etc.) the following:

$$j_{lZ} = \frac{\pi^{3/2} e}{2\Gamma\left(\frac{1+4}{2}\right)\Gamma\left(\frac{3-1}{2}\right)}\int_0^{\infty} v^3 f^*_{loo}(v)dv = \frac{\pi^{3/2} e}{m^2\Gamma\left(\frac{1+4}{2}\right)\Gamma\left(\frac{3-1}{2}\right)}\int_0^{\infty} U f^*_{loo}(U)dU \tag{22}$$

In particular

$$j_{oZ} = \pi e\int_0^{\infty} v^3 f^*_o(v)dv = K_o\int_0^{\infty} U f^*_o(U)dU \tag{23}$$

$$j_{1Z} = \frac{2\pi e}{3}\int_0^{\infty} v^3 f^*_{1Z}(v)dv = \frac{2K_o}{3}\int_0^{\infty} U f^*_{1Z}(U)dU \tag{24}$$

and

$$j_{2Z} = \frac{\pi e}{4}\int_0^{\infty} v^3 f^*_{2ZZ}(v)dv = \frac{K_o}{4}\int_0^{\infty} U f^*_{2ZZ}(U)dU \tag{25}$$

Thus up to $l = 2$

$$j_z = K_o\int_0^{\infty} U\left[f^*_o(U) - \frac{2}{3} f^*_{1Z}(U) + \frac{1}{4} f^*_{2ZZ}(U)\right]dU \tag{26}$$

c. Electron Current Density for any Orientation of the Plane Probe

Let the coordinate system in the plasma be xyz with the z-axis along the anode to cathode direction, parallel to a constant external electric field within the active discharge. The previous results obtained for a plane probe, with normal oriented along the Z-axis and coordinate system XYZ attached to it, can be related to the xyz system. We perform a transformation from the xyz to the XYZ system by θ-ϕ rotations, where θ and ϕ are Eulerian angles[2,3]. The ϕ rotation is performed first about the z-axis in the xy plane, changing to a coordinate system x'y'z' with ϕ as the angle between the x and x' axes. The θ rotation is performed next about the x' or X-axis with θ as the angle between the new Z and original z-axes (see Figure 2). Let f^* and f be, respectively, the electron distribution functions in the coordinate systems attached to the probe and to the plasma. The rotation matrix is

$$R = R_\theta R_\phi = \begin{pmatrix} \cos\phi & \sin\phi & 0 \\ -\cos\theta\sin\phi & \cos\theta\cos\phi & \sin\theta \\ \sin\theta\sin\phi & -\sin\theta\cos\phi & \cos\theta \end{pmatrix} \qquad (27)$$

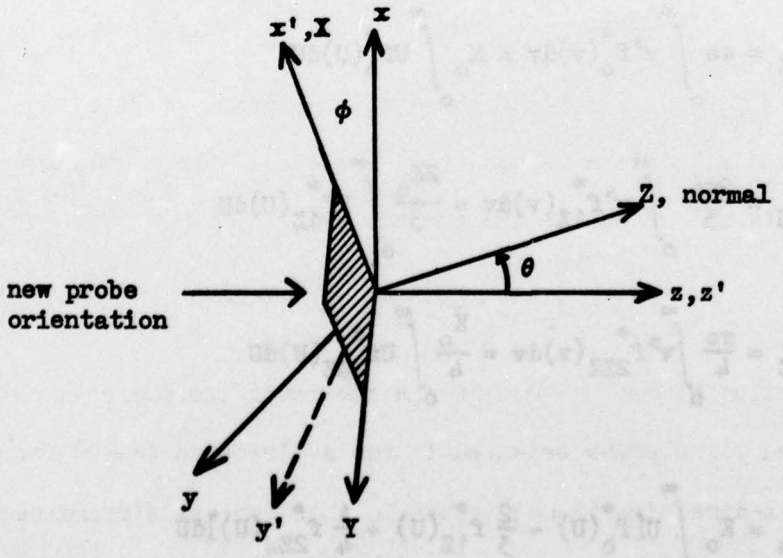

Figure 2. Eulerian Angle Transformations from Coordinate Systems xyz to XYZ

The components of f transform thus:

$$f^*_o = f_o, \quad f^*_{1i} = \sum_j R_{ij} f_{1j} \quad \text{and} \quad f^*_{2ik} = \sum_{jl} R_{ij} R_{kl} f_{2jl} \tag{28}$$

In the matrix notation

$$\begin{bmatrix} f^*_{1X} \\ f^*_{1Y} \\ f^*_{1Z} \end{bmatrix} = \begin{bmatrix} R_{Xx} & R_{Xy} & R_{Xz} \\ R_{Yx} & R_{Yy} & R_{Yz} \\ R_{Zx} & R_{Zy} & R_{Zz} \end{bmatrix} \begin{bmatrix} f_{1x} \\ f_{1y} \\ f_{1z} \end{bmatrix} \tag{29}$$

and

$$\begin{bmatrix} f^*_{2XX} & f^*_{2XY} & f^*_{2XZ} \\ f^*_{2YX} & f^*_{2YY} & f^*_{2YZ} \\ f^*_{2ZX} & f^*_{2ZY} & f^*_{2ZZ} \end{bmatrix} = \begin{bmatrix} R_{Xx} & R_{Xy} & R_{Xz} \\ R_{Yx} & R_{Yy} & R_{Yz} \\ R_{Zx} & R_{Zy} & R_{Zz} \end{bmatrix} \begin{bmatrix} f_{2xx} & f_{2xy} & f_{2xz} \\ f_{2yx} & f_{2yy} & f_{2yz} \\ f_{2zx} & f_{2zy} & f_{2zz} \end{bmatrix} \begin{bmatrix} R_{xX} & R_{yX} & R_{zX} \\ R_{xY} & R_{yY} & R_{zY} \\ R_{xZ} & R_{yZ} & R_{zZ} \end{bmatrix} \tag{30}$$

In particular

$$f^*_{1Z} = f_{1x} \sin\theta \sin\phi - f_{1y} \sin\theta \cos\phi + f_{1z} \cos\theta \tag{31}$$

$$f^*_{2ZZ} = f_{2xx} \sin^2\theta \sin^2\phi + f_{2yy} \sin^2\theta \cos^2\phi + f_{2zz} \cos^2\theta - 2f_{2xy} \sin^2\theta \sin\phi \cos\phi + 2f_{2xz} \sin\theta \cos\theta \sin\phi - 2f_{2yz} \sin\theta \cos\theta \cos\phi \tag{32}$$

We obtain $j = j_o - j_{1\theta\phi} + j_{2\theta\phi}$ with the three contributions given by Eqs. (11) to (13) and f^*_{1Z} and f^*_{2ZZ} given in Eqs. (31) and (32). When $\theta = 0$, only f_{1z} and f_{2zz} contribute, and we denote the current by

$$j = j_o - j_{1z} + j_{2z} \tag{33}$$

The f_{1z} part of f remains only if one subtracts the currents obtained from the one-sided plane probe oriented in the z-direction ($\theta = 0$) from that oriented in the -z-direction ($\theta = \pi$). Denote this current difference by j_{z-}. Then

$$j_{z-} = -\frac{4}{3} K_o \int_{V_p}^{\infty} U[1 - (V_p/U)^{3/2}] f_{1z}(U) dU \qquad (34)$$

By so doing, the $j_{1z} = -\frac{1}{2} j_{z-}$ part can be deduced. Adding the currents on both sides gives

$$j_{z+} = 2K_o \int_{V_p}^{\infty} \left\{ [U - eV_p] f_o(U) + \frac{1}{4} [U + 2V_p - 3V_p^2/U] f_{2zz}(U) \right\} dU \qquad (35)$$

which involves f_o and f_{2zz} only. Consider now slow rotation of the plane probe around the x-axis with angular velocity less than v_e/λ_s, where v_e is the electron thermal velocity and λ_s is the sheath thickness. The average current density after a complete revolution is

$$\bar{j}_{\theta\phi/x} = \frac{1}{2\pi} \int_o^{2\pi} j_{\theta\phi}(\phi = 0, \theta) d\theta$$

$$= K_o \int_{V_p}^{\infty} \left\{ (U - V_p) f_o(U) - \frac{1}{8} [U + 2V_p - 3V_p^2/U] f_{2xx}(U) \right\} dU \qquad (36)$$

which depends on f_o and f_{2xx} only. Similarly, rotation about the y-axis gives $\bar{j}_{\theta\phi/y}$ with f_{2yy}'s replacing f_{2xx}, and rotation around an i-axis located in the xy plane gives $\bar{j}_{\theta\phi/i}$ with f_{2ii}'s replacing f_{2xx}. If j_o is obtainable by some other means — a spherical probe will do as is shown later — then Eqs. (35) and (36), after subtracting j_o, will contain only the $f_{\ell 2}$ components, and the j_{2z} part can be separated.

d. Derivatives of Current with Respect to Potential and Deduction of the Components of the Distribution function

In the case of an isotropic distribution f_o, the second derivative of j with respect to V_p (in the retarding region) is proportional to $f_o(V_p)$. This result has been used to derive the distribution function

from probe characteristics. For anisotropic distributions, it turns out that the second derivative includes terms in $\underset{\sim}{f}_1$ and $\underset{\approx}{f}_2$ besides f_o:

$$j_{\theta\phi} = K_o \int_{V_p}^{\infty} \left\{ [U-V_p] f_o(U) - \frac{2}{3} U[1-(V_p/U)^{3/2}] f^*_{1Z}(U) + \frac{1}{4} [U+2V_p - 3V_p^2/U] f^*_{2ZZ}(U) \right\} dU \tag{37}$$

$$\frac{dj_{\theta\phi}}{dV_p} = - K_o \int_{V_p}^{\infty} \left\{ f_o(U) - \left(\frac{V_p}{U}\right)^{\frac{1}{2}} f^*_{1Z}(U) + \frac{1}{2} \left(\frac{3V_p}{U} - 1\right) f^*_{2ZZ}(U) \right\} dU \tag{38}$$

$$\frac{d^2 j_{\theta\phi}}{dV_p^2} = \frac{1}{2} K_o \int_{V_p}^{\infty} \left\{ \frac{f^*_{1Z}(U)}{(UV_p)^{\frac{1}{2}}} - \frac{3}{U} f^*_{2ZZ}(U) \right\} dU + K_o [f_o(V_p) - f^*_{1Z}(V_p) + f^*_{2ZZ}(V_p)] \tag{39}$$

Because of the integrals remaining in Eq. (39), one cannot get directly f_o, f^*_{1Z}, and f^*_{2ZZ} from $d^2 j_{\theta\phi}/dV_p^2$.

Suppose, however, that the j_o, j_1, and j_2 parts of $j = j_o - j_1 + j_2$ can be separately deduced. (Let the $\theta\phi$ additional subscripts on j_1 and j_2 be understood below.) In the previous subsection, we indicated that this was possible. Then f_o is obtainable from j_o given in Eq. (11) in the usual manner:

$$f_o(V_p) = \frac{1}{K_o} \frac{d^2 j_o}{dV_p^2} \tag{40}$$

From Eq. (12), we can deduce f^*_{1Z} by differentiation in the following manner:

$$f^*_{1Z}(V_p) = \frac{1}{K_o} V_p^{\frac{1}{2}} \frac{d}{dV_p} \left[\frac{1}{V_p^{\frac{1}{2}}} \frac{dj_1(V_p)}{dV_p} \right] \tag{41}$$

To derive f^*_{2ZZ}, we need the integral of j_2 in addition to its derivatives. We note that

$$\int_{V_p}^{\infty} \frac{j_2(V)}{V^{3/2}} dV = - \frac{1}{2} K_o \int_{V_p}^{\infty} \left[2V_p^{\frac{1}{2}} - V_p^{3/2}/U - U/V_p^{\frac{1}{2}} \right] f^*_{2ZZ}(U)\, dU \tag{42}$$

Using Eq. (42) and the j_2 parts of Eqs. (37) to (39), we can now solve for f^*_{2ZZ} to give

$$f^*_{2ZZ} = \frac{1}{K_o}\left\{\frac{d^2 j_2}{dV_p^2} - \frac{3}{2V_p}\frac{dj_2}{dV_p} + \frac{3}{4V_p^2} j_2 - \frac{3}{8V_p^{3/2}}\int_{V_p}^{\infty}\frac{j_2(V)}{V^{3/2}}\,dV\right\} \tag{43}$$

Thus f_o, f^*_{1Z}, and f^*_{2ZZ} can be deduced if the currents j_o, j_1, and j_2 in $j = j_o - j_1 + j_2$ can be separated.

3. THE SPHERICAL PROBE

a. Surface Integration

The total current to a probe is the integral of $j_{\theta\phi}$ over the probe area. For a plane probe, this is simply $j_{\theta\phi}$ times the surface area, A. Edge effects can be reduced by using a flat ring concentric with a flat disk, both of which have the potential V_p, but only the current from the disk is analyzed. A sphere has no edge problems, although its support may introduce unwanted effects.

The total current to a spherical probe is

$$I = \int j_{\theta\phi}\,dA = \int_{\theta=o}^{\pi}\int_{\phi=o}^{2\pi} j_{\theta\phi} r_p^2 \sin\theta\,d\theta\,d\phi \tag{44}$$

where r_p is the probe radius. We show in the next subsection that only the f^*_{1oo} spherical harmonic components, or f_o, f^*_{1Z}, and f^*_{2ZZ} up to second order, contribute to $j_{\theta\phi}$. Thus $j_{\theta\phi}$ can be written as

$$j_{\theta\phi} = j_o - j_1 + j_2 = j_o - \sum_i R_{zi} j_{1i} + \sum_{jl} R_{zj} R_{zl} j_{2jl} \tag{45}$$

similar to Eq. (28) for the f components. From Eq. (27) for R or inspecting Eqs. (29) to (32), one obtains

$$\int j_o dA = 4\pi r_p^2 j_o, \quad \int j_1 dA = 0$$

and

$$\int j_2 dA = \frac{4}{3}\pi r_p^2 (j_{2xx} + j_{2yy} + j_{2zz}) = 0 \tag{46}$$

since j_2 is related to f^*_{2ZZ} and the $\underset{\approx}{f}_2$ tensor is traceless, viz.,it satisfies $f_{2xx} + f_{2yy} + f_{2zz} = 0$. Thus,we note that I is related only to j_o, or

$$I = 4\pi r_p^2 j_o \tag{47}$$

The above assumes that the sheath surface is spherical and concentric with the probe. This is valid if the perturbations due to $\underset{\sim}{f}_1$ and $\underset{\approx}{f}_2$ or j_1 and j_2 are small.

b. Retarding Region

Consider an element of spherical surface at the sheath position, $r = r_s$, and let the normal be in the Z-direction. In the XY plane we write

$$v_X = q \sin\Phi, \quad v_Y = q\cos\Phi \quad \text{and} \quad q^2 = v_X^2 + v_Y^2 \tag{48}$$

A charged particle moving from the sheath surface to the probe surface conserves its momentum and energy within the collisionless sheath, so that

$$r_p q_p = r_s q_s \quad \text{and} \quad v_{Zp}^2 = v_{Zs}^2 + q_s^2 - q_p^2 - [2(V_p - V_s)/m] \tag{49}$$

Henceforth we write V_p instead of $V_p - V_s$ with the understanding that V_p is measured with respect to V_s. In order for the particle to reach the probe, we require $v_{Zp}^2 \geq 0$ and $v_{Zs}^2 \geq 0$,and the condition on q_s is $q_s^2 \leq q_1^2$, where

$$q_1^2 = \frac{r_p^2}{r_s^2 - r_p^2}[v_{Zs}^2 - v_o^2] \quad \text{and} \quad v_o = \left(\frac{2V_p}{m}\right)^{\frac{1}{2}} \tag{50}$$

Henceforth subscript s is to be understood on v_Z and q.

The current δI through a spherical element of surface at $r = r_s$ can now be written as

$$\frac{\delta I}{e r_s^2} = \int_{-\infty}^{-v_o} v_Z dv_Z \int_0^{q_1} q dq \int_0^{2\pi} d\Phi \, f^*(v_Z, q\sin\Phi, q\cos\Phi) \qquad (51)$$

Substituting Eq. (3) for f^* into this expression and integrating over Φ yield

$$\frac{\delta I}{e r_s^2} = 2\pi \int_{-\infty}^{-v_o} v_Z dv_Z \int_0^{q_1} q dq \sum_1 f^*_{1oo} P_1(\cos\theta) \qquad (52)$$

Hence the current is related only to the f^*_{1oo} components, and δI_2 is proportional to f^*_{2ZZ} for any orientation of the spherical surface. These facts are used in the previous subsection to show that I_1 and I_2 do not contribute upon integration over solid angle. We are therefore interested here only in δI_o, viz.,

$$\frac{\delta I_o}{e r_s^2} = 2\pi \int_{-\infty}^{-v_o} v_Z dv_Z \int_0^{q_1} q dq \, f_o(v_Z, q) \qquad (53)$$

In a spherical coordinate system with $v_Z = v\cos\theta$ and $q = v\sin\theta$ (see Figure 3) we find

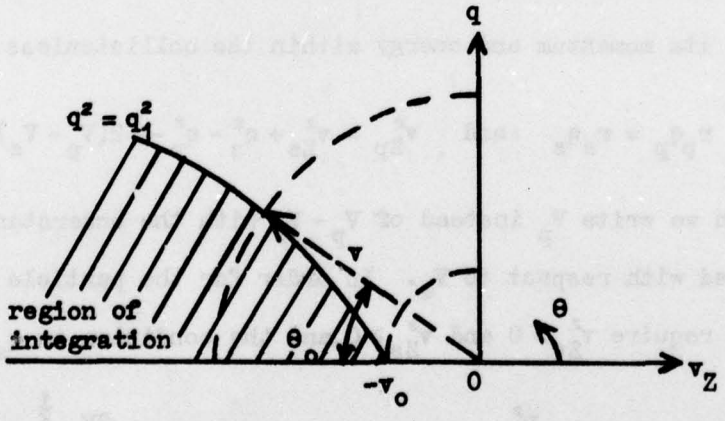

Figure 3. Spherical Velocity Space in the Retarding Region. If $v \leq |v_o|$, the integration region is nil. If $v \geq |v_o|$, the integration region lies between $\theta = \pi - \theta_o$ or $q^2 = q_1^2$ and $\theta = \pi$

$$\frac{\delta I_o}{e r_s^2} = 2\pi \int_{\infty}^{v_o} v^3 dv\, f_o(v) \int_{\pi-\theta_o}^{\pi} d\theta \sin\theta \cos\theta \tag{54}$$

The angle θ_o is here defined by the $q^2 = q_1^2$ equality, which is

$$v^2 \sin^2\theta_o = \frac{r_p^2}{r_s^2 - r_p^2}\left[v^2\cos^2\theta_o - v_o^2\right] \quad \text{or} \quad \sin^2\theta_o = \frac{r_p^2}{r_s^2}\left[1 - \left(\frac{v_o}{v}\right)^2\right] \tag{55}$$

Integrating Eq. (53) yields

$$\frac{\delta I_o}{e r_s^2} = \pi \frac{r_p^2}{r_s^2} \int_{v_o}^{\infty} v^3 dv \left[1 - \left(\frac{v_o}{v}\right)^2\right] f_o(v) dv \tag{56}$$

or

$$j_o = \frac{\delta I_o}{r_p^2} = \pi e \int_{v_o}^{\infty} v dv [v^2 - v_o^2] f_o(v) dv \tag{57}$$

and

$$I = 4\pi r_p^2 j_o = 4\pi \delta I_o = \frac{8\pi^2 r_p^2 e}{m^2} \int_{V_p}^{\infty} [U - V_p]\, f_o(U) dU \tag{58}$$

This result shows that, as far as f_o is concerned, the j_o contributions for the plane and spherical probes are identical and independent of r_s. It is known that this is true for the cylindrical probe as well, as will be shown later.

For the spherical probe, the f_1 and f_2 terms give no net contribution to the total current. The second derivative of I can then be used to determine the f_o term:

$$f_o(V_p) = \frac{m^2}{8\pi^2 r_p^2 e} \frac{d^2 I}{dV_p^2} \tag{59}$$

c. Accelerating Region

For an accelerating potential, the sign of the $2(V_p - V_s)/m$ term in Eq. (49) is changed, so that in Eq. (50) the quantity q_1 is now

$$q_1 = \frac{r_p^2}{r_s^2 - r_p^2}\left[v_Z^2 + v_o^2\right] \equiv \beta\left[v_Z^2 + v_o^2\right] \quad \text{with} \quad \beta \equiv \frac{r_p^2}{r_s^2 - r_p^2} \tag{60}$$

Also the limits on v_Z are now $-\infty$ to 0. Thus Eq. (52) reads

$$\frac{\delta I}{r_s^2} = 2\pi e \int_{-\infty}^{0} v_Z dv_Z \int_0^{q_1} q\,dq \sum_l f_{loo}(v_Z, q) P_l(\cos\theta) \tag{61}$$

As before, we are interested here only in the $l = 0$ term since the $l = 1$ and $l = 2$ terms give zero contribution. In a spherical coordinate system (see Figure 4), we find

$$\frac{\delta I_o}{r_s^2} = 2\pi e \int_{\infty}^{\sqrt{\beta}v_o} v^3 dv\, f_o(v) \int_{\pi-\theta_o}^{\pi} d\theta \sin\theta\cos\theta + 2\pi e \int_{\sqrt{\beta}v_o}^{0} v^3 dv\, f_o(v) \int_{\pi/2}^{\pi} d\theta \sin\theta\cos\theta \tag{62}$$

where θ_o is given by $q \equiv v\cos\theta_o = q_1$

or

$$\sin^2\theta_o = \frac{r_p^2}{r_s^2}\left[1 + \left(\frac{v_o}{v}\right)^2\right] \tag{63}$$

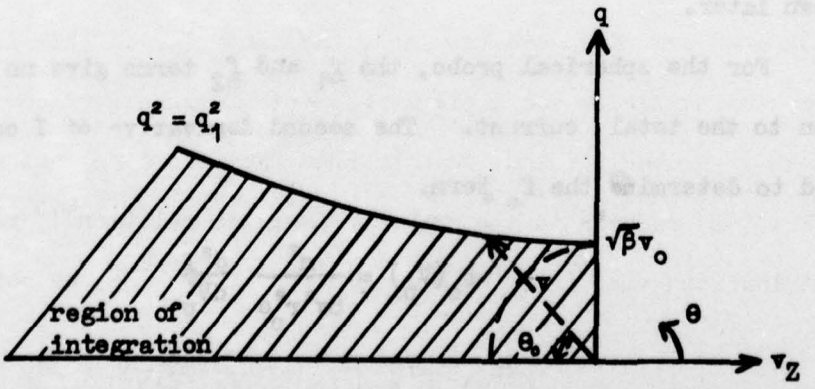

Figure 4. Spherical Velocity Space in the Accelerating Region. If $v < |\sqrt{\beta}v_o|$, the angle θ varies from $\pi/2$ to π. If $v > |\sqrt{\beta}v_o|$, the angle θ varies from $\theta = \pi - \theta_o$ or $q^2 = q_1^2$ to $\theta = \pi$

Integrating Eq. (62) yields

$$\frac{\delta I_o}{r_s^2} = \pi e \int_0^{\sqrt{\beta}v_o} dv\, v^3 f_o(v) + \pi e \frac{r_p^2}{r_s^2} \int_{\sqrt{\beta}v_o}^{\infty} dv\, v^3 f_o(v) \left[1 + \left(\frac{v_o}{v}\right)^2\right] \qquad (64)$$

Now $j_o = \delta I_o / r_p^2$ and $I = 4\pi r_p^2 j_o$, giving

$$I = 4\pi^2 e \left\{ r_s^2 \int_0^{\sqrt{\beta}v_o} dv\, v^3 f_o(v) + r_p^2 \int_{\sqrt{\beta}v_o}^{\infty} dv\, v\, f_o(v)[v^2 + v_o^2] \right\}$$

$$= \frac{8\pi^2 e}{m^2} \left\{ r_s^2 \int_0^{\beta V_p} dU\, U f_o(U) + r_p^2 \int_{\beta V_p}^{\infty} dU f_o(U)[U + V_p] \right\} \qquad (65)$$

If the sheath position is close to the probe radius, as is often the case in the pressure range above a few torr, we approximate $r_s \approx r_p$ and $\beta >> 1$ to give

$$I = \frac{8\pi^2 e r_p^2}{m^2} \int_0^{\infty} dU\, U f_o(U) \qquad (66)$$

Note that this is the same result as for a planar element of surface integrated over a sphere (see Eqs. (47) and (23)). This is reasonable since the particles see a planar element of probe surface if the sheath thickness is negligible. We also note that the more general expression in Eq. (65) reduces to the standard Langmuir relation[4,5] for a Maxwellian distribution; viz., if $f_o(U) = n_o(m/2\pi kT_e)^{3/2} e^{-U/kT_e}$, we obtain

$$I = 4\pi r_p^2 e n_o \left(\frac{kT_e}{2\pi m}\right)^{\frac{1}{2}} \left\{ \frac{r_s^2}{r_p^2} \left[1 - \exp\left(-\frac{\beta V_p}{kT_e}\right)\right] + \exp\left(-\frac{\beta V_p}{kT_e}\right) \right\} \qquad (67)$$

4. THE CYLINDRICAL PROBE

a. Surface Integration

The total current to a cylindrical probe is

$$I = r_p L \int j_{\theta\phi} d\alpha \tag{68}$$

where α is θ or ϕ depending on the orientation of the cylindrical axis and L is the length of the cylinder. Let the axis be oriented along the X-axis. Then from Eq. (31), we have

$$j_{1\theta\phi} = j_{1x}\sin\theta\sin\phi - j_{1y}\sin\theta\cos\phi + j_{1z}\cos\theta$$

We assume again that the sheath is cylindrically concentric with the probe. This implies that the $\underset{\sim}{f}_1$ and $\underset{\sim}{f}_2$ perturbations are small. We can integrate over θ from 0 to 2π and find that $\int j_{1\theta\phi} d\alpha = 0$, so that

$$I = r_p L \int [j_{o\theta\phi} + j_{2\theta\phi}] d\alpha = I_o + I_2 \tag{69}$$

In the next subsection, we evaluate the I_o and I_2 contributions.

b. Retarding Region

Consider a strip element of cylindrical surface at the sheath position, $r = r_s$. Let the axis be in the X-direction and the normal to the strip be in the Z-direction. The current element δI passing through $r = r_s$ over a length L is

$$\frac{\delta I}{e r_s L} = \int_{-\infty}^{-v_o} v_Z dv_Z \int_{-\infty}^{\infty} dv_X \int_{-q_1}^{q_1} dv_Y f^*(v_Z, v_X, v_Y) \tag{70}$$

Here q_1 is obtained from momentum and energy conservation relations for a particle moving from the sheath position to the probe, namely,

$$r_p v_{Yp} = r_s v_{Ys} \quad \text{and} \quad v_{Zp}^2 = v_{Zs}^2 + v_{Ys}^2 - v_{Yp}^2 - [2(V_p - V_s)/m] \tag{71}$$

The condition for a particle to reach the probe is $v_{Zp}^2 \geq 0$ and $v_{Zs}^2 \geq 0$ or $v_{Ys}^2 \leq q_1^2$, where

$$q_1^2 = \frac{r_p^2}{r_s^2 - r_p^2} [v_{Zs}^2 - v_o^2] \quad \text{and} \quad v_o^2 = \frac{2V_p}{m} \tag{72}$$

with V_p denoting $V_p - V_s$. Also subscripts on v_Z, v_Y, and v_X are to be understood henceforth.

Let us first integrate Eq. (70) in the XY plane over Φ. Let

$$q^2 = v_X^2 + v_Y^2, \quad v_X = q\cos\Phi, \quad v_Y = q\sin\Phi$$

Referring to Figure 5, we see that, if $q^2 \leq q_1^2$, then the limits on Φ are 0 to 2π. If $q^2 \geq q_1^2$, then the Φ limits are from $-\Phi_o$ to Φ_o and from $\pi - \Phi_o$ to $\pi + \Phi_o$. Here Φ_o is determined by the condition that $v_Y^2 = q_1^2$ or

$$\sin\Phi_o = \frac{q_1}{q} = \left[\frac{r_p^2}{r_s^2 - r_p^2}\left(\frac{v_Z^2 - v_o^2}{q^2}\right)\right]^{\frac{1}{2}} \tag{73}$$

Let us now substitute the spherical harmonic expansion in Eq. (3) for f^* into Eq. (70).

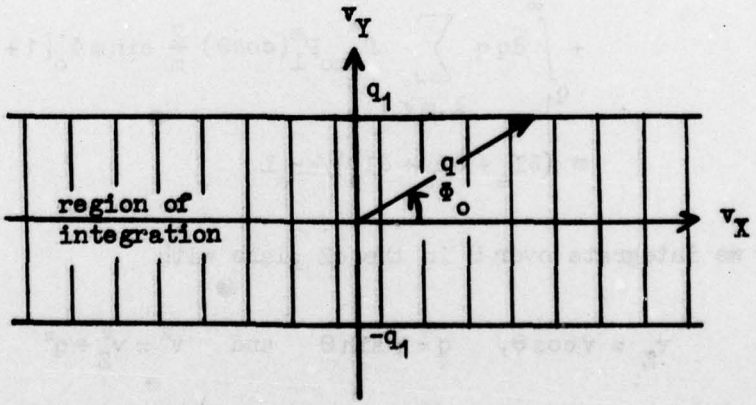

Figure 5. Velocity XY Plane for the Cylindrical Probe in the Retarding Region

Then

$$\frac{\delta I}{er_s L} = \sum_{lms} \int_{-\infty}^{-v_o} v_Z dv_Z \left\{ \int_o^{q_1} q\,dq\, f^*_{lms} P_l^m(\cos\theta) \int_o^{2\pi} d\Phi [\delta_{os} \cos m\Phi + \delta_{1s} \sin m\Phi] \right.$$

$$+ \int_{q_1}^{\infty} q\,dq\, f^*_{lms} P_l^m(\cos\theta) \int_{-\Phi_o}^{\Phi_o} d\Phi [\delta_{os} \cos m\Phi + \delta_{1s} \sin m\Phi]$$

$$\left. + \int_{q_1}^{\infty} q\,dq\, f^*_{lms} P_l^m(\cos\theta) \int_{\pi-\Phi_o}^{\pi+\Phi_o} d\Phi [\delta_{os} \cos m\Phi + \delta_{1s} \sin m\Phi] \right\} \qquad (74)$$

In the first term, we obtain a contribution only when $m = 0$ and $s = 0$. In the second plus third terms, consider first the $m = 0$ term. The Φ integration then contributes $4\Phi_o \delta_{os} \delta_{om}$. Consider now the $m \geq 1$ terms. The δ_{1s} terms give zero contributions. The δ_{os} contribution in the second term cancels that in the third unless m is even, so that the Φ integration for both these terms gives $(2/m)[1 + (-1)^m] \sin m\Phi_o$. Hence we obtain

$$\frac{\delta I}{er_s L} = \int_{-\infty}^{-v_o} v_Z dv_Z \left\{ \int_o^{q_1} dq\, q \sum_l 2\pi f^*_{loo} P_l(\cos\theta) + \int_{q_1}^{\infty} dq\, q \sum_l f^*_{loo} P_l(\cos\theta) 4\Phi_o \right.$$

$$\left. + \int_{q_1}^{\infty} dq\, q \sum_{l,m\geq 1} f^*_{lmo} P_l^m(\cos\theta) \frac{2}{m} \sin m\Phi_o [1 + (-1)^m] \right\}$$

$$= (\delta I_a + \delta I_b + \delta I_c)/er_s L \qquad (75)$$

Now we integrate over θ in the qZ plane with

$$v_Z = v\cos\theta, \quad q = v\sin\theta \quad \text{and} \quad v^2 = v_Z^2 + q^2$$

Referring now to Figure 3 for the first term in Eq. (75), we can immediately write

$$\frac{\delta I_a}{er_s L} = 2\pi \sum_{1}^{\infty} \int_{v_o}^{} v^3 dv f^*_{loo}(v) \int_{\pi-\theta_o}^{\pi} d\theta \sin\theta\cos\theta \; P_1(\cos\theta)$$

where

$$\sin^2\theta_o = \frac{r_p^2}{r_s^2}\left[1 - \left(\frac{v_o}{v}\right)^2\right] \tag{76}$$

Let $x = -\cos\theta$. Then, since $P_1(-x) = (-1)^1 P_1(x)$, we obtain

$$\frac{\delta I_a}{er_s L} = 2\pi \sum_{1}^{\infty} \int_{v_o}^{\infty} v^3 dv \; f^*_{loo}(v) \int_{\cos\theta_o}^{1} dx \, x \, (-1)^1 P_1(x) \tag{77}$$

Let us refer now to Figure 6, which indicates the region of integration for the second and third terms in Eq. (75). If $v \leq |v_o|$, there is no contribution.

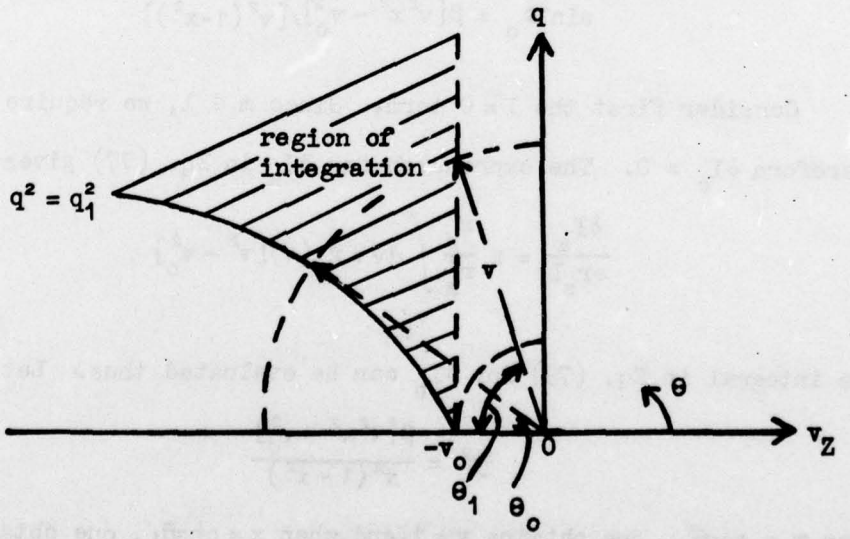

Figure 6. Spherical Velocity Space in the Retarding Region in the Investigation for a Cylindrical Probe

If $v \geq |v_o|$, then the limits on θ are $\pi - \theta_1$ to $\pi - \theta_o$, where $\sin^2\theta_o$ is given above in Eq. (76) and

$$\cos\theta_1 = v_o/v \tag{78}$$

Thus, substituting Eq. (73) for Φ_o and letting $x = -\cos\theta$, we obtain with

$\beta = r_p^2/(r_s^2 - r_p^2)$

$$\frac{\delta I_b}{e r_s L} = \sum_1 \int_{v_o}^{\infty} dv\, v^3\, f^*_{1oo}(v) \int_{\cos\theta_1}^{\cos\theta_o} dx\, x\, (-1)^1 P_1(x) 4 \sin^{-1} \left\{ \left[\frac{\beta[v^2x^2 - v_o^2]}{v^2(1-x^2)} \right]^{\frac{1}{2}} \right\} \tag{79}$$

For δI_c we write

$$\frac{\delta I_c}{e r_s L} = \int_{v_o}^{\infty} dv\, v^3 \sum_{l,m \geq 1} f^*_{lmo} \int_{\cos\theta_1}^{\cos\theta_o} dx\, x\, P_l^m(-x)\, \frac{2}{m}\, \sin m\Phi_o [1 + (-1)^m] \tag{80}$$

with Φ_o given by

$$\sin^2\Phi_o = \beta[v^2x^2 - v_o^2]/[v^2(1-x^2)] \tag{81}$$

Consider first the $l = 0$ term. Since $m \leq l$, we require $m = 0$ and therefore $\delta I_c = 0$. The expression for δI_a in Eq. (77) gives immediately

$$\frac{\delta I_a}{e r_s L} = \pi \frac{r_p^2}{r_s^2} \int_{v_o}^{\infty} dv\, v\, f_o(v)[v^2 - v_o^2] \tag{82}$$

The integral in Eq. (79) for δI_b can be evaluated thus. Let

$$y^2 = \frac{\beta[v^2x^2 - v_o^2]}{v^2(1-x^2)} \tag{83}$$

When $x = \cos\theta_o$, one obtains $y = 1$, and, when $x = \cos\theta_1$, one obtains $y = 0$. Equation (79) becomes

$$\frac{\delta I_b}{e r_s L} = \int_{v_o}^{\infty} dv\, v^3 f_o(v) \left[1 - \left(\frac{v_o}{v}\right)^2\right] \int_0^1 \frac{4\beta y\, dy \sin^{-1} y}{(y^2 + \beta)^2} \tag{84}$$

Now

$$\int \frac{y\,dy\,\sin^{-1}y}{(y^2+\beta)^2} = \frac{-\sin^{-1}y}{2(y^2+\beta)} - \frac{1}{2(\beta+\beta^2)^{1/2}}\sin^{-1}\left[\left(\frac{\beta(1-y^2)}{\beta+y^2}\right)^{\frac{1}{2}}\right] \qquad (85)$$

and

$$\int_0^1 \frac{y\,dy\,\sin^{-1}y}{(y^2+\beta)^2} = \frac{\pi}{4}\left[\frac{1}{(\beta+\beta^2)^{\frac{1}{2}}} - \frac{1}{(1+\beta)}\right]$$

so that

$$\frac{\delta I_b}{er_s L} = \pi \int_{v_o}^{\infty} dv\, v\, f_o(v)[v^2 - v_o^2]\left(\frac{r_p}{r_s} - \frac{r_p^2}{r_s^2}\right) \qquad (86)$$

Adding Eqs. (82) and (86) yields

$$\frac{\delta I_o}{er_p L} = \pi \int_{v_o}^{\infty} dv\, v\, f_o(v)[v^2 - v_o^2]$$

Thus $\delta I_o = j_o r_p L$ is independent of r_s, as mentioned previously. Performing the integral over α from 0 to 2π in Eq. (69) yields with $U = mv^2/2$

$$I_o = 2\pi r_p L j_o = \frac{4\pi^2 r_p L e}{m^2} \int_{V_p}^{\infty} dU f_o(U)[U - V_p] \qquad (87)$$

This result for j_o is the same as for the planar or spherical probe but it is multiplied here instead by the cylindrical area, $2\pi r_p L$.

Consider now the $l = 2$ terms. As mentioned in the previous subsection, the $l = 1$ term integrates to zero over α. For $l = 2$, we equate $f^*_{2oo} = f^*_{2ZZ}$ (see Eq. (4)) and $P_2(x) = \frac{1}{2}(3x^2 - 1)$. Equation (77) for δI_a integrates immediately to give

$$\frac{\delta I_a}{er_s L} = \pi \int_{v_o}^{\infty} dv\, v^3\, f^*_{2ZZ}(v)\left[1 - \left(\frac{v_o}{v}\right)^2\right]\frac{r_p^2}{r_s^2}\left[1 - \frac{3}{4}\frac{r_p^2}{r_s^2}\left(1 - \left(\frac{v_o}{v}\right)^2\right)\right] \qquad (88)$$

after Eq. (76) for $\sin^2\theta_o$ is substituted. With the substitution for y in Eq. (83), δI_b in Eq. (79) becomes

$$\frac{\delta I_b}{er_s L} = \int_{v_o}^{\infty} dv\, v^3 f^*_{2ZZ}(v)\left[1-\left(\frac{v_o}{v}\right)^2\right]\int_0^1 \frac{4\beta y\, dy \sin^{-1}y}{(y^2+\beta)^2}\left[1-\frac{3}{2}\frac{\beta}{(y^2+\beta)}\left(1-\left(\frac{v_o}{v}\right)^2\right)\right] \tag{89}$$

We use the formula in Eq. (85) and in addition the formulas

$$\int \frac{y\, dy \sin^{-1}y}{(y^2+\beta)^3} = -\frac{\sin^{-1}y}{4(y^2+\beta)^2} + \frac{y(1-y^2)^{\frac{1}{2}}}{8\beta(\beta+1)(y^2+\beta)} - \frac{2\beta+1}{8(\beta^2+\beta)^{3/2}}\sin^{-1}\left[\left(\frac{\beta(1-y^2)}{\beta+y^2}\right)^{\frac{1}{2}}\right] \tag{90}$$

and

$$\int_0^1 \frac{y\, dy \sin^{-1}y}{(y^2+\beta)^3} = \frac{\pi}{8(1+\beta)^2}\left[\frac{2\beta+1}{2\beta}\left(\frac{\beta+1}{\beta}\right)^{\frac{1}{2}} - 1\right] \tag{91}$$

Consequently,

$$\frac{\delta I_b}{er_s L} = \pi\int_{v_o}^{\infty} dv\, v^3 f^*_{2ZZ}(v)\left[1-\left(\frac{v_o}{v}\right)^2\right]\left[\frac{r_p}{r_s}-\frac{r_p^2}{r_s^2}+\frac{3}{4}\left(1-\left(\frac{v_o}{v}\right)^2\right)\frac{r_p}{r_s}\left(\frac{r_p^3}{r_s^3}-\frac{1}{2}\frac{r_p^2}{r_s^2}-\frac{1}{2}\right)\right] \tag{92}$$

In the expression for δI_c in Eqs. (80) and (81), we have only a contribu- from $m = 2$ for which $\sin 2\Phi_o = 2\sin\Phi_o\cos\Phi_o$. We note from Eq. (4) that $f^*_{220} = \frac{1}{6}(f^*_{2XX} - f^*_{2YY})$. Also $P_2^2(-x) = 3(1-x^2)$. Letting $y = 1-x^2$, we obtain

$$\frac{\delta I_c}{er_s L} = \int_{v_o}^{\infty} dv\, v\,(f^*_{2XX} - f^*_{2YY})\beta^{\frac{1}{2}}\int_{y_o}^{y_1} dy(a+by+cy^2)^{\frac{1}{2}} \tag{93}$$

where $\beta = r_p^2/(r_s^2 - r_p^2)$ as before, $a = -\beta(v^2 - v_o^2)$, $b = v^2(v^2 - v_o^2)(1+2\beta)$,

$c = -v^4(1+\beta)$, $\Delta \equiv 4ac - b^2 = -v^4(v^2 - v_o^2)^2$,

$$y_o = \left(\frac{\beta}{\beta+1}\right)\left(1-\left(\frac{v_o}{v}\right)^2\right) \quad \text{and} \quad y_1 = 1-\left(\frac{v_o}{v}\right)^2$$

Since c and Δ are less than zero, we use the formula

$$\int dy(a+by+cy^2)^{\frac{1}{2}} = \frac{2cy+b}{4c}(a+by+cy^2)^{\frac{1}{2}} + \frac{4ac-b^2}{8(-c)^{3/2}}\sin^{-1}\left(\frac{2cy+b}{(b^2-4ac)^{\frac{1}{2}}}\right) \tag{94}$$

At the upper and lower limits, the arguments of the $\sin^{-1}$ are, respectively, ∓ 1 and $(a + by + cy^2) = 0$. Thus

$$\int_{y_o}^{y_1} dy(a + by + cy^2)^{\frac{1}{2}} = \frac{\pi}{8} \frac{b^2 - 4ac}{(-c)^{3/2}} = \frac{\pi}{8}\left[1 - \left(\frac{v_o}{v}\right)^2\right]^2 \frac{v^2}{(1+\beta)^{3/2}} \qquad (95)$$

This yields for δI_c in Eq. (93) the following:

$$\frac{\delta I_c}{er_s^L} = \frac{\pi}{8}\frac{r_p}{r_s}\left(1 - \frac{r_p^2}{r_s^2}\right)\int_{v_o}^{\infty} dv\, v^3 \left(1 - \left(\frac{v_o}{v}\right)^2\right)^2 (f^*_{2XX} - f^*_{2YY}) \qquad (96)$$

Adding the three contributions in Eqs. (88), (92) and (96) finally gives

$$\frac{\delta I_2}{er_p^L} = \pi \int_{v_o}^{\infty} dv\, v^3 \left(1 - \left(\frac{v_o}{v}\right)^2\right)\left\{f^*_{2ZZ}\left[1 - \frac{3}{8}\left(1 - \left(\frac{v_o}{v}\right)^2\right)\left(1 + \frac{r_p^2}{r_s^2}\right)\right.\right.$$
$$\left.\left. + (f^*_{2XX} - f^*_{2YY})\left(1 - \left(\frac{v_o}{v}\right)^2\right)\frac{1}{8}\left(1 - \frac{r_p^2}{r_s^2}\right)\right\} \qquad (97)$$

Let us now perform the integration over α or θ from 0 to 2π. Then from Eq. (32) we find that

$$\int_0^{2\pi} f^*_{2ZZ} d\theta = \pi[f_{2xx}\sin^2\phi + f_{2yy}\cos^2\phi + f_{2zz} - 2f_{2xy}\sin\phi\cos\phi]$$
$$= -\pi[f_{2xx}\cos^2\phi + f_{2yy}\sin^2\phi + 2f_{2xy}\sin\phi\cos\phi]$$

since $f_{2zz} = -(f_{2xx} + f_{2yy})$. Similarly one can verify from Eqs. (27) and (30) that

$$2\pi f^*_{2XX} = \int_0^{2\pi} f^*_{2XX} d\theta = -2\int_0^{2\pi} f^*_{2YY} d\theta = -2\int_0^{2\pi} f^*_{2ZZ} d\theta \qquad (98)$$

Substituting Eq. (98) into the integral of Eq. (97) yields

$$\frac{I_2}{er_p^L} = -\frac{\pi}{4}\int_{v_o}^{\infty} f^*_{2XX} v^3 dv \left(1 - \left(\frac{v_o}{v}\right)^2\right)\left(1 + 3\left(\frac{v_o}{v}\right)^2\right) \qquad (99)$$

for any orientation. In terms of $U = mv^2/2$, this reads as

$$I_2 = r_p L \int_0^{2\pi} j_2 d\theta = -\frac{\pi^2 e r_p L}{2m^2} \int_{V_p}^{\infty} [U + 2V_p - 3V_p^2/U] f^*_{2XX}(U) dU \qquad (100)$$

It is remarkable that this expression is independent of r_s and could have been obtained from the plane probe result by integrating Eq. (13) with Eq. (32) over θ for $\phi = 0$. This operation yields Eq. (100) with f_{2xx} and generalizing to any other orientation means writing f^*_{2XX}. This component thus always refers to that along the cylindrical axis. Combining Eqs. (87) and (100), one can write generally for a cylinder oriented along the i-axis the following expression for the total current in a retarding potential:

$$I = \frac{4\pi^2 e r_p L}{m^2} \int_{V_p}^{\infty} \left\{ [U - V_p] f_o(U) - \frac{1}{8} [U + 2V_p - 3V_p^2/U] f_{2ii}(U) \right\} dU \qquad (101)$$

Thus, if $f_o(U)$ is obtained by using a spherical probe as outlined previously and if I_o is then subtracted from (101), the remaining current (I_2) variation versus V_p can yield the f_{2ii} components by using the inversion relation in Eq. (43). As a further illustration, if the cylinder axis is in the ij plane forming a 45^o angle with respect to the i and j axis, one gets

$$I = \frac{4\pi^2 e r_p L}{m^2} \int_{V_p}^{\infty} \left\{ [U - V_p] f_o(U) + \frac{1}{8} [U + 2V_p - 3V_p^2/U] [\tfrac{1}{2} f_{2kk}(U) - f_{2ij}(U)] \right\} dU \qquad (102)$$

Hence, in principle, with appropriate orientation of the cylinder axis, we can derive any component of the $\underset{\approx}{f}_2$ tensor.

c. Accelerating Region

Since the sign of the $2V_p/m$ term is changed, we redefine our quantity q_1 in Eq. (72) to be

$$q_1^2 = \beta[v_Z^2 + v_o^2] \quad \text{with} \quad \beta = r_p^2/(r_s^2 - r_p^2)$$

The limits on v_Z are now $-\infty$ to 0. Equation (75) reads for this case

$$\frac{\delta I}{er_s L} \equiv \frac{\delta I_a + \delta I_b + \delta I_c}{er_s L} = \int_{-\infty}^{0} v_Z dv_Z \left\{ \int_0^{q_1} dq\, q \sum_1 2\pi f^*_{loo} P_l(\cos\theta) \right.$$

$$\left. + \int_{q_1}^{\infty} dq\, q \sum_1 f^*_{loo} P_l(\cos\theta) 4\Phi_o + \int_{q_1}^{\infty} dq\, q \sum_{l,m\geq 1} f^*_{lmo} P_l^m(\cos\theta) \frac{2}{m} \sin m\Phi_o [1+(-1)^m] \right\} \tag{103}$$

where

$$\sin^2\Phi_o = \left(\frac{q_1}{q}\right)^2 = \frac{\beta[v_Z^2 + v_o^2]}{q^2} \tag{104}$$

We proceed with the integration over θ in the qZ plane. The first term in Eq. (103), δI_a, can be evaluated upon considering Figure 4, namely,

$$\frac{\delta I_a}{2\pi er_s L} = \sum_1 \int_{\infty}^{\sqrt{\beta}v_o} v^3 dv f^*_{loo}(v) \int_{\pi-\theta_o}^{\pi} d\theta \sin\theta\cos\theta\, P_l(\cos\theta) + \sum_1 \int_{\sqrt{\beta}v_o}^{0} v^3 dv f^*_{loo}(v) \int_{\pi/2}^{\pi} d\theta \sin\theta\cos\theta P_l(\cos\theta)$$

where

$$\sin^2\theta_o = \frac{r_p^2}{r_s^2}\left[1 + \left(\frac{v_o}{v}\right)^2\right] \tag{105}$$

Let $x = -\cos\theta$. Then

$$\frac{\delta I_a}{2\pi er_s L} = \sum_1 \int_{\sqrt{\beta}v_o}^{\infty} v^3 dv f^*_{loo}(v) \int_{\cos\theta_o}^{1} dx\, x\,(-1)^l P_l(x) + \sum_1 \int_{o}^{\sqrt{\beta}v_o} v^3 dv f^*_{loo}(v) \int_{0}^{1} dx\, x(-1)^l P_l(x) \tag{106}$$

Let us refer now to Figure 7 for the integrations in δI_b and δI_c. If $v \leq |\sqrt{\beta}v_o|$, there is no contribution. If $v > |\sqrt{\beta}v_o|$, then the limits on θ are $\pi/2$ to $\pi - \theta_o$, where θ_o is given in Eq. (105). Thus substituting Eq. (104) for Φ_o and letting $x = -\cos\theta$, we obtain for δI_b

$$\frac{\delta I_b}{er_s L} = \sum_1 \int_{\sqrt{\beta}v_o}^{\infty} dv\, v^3 f^*_{loo}(v) \int_{o}^{\cos\theta_o} dx\, x\,(-1)^l P_l(x) 4\sin^{-1}\left\{\left[\frac{\beta(v^2x^2 + v_o^2)}{v^2(1-x^2)}\right]^{\frac{1}{2}}\right\} \tag{107}$$

For δI_c we write

$$\frac{\delta I_c}{er_s^2 L} = \int_{\sqrt{\beta}v_o}^{\infty} dv\, v^3 \sum_{l,m\geq 1} f^*_{lmo} \int_0^{\cos\theta_o} dx\, x\, P_l^m(-x)\, \frac{2}{m} \sin m\Phi_o [1 + (-1)^m] \qquad (108)$$

with Φ_o given by

$$\sin^2\Phi_o = \beta[v^2x^2 + v_o^2]/[v^2(1-x^2)] \qquad (109)$$

Consider first the $l = 0$ term. Again $\delta I_c = 0$ since $m = 0$. The expression for δI_a in Eq. (106) yields

$$\frac{\delta I_a}{er_s^2 L} = \pi \left[\frac{r_p^2}{r_s^2} \int_{\sqrt{\beta}v_o}^{\infty} dv\, v^3\, f_o(v) \left(1 + \left(\frac{v_o}{v}\right)^2\right) + \int_0^{\sqrt{\beta}v_o} dv\, v^3 f_o(v) \right] \qquad (110)$$

As far as δI_b is concerned, we obtain, instead of Eq. (84) previously, the expression

$$\frac{\delta I_b}{er_s^2 L} = \int_{\sqrt{\beta}v_o}^{\pi} dv\, v^3\, f_o(v) \left[1 + \left(\frac{v_o}{v}\right)^2\right] \int_{\sqrt{\beta}v_o/v}^{1} \frac{4\beta\, y\, dy \sin^{-1} y}{(y^2+\beta)^2} \qquad (111)$$

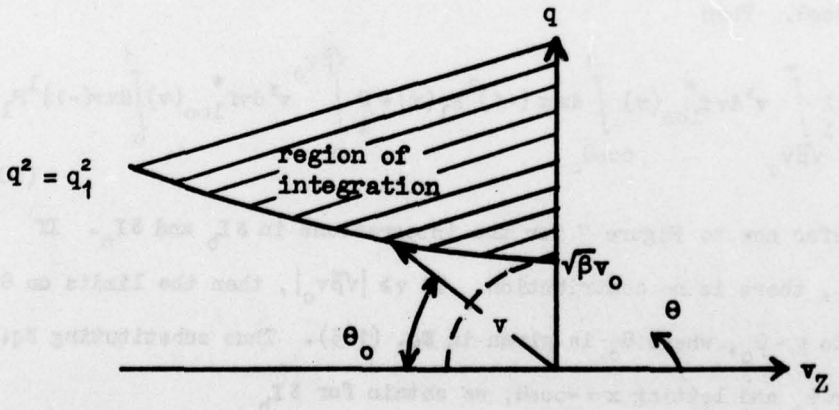

Figure 7. Spherical Velocity Space in the Accelerating Region in the Integrations for a Cylindrical Probe

where

$$y^2 = \frac{\beta[v^2x^2 + v_o^2]}{v^2(1-x^2)} \tag{112}$$

and $y = 1$ when $x = \cos\theta_o$ and $y = \sqrt{\beta}v_o/v$ when $x = 0$. We now use Eq. (85) and obtain

$$\frac{\delta I_b}{er_s^L} = 4\beta \int_{\sqrt{\beta}v_o}^{\infty} dv\, v^3 f_o(v) \left[1 + \left(\frac{v_o}{v}\right)^2\right] \left\{ -\frac{\pi}{4(\beta+1)} + \frac{\sin^{-1}(v_o\sqrt{\beta}/v)}{2\beta(1 + v_o^2/v^2)} + \frac{1}{2(\beta+\beta^2)^{\frac{1}{2}}} \cdot \right.$$

$$\left. \cdot \sin^{-1}\left\{\left[\frac{1 - \beta v_o^2/v^2}{1 + v_o^2/v^2}\right]^{\frac{1}{2}}\right\}\right\} \tag{113}$$

Adding Eqs. (110) and (113) gives for $\delta I_o = I_o/2\pi = j_o r_p L$ the following :

$$\frac{I_o}{2\pi er_s L} = \pi \int_o^{\sqrt{\beta}v_o} dv\, v^3 f_o(v) + 2\int_{\sqrt{\beta}v_o}^{\infty} dv\, v^3 f_o(v) \left\{\sin^{-1}\left(\frac{\sqrt{\beta}v_o}{v}\right) + \frac{r_p}{r_s}\left(1 + \left(\frac{v_o}{v}\right)^2\right)\sin^{-1}\left\{\left[\frac{v^2 - \beta v_o^2}{v^2 + v_o^2}\right]^{\frac{1}{2}}\right\}\right\} \tag{114}$$

Equation (114) reduces to proper values in known limits. If $f_o(v)$ is a Maxwellian distribution, Eq. (114) reduces to Langmuir's result[4,5]:

$$I_o = 2\pi er_p L n_o \left(\frac{kT_e}{2\pi m}\right)^{\frac{1}{2}} \left\{\frac{r_s}{r_p}\Phi\left[\left(\frac{\beta V_p}{kT_e}\right)^{\frac{1}{2}}\right] + \exp\left(\frac{V_p}{kT_e}\right)\left[1 - \Phi\left(\left(\frac{V_p(1+\beta)}{kT_e}\right)^{\frac{1}{2}}\right)\right]\right\} \tag{115}$$

where Φ is the error function. Also, when $r_s >> r_p$ or $\beta << 1$, we can approximate Eq. (114) by

$$I_o = 4\pi er_p L \int_o^{\infty} dv\, v^3 f_o(v) \left\{\frac{v_o}{v} + \left(1 + \left(\frac{v_o}{v}\right)^2\right)\sin^{-1}\left[\left(1 + \left(\frac{v_o}{v}\right)^2\right)^{-\frac{1}{2}}\right]\right\}$$

$$= \frac{8\pi er_p L}{m^2} \int_o^{\infty} \left\{(UV_p)^{\frac{1}{2}} + (U + V_p)\sin^{-1}\left[\left(\frac{U}{U+V_p}\right)^{\frac{1}{2}}\right]\right\} f_o(U)dU \tag{116}$$

Equation (116) agrees with the recent expression given by Polychronopulos[6]. Finally, when $r_s \approx r_p$ or $\beta >> 1$, we can reduce Eq. (114) to

$$I_o = 2\pi^2 er_p L \int_o^\infty dv\, v^3 f_o(v) = \frac{4\pi^2 er_p L}{m^2} \int_o^\infty dU\, U f_o(U) \qquad (117)$$

which is identical to the plane probe result in Eq. (11) integrated over a cylindrical surface $2\pi r_p L$. An incoming particle effectively sees a planar element of surface if the sheath thickness is small.

We now proceed to the $l = 2$ results for the particle acceleration regime. Evaluating Eq. (106) or I_a for $l = 2$ gives

$$\frac{\delta I_a}{er_s L} = \frac{\pi}{4} \int_o^{\sqrt{\beta} v_o} dv\, v^3 f^*_{2ZZ} + \frac{\pi r_p^2}{r_s^2} \int_{\sqrt{\beta} v_o}^\infty dv\, v^3 f^*_{2ZZ} \left[1 + \left(\frac{v_o}{v}\right)^2\right] \left[1 - \frac{3}{4} \frac{r_p^2}{r_s^2} \left(1 + \left(\frac{v_o}{v}\right)^2\right)\right] \qquad (118)$$

using $f^*_{2oo} = f^*_{2ZZ}$ and $P_2(x) = (3x^2 - 1)/2$. The expression in Eq. (107) for I_b can be evaluated with the substitution of y^2 in Eq. (112), similarly to the method leading to Eq. (111). The corresponding relation is

$$\frac{\delta I_b}{er_s L} = \int_{\sqrt{\beta} v_o}^\infty dv\, v^3 f^*_{2ZZ}(v) \left[1 + \left(\frac{v_o}{v}\right)^2\right] \int_{\sqrt{\beta} v_o / v}^1 dy \frac{4\beta y \sin^{-1} y}{(y^2 + \beta)^2} \left[1 - \frac{3}{2} \frac{\beta(1 + v_o^2/v^2)}{y^2 + \beta}\right] \qquad (119)$$

Using Eqs. (85) and (90), we obtain

$$\begin{aligned} \frac{\delta I_b}{er_s L} = \int_{\sqrt{\beta} v_o}^\infty dv\, v^3 f^*_{2ZZ}(v) \Bigg\{ & \frac{1}{2} \sin^{-1}\left(\frac{\sqrt{\beta} v_o}{v}\right) + \frac{3\pi}{4} \left(1 + \left(\frac{v_o}{v}\right)^2\right)^2 \left(\frac{r_p}{r_s}\right)^4 - \pi \left(1 + \left(\frac{v_o}{v}\right)^2\right) \frac{r_p^2}{r_s^2} \\ & + 2 \frac{r_p}{r_s} \left(1 + \left(\frac{v_o}{v}\right)^2\right) \left[1 - \frac{3}{8} \left(1 + \left(\frac{v_o}{v}\right)^2\right) \left(\frac{r_p^2}{r_s^2} + 1\right)\right] \sin^{-1} \left[\left(\frac{v^2 - \beta v_o^2}{v^2 + v_o^2}\right)^{\frac{1}{2}}\right] \\ & + \frac{3}{4} \frac{r_p^2}{r_s^2} \left(\frac{r_s^2 - r_p^2}{r_p^2}\right)^{\frac{1}{2}} \frac{v_o}{v} \left(1 + \left(\frac{v_o}{v}\right)^2\right) \left[1 - \left(\frac{r_p^2}{r_s^2 - r_p^2}\right) \left(\frac{v_o}{v}\right)^2\right]^{\frac{1}{2}} \Bigg\} \end{aligned} \qquad (120)$$

Next we evaluate δI_c in Eq. (108). Only the $m = 2$ term contributes. We use $P_2^2(-x) = 3(1 - x^2)$ and $f^*_{220} = \frac{1}{6}(f^*_{2XX} - f^*_{2YY})$. We are led to a relation similar to Eq. (93), namely,

$$\frac{\delta I_c}{er_s^L} = \int_{\sqrt{\beta}v_o}^{\infty} dv\, v\, (f^*_{2XX} - f^*_{2YY})\beta^{\frac{1}{2}} \int_{\sin^2\theta_o}^{1} dy(a + by + cy^2)^{\frac{1}{2}} \qquad (121)$$

where

$$y = 1 - x^2, \quad a = -\beta(v^2 + v_o^2)^2, \quad b = v^2(v^2 + v_o^2)(1 + 2\beta),$$

$$c = -v^4(1+\beta), \quad \Delta = 4ac - b^2 = -v^4(v^2 + v_o^2)^2$$

$$2c + b = v^2[v_o^2(1 + 2\beta) - v^2] \quad \text{and} \quad a + b + c = v_o^2(v^2 - \beta v_o^2)$$

Since c and Δ are less than zero, we use again the formula in Eq. (94) to yield

$$\frac{\delta I_c}{er_s^L} = \frac{1}{4}\int_{\sqrt{\beta}v_o}^{\infty} dv(f^*_{2XX} - f^*_{2YY}) \left\{\frac{r_p^2}{r_s^2}\left(\frac{r_s^2 - r_p^2}{r_p^2}\right)^{\frac{1}{2}}\left[v^2 - v_o^2\left(1 + \frac{2r_p^2}{r_s^2 - r_p^2}\right)\right] v_o\left[1 - \left(\frac{v_o}{v}\right)^2 \frac{r_p^2}{r_s^2 - r_p^2}\right]^{\frac{1}{2}}\right.$$

$$\left. + \left(\frac{r_p}{r_s} - \frac{r_p^3}{r_s^3}\right)\left(1 + \left(\frac{v_o}{v}\right)^2\right)^2 v^3 \sin^{-1}\left[\left(\frac{v^2 - \beta v_o^2}{v^2 + v_o^2}\right)^{\frac{1}{2}}\right]\right\} \qquad (122)$$

We have used the relationship illustrated in Figure 8 that

$$\xi = \sin^{-1}\left[\frac{v_o^2(1+2\beta) - v^2}{v^2 + v_o^2}\right] = \frac{\pi}{2} - 2\chi = \frac{\pi}{2} - 2\sin^{-1}\left[\left(\frac{v^2 - \beta v_o^2}{v^2 + v_o^2}\right)^{\frac{1}{2}}\right] \qquad (123)$$

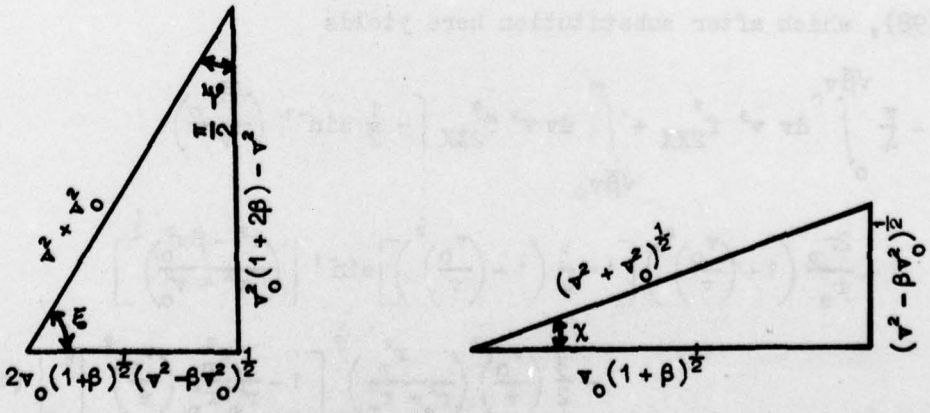

Figure 8. Relationship Between the Angles ξ and χ. Note that $\sin(\pi/2 - \xi) = 2\sin\chi\cos\chi$ or $\pi/2 - \xi = 2\chi$

Combining the three parts in Eqs. (118), (120), and (122), we finally obtain

$$\frac{\delta I_2}{e r_s L} = \frac{\pi}{4}\int_0^{\sqrt{\beta}v_o} dv\, v^3 f^*_{2ZZ} + \int_{\sqrt{\beta}v_o}^{\infty} dv\, v^3 f^*_{2ZZ}\left\{\frac{1}{2}\sin^{-1}\left(\frac{\sqrt{\beta}v_o}{v}\right)\right.$$

$$+\frac{2r_p}{r_s}\left(1+\left(\frac{v_o}{v}\right)^2\right)\left[1-\frac{3}{8}\left(1+\left(\frac{v_o}{v}\right)^2\right)\left(\frac{r_p^2}{r_s^2}+1\right)\right]\sin^{-1}\left[\left(\frac{v^2-\beta v_o^2}{v^2+v_o^2}\right)^{\frac{1}{2}}\right]$$

$$\left.+\frac{3}{4}\frac{r_p^2}{r_s^2}\left(\frac{r_s^2-r_p^2}{r_p^2}\right)^{\frac{1}{2}}\frac{v_o}{v}\left(1+\left(\frac{v_o}{v}\right)^2\right)\left[1-\frac{r_p^2}{r_s^2-r_p^2}\left(\frac{v_o}{v}\right)^2\right]^{\frac{1}{2}}\right\}$$

$$+\frac{1}{4}\int_{\sqrt{\beta}v_o}^{\infty} dv(f^*_{2XX}-f^*_{2YY})\left\{\frac{r_p^2}{r_s^2}\left(\frac{r_s^2-r_p^2}{r_p^2}\right)^{\frac{1}{2}}\left[v^2-v_o^2\left(1+\frac{2r_p^2}{r_s^2-r_p^2}\right)\right]v_o\left[1-\frac{r_p^2}{r_s^2-r_p^2}\left(\frac{v_o}{v}\right)^2\right]^{\frac{1}{2}}\right.$$

$$\left.+\left(\frac{r_p}{r_s}-\frac{r_p^3}{r_s^3}\right)\left(1+\left(\frac{v_o}{v}\right)^2\right)v^3\sin^{-1}\left[\left(\frac{v^2-\beta v_o^2}{v^2+v_o^2}\right)^{\frac{1}{2}}\right]\right\} \qquad (124)$$

The above applies to a cylindrical strip whose exis is along the X axis and whose normal is in the Z-direction. Let us now integrate over all such strips by letting θ vary from 0 to 2π. We obtain the result in Eq. (98), which after substitution here yields

$$\frac{I_2}{e\pi r_s L} = -\frac{\pi}{4}\int_0^{\sqrt{\beta}v_o} dv\, v^3 f^*_{2XX} + \int_{\sqrt{\beta}v_o}^{\infty} dv\, v^3 f^*_{2XX}\left\{-\frac{1}{2}\sin^{-1}\left(\frac{\sqrt{\beta}v_o}{v}\right)\right.$$

$$-\frac{2r_p}{r_s}\left(1+\left(\frac{v_o}{v}\right)^2\right)\left[1-\frac{3}{4}\left(1+\left(\frac{v_o}{v}\right)^2\right)\right]\sin^{-1}\left[\left(\frac{v^2-\beta v_o^2}{v^2+v_o^2}\right)^{\frac{1}{2}}\right]$$

$$\left.-\frac{3}{2}\left(\frac{v_o}{v}\right)^3\left(\frac{r_p^2}{r_s^2-r_p^2}\right)^{\frac{1}{2}}\left[1-\frac{r_p^2}{r_s^2-r_p^2}\left(\frac{v_o}{v}\right)^2\right]^{\frac{1}{2}}\right\} \qquad (125)$$

This is our final result. When $r_s >> r_p$ or $\beta << 1$, it reduces to

$$\frac{I_2}{e\pi r_p L} = -\frac{1}{2}\int_o^\infty dv\, v^3 f^*_{2XX}(v) \left\{\frac{v_o}{v}\left(1+3\left(\frac{v_o}{v}\right)^2\right)+\left(1+\left(\frac{v_o}{v}\right)^2\right)\left(1-3\left(\frac{v_o}{v}\right)^2\right)\sin^{-1}\left[\left(1+\left(\frac{v_o}{v}\right)^2\right)^{-\frac{1}{2}}\right]\right.$$

or

$$I_2 = -\frac{e\pi r_p L}{m^2}\int_o^\infty dU\, U f^*_{2XX}(U) \left\{\left(\frac{V_p}{U}\right)^{\frac{1}{2}}\left(1+\frac{3V_p}{U}\right)+\left(1+\frac{V_p}{U}\right)\left(1-\frac{3V_p}{U}\right)\sin^{-1}\left[\left(\frac{U}{U+V_p}\right)^{\frac{1}{2}}\right]\right\} \tag{126}$$

When $r_s \approx r_p$ or $\beta >> 1$, we obtain

$$I_2 = -\frac{e\pi^2 r_p L}{2m^2}\int_o^\infty dU\, U f^*_{2XX}(U) \tag{127}$$

which again is equivalent to a planar surface element (see Eq. (25)) integrated over θ (see Eq. (32)) from 0 to 2π.

5. THE SPHERICAL GRID SYSTEM

A different type of electrostatic analyzer is the spherical grid system, illustrated in Figure 9.

Let the normal to the hole in the plate be along the Z-axis. Then, after integration over Φ, we obtain for a retarding potential

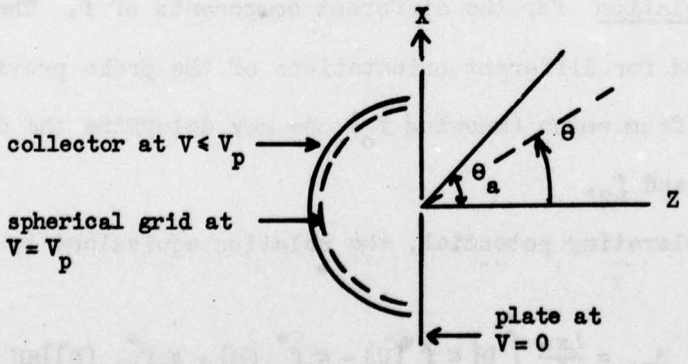

Figure 9. The Spherical Grid System

$$j_{\theta\phi} = 2\pi e \int_{v_o}^{\infty} \int_{o}^{\theta_a} dv\, v^3 \sum_{l} f^*_{loo} P_l(\cos\theta)(-1)^l \sin\theta\cos\theta d\theta \qquad (128)$$

where θ_a is the acceptance angle and $v_o \equiv (2V_p/m)^{\frac{1}{2}}$. Integration over θ gives

$$j_{\theta\phi} = 2\pi e \int_{v_o}^{\infty} dv\, v^3 \sum_{l} f^*_{loo}(-1)^l \kappa_l \qquad (129)$$

where, using Eq. (16), we have

$$\kappa_n = \frac{1}{(2n+1)}\left[\left(\frac{n+1}{2n+3}\right)(P_n(\cos\theta_a) - P_{n+2}(\cos\theta_a)) + \left(\frac{n}{2n-1}\right)(P_{n-2}(\cos\theta_a) - P_n(\cos\theta_a))\right]$$

In particular for l up to 2, we obtain

$$j_{\theta\phi} = \frac{4\pi e}{m^2} \int_{V_p}^{\infty} U[\kappa_o f_o(U) - \kappa_1 f^*_{1Z}(U) + \kappa_2 f^*_{2ZZ}(U)]dU \qquad (130)$$

with

$$\kappa_o = \tfrac{1}{2}\sin^2\theta_a, \quad \kappa_1 = \tfrac{1}{3}(1 - \cos^3\theta_a) \quad \text{and} \quad \kappa_2 = \tfrac{1}{8}\sin^2\theta_a(1 + 3\cos^2\theta_a) \qquad (131)$$

Differentiation yields

$$\frac{dj_{\theta\phi}}{dV_p} = -\frac{4\pi e}{m^2}\left\{V_p[\kappa_o f_o(V_p) - \kappa_1 f^*_{1Z}(V_p) + \kappa_2 f^*_{2ZZ}(V_p)]\right\} \qquad (132)$$

For this kind of probe then, the first derivative of j with respect to V_p gives a <u>linear relation</u> for the different components of f. The current densities obtained for different orientations of the probe provide a set of linear equations from which (knowing f_o) one may determine the different components of $\underset{\sim}{f}_1$ and $\underset{\approx}{f}_2$.

For an accelerating potential, the relation equivalent to Eq. (130) is

$$j_{\theta\phi} = \frac{4\pi e}{m^2} \int_{o}^{\infty} U[\kappa_o f_o(U) - \kappa_1 f^*_{1Z}(U) + \kappa_2 f^*_{2ZZ}(U)]dU \qquad (133)$$

6. SUMMARY

We summarize here the results in this section for various probes including anisotropic terms, up to $f_{\underset{\sim}{2}}$ terms in the distribution function. In the retarding potential region, the current intercepted by a one-sided flat disk of area A is (see Eqs. (11) to (13))

$$I = \frac{2\pi eA}{m^2}\int_{V_p}^{\infty} dU \left\{ (U - V_p) f_o(U) - \frac{2}{3} U \left[1 - \left(\frac{V_p}{U}\right)^{3/2} \right] f^*_{1Z}(U) + \frac{1}{4}\left[U + 2V_p - 3V_p^2/U \right] f^*_{2ZZ}(U) \right\} \tag{134}$$

Here V_p is the retarding potential and a star on f allows for a $\theta\phi$ rotation of the disk according to Eqs. (31) and (32). The Z axis is the direction of the normal in this coordinate system attached to the probe. In the accelerating potential region (see Eq. (26))

$$I = \frac{2\pi eA}{m^2}\int_{o}^{\infty} dU \left\{ f_o(U) - \frac{2}{3} f^*_{1Z}(U) + \frac{1}{4} f^*_{2ZZ}(U) \right\} U \tag{135}$$

A spherical probe with surface area A collects in a retarding potential (see Eq. (58))

$$I = \frac{2\pi eA}{m^2}\int_{V_p}^{\infty} dU (U - V_p) f_o(U) \tag{136}$$

and in an accelerating potential (see Eq. (65))

$$I = \frac{2\pi eA}{m^2}\left\{ \frac{r_s^2}{r_p^2}\int_{o}^{\beta V_p} dU\, U\, f_o(U) + \int_{\beta V_p}^{\infty} dU (U + V_p) f_o(U) \right\} \tag{137}$$

where r_s is the sheath radius, r_p is the probe radius, and $\beta = r_p^2/(r_s^2 - r_p^2)$. For a thin sheath, $r_s \approx r_p$, $\beta \gg 1$, and Eq. (137) reduces to

$$I = (2\pi eA/m^2)\int_{o}^{\infty} dU\, U\, f_o(U) \tag{138}$$

A cylindrical probe has contributions from f_o and $\underset{\approx}{f}_2$. In a retarding potential (see Eq. (101))

$$I = \frac{2\pi eA}{m^2} \int_{V_p}^{\infty} dU \left\{ (U - V_p) f_o(U) - \frac{1}{8} [U + 2V_p - 3V_p^2/U] f^*_{2XX}(U) \right\} \tag{139}$$

where X signifies the axis of the cylinder and A is its surface area. In an accelerating potential (see Eqs. (114) and (125))

$$I = \frac{2\pi eA}{m^2} \left\{ \frac{r_s}{r_p} \int_o^{\beta V_p} dU\, U f_o(U) + \frac{2}{\pi} \int_{\beta V_p}^{\infty} dU\, U f_o(U) \left\{ \frac{r_s}{r_p} \sin^{-1} \left[\left(\frac{\beta V_p}{U} \right)^{\frac{1}{2}} \right] \right.\right.$$

$$\left.\left. + \left(1 + \frac{V_p}{U} \right) \sin^{-1} \left[\left(\frac{U - \beta V_p}{U + V_p} \right)^{\frac{1}{2}} \right] \right\} - \frac{r_s}{8 r_p} \int_o^{\beta V_p} dU\, U f^*_{2XX}(U)$$

$$- \frac{1}{4\pi} \int_{\beta V_p}^{\infty} dU\, U f^*_{2XX}(U) \left\{ \frac{r_s}{r_p} \sin^{-1} \left[\left(\frac{\beta V_p}{U} \right)^{\frac{1}{2}} \right] \right.$$

$$\left. + \left(1 + \frac{V_p}{U} \right) \left(1 - \frac{3V_p}{U} \right) \sin^{-1} \left[\left(\frac{U - \beta V_p}{U + V_p} \right)^{\frac{1}{2}} \right] + 3 \left(\frac{V_p}{U} \right)^{3/2} \left(\frac{r_s^2}{r_s^2 - r_p^2} \right)^{\frac{1}{2}} \left[1 - \frac{r_p^2}{r_s^2 - r_p^2} \left(\frac{V_p}{U} \right) \right]^{\frac{1}{2}} \right\} \tag{140}$$

For a thin sheath, Eq. (140) reduces to

$$I = \frac{2\pi eA}{m^2} \int_o^{\infty} dU\, U \left\{ f_o(U) - \frac{1}{8} f^*_{2XX}(U) \right\} \tag{141}$$

A spherical grid system, with hole area A, collects in a retarding potential

$$I = \frac{4\pi eA}{m^2} \int_{V_p}^{\infty} dU [\kappa_o f_o(U) - \kappa_1 f^*_{1Z}(U) + \kappa_2 f^*_{2ZZ}(U)] U \tag{142}$$

where the κ_n's depend on the hole acceptance angle and are given in Eq. (131). In an accelerating potential (see Eq. (133))

$$I = \frac{4\pi eA}{m^2} \int_0^\infty dU[\kappa_o f_o(U) - \kappa_1 f^*_{1Z}(U) + \kappa_2 f^*_{2ZZ}(U)]U \tag{143}$$

By using several probes or different orientations in a retarding potential case, the I_o, I_1, and I_2 current contributions in $I = I_o - I_1 + I_2$ can be separated from each other. Then from I_o for the plane, sphere or cylinder, one can obtain f_o by Eq.(40), i.e.,

$$f_o(eV_p) = \frac{m^2}{2\pi eA} \frac{d^2 I_o(V_p)}{dV_p^2} \tag{144}$$

From I_1 for the plane, one derives f^*_{1Z} (see Eq. (41)):

$$f^*_{1Z}(eV_p) = \frac{m^2}{2\pi eA} V_p^{\frac{1}{2}} \frac{d}{dV_p}\left[\frac{1}{V_p^{\frac{1}{2}}} \frac{dI_1(V_p)}{dV_p}\right] \tag{145}$$

where Z is the direction perpendicular to the plane. From I_2 for the plane or cylinder one obtains (see Eq. (43))

$$cf^*_{2ii} = \frac{m^2}{2\pi eA}\left\{\frac{d^2 I_2}{dV_p^2} - \frac{3}{2V_p}\frac{dI_2}{dV_p} + \frac{3}{4V_p^2} I_2 - \frac{3}{8V_p^{3/2}} \int_{V_p}^\infty \frac{I_2(V)dV}{V^{3/2}}\right\} \tag{146}$$

where $c = 1$ for a plane and $c = -\frac{1}{2}$ for a cylinder. Also, i is the direction perpendicular to a plane surface or the axial direction for the case of a cylinder. For a spherical grid system with normal in the Z-direction, the first derivative gives directly a linear combination of the f's (see Eq. (132)), namely,

$$\kappa_o f_o(V_p) - \kappa_1 f^*_{1Z}(V_p) + \kappa_2 f^*_{2ZZ}(V_p) = -\frac{m^2}{4\pi eA}\frac{dI}{dV_p} \tag{147}$$

from which for different orientations one can sort out the various parts.

SECTION III

ADDITIONAL CORRECTION TERMS DUE TO THE EXTERNAL ELECTRIC FIELD

1. INTRODUCTION

In Section II, it was assumed that the electric field, E, in the plasma multiplied by the sheath dimension, λ_s, was negligible compared to the probe potential, V_p. In certain discharges, E may be of the order of kV/m, which means that for sheath thickness of the order of 1mm, $E\lambda_s$ becomes comparable to the probe potential. When this is the case, the previous expressions for the current collected by the probe should be corrected, since the effective potential between the sheath boundary and the probe can be substantially different than V_p and the correction terms can provide contributions to the current comparable to those due to higher order anisotropic parts of the distribution function. Here we give the new expressions for the current intercepted by a probe when the influence of the external electric field around the probe is taken into account.

In doing this, we assume, however, that $E\lambda_s$ is still small compared to V_p so that we can ignore angular variations of the sheath thickness due to E. This approximation allows us to avoid the treatment of non-symmetrical sheaths and the case where spherical or cylindrical probes have accelerating and retarding regions on opposite sides which make the calculations almost impossible. On the other hand, this approximation may force us to omit diagnostics pertaining to the lowest energy (U) domain of the distribution function, namely, $U < eE\lambda_s$. However, since λ_s also decreases with V_p, then, if $V_p >> eE\lambda_s$ for large V_p, this condition is usually obeyed, although possibly to a lesser extent, at lower V_p.

In the first subsection, the current density intercepted by a plane probe with the normal making an angle θ with respect to $\underset{\sim}{E}$ is expressed in terms of the spherical harmonics of the electron distribution function f_0, $\underset{\sim}{f}_1$, and $\underset{\approx}{f}_2$, including the above correction terms. Only the retarding case is considered since, for the accelerating case, the expressions for the current are the same as when E = 0. Expressions for the limiting case of $eE\lambda_s << V_p$ are also given.

Following the plane probe, the spherical and cylindrical probes are analyzed. We first derive the general case for an arbitrary ratio of sheath to probe radius, r_s/r_p, and express the results in the limit when $eE\lambda_s << V_p$ for both the retarding and accelerating regions. The cylindrical probe is assumed oriented along an axis perpendicular to the electric field $\underset{\sim}{E}$. When oriented along the electric field, we get the same results as when $E\lambda_s = 0$. For the perpendicular cylindrical probe, integration over θ cannot be performed analytically for arbitrary r_s/r_p, which implies in this case a double numerical integration to calculate the current.

Next, an approximate analysis of the sheath thickness λ_s is presented. This evaluation is required for the evaluation of $E\lambda_s$, which appears in the expressions of the currents. We assume that the electron contribution to λ_s is mainly determined by the isotropic part of the electron velocity distribution and by the probe potential. The ion drift is assumed monoenergetic and is related to the electron thermal energy by the Bohm sheath criterion. These approximations are justified if we consider $E\lambda_s$ as a correction term; otherwise the analysis becomes extremely complex. The effects of negative ions on λ_s, on the Bohm criterion, and on the ion saturation current are also presented.

Finally, we treat the inverse problem of deriving the electron energy distribution from the current with the additional correction terms. We find that we can deduce f_o, f_{1z}, and f_{2zz} from the currents intercepted by a plane probe oriented along five independent directions. Results are given when the orientations $\theta = 0$, $\pi/4$, $\pi/2$, $3\pi/4$, and π are chosen. The utilization of different probe geometries under circumstances when $E\lambda_s$ is non-negligible (as proposed in Section II) is not practical because we can hardly separate the different orders of anisotropy if we include the correction terms. Thus, to determine the anisotropic terms of the electron distribution function, a plane probe is most sensitive. A design of a plane probe is given in Appendix B.

As in Section II, we assume here again a collisionless sheath in a low pressure plasma. Most of the fall in the potential that is applied to the probe is assumed to occur in this region, and the electric field outside of this region is associated only with the external electric field. This is valid if the mean free path is much greater than the sheath width and greater than the probe radius. At higher pressures, there exists a quasi-collisional sheath outside of the collisionless sheath. In Sections IV and V, the combined sheaths will be discussed.

2. THE PLANE PROBE WITH CORRECTION TERMS

Let the external electric field $\underset{\sim}{E}$ be oriented along the z-axis in the anode to cathode direction, and let θ be the angle between the normal to the one-sided plane probe measured with respect to the z-axis. The magnitude of the effective potential between the sheath boundary and the probe when it is retarding particles can be written as $V_p - V_a^*$, where V_p is the

magnitude of the probe potential with respect to the potential at the sheath edge (when the probe is oriented parallel to E with $\theta = \pm \pi/2$). Letting λ_s designate the sheath thickness, we note that $V_a^* = |eE\lambda_s| \cos\theta = V_a \cos\theta$ is the magnitude of the potential drop of the external electric field across the sheath and e is the magnitude of the electron charge. (Remember that we assume $V_p > V_a^*$ throughout the calculations here.) Presently, we will include the effects of V_a^* which were neglected in our previous analyses. However, we neglect the small potential bump ΔV with respect to potential at the sheath boundary which appears in the sheath at the point where $\underset{\sim}{E} + \underset{\sim}{E}_p = 0$ when $\underset{\sim}{E}_p \cdot \underset{\sim}{E} < 0$ (where $\underset{\sim}{E}_p$ is the electric field due to the probe). For $V_p > V_a^*$, $\Delta V << V_a^*$ and neglecting it does not affect the results too much.

For the accelerating region, the current density intercepted by the probe is independent of the effective potential, so that we get the same expression as for $\underset{\sim}{E} = 0$. That is,

$$j_{\theta\phi} = K_o \int_o^\infty U \left[f_o(U) - \frac{2}{3} f_{1Z}^*(U) + \frac{1}{4} f_{2ZZ}^*(U) \right] dU \qquad (148)$$

for the probe oriented along the (θ,ϕ)-direction (see Eq. (26)) with $K_o = 2\pi e/m^2$ and $f_{1Z}^*(U)$ and $f_{2ZZ}^*(U)$ given by Eqs. (31) and (32).

For the retarding region, we obtain the following for the current density intercepted by a probe oriented along the (θ,ϕ)-direction:

$$j_{\theta\phi} = j_{0\theta\phi} - j_{1\theta\phi} + j_{2\theta\phi} \qquad (149)$$

with

$$j_{0\theta\phi} = K_o \int_{V_p - V_a^*}^\infty [U - (V_p - V_a^*)] f_o(U) dU \qquad (150)$$

$$j_{1\theta\phi} = \frac{2}{3} K_o \int_{V_p - V_a^*}^{\infty} U \left[1 - \left(\frac{V_p - V_a^*}{U} \right)^{3/2} \right] f_{1Z}^*(U) dU \qquad (151)$$

$$j_{2\theta\phi} = \frac{1}{4} K_o \int_{V_p - V_a^*}^{\infty} [U + 2(V_p - V_a^*) - 3(V_p - V_a^*)^2/U] \, f_{2ZZ}^*(U) dU \qquad (152)$$

which are the same equations as Eqs. (11) to (13) after replacing V_p by the effective potential $V_p - V_a^*$.

When $V_a^* \ll V_p$, we obtain after neglecting terms of order higher than $(V_a^*)^2$ the approximate relations:

$$j_{0\theta\phi} \approx K_o \int_{V_p}^{\infty} (U - V_p) f_o(U) dU + K_o V_a^* \int_{V_p}^{\infty} f_o(U) dU + \tfrac{1}{2} K_o (V_a^*)^2 f_o(V_p) \qquad (153)$$

$$j_{1\theta\phi} \approx \frac{2}{3} K_o \int_{V_p}^{\infty} U \left[1 - \left(\frac{V_p}{U} \right)^{3/2} \right] f_{1Z}^*(U) dU + K_o V_a^* \int_{V_p}^{\infty} \left(\frac{V_p}{U} \right)^{\frac{1}{2}} f_{1Z}^*(U) dU$$

$$- \frac{1}{4} K_o (V_a^*)^2 \int_{V_p}^{\infty} \frac{f_{1Z}^*(U) dU}{(V_p U)^{\frac{1}{2}}} + \frac{1}{2} K_o (V_a^*)^2 f_{1Z}^*(V_p) \qquad (154)$$

$$j_{2\theta\phi} \approx \frac{1}{4} K_o \int_{V_p}^{\infty} [U + 2V_p - 3V_p^2/U] f_{2ZZ}^*(U) dU + \frac{1}{2} K_o V_a^* \int_{V_p}^{\infty} \left(\frac{3V_p}{U} - 1 \right) f_{2ZZ}^*(U) dU$$

$$- \frac{3}{4} K_o (V_a^*)^2 \int_{V_p}^{\infty} f_{2ZZ}^*(U) U^{-1} dU + \frac{1}{2} K_o (V_a^*)^2 f_{2ZZ}^*(V_p) \qquad (155)$$

These results are obtained by first considering separately the integrals

from V_p to ∞ and from $V_p - V_a^*$ to V_p. In the latter, we approximate $f(U) \approx f(V_p)$, then take it outside of the integral and perform the remaining integration over U to yield the above indicated terms. The approximation on f also requires the assumption that higher order Taylor expansion terms are negligible, viz., $|V_a(\partial \ln f/\partial V_p)| \ll 1$. All terms except the first in Eqs. (153) to (155) are the corrections due to external electric field $\underset{\sim}{E}$. The first terms for $j_{0\phi}$ and $j_{1\theta\phi}$ in Eqs. (153) and (154) have already been obtained recently by Lukovnikov[7], using a less general approach. The third term of Eq. (153) is comparable to the first term of Eq. (155) when $|f_0/f_2| \sim (V_p/V_a)^2$, so that, if one is interested in including the f_2 contribution, the effect due to V_a should be included as well.

3. THE SPHERICAL PROBE WITH CORRECTION TERMS

For the spherical probe, the magnitude of the effective probe potential is $V_p \mp V_a^*$ where the $\mp$ sign is used, depending, respectively, on whether the probe is retarding or accelerating. Here V_a^* has to be redefined in terms of the potential variation around a conducting sphere in an external electric field. This is well known to be

$$V_a^* = eE(r_s - r_p^3/r_s^2)\cos\theta = V_a \cos\theta \tag{156}$$

where r_s is distance from the center, in particular the sheath position, and r_p is the probe radius. If λ_s is the sheath thickness and $r_s = r_p + \lambda_s \approx r_p$, then

$$V_a^* \approx 3\lambda_s eE \cos\theta = V_a \cos\theta \tag{157}$$

where we redefine $V_a = eE(r_s - r_p^3/r_s^2) \approx 3\lambda_s eE$ for a sphere. We assume that the sheath is spherically concentric with the probe, i.e., λ_s is not a function of θ.

a. Retarding Region

For the retarding case, the total current intercepted by a sphere is

$$I = \int j_{\theta\phi} dA = \int_{\theta=o}^{\pi} \int_{\phi=o}^{2\pi} j_{\theta\phi} r_p^2 \sin\theta \, d\theta \, d\phi \tag{158}$$

where

$$j_{\theta\phi} = j_{0\theta\phi} - j_{1\theta\phi} + j_{2\theta\phi} = (\delta I_0 - \delta I_1 + \delta I_2)/r_p^2 = \delta I/r_p^2 \tag{159}$$

is the current density on the element area located at (r_p, θ, ϕ) and δI is the current through a spherical element at (r_s, θ, ϕ). It has been shown in Eq. (52) that

$$\frac{\delta I}{e r_s^2} = 2\pi \int_{-\infty}^{-v_o} v_Z dv_Z \int_o^{q_1} q \, dq \sum_{l=0}^{2} f_{loo}^* P_l(\cos\theta) \tag{160}$$

where θ is the angle of the electron velocity $\underset{\sim}{v}$ with respect to the normal to the spherical element at (r_s, θ, ϕ) and where $v_Z = v\cos\theta$, $q = v\sin\theta$, $v_o = (2V_p/m)^{\frac{1}{2}}$, and q_1 given in Eq. (50). Summation in Eq. (160) has been truncated at $l = 2$ since it is assumed that higher order terms are negligible. After changing variables $[v = (v_Z^2 + q^2)^{\frac{1}{2}}$ and $\theta = \tan^{-1} q/v_Z]$ and integrating over θ using Eq. (16) and Figure 3, we obtain

$$\frac{\delta I}{e r_s^2} = 2\pi \sum_{l=0}^{2} \frac{(-1)^l}{2l+1} \int_{v_o}^{\infty} dv \, v^3 f_{loo}^* \left\{ \frac{l+1}{2l+3} [P_l - P_{l+2}] + \frac{l}{2l-1} [P_{l-2} - P_l] \right\} \tag{161}$$

where the argument of the Legendre polynomials is

$$\cos\theta_o = \left[1 - \frac{r_p^2}{r_s^2} \left(1 - \frac{v_o^2}{v^2} \right) \right]^{\frac{1}{2}} \tag{162}$$

and $P_l(-\cos\theta_o) = (-1)^l P_l(\cos\theta_o)$. For an effective potential $V_p - V_a^*$, we note that

$$v_o = [2(V_p - V_a^*)/m]^{\frac{1}{2}} \tag{163}$$

Letting $l = 0$, 1, and 2, we find that $j_{0\theta\phi}$, $j_{1\theta\phi}$, $j_{2\theta\phi}$ can be written from Eq. (161) as

$$j_{0\theta\phi} = K_o \int_{V_p - V_a^*}^{\infty} (U - V_p + V_a^*) f_o(U) dU \tag{164}$$

$$j_{1\theta\phi} = \frac{2}{3} K_o \frac{r_s^2}{r_p^2} \int_{V_p - V_a^*}^{\infty} U \left\{ 1 - \left[1 - \frac{r_p^2}{r_s^2} + \frac{r_p^2}{r_s^2} \left(\frac{V_p - V_a^*}{U} \right) \right]^{3/2} \right\} f_{1Z}^*(U) dU \tag{165}$$

and

$$j_{2\theta\phi} = K_o \int_{V_p - V_a^*}^{\infty} U \left(1 - \frac{V_p - V_a^*}{U} \right) \left[1 - \frac{3}{4} \frac{r_p^2}{r_s^2} \left(1 - \frac{V_p - V_a^*}{U} \right) \right] f_{2ZZ}^*(U) dU \tag{166}$$

where $U = \frac{1}{2}mv^2$ has replaced v and where $K_o = 2\pi e/m^2$. From Eqs. (164) to (166), we can now evaluate the integrals in Eq. (158). The first integral can be written as

$$\int j_{0\theta\phi} dA = 2\pi r_p^2 K_o \int_{\theta=o}^{\pi} \int_{V_p - V_a \cos\theta}^{\infty} (U - V_p + V_a \cos\theta) f_o(U) \sin\theta \, d\theta dU$$

$$= 2\pi r_p^2 K_o \left[\int_{V_p}^{\infty} \int_{o}^{\pi} + \int_{V_p - V_a}^{V_p} \int_{o}^{\theta_2} - \int_{V_p}^{V_p + V_a} \int_{\theta_2}^{\pi} \right] (U - V_p + V_a \cos\theta) f_o(U) dU \sin\theta \, d\theta$$

where

$$\cos\theta_2 = (V_p - U)/V_a, \quad 0 \le \theta_2 \le \pi \tag{167}$$

The double integrals can be reduced to a single one by first integrating over θ. The subdivision of the areas of integration is illustrated in

Figure 10. Integration over θ yields

$$\int j_{0\theta\phi}\,dA = 4\pi r_p^2 K_o \int_{V_p}^{\infty} (U - V_p) f_o(U)\,dU + \frac{\pi r_p^2 K_o}{V_a}\left[\int_{V_p - V_a}^{V_p} (U - V_p + V_a)^2 f_o(U)\,dU + \int_{V_p}^{V_p + V_a} (U - V_p - V_a)^2 f_o(U)\,dU\right] \tag{168}$$

In addition, from Eq. (31), integration over ϕ leaves only the f_{1z} part of f_{1Z}^*, and we have

$$\int j_{1\theta\phi}\,dA = \frac{4}{3}\pi r_s^2 K_o \int_{\theta=0}^{\pi}\int_{V_p - V_a\cos\theta}^{\infty} [U^{3/2} - (a_1 - b_1\cos\theta)^{3/2}] f_{1z}(U)\cos\theta\sin\theta U^{-\frac{1}{2}}\,dU\,d\theta \tag{169}$$

with

$$a_1(U) = \left(1 - \frac{r_p^2}{r_s^2}\right) U + \frac{r_p^2}{r_s^2} V_p \tag{170}$$

$$b_1 = \frac{r_p^2}{r_s^2} V_a = \frac{r_p^2}{r_s^2}\left(r_s - \frac{r_p^2}{r_s^2}\right) eE \tag{171}$$

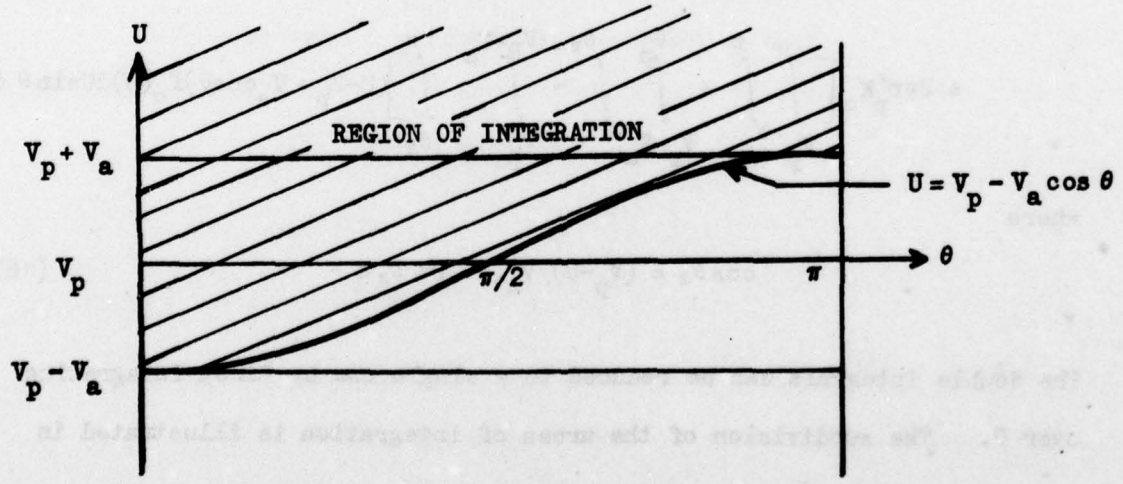

Figure 10. Double Integration over θ and U for a Spherical Probe

(For $r_p \approx r_s$, $a_1 \approx V_p$ and $b_1 \approx V_a$.) Subdividing the areas similar to that shown in Figure 10 and integrating over θ yield

$$\int j_{1\theta\phi}\,dA = \frac{8}{15}\pi r_s^2 K_o \int_{V_p}^{\infty} \left\{ \frac{1}{b_1 U^{\frac{1}{2}}} \left[(a_1 - b_1)^{5/2} + (a_1 + b_1)^{5/2} \right] + \frac{2}{7 b_1^2 U^{\frac{1}{2}}} \left[(a_1 - b_1)^{7/2} - (a_1 + b_1)^{7/2} \right] \right\} \cdot f_{1z}(U)\,dU$$

$$+ \frac{2}{3}\pi r_s^2 K_o \int_{V_p - V_a}^{V_p + V_a} U \left[\frac{V_a^2 - (U - V_p)^2}{V_a^2} \right] f_{1z}(U)\,dU$$

$$+ \frac{8}{15}\pi r_s^2 K_o \int_{V_p - V_a}^{V_p} \left\{ \frac{1}{b_1 U^{\frac{1}{2}}} \left[(a_1 - b_1)^{5/2} + \frac{(U - V_p)}{V_a} U^{5/2} \right] + \frac{2}{7 b_1^2 U^{\frac{1}{2}}} \left[(a_1 - b_1)^{7/2} - U^{7/2} \right] \right\} f_{1z}(U)\,dU$$

$$- \frac{8}{15}\pi r_s^2 K_o \int_{V_p}^{V_p + V_a} \left\{ \frac{1}{b_1 U^{\frac{1}{2}}} \left[(a_1 + b_1)^{5/2} - \frac{(U - V_p)}{V_a} U^{5/2} \right] + \frac{2}{7 b_1^2 U^{\frac{1}{2}}} \left[U^{7/2} - (a_1 + b_1)^{7/2} \right] \right\} f_{1z}(U)\,dU \tag{172}$$

Also, from Eq. (32), integration over ϕ leaves only the f_{2ii} components of f^*_{2ZZ}. We associate $\underset{\sim}{f}_2$ with the external $\underset{\sim}{E}$, which has ϕ symmetry in the uniform region of the plasma. Also, since $\underset{\sim}{f}_2$ is traceless, we can write

$$f_{2xx} = f_{2yy} = -\tfrac{1}{2} f_{2zz} \tag{173}$$

and obtain

$$\int j_{2\theta\phi}\,dA = 2\pi r_p^2 K_o \int_{\theta=0}^{\pi} \int_{V_p - V_a \cos\theta}^{\infty} (a_2 + b_2 \cos\theta + c_2 \cos^2\theta)(\cos^2\theta - \tfrac{1}{2}\sin^2\theta)\sin\theta f_{2zz}(U)\,dU\,d\theta \tag{174}$$

with

$$a_2(U) = (U - V_p)\left[1 - \frac{3}{4}\frac{r_p^2}{r_s^2}\left(1 - \frac{V_p}{U} \right) \right] \tag{175}$$

$$b_2(U) = V_a\left[1 - \frac{3}{2}\frac{r_p^2}{r_s^2}\left(1 - \frac{V_p}{U}\right)\right] \tag{176}$$

$$c_2(U) = -\frac{3}{4}\frac{r_p^2}{r_s^2}\frac{V_a^2}{U} \tag{177}$$

Integration over θ as before yields

$$\int j_{2\theta\phi}dA = \frac{8}{15}\pi r_p^2 K_o \int_{V_p}^{\infty} c_2 f_{2zz}(U)dU$$

$$+ \pi r_p^2 K_o \int_{V_p-V_a}^{V_p+V_a} [a_2\cos\theta_2\sin^2\theta_2 + \tfrac{1}{2}\, b_2(1 - \cos^4\theta_2 - \tfrac{1}{2}\sin^4\theta_2)$$
$$+ c_2(\tfrac{1}{3}\cos^3\theta_2 - \tfrac{3}{5}\cos^5\theta_2)]f_{2zz}(U)dU$$

$$+ \frac{4}{15}\pi r_p^2 K_o\left[\int_{V_p-V_a}^{V_p} c_2 f_{2zz}(U)dU - \int_{V_p}^{V_p+V_a} c_2 f_{2zz}(U)dU\right] \tag{178}$$

where θ_2 is given by Eq. (167). Summation of Eqs. (168), (172) and (178) gives the current I intercepted by the spherical probe. These expressions are greatly simplified when $V_a << V_p$. In this case it is simpler to expand directly Eqs. (164) to (166). Neglecting terms of order higher than V_a^2, we get

$$\int j_{0\theta\phi}dA \approx 4\pi r_p^2 K_o \int_{V_p}^{\infty} (U - V_p)f_o(U)dU + \frac{2}{3}\pi r_p^2 K_o V_a^2 f_o(V_p) \tag{179}$$

$$\int j_{1\theta\phi}dA \approx \frac{4}{3}\pi r_p^2 K_o V_a \int_{V_p}^{\infty}\left(1 - \frac{r_p^2}{r_s^2} + \frac{r_p^2}{r_s^2}\frac{V_p}{U}\right)^{\frac{1}{2}} f_{1z}(U)dU \tag{180}$$

$$\int j_{2\theta\phi}\,dA \approx -\frac{2}{5}\,\pi\,\frac{r_p^4}{r_s^2}\,K_o\int_{V_p}^{\infty}\frac{V_a^2}{U}\,f_{2zz}(U)\,dU + \frac{4\pi}{15}\,r_p^2 K_o V_a^2 f_{2zz}(V_p) \qquad (181)$$

These same results in the limit of $r_s \approx r_p$ can also be obtained directly from Eqs. (153) to (155) after integration over a spherical area. When $r_s \gg r_p$, V_a may be an important correction to V_p, and one may have to use the more nearly exact Eqs. (168), (172), and (178) instead of Eqs. (179) to (181).

b. Accelerating Region

In the accelerating region, we write again Eqs. (158) and (159), but here Eqs. (62) and (64) have to be generalized to include the $l = 1$ and $l = 2$ terms. Using Eqs. (16), (21), and (61), we obtain

$$\frac{\delta I}{r_p^2} = \tfrac{1}{2}\pi^{3/2}\,e\,\frac{r_s^2}{r_p^2}\,\frac{1}{\Gamma\left(\frac{l+4}{2}\right)\Gamma\left(\frac{3-l}{2}\right)}\int_0^{\sqrt{\beta}v_o} dv\,v^3\,f^*_{loo}(v)$$

$$+\,\frac{2\pi e r_s^2}{r_p^2}\int_{\sqrt{\beta}v_o}^{\infty} dv\,v^3\,f^*_{loo}(v)\,\frac{1}{2l+1}\left\{\frac{l+1}{2l+3}\,(P_l - P_{l+2}) + \frac{l}{2l-1}\,(P_{l-2} - P_l)\right\} \qquad (182)$$

The argument of the Legendre polynomial P_l is

$$\cos\theta_o = \left[1 - \frac{r_p^2}{r_s^2}\,(1 + v_o^2/v^2)\right]^{\frac{1}{2}} \qquad (183)$$

Also,

$$v_o = [2(V_p + V_a^*)/m]^{\frac{1}{2}} \quad \text{and} \quad \beta = r_p^2/(r_s^2 - r_p^2) \qquad (184)$$

(Note that $\cos\theta_o$ and v_o are the same as in Eqs. (162) and (163) except for a plus sign.) For $l = 0$, 1, and 2, we obtain, respectively,

$$j_{0\theta\phi} = \frac{r_s^2}{r_p^2}\,K_o\int_o^{\beta(V_p+V_a^*)} U f_o(U)\,dU + K_o\int_{\beta(V_p+V_a^*)}^{\infty}(U+V_p+V_a^*)\,f_o(U)\,dU \qquad (185)$$

$$j_{1\theta\phi} = \frac{2}{3}\frac{r_s^2}{r_p^2} K_o \int_o^{\beta(V_p+V_a^*)} U f_{1Z}^*(U)dU + \frac{2}{3}\frac{r_s^2}{r_p^2} K_o \int_{\beta(V_p+V_a^*)}^{\infty} U\left\{1-\left[1-\frac{r_p^2}{r_s^2}\left(1+\frac{V_p+V_a^*}{U}\right)\right]^{3/2}\right\} f_{1Z}^*(U)dU \quad (186)$$

and

$$j_{2\theta\phi} = \frac{1}{4}\frac{r_s^2}{r_p^2} K_o \int_o^{\beta(V_p+V_a^*)} U f_{2ZZ}^*(U)dU + K_o \int_{\beta(V_p+V_a^*)}^{\infty} U\left(1+\frac{V_p+V_a^*}{U}\right)\left[1-\frac{3}{4}\frac{r_p^2}{r_s^2}\left(1+\frac{V_p+V_a^*}{U}\right)\right] f_{2ZZ}^*(U)dU \quad (187)$$

Integration of Eqs. (185) to (187) over the area yields

$$\int j_{0\theta\phi} dA = 4\pi K_o \left\{ r_s^2 \int_o^{\beta V_p} U f_o(U)dU + r_p^2 \int_{\beta V_p}^{\infty} (U+V_p) f_o(U)dU \right\}$$

$$-\pi K_o V_a r_p^2 \left\{ \int_{\beta(V_p-V_a)}^{\beta V_p} \left[\frac{U-\beta(V_p-V_a)}{\beta V_a}\right]^2 f_o(U)dU + \int_{\beta V_p}^{\beta(V_p+V_a)} \left[\frac{U-\beta(V_p+V_a)}{\beta V_a}\right]^2 f_o(U)dU \right\} \quad (188)$$

$$\int j_{1\theta\phi} dA = \frac{8\pi r_s^2}{15} K_o \left\{ \int_{\beta V_p}^{\infty} \left(\frac{1}{b_1 U^{1/2}} \left[(a_1-b_1)^{5/2} + (a_1+b_1)^{5/2} \right] + \frac{2}{7 b_1^2 U^{1/2}} \left[(a_1-b_1)^{7/2} - (a_1+b_1)^{7/2} \right] \right) f_{1z}(U)dU \right.$$

$$+ \int_{\beta(V_p-V_a)}^{\beta V_p} \left[\frac{1}{b_1 U^{1/2}} (a_1+b_1)^{5/2} - \frac{2}{7 b_1^2 U^{1/2}} (a_1+b_1)^{7/2} \right] f_{1z}(U)dU$$

$$\left. - \int_{\beta V_p}^{\beta(V_p+V_a)} \left[\frac{1}{b_1 U^{1/2}} (a_1-b_1)^{5/2} + \frac{2}{7 b_1^2 U^{1/2}} (a_1-b_1)^{7/2} \right] f_{1z}(U)dU \right\} \quad (189)$$

with

$$a_1(U) = \left(1-\frac{r_p^2}{r_s^2}\right) U - \frac{r_p^2}{r_s^2} V_p \quad (190)$$

and $$b_4 = (r_p^2/r_s^2)V_a \tag{191}$$

(Note that Eq. (190) for a_4 differs from Eq. (170).) Finally,

$$\int j_{2\theta\phi}\,dA = \frac{8}{15}\pi r_p^2 K_o \int_{\beta V_p}^{\infty} c_2 f_{2zz}(U)\,dU$$

$$+ \pi r_p^2 K_o \int_{\beta(V_p-V_a)}^{\beta(V_p+V_a)} \left[\left(a_2 - \frac{1}{4}\frac{r_s^2}{r_p^2}U\right)\cos\theta_3 \sin^2\theta_3 - \tfrac{1}{2}b_2(1-\cos^4\theta_3 - \tfrac{1}{2}\sin^4\theta_3) + c_2\left(\frac{1}{3}\cos^3\theta_3 - \frac{3}{5}\cos^5\theta_3\right)\right] f_{2zz}(U)\,dU$$

$$+ \frac{4\pi}{15} r_p^2 K_o \left[\int_{\beta(V_p-V_a)}^{\beta V_p} c_2 f_{2zz}(U)\,dU - \int_{\beta V_p}^{\beta(V_p+V_a)} c_2 f_{2zz}(U)\,dU\right] \tag{192}$$

with $$a_2(U) = (U+V_p)\left[1 - \frac{3}{4}\frac{r_p^2}{r_s^2}\left(1 + \frac{V_p}{U}\right)\right] \tag{193}$$

$$b_2(U) = V_a\left[1 - \frac{3}{2}\frac{r_p^2}{r_s^2}\left(1 + \frac{V_p}{U}\right)\right] \tag{194}$$

$$c_2(U) = -\frac{3}{4}\frac{r_p^2}{r_s^2}\frac{V_a^2}{U} \tag{195}$$

and $$\cos\theta_3 = (\beta V_p - U)/\beta V_a \quad , \quad 0 \leq \theta_3 < \pi \tag{196}$$

In the limit of $V_a \to 0$, these results reduce to those in Eqs. (65) to (67).

4. THE CYLINDRICAL PROBE WITH CORRECTION TERMS

For a cylindrical probe oriented along the z-axis, we get the same results as for $E = 0$ since the external electric field does not modify the potential around the probe, provided that the radius of the probe is small

compared to its length. If the cylinder is oriented along any direction other than z, the external electric field introduces a θ-variation in the effective probe potential $V_p \mp V_a^*$ which affects the current intercepted by the probe in the retarding or accelerating regions. We will treat here only the case where the cylinder is oriented perpendicularly to the z-axis (say along the x-axis). The general case of arbitrary orientation is more complicated and does not illustrate any new phenomenon. The magnitude of the potential variation around a conducting cylinder whose axis is perpendicular to an external electric field is

$$V_a^* = eE(1 - r_p^2/r_s^2)r_s \cos\theta \equiv V_a \cos\theta \tag{197}$$

or, if $r_s = r_p + \lambda_s \approx r_p$,

$$V_a^* \approx 2\lambda_s eE \cos\theta \tag{198}$$

Here r_p is the cylindrical radius, r_s is radial distance, here associated with the sheath position, and λ_s is the sheath thickness. We again assume that the sheath is cylindrically concentric with the probe. Note that V_a^* differs from the spherical case in Eq. (157) and from the plane case.

a. Retarding Region

The total current intercepted by the probe is

$$I = r_p L \int_{\theta=0}^{2\pi} j_{\theta\phi} d\theta = r_p L \sum_{l=0}^{2} (-1)^l \int_{\theta=0}^{2\pi} j_{l\theta\phi} d\theta \tag{199}$$

where L is the length of the probe and r_p is its radius. It has been shown in Eqs. (75), (77), (79), (80) that the current density $j_{l\theta\phi}$ can be written as

$$(-1)^l j_{l\theta\phi} = \frac{1}{r_p L}(\delta I_{la} + \delta I_{lb} + \delta I_{lc}) = \frac{1}{r_p L}\delta I_l \tag{200}$$

where

$$\delta I_{1a} = 2\pi e r_s L \int_{v_o}^{\infty} dv\, v^3 f^*_{1oo}(v) \int_{\cos\theta_o}^{1} dx\, x\, (-1)^1 P_1(x) \tag{201}$$

Here θ_o is the same as that given in Eq. (162) with θ's being the angle between the electron velocity $\underset{\sim}{v}$ and the normal to the cylindrical element at (r_s,θ) and $x = -\cos\theta$. Also,

$$\delta I_{1b} = e r_s L \int_{v_o}^{\infty} dv\, v^3 \, f^*_{1oo}(v) \int_{\cos\theta_1}^{\cos\theta_o} dx\, x\, (-1)^1 P_1(x) 4\Phi_o \tag{202}$$

and

$$\delta I_{1c} = e r_s L \int_{v_o}^{\infty} dv\, v^3 \sum_{m\geq 1} f^*_{1mo}(v) \int_{\cos\theta_1}^{\cos\theta_o} dx\, x\, P_1^m(-x)\, \frac{2}{m} \sin m\Phi_o [1+(-1)^m] \tag{203}$$

with

$$\cos\theta_1 = v_o/v \tag{204}$$

$$\beta = r_p^2/(r_s^2 - r_p^2) \tag{205}$$

and

$$\sin^2\Phi_o = \frac{\beta(v^2x^2 - v_o^2)}{v^2(1-x^2)} \tag{206}$$

The expressions of $j_{1\theta\phi}$ for $l = 0$ and 2 were given in Eqs. (87) and (97). For strong external electric fields, one must substitute for v_o the value of $[2(V_p - V_a^*)/m]^{\frac{1}{2}}$ in these equations to obtain

$$j_{0\theta\phi} = K_o \int_{V_p - V_a^*}^{\infty} (U - V_p + V_a^*) f_o(U)\, dU \tag{207}$$

$$j_{2\theta\phi} = K_o \int_{V_p - V_a^*}^{\infty} U \left(1 - \frac{V_p - V_a^*}{U}\right) \left\{ \left[1 - \frac{3}{8}\left(1 - \frac{V_p - V_a^*}{U}\right)\left(1 + \frac{r_p^2}{r_s^2}\right)\right] f^*_{2ZZ}(U) \right.$$

$$\left. + \frac{1}{8}\left(1 - \frac{V_p - V_a^*}{U}\right)\left(1 - \frac{r_p^2}{r_s^2}\right) [f^*_{2XX}(U) - f^*_{2YY}(U)] \right\} dU \tag{208}$$

where $K_o \equiv 2\pi e/m^2$. Since here $\phi = 0$, we note from Eq. (30) that $f^*_{2XX} = f_{2xx}$, $f^*_{2ZZ} = f_{2yy}\sin^2\theta + f_{2zz}\cos^2\theta - 2f_{2yz}\sin\theta\cos\theta$, and $f^*_{2YY} = f_{2yy}\cos^2\theta + f_{2zz}\sin^2\theta + 2f_{2yz}\sin\theta\cos\theta$. For our situation with $f_{2xx} = f_{2yy} = -\frac{1}{2} f_{2zz}$ and $f_{2yz} = 0$, we have

$$(f^*_{2XX} - f^*_{2YY}) = -\frac{3}{2}\sin^2\theta\, f_{2zz} \quad \text{and} \quad f^*_{2ZZ} = \tfrac{1}{2}(3\cos^2\theta - 1) f_{2zz} \tag{209}$$

For $l = 1$, we obtain from Eqs. (200) to (203)

$$-\delta I_1 = \frac{2\pi r_s Le}{3}\int_{v_o}^{\infty} dv\, v^3 f^*_{1Z}(v)\left[1 - \left(1 - \frac{r_p^2}{r_s^2} + \frac{r_p^2}{r_s^2}\frac{v_o^2}{v^2}\right)^{3/2}\right]$$

$$+ 4 r_s Le\beta \int_{v_o}^{\infty} dv\, v^3 f^*_{1Z}(v)\left(1 - \frac{v_o^2}{v^2}\right)\int_0^1 dy\, \frac{y\sin^{-1}y}{\left(y^2 + \dfrac{r_p^2}{r_s^2 - r_p^2}\right)^{3/2}}\left[y^2 + \frac{r_p^2}{r_s^2 - r_p^2}\,\frac{v_o^2}{v^2}\right]^{\frac{1}{2}} \tag{210}$$

where $y^2 = \beta(v^2\cos^2\theta - v_o^2)/(v^2\sin^2\theta)$. After integrating by parts the second integral of Eq. (210) and regrouping, we get

$$-\delta I_1 = \frac{2\pi r_s Le}{3}\int_{v_o}^{\infty} dv\, v^3 f^*_{1Z}(v) - \frac{4}{3} r_s Le \int_{v_o}^{\infty} dv\, v^3 f^*_{1Z}(v) \int_0^1 \left(\frac{y^2+\gamma}{y^2+\beta}\right)^{3/2} \frac{dy}{\sqrt{1-y^2}} \tag{211}$$

where

$$\gamma = \beta v_o^2/v^2 = \beta(V_p - V_a^*)/U \qquad (\beta > \gamma) \tag{212}$$

Also from Byrd and Friedman[8]

$$\int_0^1 \left(\frac{y^2+\gamma}{y^2+\beta}\right)^{3/2} \frac{dy}{\sqrt{1-y^2}} = \frac{\gamma}{2}\int_0^1 \frac{dt}{(t+\beta)}\left[\frac{t+\gamma}{(t+\beta)t(1-t)}\right]^{\frac{1}{2}} + \frac{1}{2}\int_0^1 \frac{dt}{(t+\beta)}\left[\frac{t(t+\gamma)}{(t+\beta)(1-t)}\right]^{-\frac{1}{2}}$$

$$= \frac{(\gamma+1)^{\frac{1}{2}}(\gamma-\beta)}{\beta^{\frac{1}{2}}(\beta+1)} G(k_o) + \frac{\gamma}{[\beta(\gamma+1)]^{\frac{1}{2}}} \Pi(\alpha_o^2, k_o) \tag{213}$$

with

$$t = y^2, \quad \alpha_o = (\gamma+1)^{-\frac{1}{2}} \quad \text{and} \quad k_o = \left[\frac{\beta-\gamma}{(\gamma+1)\beta}\right]^{\frac{1}{2}} \tag{214}$$

and where $G(k_o)$ and $\Pi(\alpha_o^2, k_o)$ are the complete elliptic integrals of second and third kind, respectively. (We use $G(k)$ here instead of the standard notation $E(k)$ in order not to be confused with the symbol for the electric field, E.) We can then express $j_{1\theta\phi}$ as

$$j_{1\theta\phi} = \frac{2}{3}\frac{r_s}{r_p} K_o \int_{V_p-V_a^*}^{\infty} U\left\{1 - \frac{2}{\pi}\left[\frac{(\gamma+1)^{\frac{1}{2}}(\gamma-\beta)}{\beta^{\frac{1}{2}}(\beta+1)} G(k_o) + \frac{\gamma}{[\beta(\gamma+1)]^{\frac{1}{2}}} \Pi(\alpha_o^2, k_o)\right]\right\} f_{1Z}^*(U)dU \tag{215}$$

where γ in Eq. (212) is a function of θ. Integration of Eq.(199) over θ with $j_{0\theta\phi}$, $j_{1\theta\phi}$ and $j_{2\theta\phi}$ given by Eqs. (207), (215), and (208), must now be performed. This must be done numerically for $j_{1\theta\phi}$.

For $r_s \approx r_p$, however, these relations reduce, respectively, to Eqs. (150) to (152). Integration over θ can be performed analytically after inverting the order of integration by using a figure similar to Figure 10, except that now θ varies up to 2π. Defining θ_2 as in Eq. (167), we obtain

$$\int_o^{2\pi} j_{0\theta\phi} d\theta = 2\pi K_o \int_{V_p}^{\infty} (U-V_p) f_o(U)dU + 2K_o \int_{V_p-V_a}^{V_p+V_a} V_a\left[1 - \left(\frac{U-V_p}{V_a}\right)^2\right]^{\frac{1}{2}} f_o(U)dU$$

$$+ 2K_o \int_{V_p-V_a}^{V_p} (U-V_p)\theta_2 f_o(U)dU - 2K_o \int_{V_p}^{V_p+V_a} (U-V_p)(\pi-\theta_2) f_o(U)dU \tag{216}$$

Also,

$$\int_0^{2\pi} j_{1\theta\phi}\,d\theta = -\frac{8}{15}K_o\int_{V_p}^{\infty}\left(\frac{V_p+V_a}{U}\right)^{\frac{1}{2}}\left\{V_p\left(\frac{V_p}{V_a}-1\right)K(k_1)-V_a\left[3+\left(\frac{V_p}{V_a}\right)^2\right]G(k_1)\right\}f_{1z}(U)\,dU$$

$$-\frac{4}{15}K_o\int_{V_p-V_a}^{V_p+V_a}\left(\frac{2V_p-3U}{U^{\frac{1}{2}}V_a}\right)\left[(2V_a+U)(V_p+V_a-U)(3V_a-V_p+U)\right]^{\frac{1}{2}}f_{1z}(U)\,dU$$

$$-\frac{8}{15}K_o\int_{V_p-V_a}^{V_p}\left(\frac{V_p+V_a}{U}\right)^{\frac{1}{2}}\left\{V_p\left(\frac{V_p}{V_a}-1\right)\left[K(k_1)-F(\xi_1,k_1)\right]-V_a\left[3+\left(\frac{V_p}{V_a}\right)^2\right]\left[G(k_1)-G(\xi_1,k_1)\right]\right\}\cdot f_{1z}(U)\,dU$$

$$+\frac{8}{15}K_o\int_{V_p}^{V_p+V_a}\left(\frac{V_p+V_a}{U}\right)^{\frac{1}{2}}\left\{V_p\left(\frac{V_p}{V_a}-1\right)F(\xi_1,k_1)-V_a\left[3+\left(\frac{V_p}{V_a}\right)^2\right]G(\xi_1,k_1)\right\}f_{1z}(U)\,dU \qquad (217)$$

where

$$\xi_1 = \sin^{-1}\left(\frac{V_a+V_p-U}{2V_a}\right)^{\frac{1}{2}}, \quad k_1 = \left(\frac{2V_a}{V_p+V_a}\right)^{\frac{1}{2}}$$

and where $K(k_1)$, $F(\xi_1,k_1)$, $G(k_1)$ and $G(\xi_1,k_1)$ are, respectively, the complete and incomplete elliptic integrals of first and second kind. Finally,

$$\int_0^{2\pi} j_{2\theta\phi}\,d\theta = \frac{\pi}{8}K_o\int_{V_p}^{\infty}\left(a_3+\frac{5}{4}c_3\right)f_{2zz}(U)\,dU$$

$$+\frac{1}{8}K_o\int_{V_p-V_a}^{V_p+V_a}\left[a_3\left(\theta_2+\frac{3}{2}\sin 2\theta_2\right)+2b_3\sin\theta_2\left(1+\cos^2\theta_2\right)+c_3\left(\frac{3}{16}\sin 4\theta_2+\sin 2\theta_2+\frac{5}{4}\theta_2\right)\right]f_{2zz}(U)\,dU$$

$$-\frac{\pi}{8}K_o\int_{V_p}^{V_p+V_a}\left(a_3+\frac{5}{4}c_3\right)f_{2zz}(U)\,dU \qquad (218)$$

with

$$a_3(U) = U + 2V_p + 3V_p^2/U \tag{219}$$

$$b_3(U) = 2V_a(3V_p/U - 1) \tag{220}$$

and

$$c_3(U) = -3V_a^2/U \tag{221}$$

In the limit $V_a \ll V_p$, we can also obtain simplified results by expanding Eqs. (207), (208), and (211). Using Eq. (209), we obtain

$$\int_0^{2\pi} j_{0\theta\phi}\,d\theta = 2\pi K_o \int_{V_p}^{\infty} (U - V_p) f_o(U)\,dU + \frac{\pi}{2} V_a^2 K_o f_o(V_p) \tag{222}$$

and

$$\int_0^{2\pi} j_{2\theta\phi}\,d\theta = \frac{\pi}{8} K_o \int_{V_p}^{\infty} \left[a_3 + \frac{c_3}{4}\left(3 + 2\frac{r_p^2}{r_s^2}\right)\right] f_{2zz}(U)\,dU + \frac{5\pi}{16} K_o V_a^2 f_{2zz}(V_p) \tag{223}$$

with a_3 and c_3 given by Eqs. (219) and (221). Also[8],

$$\int_0^{2\pi} j_{1\theta\phi}\,d\theta = \frac{2r_s}{r_p}\beta V_a K_o \int_{V_p}^{\infty} dU f_{1z}(U) \int_0^1 \frac{dy}{(y^2+\beta)^{3/2}} \left(\frac{y^2 + \beta V_p/U}{1 - y^2}\right)^{\frac{1}{2}}$$

$$= 2\beta^{-\frac{1}{2}} V_a K_o \int_{V_p}^{\infty} dU f_{1z}(U)(1 + \beta V_p/U)^{\frac{1}{2}} G(k_3) \tag{224}$$

where $G(k_3)$ is the complete elliptic integral of the second kind and $k_3 = [(U-V_p)/(\beta V_p + U)]^{\frac{1}{2}}$. If in addition $r_s \approx r_p$ or $\beta \gg 1$, Eq. (224) reduces to

$$\int_0^{2\pi} j_{1\theta\phi}\,d\theta = \pi K_o V_a \int_{V_p}^{\infty} (V_p/U)^{\frac{1}{2}} f_{1z}(U)\,dU \tag{225}$$

Equations (222), (223) and (225) also follow directly in these limits from Eqs. (153) to (155) after integration over a cylindrical surface.

b. Accelerating Region

In the accelerating region, the l^{th} order current density j_l on a cylindrical element is from Eqs. (106) to (108) given by

$$j_{l\theta\phi} = e\frac{r_s}{r_p}\left\{2\pi\int_{\sqrt{\beta}v_o}^{\infty} dv\, v^3 f^*_{loo}(v)\int_{\cos\theta_o}^{1} dx\, x P_l(-x) + 2\pi\int_{o}^{\sqrt{\beta}v_o} dv\, v^3 f^*_{loo}(v)\int_{o}^{1} dx\, x P_l(-x)\right.$$

$$+\int_{\sqrt{\beta}v_o}^{\infty} dv\, v^3 f^*_{loo}(v)\int_{o}^{\cos\theta_o} dx\, x P_l(-x)4\Phi_o$$

$$\left.+\int_{\sqrt{\beta}v_o}^{\infty} dv\, v^3 \sum_{m\geq 1} f^*_{lmo}(v)\int_{o}^{\cos\theta_o} dx\, x P_l^m(-x)\,\frac{2}{m}\sin m\Phi_o[1+(-1)^m]\right\} \qquad (226)$$

with θ_o, β, and v_o given by Eqs. (183) and (184) and Φ_o now given by

$$\sin\Phi_o = \left[\frac{\beta(v^2x^2+v_o^2)}{v^2(1-x^2)}\right]^{\frac{1}{2}} \qquad (227)$$

Letting $l = 0$, 1, and 2, we obtain

$$j_{0\theta\phi} = \frac{r_s}{r_p}K_o\left[\int_{o}^{\beta(V_p+V_a^*)} Uf_o(U)dU + \frac{2}{\pi}\int_{\beta(V_p+V_a^*)}^{\infty} U\left\{\sin^{-1}\left[\frac{\beta(V_p+V_a^*)}{U}\right]^{\frac{1}{2}} + \frac{r_p}{r_s}\left(1+\frac{V_p+V_a}{U}\right)\cdot\right.\right.$$

$$\left.\left.\cdot\sin^{-1}\left[\frac{U-\beta(V_p+V_a^*)}{U+V_p+V_a^*}\right]^{\frac{1}{2}}\right\}f_o(U)dU\right] \qquad (228)$$

$$j_{1\theta\phi} = \frac{2}{3}\frac{r_s}{r_p}K_o\left\{\int_{o}^{\infty} Uf^*_{1Z}(U)dU - \frac{2}{\pi}\int_{\beta(V_p+V_a^*)}^{\infty} dU\,U f^*_{1Z}(U)\int_{\sqrt{y}}^{1} dx(x^2-y)^{3/2}/[(x^2+\beta)^{3/2}(1-x^2)^{\frac{1}{2}}]\right\}$$

Integrating[8], one obtains

$$j_{1\theta\phi} = \frac{2}{3}\frac{r_s}{r_p}K_o\left\{\int_o^{\infty} U f^*_{1Z}(U)dU - \frac{2}{\pi}\int_{\beta(V_p+V_a^*)}^{\infty} U\left[\frac{\gamma^2}{\beta(\gamma+\beta)^{\frac{1}{2}}}K(k_2) - \frac{(\gamma+\beta)^{3/2}}{\beta(1+\beta)}G(k_2) + \frac{\gamma}{(\gamma+\beta)^{\frac{1}{2}}}\Pi(\alpha_1^2,k_2)\right] f^*_{1Z}(U)dU\right\} \tag{229}$$

where here

$$\gamma = \beta(V_p + V_a^*)/U, \quad \alpha_1 = (1-\gamma)^{\frac{1}{2}}, \quad k_2 = \left[\frac{\beta(1-\gamma)}{\beta+\gamma}\right]^{\frac{1}{2}}$$

and where $K(k)$, $G(k)$, and $\Pi(\alpha^2,k)$ are the complete elliptic integrals of first, second, and third kind, respectively. Finally,

$$j_{2\theta\phi} = \frac{1}{4}\frac{r_s}{r_p}K_o\int_o^{\beta(V_p+V_a^*)} U f^*_{2ZZ}(U)dU + \frac{1}{\pi}\frac{r_s}{r_p}K_o\int_{\beta(V_p+V_a^*)}^{\infty} U\left\{\frac{1}{2}\sin^{-1}\left[\frac{\beta(V_p+V_a^*)}{U}\right]^{\frac{1}{2}}\right.$$

$$+ \frac{2r_p}{r_s}\left(1+\frac{V_p+V_a^*}{U}\right)\left(\left[1-\frac{3}{8}\left(1+\frac{V_p+V_a^*}{U}\right)\left(1+\frac{r_p^2}{r_s^2}\right)\right]\sin^{-1}\left[\frac{U-\beta(V_p+V_a^*)}{U+V_p+V_a^*}\right]^{\frac{1}{2}}\right.$$

$$\left.\left. + \frac{3}{8}\frac{r_p}{r_s}\left(\frac{V_p+V_a^*}{\beta U}\right)^{\frac{1}{2}}\left[1-\frac{\beta(V_p+V_a^*)}{U}\right]^{\frac{1}{2}}\right)\right\} f^*_{2ZZ}(U)dU$$

$$+ \frac{1}{4\pi}K_o\int_{\beta(V_p+V_a^*)}^{\infty}\left\{\frac{r_p}{r_s}[U-(V_p+V_a^*)(1+2\beta)]\left(\frac{V_p+V_a^*}{\beta U}\right)^{\frac{1}{2}}\left[1-\frac{\beta(V_p+V_a^*)}{U}\right]^{\frac{1}{2}}\right.$$

$$\left. + \frac{r_p^2}{r_s^2}\frac{1}{\beta}U\left(1+\frac{V_p+V_a^*}{U}\right)^2\sin^{-1}\left[\frac{U-\beta(V_p+V_a^*)}{U+V_p+V_a^*}\right]^{\frac{1}{2}}\right\}[f^*_{2XX}(U)-f^*_{2YY}(U)]dU \tag{230}$$

When the cylinder is perpendicular to $\underset{\sim}{E}$, integration of Eqs. (228) to (230) over θ has to be performed. Once again the integration of $j_{1\theta\phi}$ must

be done numerically. For $r_s \approx r_p$ or $\beta >> 1$, these relations reduce to Eqs. (23) to (25), which are independent of V_a. The total current in that case has been given in Eq. (141). For an arbitrary ratio of r_s/r_p but for $V_a \to 0$, the result has also been given in Eq. (140), and when $r_s >> r_p$ or $\beta << 1$, this reduces to the sum of the contributions in Eq . (116) plus Eq. (126).

5. DEDUCTION OF THE DISTRIBUTION FUNCTION WITH A PLANE PROBE

Due to the complexity of the equations involved, it seems that the deduction of the distribution function from the current intercepted by the probe can be done only for $V_a << V_p$. Even then, it is not possible to separate explicitly the different components of the distribution function by using different probe geometries as we did in Section II for E = 0. However, we have from the expansion in spherical harmonics of the Boltzmann equation up to the second order for time independent and homogeneous plasmas[1]

$$\frac{e\underset{\sim}{E}\cdot\underset{\sim}{f}_1}{mv} + \frac{v}{3}\frac{\partial}{\partial v}\left(\frac{e\underset{\sim}{E}\cdot\underset{\sim}{f}_1}{mv}\right) + \left(\delta f_o/\delta t\right)_c = 0 \tag{231}$$

$$\frac{e\underset{\sim}{E}\partial f_o}{m\partial v} - \nu_1\underset{\sim}{f}_1 + \frac{2}{5v^3}\frac{\partial}{\partial v}\left(v^3\,\frac{e\underset{\sim}{E}}{m}\cdot\underset{\approx}{f}_2\right) = 0 \tag{232}$$

$$v\frac{\partial}{\partial v}\left[\frac{e\left(\underset{\approx}{E}\underset{\sim}{f}_1 + \underset{\sim}{f}_1\underset{\sim}{E}\right)}{2mv} - \frac{1}{3}\left(\frac{e\underset{\sim}{E}\cdot\underset{\sim}{f}_1}{mv}\right)\underset{\approx}{I}_2\right] - \nu_2\underset{\approx}{f}_2 = 0 \tag{233}$$

where v is the electron velocity, $\left(\delta f_o/\delta t\right)_c$ is the collision term for f_o, the ν_l's are the l^{th} order collision frequencies, and $\underset{\approx}{I}_2$ is the unit tensor. If $\underset{\sim}{E}$ is oriented along the z-axis, Eq. (233) implies that, if $(eE/m\nu v)^2 << 1$ (or the electron drift to thermal velocity is small), then $\underset{\approx}{f}_2$ is a diagonal tensor with $f_{2xx} = f_{2yy} = -\frac{1}{2}f_{2zz}$, as given in Eq. (173). This result plus Eq. (232) also means that $f_{1x} = f_{1y} = 0$, so that the only components to be

determined are f_o, f_{1z} and f_{2zz}. Also,* for $\phi = 0$, we have, as in Eq. (209), $f^*_{1z} = f_{1z} \cos\theta$, $f^*_{2zz} = \frac{1}{2}(3\cos^2\theta - 1) f_{2zz}$ and $V^*_a = V_a \cos\theta$.

When $V_a << V_p$, one can obtain the three components of f from the current intercepted by a plane probe oriented along three directions with respect to the z-axis if we omit the V_a/V_p correction and along five directions if we include terms up to $(V_a/V_p)^2$. In the latter case, the current density on a plane probe with its normal oriented at an angle θ with respect to $\underset{\sim}{E}$ can be written from Eqs. (153) to (155) as

$$j_\theta = \sum_{i=0}^{4} B_i \cos^i\theta \tag{234}$$

where

$$B_o = j_o - \tfrac{1}{2} j_2 \tag{235}$$

$$B_1 = -j_1 - V_a(j'_o - \tfrac{1}{2} j'_2) = -j_1 - V_a B'_o \tag{236}$$

$$B_2 = \tfrac{3}{2} j_2 + V_a j'_1 + \tfrac{1}{2} V_a^2 B''_o \tag{237}$$

$$B_3 = -\tfrac{3}{2} V_a j'_2 - \tfrac{1}{2} V_a^2 j''_1 \quad \text{and} \quad B_4 = \tfrac{3}{4} V_a^2 j''_2$$

Here we use new definitions for j_o, j_1, and j_2 with

$$j_o = K_o \int_{V_p}^{\infty} (U - V_p) f_o(U)\, dU \tag{238}$$

$$j_1 = \tfrac{2}{3} K_o \int_{V_p}^{\infty} U \left[1 - \left(\frac{V_p}{U}\right)^{3/2}\right] f_{1z}(U)\, dU \tag{239}$$

---

* It is interesting to note from this result that we would get no contribution from $\underset{\sim}{f}_2$ to the current intercepted by a plane probe when $\cos^2\theta = 1/3$ or for the angles $\theta = \pm 54.7^\circ$ and $\pm 125.3^\circ$.

and

$$j_2 = \frac{1}{4} K_o \int_{V_p}^{\infty} (U + 2V_p - 3V_p^2/U) f_{2zz}(U) dU \tag{240}$$

as the contributions if V_a were zero and $\theta = 0$. A prime denotes differentiation with respect to V_p. If we choose the five orientations of the probe to be $\theta = 0$, $\pi/4$, $\pi/2$, $3\pi/4$, and π, we can solve Eq. (234) to obtain

$$B_o = j_{\pi/2} \tag{241}$$

$$B_1 = \sqrt{2}\,(j_{\pi/4} - j_{3\pi/4}) - \tfrac{1}{2}(j_{2\pi} - j_{\pi}) \tag{242}$$

$$B_2 = 2(j_{\pi/4} + j_{3\pi/4}) - 3j_{\pi/2} - \tfrac{1}{2}(j_{2\pi} + j_{\pi}) \tag{243}$$

$$B_3 = (j_{2\pi} - j_{\pi}) - \sqrt{2}(j_{\pi/4} - j_{3\pi/4}) \tag{244}$$

and

$$B_4 = (j_{2\pi} + j_{\pi}) - 2(j_{\pi/4} + j_{3\pi/4} - j_{\pi/2}) \tag{245}$$

Thus, the B's can be thought of as experimentally available quantities in terms of which we can express j_o, j_1, and j_2. Equations (235) to (237) allow us to write

$$j_o = B_o + \frac{1}{3} B_2 + \frac{1}{3} V_a B_1' + \frac{1}{6} (V_a^2 B_o')' \tag{246}$$

$$j_1 = - B_1 - V_a B_o' \tag{247}$$

$$j_2 = \frac{2}{3} B_2 + \frac{2}{3} V_a B_1' + \frac{1}{3} (V_a^2 B_o')' \tag{248}$$

so that the problem now reduces to the inversion of the Eqs. (238) to (240) since j_o, j_1, and j_2 can be experimentally determined separately upon knowing the B's. We can derive f_o from j_o in the manner given in Eq. (40):

$$f_o(V_p) = \frac{1}{K_o} j_o'' \tag{249}$$

We can deduce f_{1z} from j_1 by differentiation as given in Eq. (41) and f_{2zz} from Eq. (43):

$$f_{1z}(V_p) = \frac{1}{K_o} V_p^{\frac{1}{2}} \left[\frac{1}{V_p^{\frac{1}{2}}} j_1' \right]' \tag{250}$$

$$f_{2zz}(V_p) = \frac{1}{K_o} \left[j_2'' - \frac{3}{2V_p} j_2' + \frac{3}{4V_p^2} j_2 - \frac{3}{8V_p^{3/2}} \int_{V_p}^{\infty} \frac{j_2(V_p)}{V_p^{3/2}} dV_p \right]$$

$$= -\frac{1}{K_o} \left[V_p^3 \left(V_p^{-3/2} \int_{V_p}^{\infty} \frac{j_2(V_p) dV_p}{V_p^{3/2}} \right)' \right]'' \tag{251}$$

Thus f_o, f_{1z}, and f_{2zz} can be deduced from j_o, j_1, and j_2 given by Eqs. (246) to (248), where the B's are obtained from the current density on the plane probe oriented along five directions as given by Eqs. (241) to (243). Equations (250) and (251) require a knowledge of the reference plasma potential with respect to which V_p is measured. Plasma potential can be obtained from the change (theoretically a discontinuity) in the second derivative of the I-V characteristic with the plane probe oriented at $\theta = \pi/2$, for which V_a corrections do not occur. In so doing we assume that the potential of the probe has fallen close to the plasma potential at the sheath edge. The last term of Eqs. (246) to (248) may be found to be highly inaccurate when replaced in Eqs. (249) and (251) because of the fourth order derivative involved. When $V_a \ll V_p$, these two terms can be omitted, so that Eqs. (246) to (248) can be written in terms of j's as

$$j_o \approx \frac{2}{3} (j_{\pi/4} + j_{3\pi/4}) - \frac{1}{6} (j_{2\pi} + j_{\pi}) + \frac{1}{3} V_a [\sqrt{2}(j_{\pi/4}' - j_{3\pi/4}') - \frac{1}{2} (j_{2\pi}' - j_{\pi}')] \tag{252}$$

$$j_1 \approx \frac{1}{2} (j_{2\pi} - j_{\pi}) - \sqrt{2}(j_{\pi/4} - j_{3\pi/4}) - V_a j_{\pi}'/2 \tag{253}$$

$$j_2 \approx \frac{4}{3}\,(j_{\pi/4} + j_{3\pi/4}) - 2j_{\pi/2} - \frac{1}{3}\,(j_{2\pi} + j_{\pi}) + \frac{2}{3}\,V_a[\sqrt{2}(j'_{\pi/4} - j'_{3\pi/4}) - \frac{1}{2}(j'_{2\pi} - j'_{\pi})] \tag{254}$$

In the limit $V_a \to 0$, $B_3 = B_4 = 0$, so that $j_{\pi/4}$ and $j_{3\pi/4}$ become linearly dependent on $j_{2\pi}$, j_{π}, and $j_{\pi/2}$ (see Eqs. (244) and (245)). Then

$$j_o = \frac{2}{3}\,j_{\pi/2} + \frac{1}{6}\,(j_{2\pi} + j_{\pi}) \tag{255}$$

$$j_1 = \frac{1}{2}\,(j_{\pi} - j_{2\pi}) \tag{256}$$

$$j_2 = \frac{1}{3}\,(j_{2\pi} + j_{\pi}) - \frac{2}{3}\,j_{\pi/2} \tag{257}$$

Three orientations of the plane probe are sufficient. In this same limit, the expressions for the current intercepted by the spherical and cylindrical probes are also greatly simplified. By using several probes in a retarding potential region, the I_o, I_1, and I_2 current contributions can be separated from each other by combining the responses from several probes. For example, only j_o contributes to the current of a spherical probe, and one can obtain $f_o(V_p)$ directly from Eq. (249). The j_1 contribution can be obtained from a plane probe by using Eq. (256), which, substituted in Eq. (250), gives $f_{1z}(V_p)$. Knowing j_o and j_1, one can then obtain j_2 from either the plane or cylinder, which allows us to determine $f_{2zz}(V_p)$ from Eq. (251). All these results are also derivable with the hemispherical grid system.

In the more general case, when one has to allow for V_a, the problem becomes the evaluation of $V_a = e\Phi_s$, where $f_o(U)$ has to be known to determine λ_s, as shown in the next subsection. The simplest way to get λ_s is by iteration, upon assuming first an approximate value $f_{01}(V_p)$ for $f_o(V_p)$:

$$f_{01}(V_p) \approx \frac{1}{K_o}\,[\frac{2}{3}\,j''_{\pi/2} + \frac{1}{6}\,(j''_{2\pi} + j''_{\pi})] \tag{258}$$

as given by Eqs. (249) and (255). Introducing $f_{01}(V_p)$ allows us to calculate a first approximation λ_{s1} for λ_s, which can then be reiterated.

6. EVALUATION OF THE SHEATH THICKNESS AND EFFECT OF NEGATIVE IONS

For the calculation of the current from the electron distribution function, one must know the drop of potential V_a of the external electric field across the sheath in the retarding region. This implies an evaluation of the sheath thickness λ_s for negative probe potentials in a situation where electrons still provide the dominant contribution to the current. For an anisotropic non-Maxwellian plasma and a strong external electric field, this problem is extremely difficult. However, if we consider V_a as a correction term, an approximate expression for λ_s may be acceptable. One of the assumptions is that the sheath boundary is parallel or concentric with the probe.

In many lasing plasmas, negative ions are present to an appreciable degree. Their presence influences the sheath criterion, the ion directed velocity at the sheath edge, and consequently the positive ion contribution to the current. It will be shown below that the ion saturation current is sharply reduced if the negative ion concentration is high. Also, in the electron saturation region, the effect of negative ions is to lower the electron saturation current, since, due to charge neutrality, the electron density is lower in the presence (as compared to that in the absence) of negative ions for the same positive ion density. Thus, negative ions are included in the following analysis.

The negative ion contribution, j_-, to the total current density in the electron retardation region can be derived from Eq. (150). Allowing their distribution function to be isotropic and Maxwellian, we obtain

for a plane probe

$$j_- = \Sigma n_n Z_n e \left(\frac{kT_-}{2\pi m_n}\right)^{\frac{1}{2}} \exp\left[-\left(\frac{V_p - V_a^*}{kT_-}\right)\right] \tag{259}$$

where k is Boltzmann's constant, n_n is the negative ion density, Z_n is their charge number, m_n is their mass, and T_- is their temperature. (For a spherical or cylindrical probe, this expression can be readily integrated over angle as in Eqs. (158) and (160).) Because of their greater mass when compared to the electrons, the negative ions contribute very little to the total current.

Space charge and sheath effects are determined from Poisson's equation,

$$\nabla^2 \left(\frac{V}{e}\right) = \frac{e}{\varepsilon_o} [n_e - \Sigma Z_p n_p + \Sigma Z_n n_n] \tag{260}$$

where V/e is the potential (V in joules), e is the magnitude of the electron charge, ε_o is the permittivity of free space, n_p is the positive ion density, and Z_p is the charge number. The external electric field across the discharge is taken to be constant, so that it does not cause any space charge effects. Thus V is here associated only with the potential variation caused by applying a potential to a probe inserted in the plasma.

Consider a plane probe accelerating positive ions of mass m_p and let Z be the direction of the normal to the probe. The positive ion density, n_p, within the collisionless sheath is given by

$$n_p(Z) = \iiint f_p(v_Z', v_X, v_Y) dv_Z' \, dv_X \, dv_Y$$

$$= \iiint f_p(v_Z, v_X, v_Y)(v_Z/v_Z') dv_Z dv_X dv_Y \tag{261}$$

where

$$v_Z' = \left[v_Z^2 + \frac{2}{m_p}(V - V_s)\right]^{\frac{1}{2}}$$

Henceforth, $V/e = |V/e|$ designates the magnitude of the potential within the sheath. Also, f_p is the ion velocity distribution function and V_s/e is the potential, both at the sheath edge. For simplicity, we assume that the ion velocity at the sheath edge is much greater than the ion thermal velocity. (This assumption is valid provided the negative ion concentration is less than the electron concentration.) Then f_p can be considered as a delta function, as far as the v_Z component is concerned, viz.,

$$\iint f_p(v_Z, v_X, v_Y)dv_X dv_Y = n_{ps}\delta[v_Z-(2V_i/m_p)^{\frac{1}{2}}] \tag{262}$$

where n_{ps} is the positive ion density and V_i is the ion directed energy, both at the sheath edge. Combining Eqs. (261)and (262) yields

$$n_p(Z) = n_{ps}\left(\frac{V_i}{V_i + V-V_s}\right)^{\frac{1}{2}} \tag{263}$$

For the electrons, we assume for simplicity that only the isotropic part of the distribution function contributes to the density in the sheath. Since electrons are decelerated, we have

$$n_e(Z) = \iiint f_o(v_Z', v_X, v_Y)dv_Z'dv_X dv_Y \tag{264}$$

where $v_Z' = [v_Z^2 - (2/m)(V - V_s)]^{\frac{1}{2}}$, m is the electron mass,and f_o is the isotropic part of the electron distribution function just outside of the sheath edge. The assumption that f is isotropic plus the assumption that V_i is independent of θ imply that λ_s is independent of θ. That is, as a first approximation, the external electric field is considered weak enough not to make the sheath thickness dependent on angle.

Below we restrict ourselves to a plane probe and later give the results for the sphere and cylinder. In evaluating the integral in Eq. (264) for a

position Z where the voltage is V, one notes that, when $V_p - V_s > \frac{1}{2}mv_Z^2 > V - V_s$, the electrons turn around in the sheath between the point Z and the probe surface, and we have to count them twice. When $\frac{1}{2}mv_Z^2 > V_p - V_s$, they reach the probe and we count them once. If $\frac{1}{2}mv_Z^2 < V - V_s$, we do not count them since they do not reach the point Z in the sheath. Thus we have

$$n_e(Z) = \int_{-\infty}^{\infty} dv_X \int_{-\infty}^{\infty} dv_Y \left[2 \int_{0}^{(v_o^2 - v_V^2)^{\frac{1}{2}}} f(v_Z', v_X, v_Y) dv_Z' + \int_{(v_o^2 - v_V^2)^{\frac{1}{2}}}^{\infty} f(v_Z', v_X, v_Y) dv_Z' \right]$$

$$= \int_{-\infty}^{\infty} dv_X \int_{-\infty}^{\infty} dv_Y \left[2 \int_{v_V}^{\infty} \frac{f_o(v_Z, v_X, v_Y) v_Z dv_Z}{(v_Z^2 - v_V^2)^{\frac{1}{2}}} - \int_{v_o}^{\infty} \frac{f_o(v_Z, v_X, v_Y) v_Z dv_Z}{(v_Z^2 - v_V^2)^{\frac{1}{2}}} \right] \tag{265}$$

where $v_V = [2(V - V_s)/m]^{\frac{1}{2}}$ and $v_o = [2(V_p - V_s)/m]^{\frac{1}{2}}$. We use the fact that $2\int_{v_V}^{v_o} + \int_{v_o}^{\infty} = 2\int_{v_V}^{\infty} - \int_{v_o}^{\infty}$.

Let $q^2 = v_X^2 + v_Y^2$, $dv_X dv_Y = q\, dq\, d\Phi$ and integrate over Φ to give

$$n_e(Z) = 2\pi \int_{o}^{\infty} q\, dq \left[2 \int_{v_V}^{\infty} \frac{f_o v_Z dv_Z}{(v_Z^2 - v_V^2)^{\frac{1}{2}}} - \int_{v_o}^{\infty} \frac{f_o v_Z dv_Z}{(v_Z^2 - v_V^2)^{\frac{1}{2}}} \right] \tag{266}$$

Let us change to polar coordinates with $\tan\theta = q/v_Z$ and $U = m(v_Z^2 + q^2)/2$. We obtain

$$n_e(Z) = \frac{\sqrt{2}\pi}{m^{3/2}} \left[2 \int_{V-V_s}^{\infty} f_o(U) dU \int_{o}^{\theta_V} \frac{d\theta \sin\theta\cos\theta}{[U\cos^2\theta - (V - V_s)]^{\frac{1}{2}}} - \int_{V_p - V_s}^{\infty} f_o(U) dU \int_{o}^{\theta_1} \frac{d\theta \sin\theta\cos\theta}{[U\cos^2\theta - (V - V_s)]^{\frac{1}{2}}} \right] \tag{267}$$

where $\cos^2\theta_V = mv_V^2/2U$ and $\cos^2\theta_1 = mv_o^2/2U$. Integrating over θ yields

$$n_e(Z) = \left(\frac{2}{m}\right)^{3/2} \pi \left\{ 2 \int_{V-V_s}^{\infty} dU (U - V + V_s)^{\frac{1}{2}} f_o(U) - \int_{V_p - V_s}^{\infty} dU [(U - V + V_s)^{\frac{1}{2}} - (V_p - V)^{\frac{1}{2}}] f_o(U) \right\} \tag{268}$$

If $n_e = n_{es}$ at the sheath position where $V = V_s$, one can normalize and write

$$\frac{n_e(Z)}{n_{es}} = \frac{\int_{V-V_s}^{\infty} (U-V+V_s)^{\frac{1}{2}} f_o(U)dU - \frac{1}{2}\int_{V_p-V_s}^{\infty} [(U-V+V_s)^{\frac{1}{2}} - (V_p-V)^{\frac{1}{2}}] f_o(U)dU}{\int_{o}^{\infty} U^{\frac{1}{2}} f_o(U)dU - \frac{1}{2}\int_{V_p-V_s}^{\infty} [U^{\frac{1}{2}} - (V_p-V_s)^{\frac{1}{2}}] f_o(U)dU} \tag{269}$$

For sufficiently negative potentials when V_p is much greater than the electron thermal energy, Eq. (269) reduces to

$$\frac{n_e(Z)}{n_{es}} = \int_{V-V_s}^{\infty} (U-V+V_s)^{\frac{1}{2}} f_o(U)dU \Big/ \int_{o}^{\infty} U^{\frac{1}{2}} f_o(U)dU \tag{270}$$

The negative ions are also decelerated, and the assumption that V_p is greater than their thermal energy is obeyed even for very small V_p. Furthermore their distribution function is Maxwellian. An equation similar to Eq. (270) then applies, which, for a Maxwellian distribution, reduces to

$$\frac{n_n(Z)}{n_{ns}} = \exp\left[-\left(\frac{V-V_s}{kT_-}\right)\right] \tag{271}$$

where n_{ns} is the negative ion density at the sheath edge.

Let us assume that all the positive ions have the same V_i and all the negative ions have the same T_-. Also in Eq. (260) we can define

$$n_+ = \Sigma Z_p n_p \quad \text{and} \quad n_- = \Sigma Z_n n_n \tag{272}$$

Equation (260) can be integrated once to give

$$\left(\frac{dV}{dZ}\right)^2 - \left(\frac{dV_s}{dZ}\right)^2 = \frac{2e^2}{\varepsilon_o}\int_{V_s}^{V} [n_+ - n_e - n_-]dV \tag{273}$$

where V is now the magnitude of V. From Eqs. (263), (268), and (271) we obtain

$$\int_{V_s}^{V} n_+ dV = 2n_{+s}\left\{\left[V_i(V_i + V - V_s)\right]^{\frac{1}{2}} - V_i\right\} \tag{274}$$

$$\int_{V_s}^{V} n_- dV = n_{-s}kT_-\left\{1 - \exp\left[-\left(\frac{V-V_s}{kT_-}\right)\right]\right\} \tag{275}$$

$$\int_{V_s}^{V} n_e dV = \frac{4\pi}{3}\left(\frac{2}{m}\right)^{3/2}\left\{\int_0^{\infty} dU\, U^{3/2} f_o(U) - \int_{V-V_s}^{\infty} dU f_o(U)(U+V-V_s)^{3/2}\right\}$$
$$+ \frac{2\pi}{3}\left(\frac{2}{m}\right)^{3/2}\int_{V_p-V_s}^{\infty} dU f_o(U)\left[(U-V+V_s)^{3/2} - U^{3/2} - (V_p-V)^{3/2} + (V_p-V_s)^{3/2}\right] \tag{276}$$

For large V_p, this reduces to

$$\int_{V_s}^{V} n_e dV = \frac{2}{3} n_{es}\left\{\int_0^{\infty} dU\, U^{3/2} f_o(U) - \int_{V-V_s}^{\infty} dU f_o(U)(U+V-V_s)^{3/2}\right\} \Big/ \int_0^{\infty} dU\, U^{\frac{1}{2}} f_o(U) \tag{277}$$

The Bohm criterion[9,10] requires that $(dV/dz)^2 - (dV_s/dz)^2$ be greater than or equal to zero at the sheath edge. Putting this equal to zero is the condition used to determine the positive ion energy V_i at the sheath edge. The same condition results by assuming a positive ion sheath with $n_+ \geq n_e + n_-$. If we now expand Eqs. (263), (270), and (271) or Eqs. (274) to (277) near the sheath edge where $V-V_s$ is small, we obtain

$$n_+/n_{+s} \approx 1 - (V-V_s)/2V_i \quad \text{and} \quad \int_{V_s}^{V} n_+ dV \approx n_{+s}[V-V_s-(V-V_s)^2/4V_i]$$

$$n_-/n_{-s} \approx 1 - (V-V_s)/kT_- \quad \text{and} \quad \int_{V_s}^{V} n_- dV \approx n_{-s}[V-V_s-(V-V_s)^2/2kT_-]$$

$$n_e/n_{es} \approx 1 - (V-V_s)/V_{e1} \quad \text{and} \quad \int_{V_s}^{V} n_e dV \approx n_{es}[V-V_s-(V-V_s)^2/2V_{e1}]$$

In the above,

$$V_{e1} = 2\int_0^\infty f_o(U)U^{\frac{1}{2}}dU \Big/\Big/ \int_0^\infty f_o(U)U^{-\frac{1}{2}}\,dU \tag{278}$$

defines a new average energy or temperature (V_{e1}/e in eV) for a non-Maxwellian electron distribution, which differs from the usual definition

$$V_e = 2\int_0^\infty f_o(U)U^{3/2}dU \Big/ 3\int_0^\infty f_o(U)U^{\frac{1}{2}}dU \tag{279}$$

(For a Maxwellian distribution, $V_{e1} = V_e = kT_e$, where T_e is the electron temperature.) The Bohm criterion can now be applied to the above equations with $n_{+s} = n_{es} + n_{-s}$ to yield $n_{+s}/2V_i = n_{-s}/kT_- + n_{es}/V_{e1}$ or

$$V_i = \frac{V_{e1}}{2}\,\frac{n_{+s}}{(n_{es} + V_{e1}n_{-s}/kT_-)} \tag{280}$$

This result is identical to that given in Swift and Schwar[11] and in Boyd and Thompson[12], except for the new definition for V_{e1} given in Eq. (278).

In terms of V_i, the positive ion contribution to the total current density is

$$j_+ = \Sigma Z_p n_{ps} e(2V_i/m_p)^{\frac{1}{2}} = n_{+s}(2V_i/m_p)^{\frac{1}{2}} e \tag{281}$$

When $n_{-s}V_{e1}/n_{es}kT_- << 1$, then $V_i = V_{e1}/2$. When $n_{-s}V_{e1}/n_{es}kT_- >> 1$, $V_i = kT_-n_{+s}/2n_{-s}$,

but the lowest value of V_i allowable before the delta function approximation breaks down is $V_i \geq kT_-/4\pi$. At first sight, the variation of j_+ with n_{-s}/n_{es} seems to be useful as a diagnostic to determine the percentage negative ion concentration in the plasma. However, if $V_e >> V_-$, Boyd and Thompson[12] show (for a Maxwellian electron distribution) that after the quantities at the sheath position are related to those at infinity, the positive ion current is an insensitive function of negative ion concentration except at about $n_{-\infty}/n_{e\infty} \approx 2$ where an abrupt transition occurs in V_i. A similar conclusion probably applies to a non-Maxwellian electron distribution function.

All the above quantities, such as density and electron distribution function f_o refer to the sheath position. Our previous assumption, that the ion beam is monoenergetic and has attained an energy V_i at the sheath position, implies that the sheath potential V_s/e is equal to V_i/e. If we adopt $V_s = V_i$ as is usually done, then unfortunately f_o and the densities at this sheath position differ from those in the undisturbed plasma, and corrections are necessary. Furthermore, at this position close to the probe, the voltage gradient due to the applied probe potential may not be small compared to the external electric field, as we would like it to be in order for $\underset{\sim}{f}_1$ and $\underset{\approx}{f}_2$ in our previous subsections to be related only to the external electric field. For these reasons, we do not proceed further with the usual analysis which provides the sheath radius, λ_{so}, up to the point $V = V_s = V_i$ by integrating again Eq. (273) thus:

$$\lambda_{so} = \int_{V_s}^{V_p} dV/(dV/dZ) \qquad (282)$$

Instead, we adopt Eq. (280) for V_i and let it crudely apply even at a distance further away from the probe where the densities and distribution function are close to those in the ambient plasma. If we were still to use Eq. (282), we would now choose V_s less than V_i and determined by the requirement that at the sheath position the gradient dV/dZ be much less than the magnitude of the external electric field. However, Eq. (282) involves several numerical integrations and is cumbersome. We use instead a different definition for λ_s which is much simpler analytically and numerically. We define the sheath width in terms of the effective capacitance of the sheath, and this will give a somewhat larger λ_s than that in Eq. (282).

Following Grard's[13] method, we define

$$\lambda_s = A\varepsilon_o / C_s \tag{283}$$

where C_s is the sheath capacitance, A the area of the probe, and ε_o the permittivity of vacuum. The sheath capacitance is defined as the partial derivative of the charge Q_p carried by the probe with respect to its potential V_p, $C_s = \partial Q_p / \partial V_p$. From Gauss' law, one can show that

$$C_s = - A\varepsilon_o \frac{\partial}{\partial V_p} \left(\frac{\partial V}{\partial Z} \right)_p$$

so that λ_s becomes

$$\frac{1}{\lambda_s} = - \frac{\partial}{\partial V_p} \left(\frac{\partial V}{\partial Z} \right)_p \tag{284}$$

and depends only on the potential gradient at the surface of the probe. From Eqs. (273) and (274), the relation for λ_s becomes

$$\frac{1}{\lambda_s} = \left[\left(\frac{dV_s}{dZ} \right)^2 + \frac{4n_{+s}e^2}{\varepsilon_o} \left[\left(V_i (V_i - V_s + V_p) \right)^{\frac{1}{2}} - V_i \right] - \frac{2e^2}{\varepsilon_o} \int_{V_s}^{V_p} (n_e + n_-) dV \right]^{-\frac{1}{2}}$$

$$\cdot \left\{ \frac{n_{+s}e^2}{\varepsilon_o} V_i \left[V_i (V_i - V_s + V_p) \right]^{-\frac{1}{2}} - \frac{d}{dV_p} \left[\frac{e^2}{\varepsilon_o} \int_{V_s}^{V_p} (n_e + n_-) dV \right] \right\} \tag{285}$$

where from Eq. (276)

$$\int_{V_s}^{V_p} n_e dV = -\left(\frac{2}{m}\right)^{3/2} \frac{2\pi}{3}\left\{\int_{V_p-V_s}^{\infty} dU\,[(U-V_p+V_s)^{3/2} - U^{3/2} - (V_p-V_s)^{3/2}]f_o(U) - 2\int_{o}^{V_p-V_s} dU\,U^{3/2} f_o(U)\right\} \qquad (286)$$

and

$$\frac{d}{dV_p}\int_{V_s}^{V_p} n_e dV = \left(\frac{2}{m}\right)^{3/2} \pi \int_{V_p-V_s}^{\infty} dU[(U-V_p+V_s)^{\frac{1}{2}} + (V_p-V_s)^{\frac{1}{2}}]f_o(U) \qquad (287)$$

The negative ion contributions are similarly obtained from Eq. (275). Assuming $dV_s/dZ \approx 0$ and letting V_p be measured with respect to V_s yield finally

$$\frac{\lambda_s}{\lambda_D} = \left(\frac{2n_{es}}{n_{+s}V_{e1}}\right)^{\frac{1}{2}} \frac{\left\{2[V_i(V_i+V_p)]^{\frac{1}{2}} - 2V_i - \int_o^{V_p}(n_e+n_-)dV/n_{+s}\right\}^{\frac{1}{2}}}{\left\{[V_i/(V_i+V_p)]^{\frac{1}{2}} - (d/dV_p)\int_o^{V_p}(n_e+n_-)dV/n_{+s}\right\}} \qquad (288)$$

with the Debye length given by

$$\lambda_D = (\varepsilon_o V_{e1}/n_{es}e^2)^{\frac{1}{2}} \qquad (289)$$

The main contribution to λ_s in Eq. (288) comes from the ions since the ion density in the sheath is larger than the electron density. In the absence of negative ions, Eq. (280) gives $V_i = V_{e1}/2$, and in the region $V_p >> V_{e1}$ Eq. (286) reduces to

$$\int_o^{V_p} n_e dV = \left(\frac{2}{m}\right)^{3/2} \frac{4\pi}{3}\int_o^{\infty} U^{3/2} f_o(U)dU = n_{es}V_e$$

with V_e defined in Eq. (279). Furthermore, Eq. (287) gives zero. Then we obtain a relation similar to that of Grard[13] (who assumes a Maxwellian distribution, so that $V_e = V_{e1}$):

$$\lambda_s = \sqrt{2}\,\lambda_D[(1 + 2V_p/V_{e1})^{3/2} - (1 + 2V_p/V_{e1})(1 + V_e/V_{e1})]^{\frac{1}{2}} \qquad (290)$$

This expression is plotted in Appendix A. However, in contrast to Eq. (288), the approximate formula in Eq. (290) does not reduce to $\lambda_s = 0$ at $V_p = 0$.

For a spherical or a plane probe, the expression for $n_e(r)$ has to be rederived with r as the radial distance from the center of the probe. In the electron retardation region, an analysis similar to that in Eqs. (264) to (270) yields for a spherical probe

$$n_e(r) = \left(\frac{2}{m}\right)^{3/2} \pi \left\{ 2 \int_{V-V_s}^{\infty} dU f_o(U)(U - V + V_s)^{\frac{1}{2}} - \int_{V_p-V_s}^{\infty} dU f_o(U) \left\{ (U - V + V_s)^{\frac{1}{2}} - \left[(U - V + V_s) - \frac{r_p^2}{r^2}(U - V_p + V_s)\right]^{\frac{1}{2}} \right\} \right\} \qquad (291)$$

For a cylindrical probe, we obtain

$$n_e(r) = \left(\frac{2}{m}\right)^{3/2} 2 \left\{ \pi \int_{V-V_s}^{\infty} dU f_o(U)(U - V + V_s)^{\frac{1}{2}} - \int_{V_p-V_s}^{\infty} dU\, U^{\frac{1}{2}} f_o(U) \cdot \int_0^{x_c} dx \sin^{-1}\left[\frac{r_p}{r}\left(\frac{U - V_p + V_s - Ux^2}{U - V + V_s - Ux^2}\right)^{\frac{1}{2}}\right] \right\} \qquad (292)$$

where

$$x_c = [(U - V_p + V_s)/U]^{\frac{1}{2}}$$

These expressions have to be further integrated for use in Eq. (285). Performing this operation on Eq. (291) and then evaluating the result at $V = V_p$

and $r = r_p$, we find an identical expression to that in Eq. (286). Thus for the spherical probe, the expression for λ_s in Eq. (288) is the same as for a plane. The calculation for the cylindrical probe is more tedious, but the value of λ_s, expressed in Eq. (288), is found again to be identical to that for the plane. This can be shown by integrating Eq. (292) first over V, then letting $V = V_p$ and $r = r_p$, and finally integrating over x. Thus, for any of these three geometries, Eqs. (286) to (288) or (290) provide a fair evaluation of λ_s in the retarding region. This value can be used in the previous equations for the calculation of the current from the distribution function or inversely.

For the evaluation of the sheath thickness when the probe is positively biased, attracting electrons, we can use the well-known Child-Langmuir[5,14] law. For a plane probe, we have

$$\lambda_s = \frac{2}{3}\left(\frac{2}{m}\right)^{\frac{1}{4}} V_p^{3/4}\left[\frac{\epsilon_o}{je}\left(1 + 2.66\,\frac{V_e^{\frac{1}{2}}}{V_p^{\frac{1}{2}}}\right)\right]^{\frac{1}{2}} \tag{293}$$

where the electron distribution function is assumed Maxwellian as far as the V_e/V_p correction term is concerned and where the positive and negative ion densities in the sheath are neglected. Here j is the electron current density.

For spherical and cylindrical probes, Eq. (293) has to be multiplied by respective correction factors, which are functions of r_s/r_p, as given by Langmuir and Blodgett[5,15,16]. Since these factors and also j in Eq. (293) depend on λ_s, one may have to evaluate λ_s numerically by iteration.

7. SUMMARY OF RELATIONS IN THE ELECTRON RETARDATING REGION

The presence of a strong electric field $\underset{\sim}{E}$ in the plasma modifies the potential around the probe. If $eE\lambda_s = V_a$ is comparable to, but still smaller than, the probe potential V_p, correction terms have to be added to the expressions for the current intercepted by the probe in the retarding region. For a plane probe with normal along the $(\theta-\phi)$ direction with respect to the z-axis, assuming $V_a \ll V_p$, we find in Eqs. (153) to (155)

$$j_{\theta\phi} = \sum_{l=0}^{2} (-1)^l j_{l\theta\phi} \tag{294}$$

with

$$j_{0\theta\phi} = K_o \int_{V_p}^{\infty} (U-V_p) f_o(U)dU + K_o V_a^* \int_{V_p}^{\infty} f_o(U)dU + \frac{1}{2} K_o (V_a^*)^2 f_o(V_p) \tag{295}$$

$$j_{1\theta\phi} = \frac{2}{3} K_o \int_{V_p}^{\infty} U\left[1 - \left(\frac{V_p}{U}\right)^{3/2}\right] f_{1Z}^*(U)dU + K_o V_a^* \int_{V_p}^{\infty} \left(\frac{V_p}{U}\right)^{\frac{1}{2}} f_{1Z}^*(U)dU$$

$$- \frac{1}{4} K_o (V_a^*)^2 \int_{V_p}^{\infty} \frac{f_{1Z}^*(U)dU}{(V_p U)^{\frac{1}{2}}} + \frac{1}{2} K_o (V_a^*)^2 f_{1Z}^*(V_p) \tag{296}$$

$$j_{2\theta\phi} = \frac{1}{4} K_o \int_{V_p}^{\infty} [U + 2V_p - 3V_p^2/U] f_{2ZZ}^*(U)dU + \frac{1}{2} K_o V_a^* \int_{V_p}^{\infty} \left(\frac{3V_p}{U} - 1\right) f_{2ZZ}^*(U)dU$$

$$- \frac{3}{4} K_o (V_a^*)^2 \int_{V_p}^{\infty} f_{2ZZ}^*(U) U^{-1} dU + \frac{1}{2} K_o (V_a^*)^2 f_{2ZZ}^*(V_p) \tag{297}$$

where $V_a^* = eE\lambda_s \cos\theta = V_a \cos\theta$, $K_o = 2\pi e/m^2$, and $f_{1Z}^*(E)$, $f_{2ZZ}^*(E)$ are given by Eqs. (31) and (32). For $\underset{\sim}{E}$ along the z-axis, we find from Boltzmann's equation

that

$$f^{*}_{1Z}(U) = f_{1z}(U)\cos\theta \tag{298}$$

and

$$f^{*}_{2ZZ}(U) = \tfrac{1}{2}f_{2zz}(U)(3\cos^2\theta - 1) \tag{299}$$

so that for $\theta = \pm \cos^{-1}\sqrt{3}/3 \pm \pi$ the plane probe sees no contribution to the current from $\underset{\sim}{f}_2$ and, for $\theta = \pm\pi/2$, no contribution from $\underset{\sim}{f}_1$.

For the spherical probe, in the approximation $V_a << V_p$, we obtain from Eqs. (179) to (181) in the retarding case

$$I = \sum_{l=o}^{2} (-1)^l \int j_{l\theta\phi}\,dA \tag{300}$$

with

$$\int j_{0\theta\phi}\,dA = 4\pi r_p^2 K_o \int_{V_p}^{\infty} (U - V_p) f_o(U)\,dU + \frac{2}{3}\pi r_p^2 K_o V_a^2 f_o(V_p) \tag{301}$$

$$\int j_{1\theta\phi}\,dA = \frac{4}{3}\pi r_p^2 K_o V_a \int_{V_p}^{\infty} \left(1 - \frac{r_p^2}{r_s^2} + \frac{r_p^2}{r_s^2}\frac{V_p}{U}\right)^{\frac{1}{2}} f_{1z}(U)\,dU \tag{302}$$

$$\int j_{2\theta\phi}\,dA = -\frac{2}{5}\pi \frac{r_p^4}{r_s^2} K_o \int_{V_p}^{\infty} \frac{V_a^2}{U} f_{2zz}(U)\,dU + \frac{4\pi}{15} r_p^2 K_o V_a^2 f_{2zz}(V_p) \tag{303}$$

Here $V_a = eE(r_s - r_p^3/r_s^2)$, r_s is the sheath radius, r_p is the probe radius, and $\lambda_s = r_s - r_p$.

Under the same approximations for a cylindrical probe, whose axis is perpendicular to the electric field, we obtain

$$I = r_p L \sum_{l=o}^{2} (-1)^l \int_o^{2\pi} j_{l\theta\phi}\,d\theta \tag{304}$$

with (see Eqs. (222) to (225))

$$\int_0^{2\pi} j_{0\theta\phi}\,d\theta = 2\pi K_o \int_{V_p}^{\infty} (U - V_p) f_o(U)\,dU + \frac{\pi}{2} K_o (V_a)^2 f_o(V_p) \tag{305}$$

$$\int_0^{2\pi} j_{1\theta\phi}\,d\theta = 2\beta^{-\frac{1}{2}} K_o V_a \int_{V_p}^{\infty} \left(1 + \frac{\beta V_p}{U}\right)^{\frac{1}{2}} G(k_3) f_{1z}(U)\,dU \approx \pi K_o V_a \int_{V_p}^{\infty} \left(\frac{V_p}{U}\right)^{\frac{1}{2}} f_{1z}(U)\,dU \tag{306}$$

$$\int_0^{2\pi} j_{2\theta\phi}\,d\theta = \frac{\pi}{8} K_o \int_{V_p}^{\infty} \left[U + 2V_p - \frac{3V_p^2}{U} - \frac{3}{4}\frac{V_a^2}{U}\left(3 + 2\frac{r_p^2}{r_s^2}\right)\right] f_{2zz}(U)\,dU + \frac{5\pi}{16} K_o (V_a)^2 f_{2zz}(V_p) \tag{307}$$

In Eq. (306), $k_3 = [(U - V_p)/(\beta V_p + U)]^{\frac{1}{2}}$ and $G(k_3)$ is the complete elliptic integral of the second kind. The approximation on the right-hand side of Eq. (306) applies when $r_s \approx r_p$ or $\beta \gg 1$, where $\beta = r_p^2/(r_s^2 - r_p^2)$. Also here we equate $V_a = eEr_s(1 - r_p^2/r_s^2)$.

The current intercepted by the spherical grid system is not affected by the presence of $\underset{\sim}{E}$ since the surrounding conductor prevents the external electric field from penetrating the cavity. The results are then the same as for $\underset{\sim}{E} = 0$.

An estimate of the sheath thickness λ_s can be obtained (in the absence of negative ions) if we assume that the ion drift energy, V_i, is equal to one half the electron mean energy V_{e1}, as defined in Eq. (278), and that the main contribution by the electrons comes from the isotropic part. (In the presence of negative ions, V_i is redefined in Eq. (280).) Using the definition for λ_s in Eq. (284), we have from Eq. (288)

$$\lambda_s = \left(\frac{2\varepsilon_o}{e^2 n_{+s}}\right)^{\frac{1}{2}} \frac{\left\{2[V_i(V_i + V_p)]^{\frac{1}{2}} - 2V_i - \int_0^{V_p} (n_e/n_{+s})\,dV\right\}^{\frac{1}{2}}}{\left\{[V_i/(V_i + V_p)]^{\frac{1}{2}} - (d/dV_p)\int_0^{V_p} (n_e/n_{+s})\,dV\right\}} \tag{308}$$

with the integrals given in Eqs. (286) and (287) in terms of the electron distribution function. Here n_{+s} is the positive ion density just outside the sheath. (In the presence of negative ions, add n_- to n_e and use Eq. (275).)

In order to recover the electron distribution function from the current, it seems that only the plane probe (when $V_a << V_p$) or the spherical grid system are sensitive to $\underset{\sim}{f}_1$. We show that, upon using a plane probe and retaining the correction terms up to V_a^2, we need five orientations of the probe to derive $f_o(U)$, $f_{1z}(U)$, and $f_{2zz}(U)$. If we choose these five directions to be $\theta = 2\pi,\ \pi/4,\ \pi/2,\ 3\pi/4$, and π, we have from Eqs. (249) to (251)

$$f_o(V_p) = \frac{m^2}{2\pi e} \frac{d^2 j_o}{dV_p^2} \tag{309}$$

$$f_{1z}(V_p) = \frac{m^2}{2\pi e} V_p^{\frac{1}{2}} \frac{d}{dV_p} \left(\frac{1}{V_p^{\frac{1}{2}}} \frac{d}{dV_p} j_1(V_p) \right) \tag{310}$$

and

$$f_{2zz}(V_p) = -\frac{m^2}{2\pi e} \frac{d^2}{dV_p^2} \left[V_p^3 \frac{d}{dV_p} \left(\frac{1}{V_p^{3/2}} \int_{V_p}^{\infty} \frac{j_2(V_p) dV_p}{V_p^{3/2}} \right) \right] \tag{311}$$

Here, Eqs. (241) to (248) give

$$j_o = \frac{2}{3}(j_{\pi/4} + j_{3\pi/4}) - \frac{1}{6}(j_{2\pi} + j_{\pi}) + \frac{1}{3} V_a [\sqrt{2}(j'_{\pi/4} - j'_{3\pi/4}) - \frac{1}{2}(j'_{2\pi} - j'_{\pi})] + \frac{1}{6}(V_a^2 j'_{\pi/2})' \tag{312}$$

$$j_1 = \frac{1}{2}(j_{2\pi} - j_{\pi}) - \sqrt{2}(j_{\pi/4} - j_{3\pi/4}) - V_a j'_{\pi/2} \tag{313}$$

$$j_2 = \frac{4}{3}(j_{\pi/4} + j_{3\pi/4}) - 2j_{\pi/2} - \frac{1}{3}(j_{2\pi} + j_{\pi}) \quad \frac{2}{3} V_a [\sqrt{2}(j'_{\pi/4} - j'_{3\pi/4}) - \frac{1}{2}(j'_{2\pi} - j'_{\pi})] + \frac{1}{3}(V_a^2 j'_{\pi/2})' \tag{314}$$

where the subscripts of the j's on the right side of Eqs. (312) to (314) refer to the θ-orientation of the normal to the plane probe with respect to the z-axis ($\underset{\sim}{E}$ direction) and where the prime stands for the derivative with respect to V_p.

SECTION IV

COMPUTER CALCULATIONS FOR A PLANE PROBE

1. INTRODUCTION

As part of the present work, we have numerically programmed the equations presented in Sections II and III for a one-sided plane probe, and we provide here the results. The computer programs are described in Appendix C.

Two computer programs were developed. The first one, called program FTOJ, calculates the total current intercepted by the probe for various orientations, for a given electron velocity distribution function, with components up to second order tensor terms. The second one, called program JTOF, performs the inverse operation of deriving the three components (f_o, f_{1z}, and f_{2zz}) of the electron distribution function from the current intercepted by a plane probe oriented along five different directions. The integrations and differentiations required in the main programs are performed by subroutines SUMT and DER, which are also described in Appendix C. In the following, we discuss the results of these computations.

2. RESULTS FROM PROGRAM FTOJ

We calculate the total current to a plane probe for five orientations, namely, when the normal to the probe makes angles 0, $\pi/4$, $\pi/2$, $3\pi/4$, and π radians with respect to the anode-cathode or electric field direction, $\underset{\sim}{E}$. The parameters consist of energy interval in distribution function = 0.1 eV, gas pressure, p = 0.14 torr, ratio of electron or ion density to neutral gas density = 10^{-6}, gas temperature = 300°K, probe area = 1 mm², and the gas is N_2. Several electric field values are adopted, namely, 2.1 V/cm, 4.5 V/cm, and 9 V/cm, which correspond to E/p = 15, 32.1, and 64.3 V/cm-torr, respectively, or $E/N = 4.7 \times 10^{-16}$, 10^{-15}, and 2×10^{-15} V-cm², respectively. (N is the neutral particle density.)

AD-A062 703 RCA LTD STE ANNE DE BELLEVUE (QUEBEC) RESEARCH AND D--ETC F/G 20/9
STUDY OF ELECTROSTATIC PROBES IN NONEQUILIBRIUM PLASMAS.(U)
JUN 75 I P SHKAROFSKY, A BONNIER F33615-73-C-4123
UNCLASSIFIED MNLD-75-TR-002 ARL-75-0228 NL

2 OF 3
AD
A062703

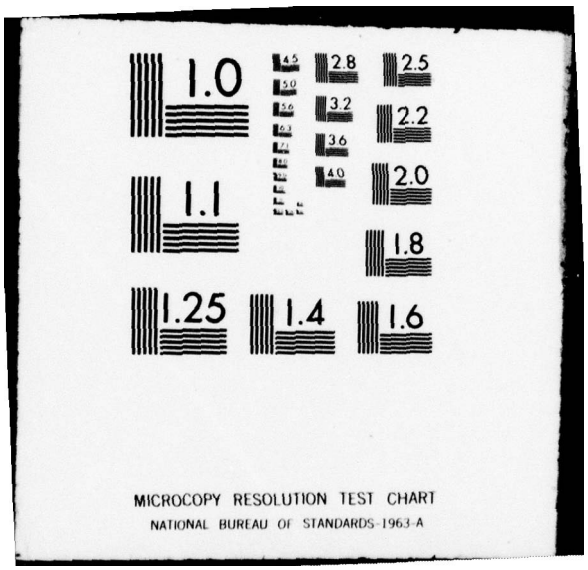
1.0
1.1
1.25
1.4
1.6
1.8
2.0
2.2
2.5
2.8
3.2
3.6
4.0
4.5
5.0
5.6
6.3
7.1
8.0
9.0
MICROCOPY RESOLUTION TEST CHART
NATIONAL BUREAU OF STANDARDS-1963-A

A solution of the Boltzmann equation including inelastic collisional effects yields the actual values of f_o, f_{1z}, and f_{2zz}, the latter two in the direction of $\underset{\sim}{E}$. The function f_o is normalized, so that

$$\int_o^\infty f_o(U)U^{\frac{1}{2}}dU = 1 \tag{315}$$

where U is the electron energy. Results for the above mentioned three electric field values in a N_2 plasma were supplied by ARL for use in the present probe analysis. These plots for f_o, f_{1z}, and f_{2zz} are illustrated later, when we compare them to the rederived results from program JTOF, but certain features are noteworthy to mention here. First, f_o deviates appreciably from a Maxwellian distribution, a result already found some time ago by Nighan[17]. At ARL, it was shown in addition by Bailey and Long[18] that the anisotropic parts, f_{1z} and f_{2zz}, can become a noticeable fraction of f_o in magnitude in certain energy regimes. These regimes are correlated to electron energies that excite strongly the gas molecules, important to know for lasing media. The purpose of the present calculations is to include both effects of a non-Maxwellian and anisotropic distribution in the response of electrostatic probes. One-sided plane probes are most sensitive to measuring the degree of anisotropy, as is indicated by the theory in Sections II and III.

Using the supplied f_o, f_{1z} and f_{2zz} input data, one computes the total current in the electron retardation region. The electron current contribution is calculated from Eqs. (149) to (152) and the ion contribution from Eq. (281).

Figure 11 illustrates results for E = 2.1 V/cm with $n_e/N = 10^{-6}$ ($n_e = 4.5\times 10^9$ cm^{-3}) and T_e = C.78 eV. We note that the curves are close together

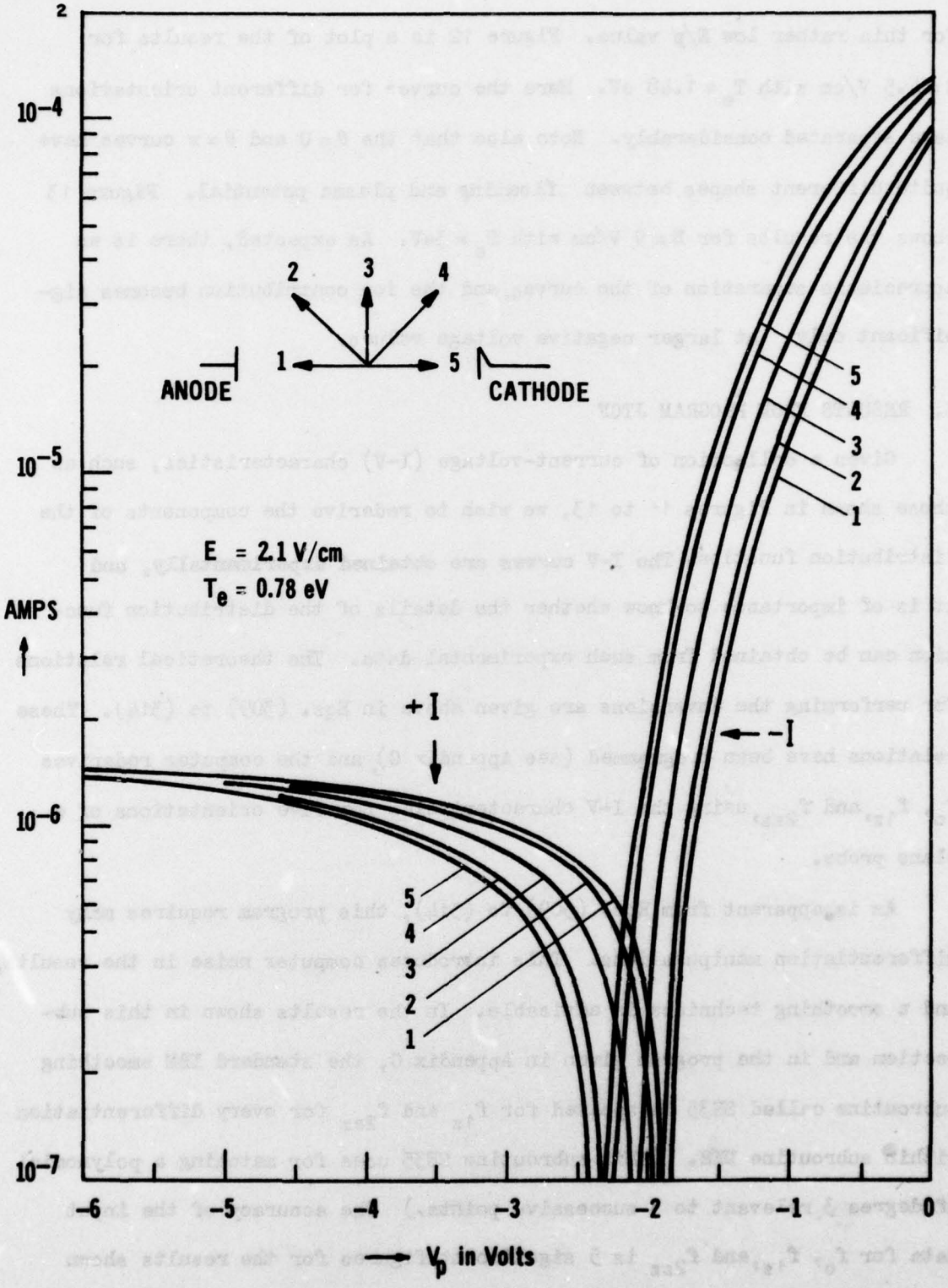

Figure 11. Current-Voltage Characteristics of a Plane Probe for Five Orientations when E = 2.1 V/cm, $\eta = 10^{-6}$ and p = 0.14 Torr in Nitrogen

for this rather low E/p value. Figure 12 is a plot of the results for $E = 4.5$ V/cm with $T_e = 1.48$ eV. Here the curves for different orientations have separated considerably. Note also that the $\theta = 0$ and $\theta = \pi$ curves have quite different shapes between floating and plasma potential. Figure 13 shows the results for $E = 9$ V/cm with $T_e = 3$eV. As expected, there is an appreciable separation of the curves, and the ion contribution becomes significant only at larger negative voltage values.

3. RESULTS FROM PROGRAM JTOF

Given a collection of current-voltage (I-V) characteristics, such as those shown in Figures 11 to 13, we wish to rederive the components of the distribution function. The I-V curves are obtained experimentally, and it is of importance to know whether the details of the distribution function can be obtained from such experimental data. The theoretical relations for performing the inversions are given above in Eqs. (309) to (314). These relations have been programmed (see Appendix C), and the computer rederives f_o, f_{1z}, and f_{2zz}, using the I-V characteristics for five orientations of a plane probe.

As is apparent from Eqs. (309) to (314), this program requires many differentiation manipulations. This introduces computer noise in the results, and a smoothing technique is advisable. In the results shown in this subsection and in the program given in Appendix C, the standard IBM smoothing subroutine called SE35 is applied for f_{1z} and f_{2zz} for every differentiation within subroutine DER. (This subroutine SE35 uses for matching a polynomial of degree 3 relevant to 5 successive points.) The accuracy of the input data for f_o, f_{1z}, and f_{2zz} is 5 significant figures for the results shown here.

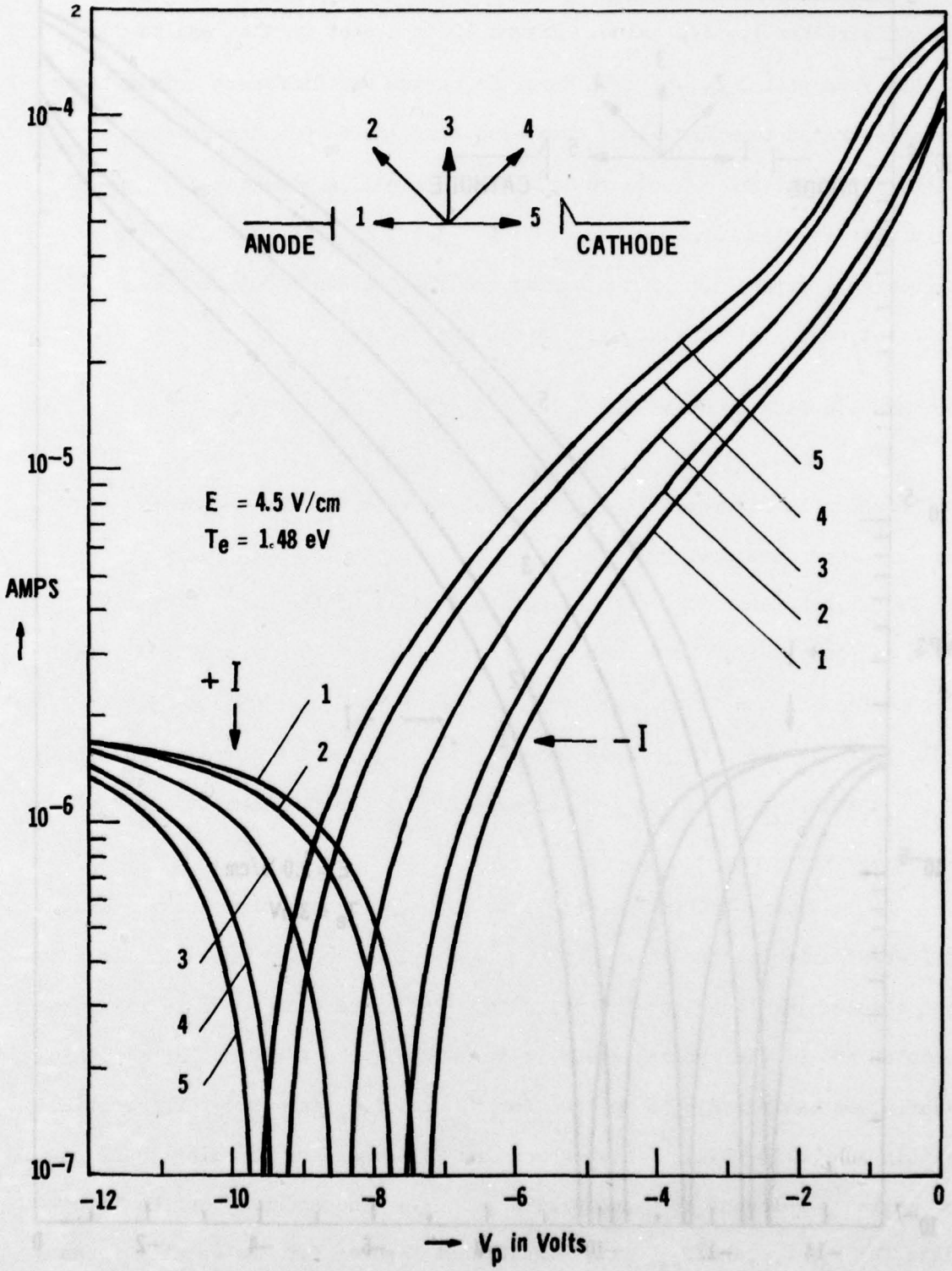

Figure 12. Current-Voltage Characteristics of a Plane Probe for Five Orientations when E = 4.5 V/cm, $\eta = 10^{-6}$ and p = 0.14 Torr in Nitrogen

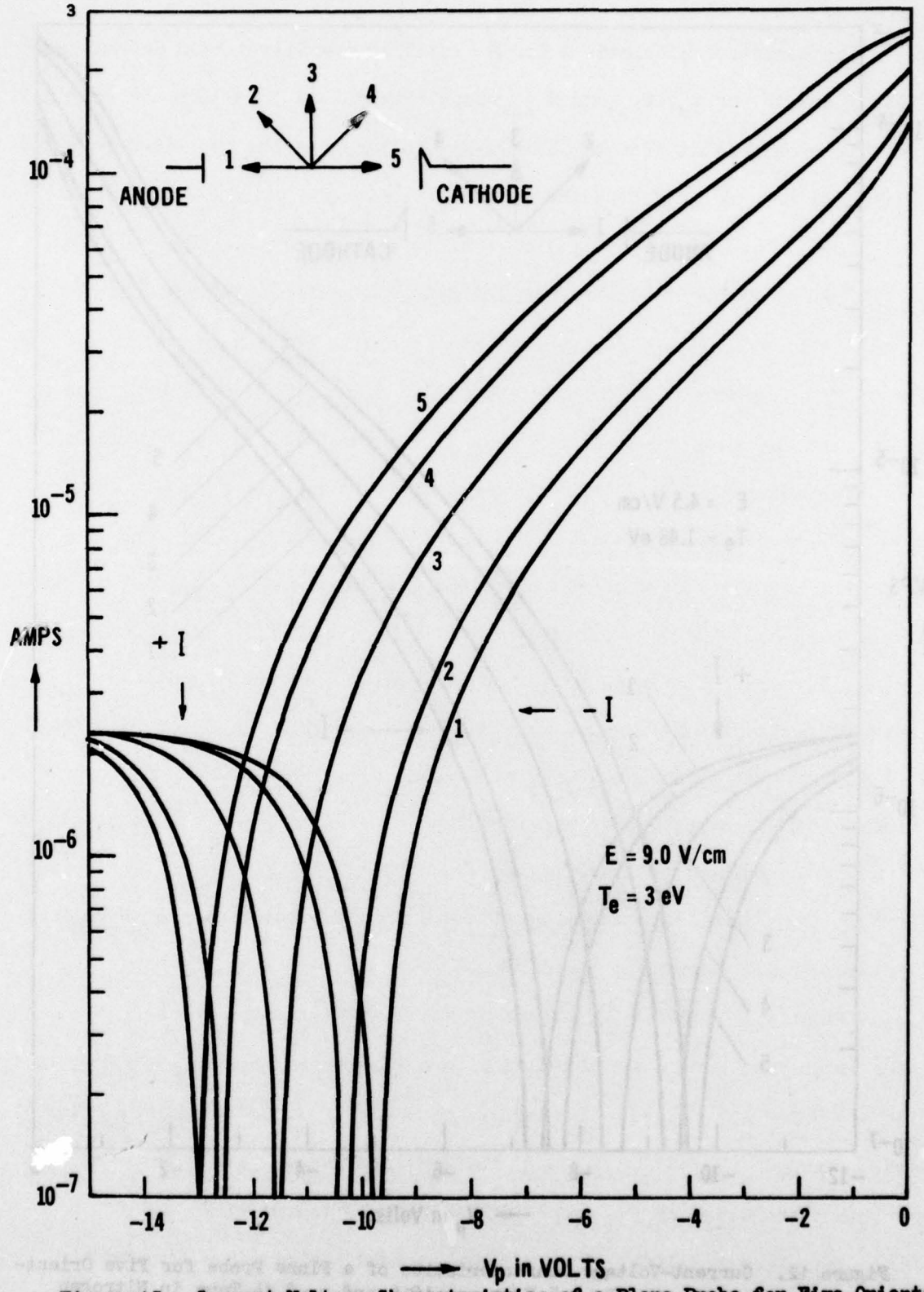

Figure 13. Current-Voltage Characteristics of a Plane Probe for Five Orientations when E = 9 V/cm, $\eta = 10^{-6}$ and p = 0.14 Torr in Nitrogen

The computer calculations for E = 2.1 V/cm are illustrated in Figures 14, 15, and 16 for f_o, f_{1z}, and f_{2zz}, respectively. We show both the original functions calculated from the Boltzmann equation and the rederived results, from the program JTOF, from the I-V characteristics. The I-V input data in Figure 11 are used from -0.1 V to -14.3 V in 0.1 V steps. We find that f_o, shown in Figure 14, is reproduced nearly exactly (to within 6%) with some deviation noticeable only near zero energy. The function $-f_{1z}$ in Figure 15 is reproduced properly around its maximum, but deviations appear near zero energy up to about 0.8 eV, and computer noise is evident at high energies above 3.8 eV. Similar remarks apply to f_{2zz} in Figure 16, but the deviations are more evident for both low and high energies.

The results for E = 4.5 V/cm are shown in Figures 17, 18, and 19. The input data use the I-V characteristics in Figure 12 from -0.1 V to -15 V in 0.1 V steps. In Figure 17, the rederived and original functions, f_o, show no noticeable difference throughout the energy range. The function, $-f_{1z}$, in Figure 18 deviates only at low energies below 0.8 eV, and some computer noise appears for energies above 10 eV. Near the maximum, only a slight difference occurs. On the other hand, stronger deviations appear for f_{2zz} in Figure 19, especially at low energies below 1 eV, and appreciable computer noise becomes apparent at 3.8 eV.

Finally, in Figures 20, 21, and 22 we show the results for E = 9 V/cm. The input data are those shown in Figure 13 with voltage varying from -0.1 to -15 V in 0.1 V steps. For this case, V_a is of the order of $eE\lambda_s$ near zero energy. ($V_a/eE\lambda_s \leq 0.1$ only for energies above 7 eV.) This is probably the cause of the errors in the deduced values of f_o and f_{1z} at the lower energy values. The rest of the curves above 4 eV follows the

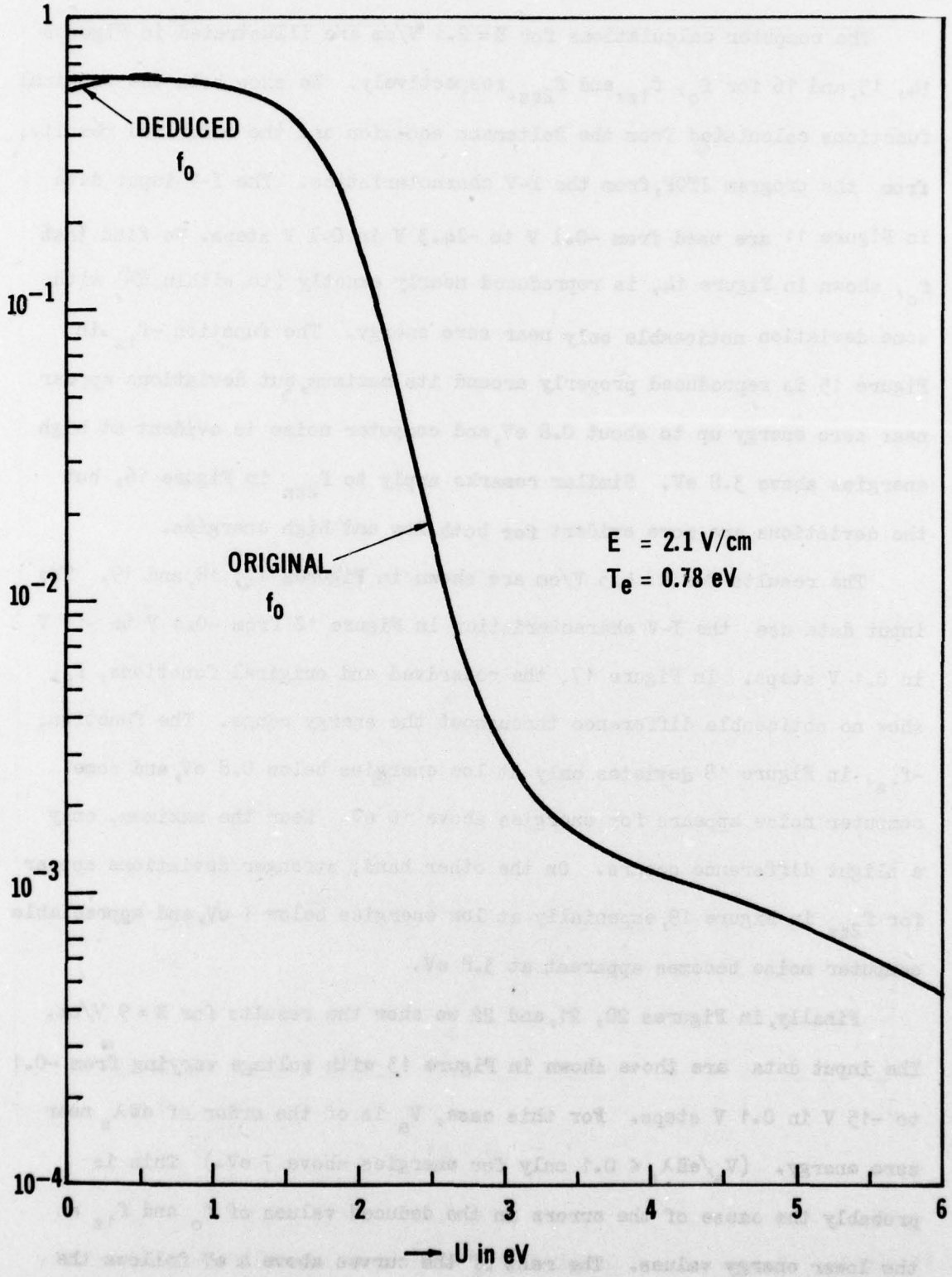

Figure 14. Comparison of Original f_o with that Deduced from Program JTOF when E = 2.1 V/cm

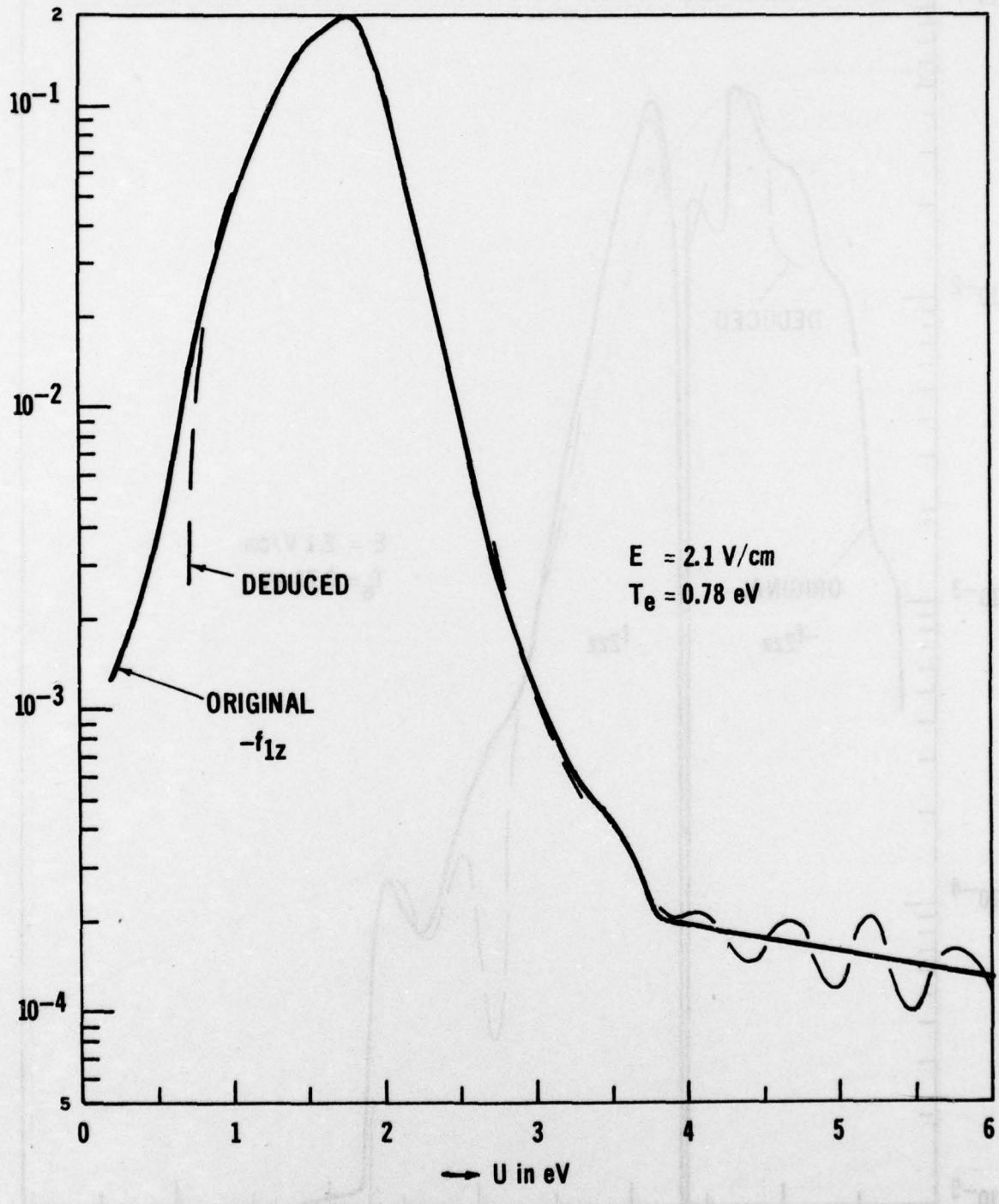

Figure 15. Comparison of Original f_{1z} with that Deduced from Program JTOF when E = 2.1 V/cm

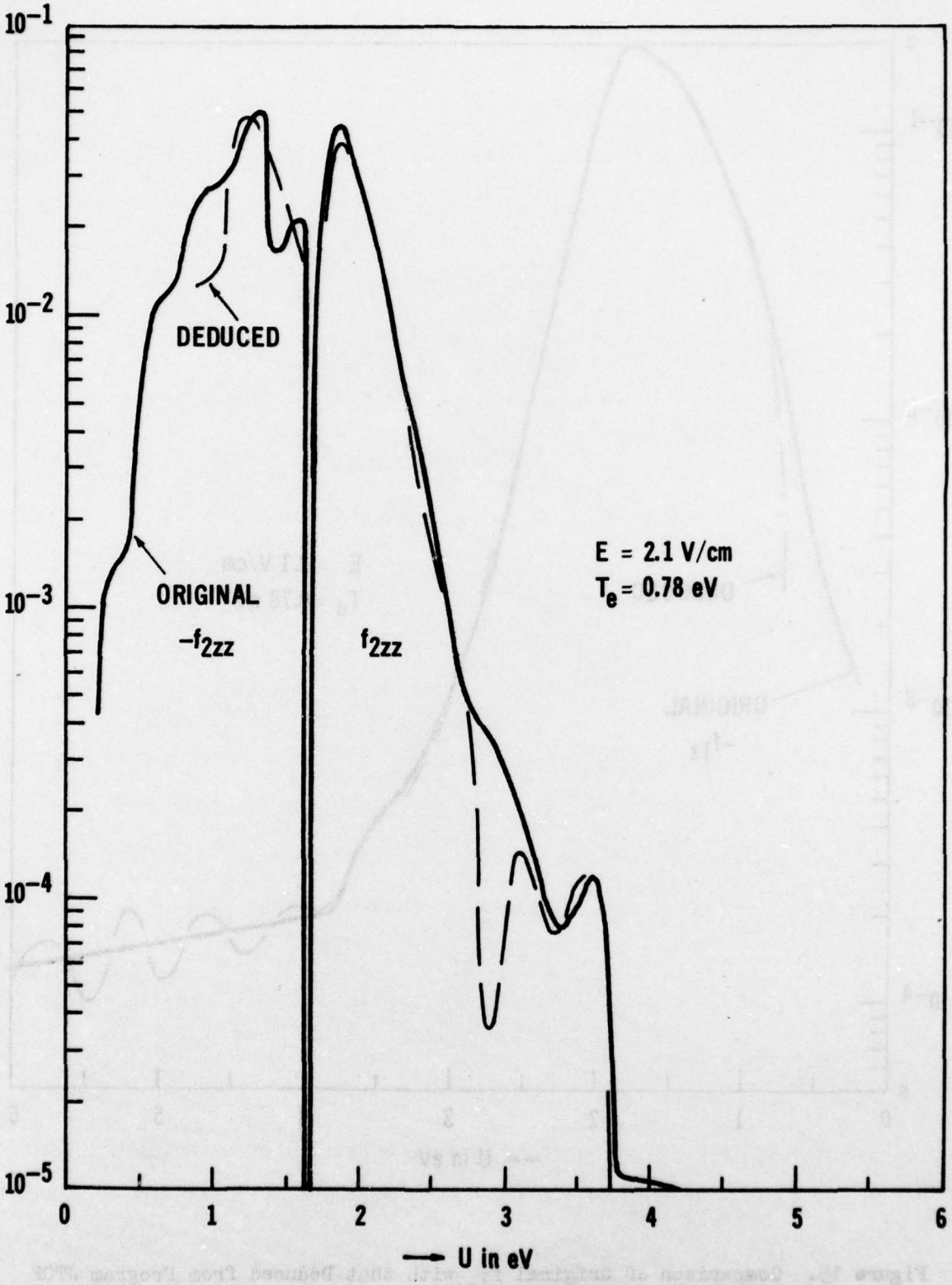

Figure 16. Comparison of Original f_{2zz} with that Deduced from Program JTOF when E = 2.1 V/cm

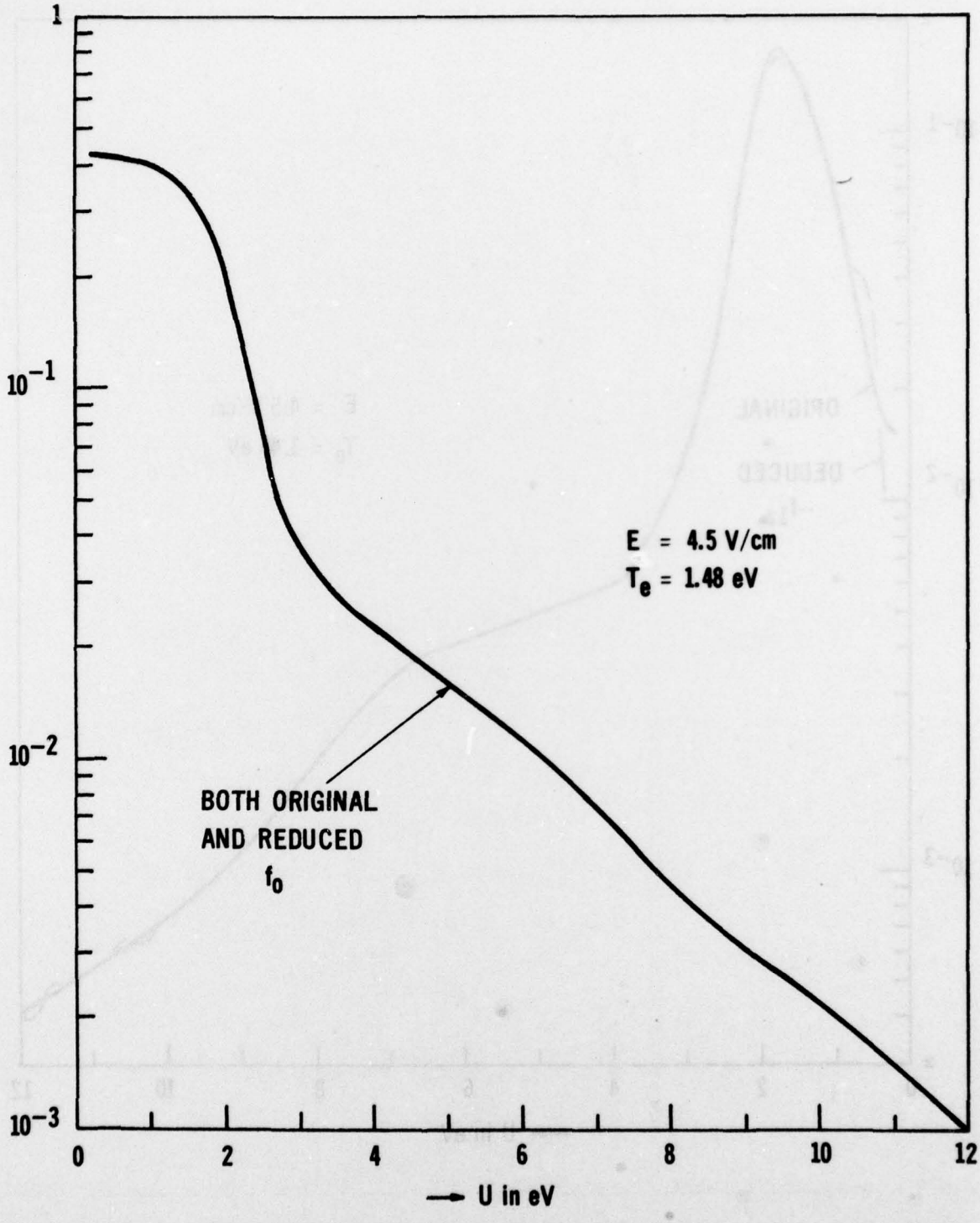

Figure 17. Agreement of Original f_o with that Deduced from Program JTOF when E = 4.5 V/cm

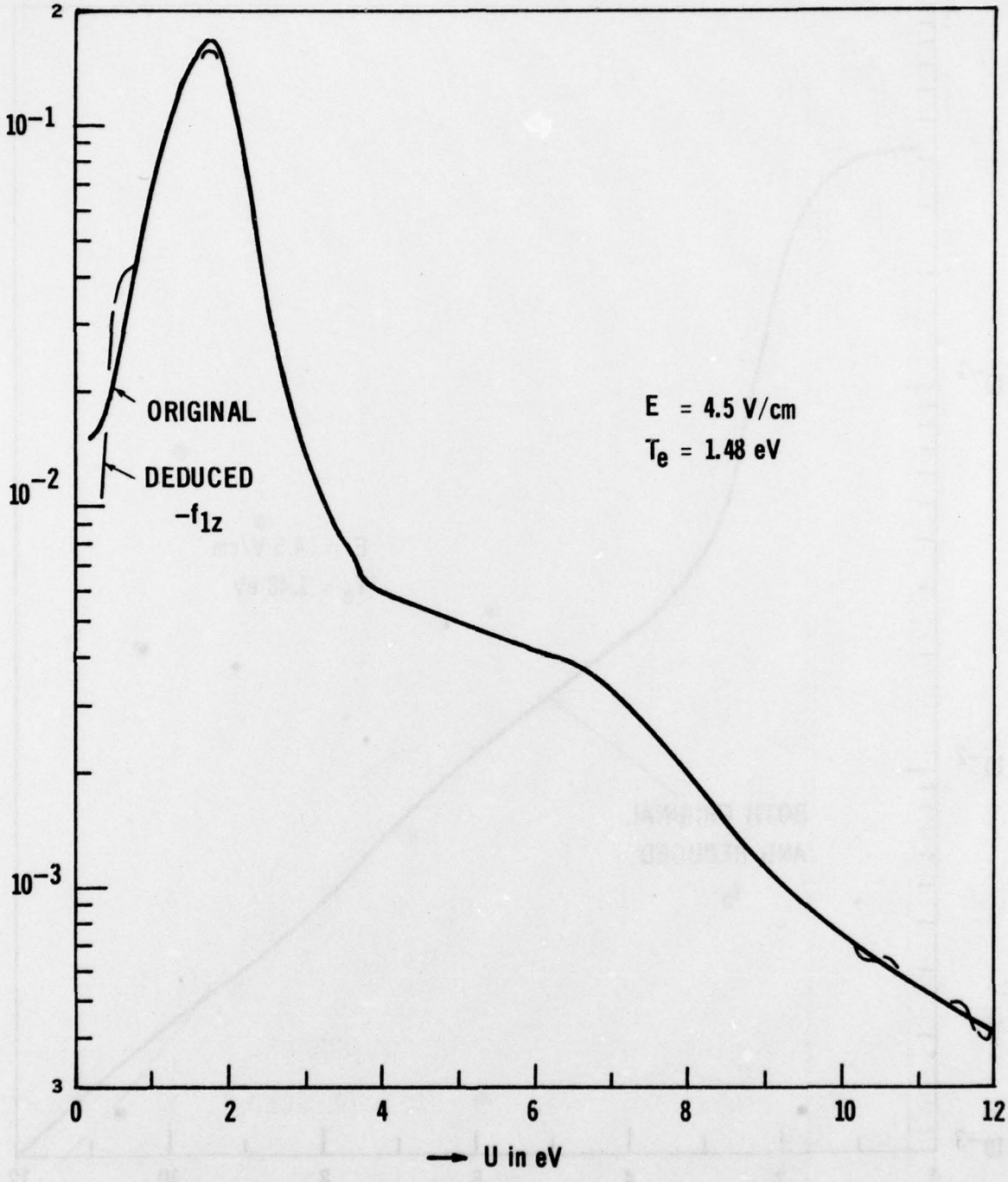

Figure 18. Comparison of Original f_{1z} with that Deduced from Program JTOF when E = 4.5 V/cm

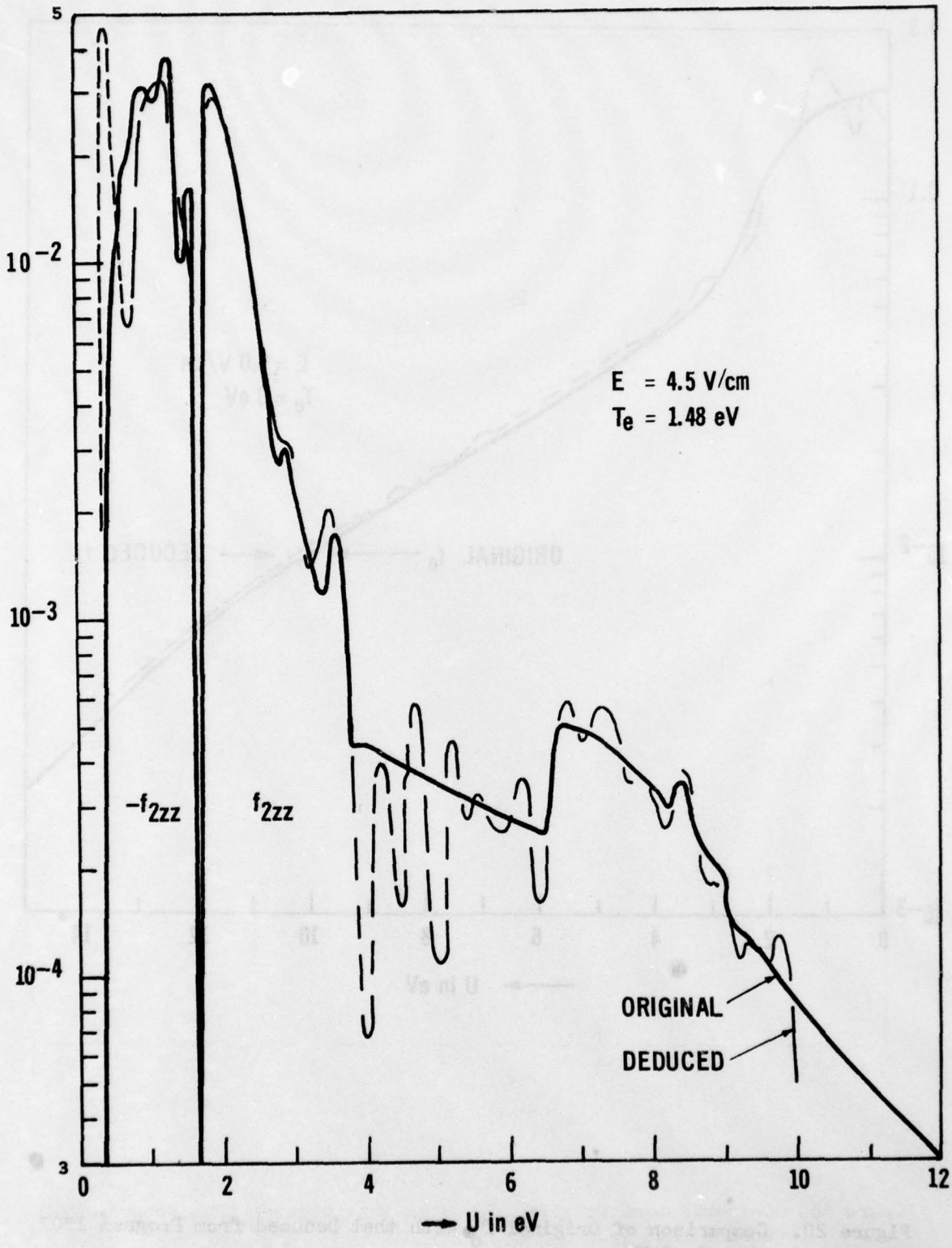

Figure 19. Comparison of Original f_{2zz} with that Deduced from Program JTOF when E = 4.5 V/cm

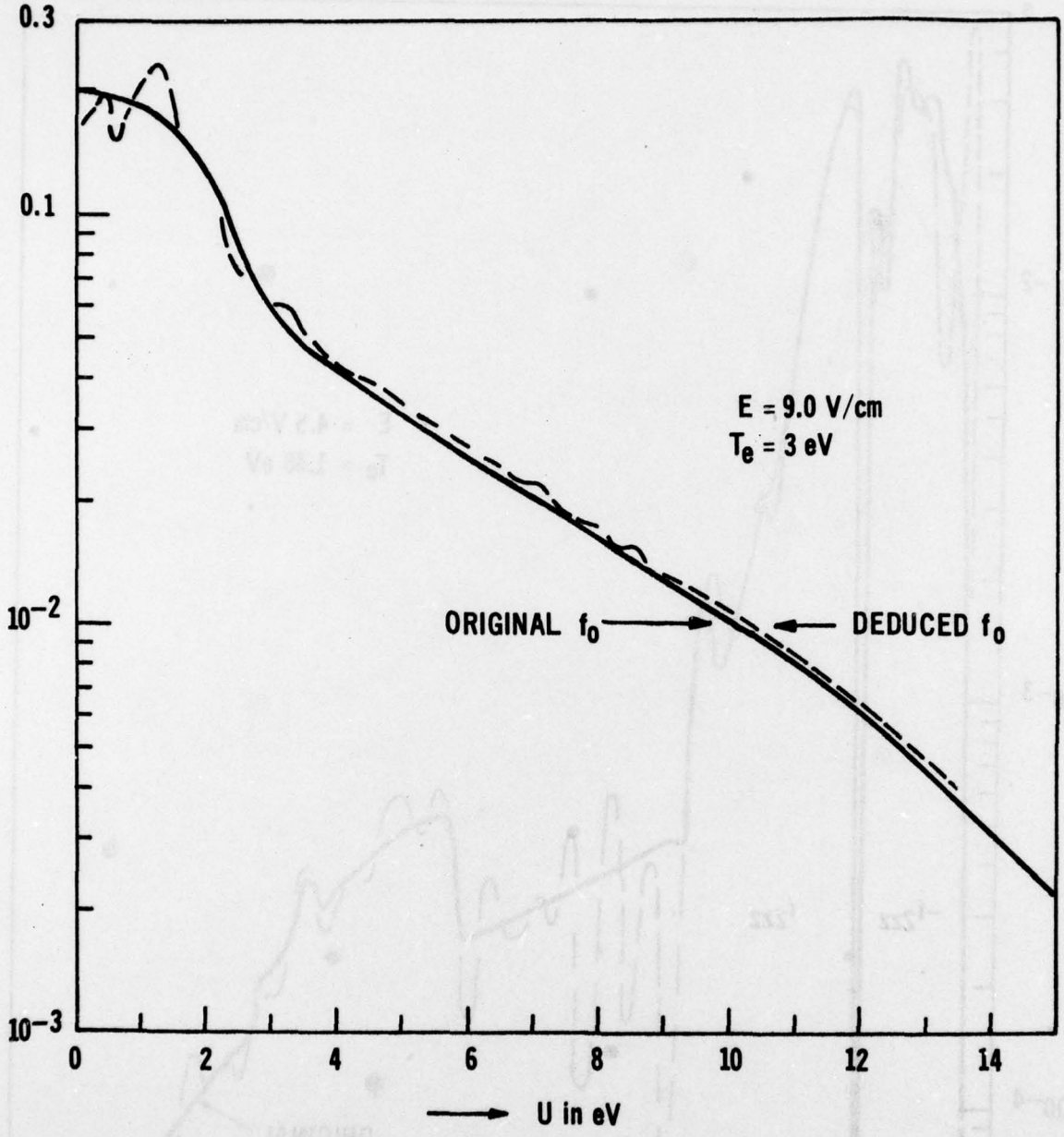

Figure 20. Comparison of Original f_o with that Deduced from Program JTOF when E = 9 V/cm

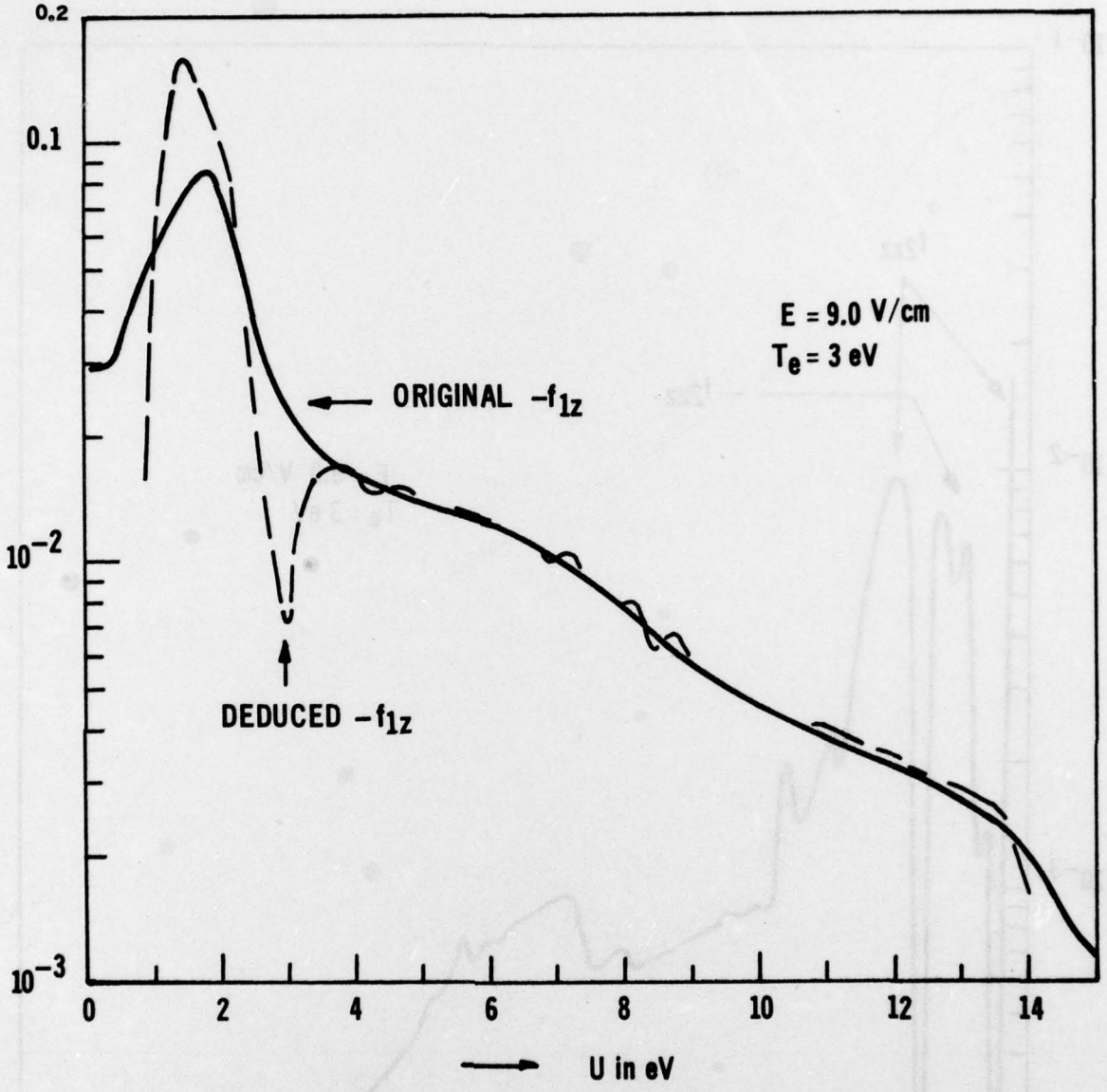

Figure 21. Comparison of Original f_{1z} with that Deduced from Program JTOF when E = 9 V/cm

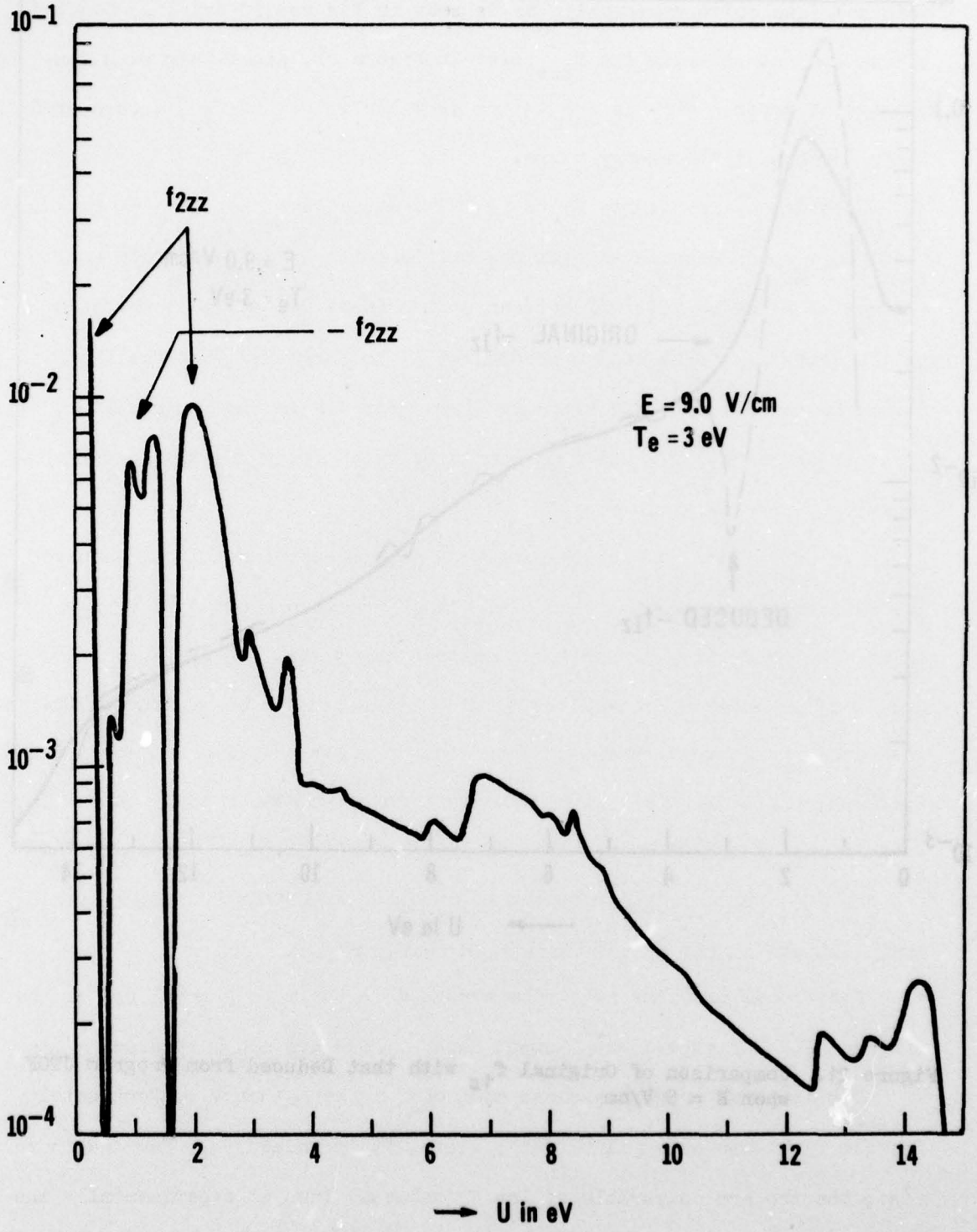

Figure 22. Original f_{2zz} when E = 9 V/cm

original data quite reasonably, as is seen in Figures 20 and 21. Deduced values are not shown in the f_{2zz} plot in Figure 22, since they were completely in error. This is due to the very low values of f_{2zz} as compared to f_o throughout the energy range.

Consider again Figures 14 to 19. The deviations near zero energy in these curves are associated with the difficulties in differentiation procedures when the ΔU interval between points (here 0.1 eV) is comparable to the energy, U. For better precision, it is suggested that the interval should be taken to be 0.01 eV up to 1 eV. For use in the program FTOJ, input values of f_o, f_{1z}, and f_{2zz} should be calculated from the Boltzmann equation with such a finer grid.

The deviations at higher energy are due to computer noise. Whenever the derived values of $|f_{1z}|$ and $|f_{2zz}|$ are less than about 1/20 of f_o, errors in computation can arise in calculating j_1 and j_2 (see Eqs. (313) and (314)). Large values of the total current have to be subtracted from each other for several probe orientations in order to yield the small differences, j_1 and j_2. This gives rise to error in addition to the noise which originates from subsequent differentiations. These wiggles in the f_{1z} and f_{2zz} curves could probably be smoothened further by additional manipulations acting only in this high energy regime.

Additional problems are to be expected in the more general use of the program JTOF for experimental input data. These are now discussed.

The computer program assumes that $eE\lambda_s$ is less than V_p. Fortunately for the first two cases illustrated above, it is indeed so. For the third case, the two are comparable at low V_p values. Thus, if experimentally the electric field is very strong ($E/p > 60$ V/cm-torr), large errors can be expected due to this cause.

The total current includes the ion current contribution. This contribution dominates at large negative voltages, and the electron part calculated from the total current will be subject to error. Thus, the distribution function components that can be deduced are limited at the high energy end (at several times thermal energy) due to this cause.

Experimental data from plane probes under certain circumstances do show[19] and under others do not show[20] clearly the break or discontinuity in the curves which is expected to occur at the plasma potential point. We note that Eqs. (310) and (311) require a knowledge of V_p with respect to plasma potential. Thus an error can arise if the exact plasma potential reference point has not been properly identified in the V_p input tabulated data.

4. SENSITIVITY OF RESULTS FROM PROGRAM JTOF TO INPUT DATA ACCURACY

Prior to the above calculations, we checked the sensitivity of the JTOF program to the accuracy of the input data. We inserted I-V characteristics with significant figures decreasing from 5 to 4 to 3 decimal places and checked the output results.

A different smoothing method is adopted for these results. The IBM subroutine SE13 is used to smoothen f_{1z} and f_{2zz}. In contrast to SE35, subroutine SE13 uses a polynomial of degree one relevant to three successive points. Smoothing is done both in the differentiation subroutine DER and at the end of the deduction of f_{1z} and f_{2zz}. This method was abandoned for the results shown in the previous subsection since it rounds off too much the regions around the maximum and it also decreases the height of the maximum, as is evident in the results presented below.

The results are illustrated in Figures 23, 24, and 25 for E = 2.1 V/cm. These calculations show that the accuracy of the input data can be reduced from 5 to 3 significant digits with no appreciable degradation of the accuracy around the maximum values, although the noise content at the higher energy values increases substantially.

In conclusion, we see that it is possible, by using numerical means, to diagnose the anisotropy of a plasma with an imposed external electric field, by using the experimental results measured with a plane probe. Also, there is room for improvement of the computer programs as indicated above.

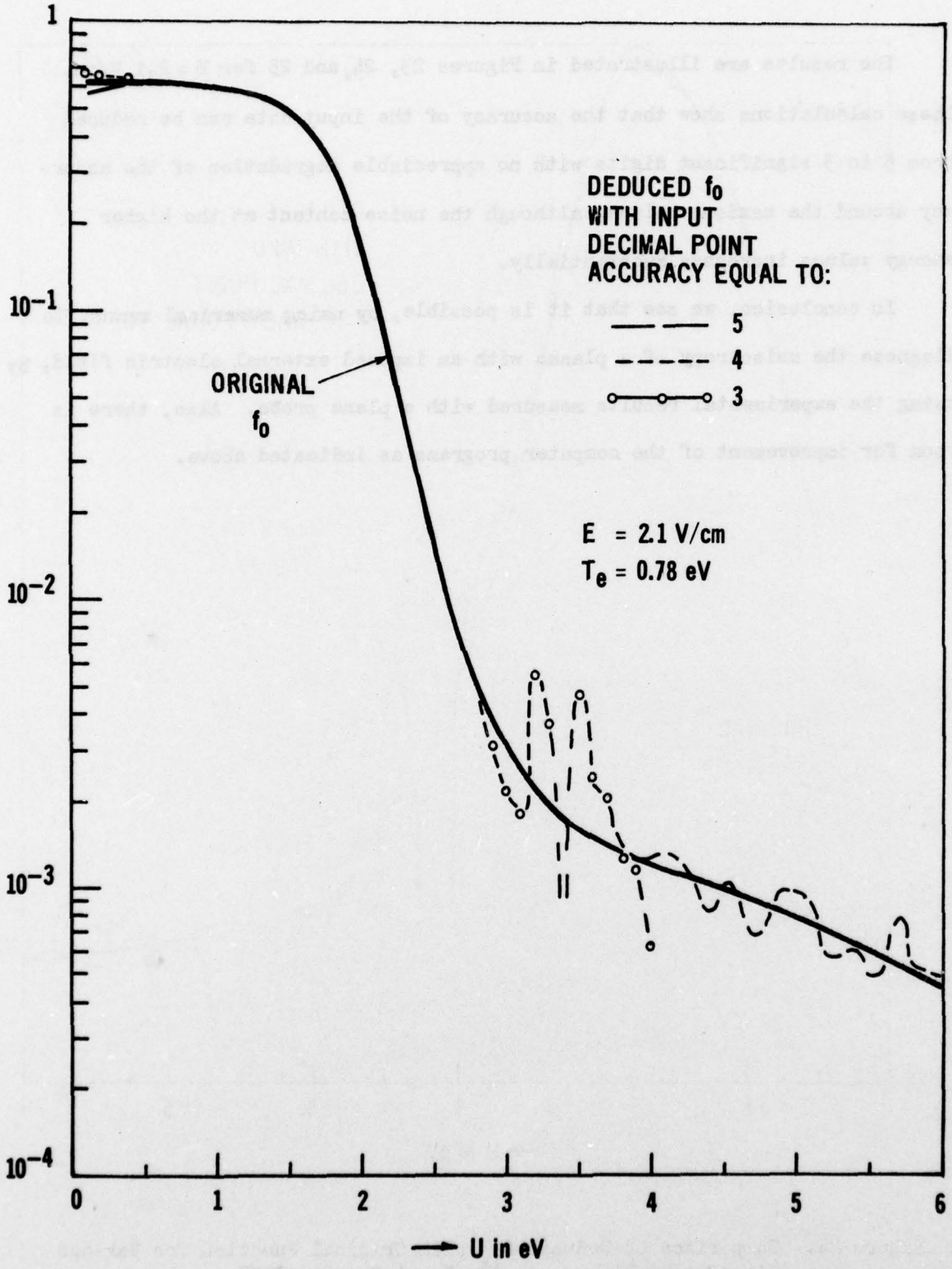

Figure 23. Comparison of Deduced f_o with Original Function for Various Significant Figures in the Input Data to JTOF

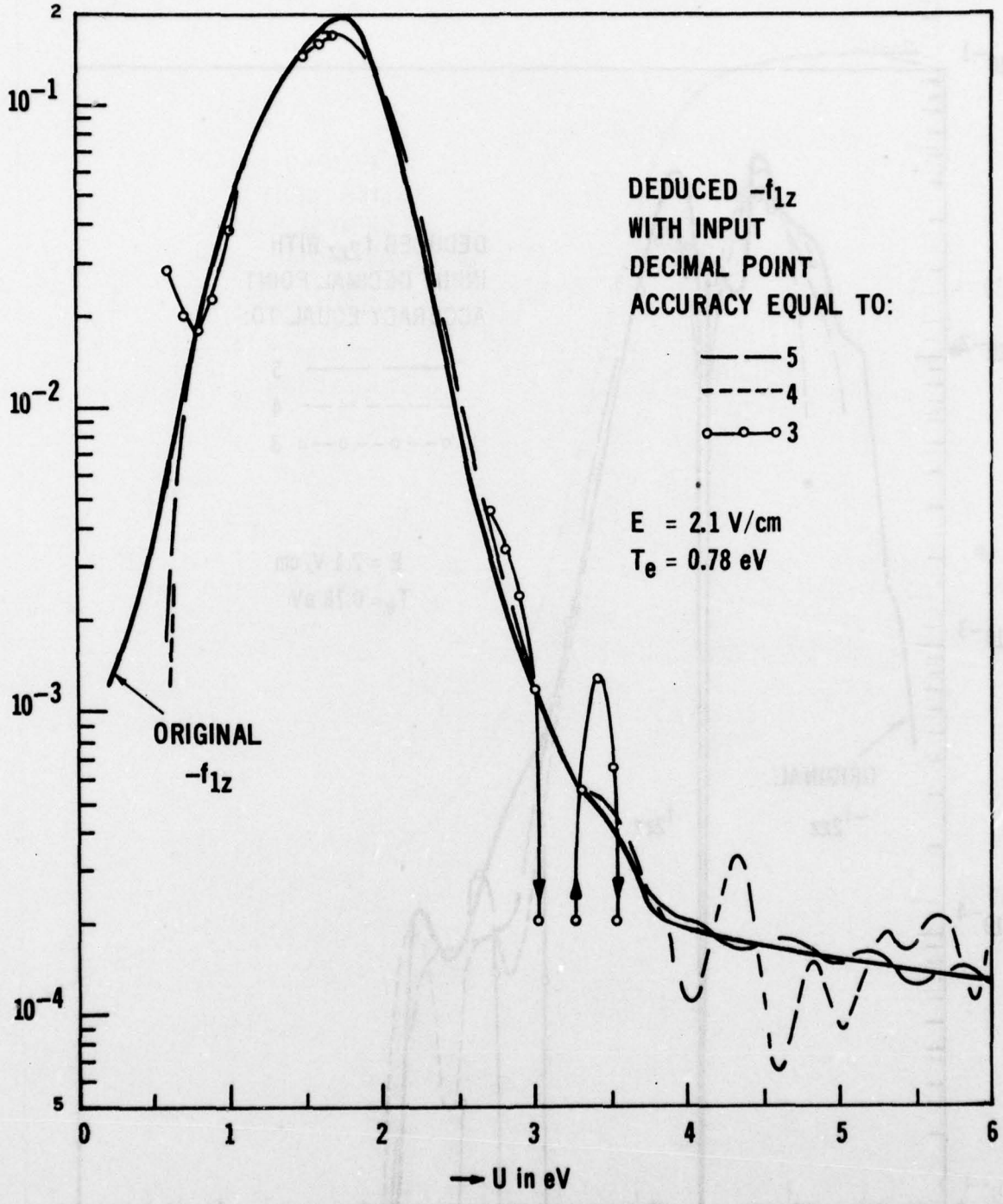

Figure 24. Comparison of Deduced f_{1z} with Original Function for Various Significant Figures in the Input Data to JTOF

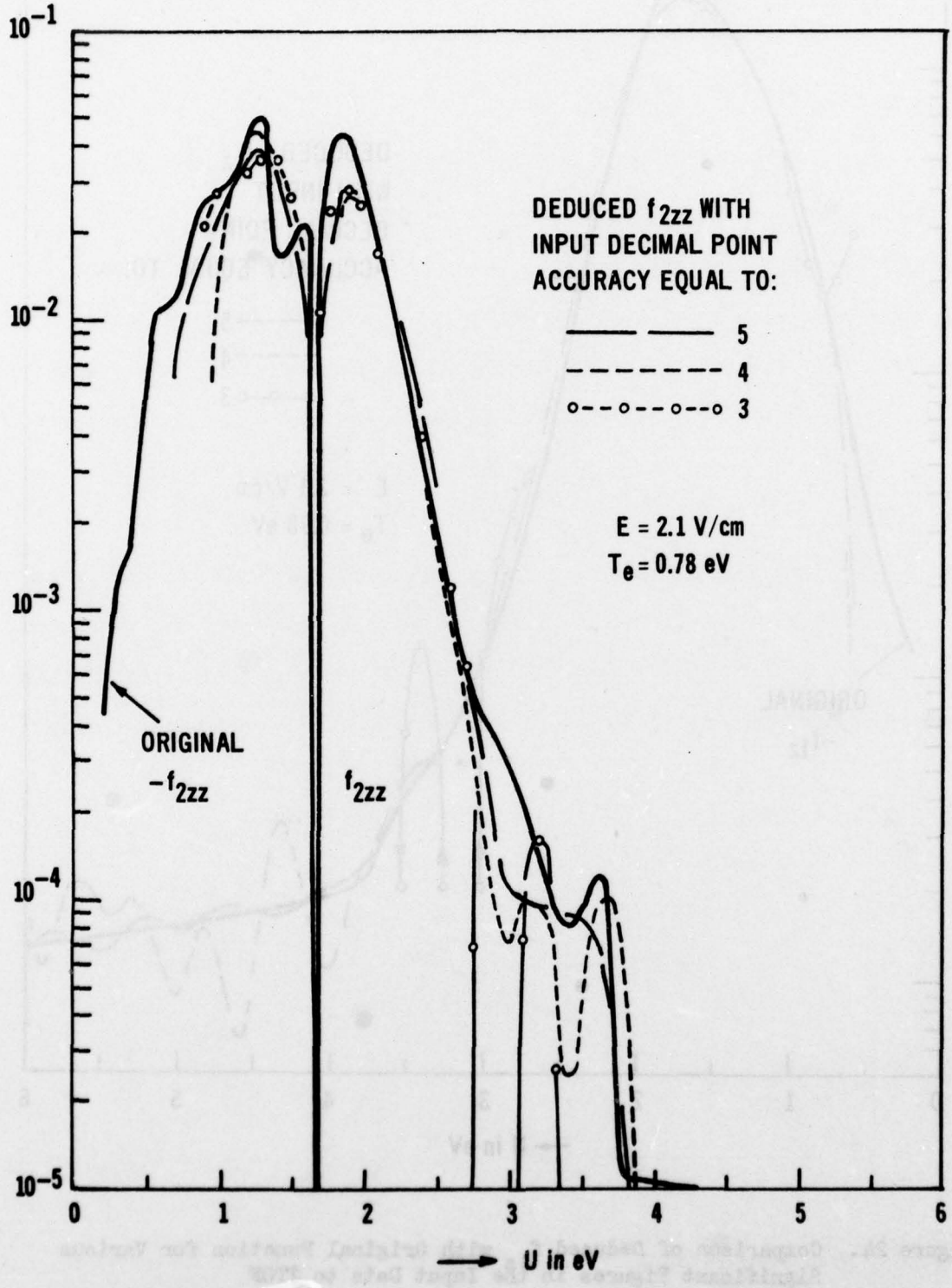

Figure 25. Comparison of Deduced f_{2zz} with Original Function for Various Significant Figures in the Input Data to JTOF

SECTION V

QUASICOLLISIONAL PROBE ANALYSIS

1. INTRODUCTION

The sheath surrounding an electrostatic probe becomes quasicollisional when the mean free path, l_c, is comparable to the probe radius, r_p. In Appendix B, we find that this occurs even at low pressures above 0.1 torr in nitrogen for probe sizes of the order of 1mm. Plasmas found in lasing media often fall into this regime. In the following, we discuss the quasi-collisional theory for the situation of a probe which is retarding electrons.

The different regimes that can occur are illustrated in Figure 26, which is a schematic diagram used by Wassertrom et al[24]. It can be seen from Appendix B (see Figure 31 there) for lower probe voltages that, as the pressure is increased from below 0.1 torr to about 40 torr, one passes from (a) region C with $l_c > r_p > \lambda_s$ through (b) region A with $r_p > l_c > \lambda_s$ and then to (c) region B or $r_p > \lambda_s > l_c$. Pure collisionless theory, as given in previous sections,

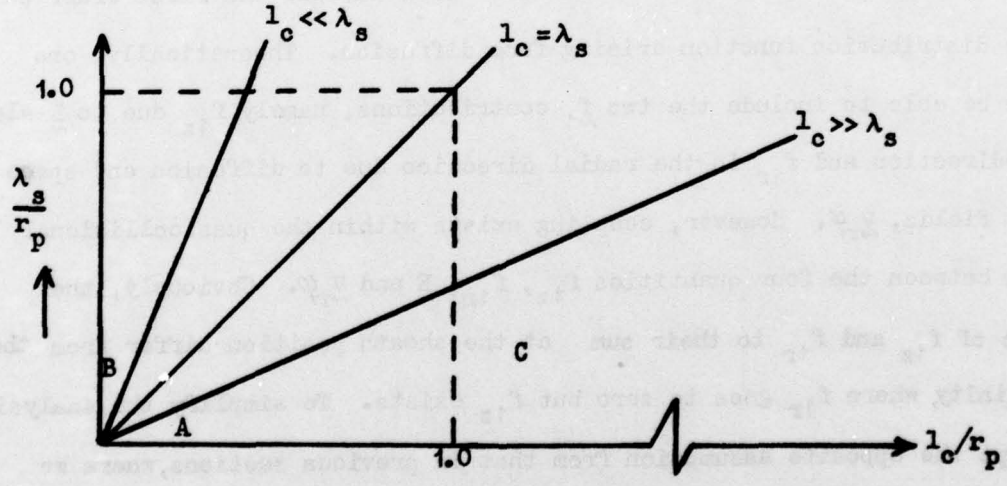

Figure 26. Mean Free Path, l_c, Versus Sheath Thickness, λ_s, Illustrating Various Regimes

strictly applies only if the conditions in region C are well satisfied. A quasicollisional situation applies in region A as well as in the transition from C to A. Region B is the continuum limit, where $\lambda_s >> l_c$, and a summary of relevant theories based on diffusion and mobility has been previously given by Johnston[25]. In this section, we consider region A, $r_p \geq l_c > \lambda_s$, and in the next section we consider region B, $r_p > \lambda_s > l_c$. In the former situation, we still use kinetic theory, and we discuss below the methods due to Swift[26] and Lukovnikov and Novgorodov[27]. In the second situation, the theory we discuss is based on a combination of free fall and continuum theories using the moment relations, following that given by Waymouth[28] and Wilkins and Katra[29]. For both situations, we provide new relations extending the works of the above authors.

We allow an arbitrary dependence for the zeroth order of the distribution function, f_o, but, in order to make the analysis less formidable, we do not include the first and second orders of anisotropy due to the external electric field. Instead, we provide new relations which include the first order part of the distribution function arising from diffusion. Theoretically, one should be able to include the two $\underset{\sim}{f}_1$ contributions, namely, f_{1z} due to $\underset{\sim}{E}$ along the z-direction and f_{1r} in the radial direction due to diffusion and space charge fields, $\underset{\sim}{\nabla}_r\varphi$. However, coupling exists within the quasicollisional sheath between the four quantities f_{1z}, f_{1r}, $\underset{\sim}{E}$ and $\underset{\sim}{\nabla}_r\varphi$. Obviously, the ratios of f_{1z} and f_{1r} to their sum at the sheath position differ from those at infinity, where f_{1r} goes to zero but f_{1z} exists. To simplify the analysis, we adopt the opposite assumption from that in previous sections, where we associated $\underset{\sim}{f}_1$ with f_{1z}, and we associate $\underset{\sim}{f}_1$ with f_{1r} only in the following work.

2. APPROACHES BASED ON ANALYSES OF SWIFT AND LUKOVNIKOV

When $l_c \lesssim r_p$, the electron diffusion rate is not high enough to compensate for the drain of electrons from the plasma to the probe. Thus f_o at infinity differs from f_o^s at the collisionless sheath edge. Furthermore, the drain of particles causes the distribution function to become anisotropic.

Assume for the moment that the distribution function at the sheath position is isotropic, so that only the f_o^s part is of importance. (This is modified in the next subsection.) At the sheath position, we can apply Eqs. (134), (136), and (139) (essentially the same result for all three respective geometries - plane, sphere, and cylinder) to yield the incremental current, dI, to the probe associated with the energy interval, dU, namely,

$$dI = AK_o(U - V_p)[f_o^s(U)dU] \tag{316}$$

where A is the area of the probe and $K_o = 2\pi e/m^2$. This equation applies only within the collisionless part of the sheath. We are free to choose f_o^s at any position within the collisionless region provided we interpret V_p as measured with respect to V_s (the potential due to the probe) at the same position. We choose this position to be the furthest possible, namely, at a distance of one mean free path, l_c, from the probe surface.

The current reaching the probe is controlled by diffusion from the outside medium through the quasicollisional part of the sheath. The procedure is to calculate in this region f_o^s and relate it to f_o at infinity, which is then substituted into Eq. (316). A basic assumption used in this section is that the diffusion process is free rather than ambipolar. This

allows us to omit ion and space charge effects, but this applies only for very large ratios of electron to ion temperature, i.e., $T_e/T_+ >> 1$. For any point r within the quasicollisional sheath, which is at least one mean free path from the probe, kinetic theory[1] gives

$$f_{1r} = - l_c \partial f_o / \partial r \tag{317}$$

where f_{1r} is the anisotropic part of the distribution function due to diffusion. The mean free path is given by

$$l_c = v/\nu_1 = (2U/m)^{\frac{1}{2}}/\nu_1 \tag{318}$$

where ν_1 is the electron collision frequency for momentum transfer, $U = mv^2/2$ is the electron kinetic energy, and v is its speed. The incremental diffusion current due to f_{1r} is

$$\frac{dI}{A_r} = - \frac{4\pi e}{3} f_{1r} v^3 dv = \frac{8\pi e l_c U}{3m^2} \frac{\partial [f_o dU]}{\partial r} \tag{319}$$

where e is the magnitude of the electron charge and A_r is the sheath area at position r through which the charge is passing.

We now have to specify the geometry, and we consider, consecutively, the one-sided plane, sphere, and cylinder. The spherical case has been analyzed by Swift[26] and the cylindrical case by Lukovnikov and Novgorodov[27]. (Note that Lukovnikov's f_o is equal to our $f_o 2\pi (2e/m)^{3/2}/n_e$ and Swift's f_o is equal to our $f_o 4\pi (2eU)^{\frac{1}{2}}/m^{3/2}$.)

It is difficult to specify a normalizing area A_r to give the current sufficiently far away from the one sided probe of radius r_p. For distances in the normal direction, Z, less than r_p, a reasonable approximation is $A_r = \pi (r_p^2 + Z^2)$. Thus Eq. (319) becomes

$$dI = \frac{8\pi e l_c U}{3m^2} \frac{\partial}{\partial Z} (f_o dU)\pi(r_p^2 + Z^2) \tag{320}$$

Since dI doesn't change with Z, we can integrate over Z from the start of the quasicollisional sheath, $Z = l_c$, where $f = f_o^s$, to $Z = r_p$ (if $l_c \leq r_p$), where $f = f_o$, its value within the ambient plasma. We obtain from Eq. (320)

$$f_o^s dU = f_o dU - \frac{dI\, 3m^2}{32\pi e l_c r_p U} \left(1 - \frac{4}{\pi} \tan^{-1} \frac{l_c}{r_p}\right) \tag{321}$$

We can now substitute this into Eq. (316). Note that $A = \pi r_p^2$ and $K_o = 2\pi e/m^2$. Solving for dI and integrating from V_p to ∞ finally yield

$$I = AK_o \int_{V_p}^{\infty} \frac{(U - V_p) f_o dU}{1 + \frac{3\pi r_p}{16 l_c}\left(1 - \frac{V_p}{U}\right)\left(1 - \frac{4}{\pi} \tan^{-1} \frac{l_c}{r_p}\right)} \tag{322}$$

Since we assumed $l_c \leq r_p$, this relation is not valid if $l_c > r_p$, but nonetheless the correction term in the denominator goes to zero for $l_c >> r_p$. The $\tan^{-1}$ term is usually negligible for $r_p >> l_c$. For a probe with a guard ring having an overall radius equal to R_p, one has to change the ratio l_c/r_p to l_c/R_p in the denomenator but leave $A = \pi r_p^2$ the same.

The spherical probe is simple to analyze. Here, $A_r = 4\pi r^2$, where r is radial distance from the center of the probe. Thus,

$$dI = \frac{8\pi e l_c U}{3m^2} \frac{\partial}{\partial r} (f_o dU)\, 4\pi r^2 \tag{323}$$

Integration from $r = r_p + l_c$, where $f_o = f_o^s$, to infinity, where f_o is its value, gives

$$f_o^s dU = f_o dU - \frac{dI 3m^2}{32\pi^2 e l_c (r_p + l_c)} \tag{324}$$

We substitute this expression into Eq.(316) and note that $A = 4\pi r_p^2$. Integrating

from V_p to ∞ yields

$$I = AK_o \int_{V_p}^{\infty} \frac{(U - V_p) f_o \, dU}{1 + \frac{3}{4} \frac{r_p^2}{l_c (r_p + l_c)} \left(1 - \frac{V_p}{U}\right)} \tag{325}$$

This is the result given by Swift[26].

Consider now the cylindrical case. Lukovnikov and Novgorodov[27] take the normalizing area as $A_r = 2\pi r L(1 + 2r/L)$, where r is radial distance from the cylindrical axis and L is the length of the cylinder ($L >> r$). The factor $(1 + 2r/L)$ allows for end effect corrections. Consequently, we have

$$dI = \frac{8\pi e l_c U}{3m^2} \frac{\partial}{\partial r} (f_o \, dU) 2\pi r L \left(1 + \frac{2r}{L}\right) \tag{326}$$

Integrating from $r = r_p + l_c$ to ∞ and equating f_o^s to the value of f_o at $r_p + l_c$ give

$$f_o^s dU = f_o dU - \frac{dI}{16\pi^2 e l_c L U} \frac{3m^2}{} \ln \left(1 + \frac{L}{2(r_p + l_c)}\right) \tag{327}$$

Lukovnikov and Novgorodov omit the l_c part in the ln term, assuming that $l_c < r_p$. We again substitute this expression into Eq. (316) with $A = 2\pi r_p L$ and obtain the result

$$I = AK_o \int_{V_p}^{\infty} \frac{(U - V_p) f_o \, dU}{1 + \frac{3}{4} \frac{r_p}{l_c} \left(1 - \frac{V_p}{U}\right) \ln \left(1 + \frac{L}{2(r_p + l_c)}\right)} \tag{328}$$

This result differs from Lukovnikov and Novgorodov by a factor $(r_p/r_s)(1+2r_s/L)$ both in A and in the second term in the denominator. The $(1 + 2r_s/L)$ factor can be accounted for by allowing for edge effects, which modifies A to $A = 2\pi r_p L(1 + 2r_s/L)$. In any case this correction is negligible since $2r_s << L$. Their r_p/r_s factor, however, seems to be a mistake and stems from the fact that in their calculation of Eq.(316), which is the same as Eq. (87) in Section II,

they have omitted the I_b contribution in Eq. (86) and have used only the I_a contribution to I, which gives a r_p/r_s factor in front. We also wish to mention that taking the limit to cylindrical geometry from an ellipsoidal geometry provides the slightly different expression, $A_r = 2\pi rL(1 + 4r/\pi L)$. Redoing the above analysis yields **the same expressions as above but** with the factor $\frac{1}{2}$ in the logarithm replaced by $\pi/4$. This is a negligible correction, but it is adopted below.

Summarizing, we can write

$$f_o^s dU = f_o dU - dI\psi/2UAK_o \tag{329}$$

$$\frac{I}{AK_o} = \int_{V_p}^{\infty} \frac{(U - V_p) f_o dU}{1 + \frac{\psi}{2}\left(1 - \frac{V_p}{U}\right)} \tag{330}$$

where

for a plane
$$\psi = \frac{3\pi r_p}{8l_c}\left(1 - \frac{4}{\pi}\tan^{-1}\frac{l_c}{r_p}\right), \quad l_c \leq r_p \tag{331}$$

for a sphere
$$\psi = \frac{3r_p}{2l_c(1 + l_c/r_p)} \tag{332}$$

and for a cylinder
$$\psi = \frac{3r_p}{2l_c} \ln\left[1 + \frac{\pi L}{4(r_p + l_c)}\right] \tag{333}$$

We note that for the sphere and cylinder, ψ goes to zero when $l_c >> r_p$, which is the collisionless limit.

We can also investigate the task of deriving f_o from the current. We assume a constant mean free path, viz., l_c independent of U. Differentiating Eq. (330) twice with respect to V_p yields

$$\frac{d^2 I/dV_p^2}{AK_o} = f_o(V_p)[1 - \Gamma\psi] \tag{334}$$

where

$$\Gamma = \frac{1}{f_o(V_p)} \int_{V_p}^{\infty} \frac{U^{-1} f_o(U) dU}{\left[1 + \frac{\psi}{2}\left(1 - \frac{V_p}{U}\right)\right]^3} \tag{335}$$

An iteration process can now be used to derive the correct f_o from d^2I/dV_p^2.

It is normally assumed that the space potential is obtained from either the discontinuity or zero value of d^2I/dV_p^2. Equation (334), however, indicates that caution is necessary since the plasma potential can be incorrectly associated with the point $\Gamma\psi = 1$.

3. MODIFIED APPROACH

The above theory is subject to two basic assumptions, mentioned in the previous subsection. First, the space charge potential and ambipolar diffusion effects are omitted in favor of free electron diffusion. Secondly, f_o^s is assumed isotropic. The first assumption on free diffusion is valid (see Section VI, where we do not make this approximation) only if

$$T_e/T_+ \gg 1 \quad \text{and} \quad T_e/T_+ \gg I_+ D_e / I_e D_+ \tag{336}$$

where T_+, I_+, and D_+ are the respective ion temperature, probe current magnitude, and diffusion coefficient and T_e, I_e, and D_e are the corresponding quantities for electrons. Admittedly, this may be difficult to satisfy. The second condition, that f_o^s be isotropic, is contradictory to the basic concept of a diffusion process from the plasma caused by f_{1r} due to gradients in f_o. This anisotropic part exists even if we omit f_{1z} and f_{2zz} due to an external electric field. Below we correct the previous analysis to include the f_{1r} contribution.

A radial f_{1r}^s at the sheath position in addition to f_o^s gives rise to contributions to the current increment through the collisionless

sheath edge. Generally we can write

$$\frac{dI}{AK_o} = (U - V_p)f_o^s dU - \frac{2}{3} U\, H(U) f_{1r}^s dU \tag{337}$$

Equation (12) gives for a plane probe

$$H(U) = 1 - (V_p/U)^{3/2} \tag{338}$$

For a sphere, we note that f_{1r} is in the radial direction, independent of θ and ϕ, in contrast to f_{1z}, which is in the z-direction and which integrated to zero over a spherical area. Thus, combining the respective relations in Eqs. (164) and (165) with $V_a = 0$ gives for a sphere

$$H(U) = \frac{r_s^2}{r_p^2}\left\{1 - \left[1 - \frac{r_p^2}{r_s^2} + \frac{r_p^2}{r_s^2}\frac{V_p}{U}\right]^{3/2}\right\} \tag{339}$$

Similarly for a cylinder, we adopt Eqs. (207) and (215) with $V_a = 0$, namely,

$$H(U) = \frac{r_s}{r_p}\left\{1 - \frac{2}{\pi}\left[\frac{(\gamma+1)^{\frac{1}{2}}(\gamma-\beta)}{\beta^{\frac{1}{2}}(\beta+1)} G(k_o) + \frac{\gamma}{\beta^{\frac{1}{2}}(\gamma+1)^{\frac{1}{2}}} \Pi\,(\alpha_o^2, k_o)\right]\right\} \tag{340}$$

where

$$\beta = \frac{r_p^2}{r_s^2 - r_p^2}\,, \quad \gamma = \beta\,\frac{V_p}{U}\,, \quad k_o = \left[\frac{\beta-\gamma}{\beta(\gamma+1)}\right]^{\frac{1}{2}}, \text{ and } \alpha_o = \frac{1}{(\gamma+1)^{\frac{1}{2}}}\,.$$

Also $G(k_o)$ and $\Pi(\alpha_o^2, k_o)$ are the complete elliptic functions of the second and third kind, respectively. As previously, we associate r_s with a distance one mean free path away from the probe surface, $r_s = r_p + l_c$, and also V_p is measured with respect to the potential at r_s.

For later use, the following limits are given. When $l_c \ll r_p$ or $r_s \approx r_p$ or $\beta \gg 1$, the three relations, Eqs. (338) to (340), reduce to the same limit, namely,

$$H(U) = 1 - (V_p/U)^{3/2} \tag{341}$$

When $l_c >> r_p$ or $r_s >> r_p$ or $\beta << 1$, we obtain the following limits from the three equations:

for a plane $$H(U) = 1 - (V_p/U)^{3/2} \tag{342}$$

for a sphere $$H(U) = (3/2)(1 - V_p/U) \tag{343}$$

for a cylinder $$H(U) = (2/\pi)[(2 - V_p/U)G(k_o) - (V_p/U)K(k_o)] \tag{344}$$

where $K(k_o)$ is the complete elliptic function of the first kind and $k_o \approx (1-V_p/U)^{\frac{1}{2}}$. Thus, in both limits, H(U) becomes independent of r_s/r_p.

We match at r_s the value of f_{1r}^s to its value obtained from quasicollisional theory. We note from Eqs. (317) and (319) that

$$f_{1r}^s dU = -l_c \frac{\partial}{\partial r}(f_o^s dU) = -\frac{3m^2 dI}{A_r^s 8\pi e U} = -\frac{3dI}{4K_o A_r^s U} \tag{345}$$

where for a plane $$A_r^s = \pi(r_p^2 + l_c^2) = A(1 + l_c^2/r_p^2) \tag{346}$$

for a sphere $$A_r^s = 4\pi(r_p + l_c)^2 = A(1 + l_c/r_p)^2 \tag{347}$$

for a cylinder $$A_r^s = 2\pi(r_p + l_c)L\left(1 + \frac{2(r_p + l_c)}{L}\right) \approx A(1 + l_c/r_p) \tag{348}$$

where A is the area of the particular probe. Matching the two f_{ir}^s and using Eq. (299) for $f_o^s dU$ yield after substitution into Eq. (337)

$$\frac{dI}{AK_o} = (U - V_p)\left[f_o dU - \frac{dI\psi}{2UAK_o}\right] + \frac{dI\, H(U)}{2A_r^s K_o} \tag{349}$$

Collecting terms and integrating from V_p to ∞ yield with $\zeta \equiv A/A_r^s$

$$I = AK_o \int_{V_p}^{\infty} \frac{(U - V_p) f_o dU}{1 + \frac{\psi}{2}\left(1 - \frac{V_p}{U}\right) - \frac{\zeta}{2} H(U)} \tag{350}$$

where for a plane $$\zeta = (1 + l_c^2/r_p^2)^{-1} \tag{351}$$

for a sphere $$\zeta = (1 + l_c/r_p)^{-2} \tag{352}$$

for a cylinder $$\zeta = (1 + l_c/r_p)^{-1} \tag{353}$$

and the corresponding ψ values are given in Eqs. (331) to (333).

If we substitute dI from Eq. (349) into Eqs. (329) and (345) for f_o^s and f_{1r}^s, respectively, we also obtain the relationships of these quantities to f_o at infinity. These are

$$f_o^s dU = f_o dU - \frac{dI\psi}{2UAK_o} = f_o dU \left[\frac{1 - \frac{\zeta}{2} H(U)}{1 + \frac{\psi}{2}\left(1 - \frac{V_p}{U}\right) - \frac{\zeta}{2} H(U)} \right] \tag{354}$$

and

$$f_{1r}^s dU = -\frac{3}{4}\zeta\left(1 - \frac{V_p}{U}\right) f_o dU \left[1 + \frac{\psi}{2}\left(1 - \frac{V_p}{U}\right) - \frac{\zeta}{2} H(U) \right]^{-1} \tag{355}$$

The above analysis contains our new results, extending the previous relation in Eq. (330).

If $l_c >> r_p$, then $\zeta \to 0$ and H(U) reduces to Eqs. (342) to (344). Hence, this term and the ψ term (see Eqs. (331) to (333), which also go to zero) do not contribute in the collisionless limit. If $l_c << r_p$, then $\zeta \approx 1$ and $H(U) \approx 1 - (V_p/U)^{3/2}$. The physical meaning of this term is associated with the "blocking" action of the probe. It is also related to the "K" factor in Swift[11] (p. 210). When the mean free path is very large, the outside plasma does not "see" the probe. When it is smaller than the radius, the plasma is influenced by the obstacle, and the distribution function has to readjust accordingly. It can be seen that the ζ and ψ corrections are of comparable magnitude when $r_p \sim l_c$ but are of opposite signs. Both should be included in a proper quasicollisional probe analysis. It is, however, true that, if $r_p >> l_c$, the ψ correction is more important than the ζ correction, which may explain why no consideration was given to the latter by Lukovnikov.

SECTION VI

HYBRID PROBE ANALYSIS IN THE CONTINUUM REGIME

1. INTRODUCTION

In this section, we provide a generalized formulation for the operation of a probe in a high pressure plasma where $r_p > \lambda_s > l_c$. The method is based on the hybrid theory as formulated by Waymouth[28] and Wilkins and Katra[29]. Consequently, we will not cover all the other methods for the continuum regime, which were reviewed by Johnston[25].

Hybrid theory essentially combines the results from the thin collisionless part of the sheath adjacent to the probe to the results from the ambipolar layer valid in most of the sheath as calculated in the continuum limit. The electrostatic space charge potential is included in the latter layer here, in contrast to Section V. A proper hybrid theory deduces a Boltzmann line if f_o is a Maxwellian distribution and also resolves a problem pointed out by Blue and Ingold[30] and by Wilkins and Katra[29]. In many continuum theories, one has the erroneous boundary condition that the density at the probe is zero, and this leads formally to an infinite drift velocity. The hybrid theory given here does not have this problem.

Nearly all theories assume a Maxwellian distribution for f_o, and averaged quantities are based on this distribution. Here we do not restrict the form of f_o. Furthermore, we match proper relations for the flow (f_{1r} effects) at the collisionless edge by using our results in Section II. Other authors, who did not have these results in Section II, either omitted these effects (as Waymouth did) or adopted an **ad hoc** form (as Wilkins and Katra did) for these relations. For these reasons, our results differ from others. In the following we point out how our generalized results relate to these previous analyses.

2. GENERALIZED MOMENT APPROACH

As in Section V, we are concerned here with two components of the distribution function, f_o^s and f_{1r}^s, both at the boundary between the free fall (or collisionless) part of the sheath and the collisional part. Below, we use the word "boundary" to designate this position at r_s. The form of f_o in the plasma is allowed to be arbitrary. The directed part f_{1r} is associated with radial flow due to gradients and space charge fields in the plasma. Let V_s be the potential caused by the probe at the r_s boundary, so that V_s is the difference between the potential at the boundary and the plasma potential, the latter taken as zero. The probe potential V_p is measured with respect to plasma potential. We investigate below both the acceleration and retardation regions.

The method uses moment relations based on averages of the distribution function. We define the following averages, for either electrons or ions, where n_s is the density at the boundary:

$$n_s = 4\pi \int_o^\infty f_o^s(v) v^2 \, dv \tag{356}$$

$$\bar{v} = (4\pi/n_s) \int_o^\infty f_o^s(v) v^3 \, dv \tag{357}$$

$$D = (4\pi/3n_s) \int_o^\infty f_o^s(v)(v^4/\nu_1) dv \tag{358}$$

$$\mu = \frac{4\pi e}{3mn_s} \int_o^\infty f_o^s(v) \frac{d}{dv}\left(\frac{v^3}{\nu_1}\right) dv \tag{359}$$

Here D is the diffusion coefficient of a species, μ is its mobility, ν_1 is

its collision frequency for momentum transfer, v is its speed, and $\bar{v}$ is its averaged speed. We also define

$$v_o = [2(V_p - V_s)/m]^{\frac{1}{2}} \tag{360}$$

In the continuum regime, we note that $r_p > \lambda_s > l_c$. Hence, the collisionless part of the sheath (of order l_c) is very close to the probe, and one can use the thin plane sheath approximation ($r_s = r_p + l_c \approx r_p$). In the case of particle retardation, we have from Eqs. (7) and (8) the following result for the current density to the probe,

$$\frac{I}{A} = j = j_o - j_1 = \pi e \int_{v_o}^{\infty} [v(v^2 - v_o^2) f_o^s(U) - \frac{2}{3}(v^3 - v_o^3) f_{1r}^s(v)] dv \tag{361}$$

and, in the acceleration case, we have from Eqs. (23) and (24)

$$\frac{I}{A} = j_o - j_1 = \pi e \int_{0}^{\infty} v^3 [f_o^s(v) - \frac{2}{3} f_{1r}^s(v)] dv \tag{362}$$

Since $r_s \approx r_p$ and $A \approx A_r^s$, these relations also give the current densities at the boundary, r_s.

Collisional theory provides the form of f_{1r} inside the collisional part of the sheath. We include the space charge potential, φ, associated with charge imbalance and ambipolar effects. Now f_{1r} is related to gradients in f_o and in φ, and in particular at the boundary it is given by

$$f_{1r}^s = -\frac{v}{\nu_1}\left[\frac{\partial f_o^s}{\partial r} \pm \frac{e}{mv}\frac{\partial \varphi}{\partial r}\frac{df_o^s}{dv}\right] \tag{363}$$

where the upper sign refers to electrons and the lower sign to positive ions. Substituting this into Eq. (361) gives for a retardation case

$$j_1 = -\frac{2\pi e}{3}\int_{v_o}^{\infty} dv \, \frac{v(v^3 - v_o^3)}{\nu_1}\left(\frac{\partial f_o^s}{\partial r} \pm \frac{e}{mv}\frac{\partial \varphi}{\partial r}\frac{df_o^s}{dv}\right) \tag{364}$$

For an acceleration case we have the same result with $v_o = 0$.

For later use, we define the following ratios for a retardation case, making use of Eqs. (357) to (359):

$$W_o \equiv \frac{\int_{v_o}^{\infty} v(v^2 - v_o^2) f_o^s(v)\,dv}{\int_0^{\infty} v^3 f_o^s(v)\,dv} = \frac{4\pi}{n_s \bar{v}} \int_{v_o}^{\infty} v(v^2 - v_o^2) f_o^s(v)\,dv \tag{365}$$

$$W_1 \equiv \frac{\int_{v_o}^{\infty} (v/\nu_1)(v^3 - v_o^3) f_o^s(v)\,dv}{\int_0^{\infty} (v^4/\nu_1) f_o^s(v)\,dv} = \frac{4\pi}{3n_s D} \int_{v_o}^{\infty} \frac{v}{\nu_1} (v^3 - v_o^3) f_o^s(v)\,dv \tag{366}$$

$$W_2 \equiv \frac{\int_{v_o}^{\infty} f_o^s(v) \frac{d}{dv}\left(\frac{v^3 - v_o^3}{\nu_1}\right) dv}{\int_0^{\infty} f_o^s(v) \frac{d}{dv}\left(\frac{v^3}{\nu_1}\right) dv} = \frac{4\pi e}{3n_s m\mu} \int_{v_o}^{\infty} f_o^s(v) \frac{d}{dv}\left(\frac{v^3 - v_o^3}{\nu_1}\right) dv \tag{367}$$

For an acceleration case, these ratios are redefined as

$$W_o = W_1 = W_2 = 1 \tag{368}$$

We postulate now the basic assumption in this section, that $f_o^s/n_s = f_o/n_o$, its value within the plasma, so that f_o/n does not vary with position within the collisional part of the sheath. This is obviously only an approximation since the form of f_o is generally a complicated function of position and velocity within the sheath. The assumption supposes that all the spatial variation can be described in terms of the velocity averaged quantity n_s.

Referring now to Eqs. (357) to (359) and (365) to (367), we see that according to this assumption the quantities $\bar{v}$, D, μ, W_o, W_1, and W_2 do not vary with position since all integrals are normalized with respect to n_s.

With the new definitions in Eqs. (365) to (368), we can rewrite Eqs. (361) to (364), the relations for the current densities j_o and j_1 at the boundary, in the following forms:

$$j_o = n_s \bar{v}\, eW_o/4 \tag{369}$$

and

$$j_1 = -\frac{e}{2}\left[W_1 \frac{\partial}{\partial r}(Dn_s) \mp n_s \frac{\partial \varphi}{\partial r} \mu W_2\right] \tag{370}$$

The latter term is obtained by integration by parts in Eq. (364). Recall also that the upper sign applies to electrons and the lower sign to positive ions.

We require another set of relations giving the variation of n and φ with r in the collisional part of the sheath. From the momentum or flux conservation equation, we have, in particular at the boundary, the relation

$$\frac{\partial}{\partial r}(Dn_s) \mp \mu n_s \frac{\partial \varphi}{\partial r} = \frac{j}{e} \tag{371}$$

where j, as before, is the current density. Substituting $\partial\varphi/\partial r$ from Eqs. (371) into (370) gives for $j = j_o - j_1$ the expression

$$j = \frac{1}{4} n_s \bar{v} e\, W_o + \frac{e}{2}(W_1 - W_2)\frac{\partial}{\partial r}(Dn_s) + \tfrac{1}{2} W_2 j \tag{372}$$

Consider now the ambipolar effects obtained by combining the following electron (subscript e) and positive ion (subscript +) momentum relations within the collisional part of the sheath,

$$D_e \frac{\partial n_e}{\partial r} - \mu_e n_e \frac{\partial \varphi}{\partial r} = \frac{j_e}{e} \tag{373}$$

$$D_+ \frac{\partial n_+}{\partial r} + \mu_+ n_+ \frac{\partial \varphi}{\partial r} = \frac{j_+}{e} \tag{374}$$

We adopt the quasi-neutral approximation, namely, $n_e \approx n_+ = n$. Solving for n gives

$$\frac{e\partial n}{\partial r} = \frac{j_e\mu_+ + j_+\mu_e}{D_e\mu_+ + D_+\mu_e} = \frac{j_+D_e + \tau j_e D_+}{D_+D_e(1+\tau)} \tag{375}$$

where

$$\tau = \mu_+ D_e/\mu_e D_+ \tag{376}$$

For a Maxwellian distribution $\tau = e_+T_e/eT_+$, so that an order of magnitude value of τ is T_e/T_+. Note that j_e and j_p depend on the position r.

The integration of Eq. (375) for various geometries is given by Su and Kiel[31] and is summarized in Johnston[25]. (Note that their J is equal to our $(jA/4\pi eDn_o r_p)$, where n_o is the density outside of the sheath in the bulk of the plasma.) The quasi-neutral or ambipolar approximation yields in particular for n_s at the boundary

$$\frac{n_s}{n_o} = 1 - \left[\frac{j_+D_e + \tau j_e D_+}{D_+D_e(1+\tau)}\right] \frac{s_p A}{4\pi e n_o r_p} \tag{377}$$

where for a two-sided disc $s_p = \pi/2$ and for a one sided disc $s_p = \pi$, so that in either case

$$s_p A = \pi^2 r_p^2 \tag{378}$$

for a sphere $$s_p = 1 \text{ and } s_p A = 4\pi r_p^2 \tag{379}$$

and for a cylinder

$$s_p = \frac{2r_p}{L} \ln\left(\frac{\pi L}{4r_p}\right) \text{ and } s_p A = 4\pi r_p^2 \ln\left(\frac{\pi L}{4r_p}\right) \tag{380}$$

In the limit $\tau >> j_+D_e/j_eD_+$ and $\tau >> 1$, Eq. (377) reduces to

$$\frac{n_s}{n_o} \approx 1 - \frac{j_e s_p A}{4\pi e n_o r_p D_e} \tag{381}$$

We can compare Eq. (381) with the results in Section V. If Eq. (329) is integrated after multiplication by $4\sqrt{2}\pi\, U^{\frac{1}{2}}/m^{3/2}$, then the result will agree with Eq. (381) in the limit $l_c << r_p$ upon identifying $D_e = l_c v/3$ and $\psi l_c = 3As_p/(8\pi r_p)$, where ψ is given by Eqs. (331) to (333) for various geometries.

We now wish to solve for φ. Eliminating $\partial n/\partial r$ between Eqs. (373) and (374) and then substituting Eq. (375) yield

$$\frac{\partial \varphi}{\partial r} = \left[\frac{j_+ D_e - j_e D_+}{j_+ D_e + \tau j_e D_+}\right] \frac{D_e}{\mu_e} \frac{\partial \ln n}{\partial r} \tag{382}$$

Since the ratio within the brackets is independent of n or r, we can integrate to give $\mu_e \varphi/D_e$ equal to the bracket times $\ln n/n_o$. In particular, at the boundary we set $\varphi_s = V_s/e$ and we obtain

$$\frac{\mu_e V_s}{eD_e} = \left[\frac{j_+ D_e - j_e D_+}{j_+ D_e + \tau j_e D_+}\right] \ln \frac{n_s}{n_o} \tag{383}$$

We now examine the separate electron and ion current densities and insert the relevant subscripts. Substitute Eq. (375) into (372) to derive the following relations for the two species:

$$j_e = \tfrac{1}{4} n_s \bar{v}_e e W_{oe} + \frac{1}{2(1+\tau)} \left[j_e (W_{2e} + \tau W_{1e}) + j_+ (W_{1e} - W_{2e}) \frac{D_e}{D_+} \right] \tag{384}$$

$$j_+ = \tfrac{1}{4} n_s \bar{v}_+ e W_{o+} + \frac{1}{2(1+\tau)} \left[j_+ (\tau W_{2+} + W_{1+}) + j_e (W_{1+} - W_{2+}) \frac{D_+ \tau}{D_e} \right] \tag{385}$$

Define the following normalized parameters:

$$\tilde{j}_{e,+} = \frac{4 j_{e,+}}{n_o e \bar{v}_{e,+}}, \quad \rho_e = \frac{A\tau \bar{v}_e}{8\pi r_p D_e (1+\tau)}, \quad \rho_+ = \frac{A\bar{v}_+}{8\pi r_p D_+ (1+\tau)} \tag{386}$$

(To compare with Waymouth[28], his $Q_{e,i}$ are equal to our $\rho_{e,+} s_p/2$. To compare with Wilkins and Katra[29], their $j_{e,i}$ are our $\tilde{j}_{e,+}$ and their $\beta_{e,i}$ are our $\rho_{e,+}$. Their geometries also refer to a sphere with $A = 4\pi r_p^2$.) Then we can write for Eqs. (377) and (383)

$$\frac{n_s}{n_o} = 1 - \tfrac{1}{2} s_p(\rho_e \tilde{j}_e + \rho_+ \tilde{j}_+) \tag{387}$$

and

$$\frac{\mu_e V_s}{eD_e} = \frac{\tau\rho_+ \tilde{j}_+ - \rho_e \tilde{j}_e}{\tau(\rho_e \tilde{j}_e + \rho_+ \tilde{j}_+)} \ln \frac{n_s}{n_o} \tag{388}$$

Equations (384) and (385) can be similarly normalized. After substituting n_s/n_o into them, they become

$$\tilde{j}_e\left[1 + \tfrac{1}{2} W_{oe}\rho_e s_p - \frac{1}{2(1+\tau)}(W_{2e} + \tau W_{1e})\right] + \tilde{j}_+\left[\tfrac{1}{2} W_{oe}\rho_+ s_p - \frac{\tau}{2(1+\tau)}\frac{\rho_+}{\rho_e}(W_{1e} - W_{2e})\right] = W_{oe}$$

$$\tilde{j}_e\left[\tfrac{1}{2} W_{o+}\rho_e s_p - \frac{1}{2(1+\tau)}\frac{\rho_e}{\rho_+}(W_{1+} - W_{2+})\right] + \tilde{j}_+\left[1 + \tfrac{1}{2} W_{o+}\rho_+ s_p - \frac{1}{2(1+\tau)}(W_{1+} + \tau W_{2+})\right] = W_{o+}$$

These two equations can be solved to yield separate relations for $\tilde{j}_e$ and $\tilde{j}_+$. We define the cross denomenator, Λ:

$$\Lambda = \left[1 - \frac{W_{2e} + \tau W_{1e}}{2(1+\tau)}\right]\left[1 - \frac{W_{1+} + \tau W_{2+}}{2(1+\tau)}\right] + \tfrac{1}{2} W_{oe}\rho_e s_p(1 - \tfrac{1}{2}W_{2+}) + \tfrac{1}{2} W_{o+}\rho_+ s_p(1 - \tfrac{1}{2}W_{2e}) - \frac{\tau}{4(1+\tau)^2}(W_{1e} - W_{2e})(W_{1+} - W_{2+}) \tag{389}$$

The solutions for $\tilde{j}_e$ and $\tilde{j}_+$ are

$$\tilde{j}_e = \left\{ W_{oe}\left[1 - \frac{W_{1+} + \tau W_{2+}}{2(1+\tau)}\right] + W_{o+}\frac{\tau}{2(1+\tau)}\frac{\rho_+}{\rho_e}(W_{1e} - W_{2e})\right\}/\Lambda \tag{390}$$

and

$$\tilde{j}_+ = \left\{ W_{o+}\left[1 - \frac{W_{2e} + \tau W_{1e}}{2(1+\tau)}\right] + \frac{W_{oe}}{2(1+\tau)}\frac{\rho_e}{\rho_+}(W_{1+} - W_{2+})\right\}/\Lambda \tag{391}$$

If we substitute these values into n_s in Eq. (387) and into V_s in Eq. (388), we finally obtain

$$\frac{n_s}{n_o} = 1 - \frac{s}{2\Lambda}\left[\rho_e W_{oe}(1 - \tfrac{1}{2}W_{2+}) + \rho_+ W_{o+}(1 - \tfrac{1}{2}W_{2e})\right] \tag{392}$$

and

$$\frac{\mu_e V_s}{eD_e} = \left\{\frac{\tau\rho_+ W_{o+}(1-\frac{1}{2}W_{1e}) - \rho_e W_{oe}(1-\frac{1}{2}W_{1+})}{\tau[\rho_e W_{oe}(1 - \frac{1}{2}W_{2+}) + \rho_+ W_{o+}(1 - \frac{1}{2}W_{2e})]}\right\} \ln \frac{n_s}{n_o} \tag{393}$$

Equations (389) to (393) are our final results.

The procedure for calculating I-V characteristics is similar to that required in Waymouth's method. The steps are as follows:

1) Given forms of $f_o/n_o = f_o^s/n_s$ for electrons and ions, integrate Eqs. (357) to (359) to derive $\bar{v}$, D, and μ for each species, and then calculate τ in Eq. (376).

2) Adopt a value for $V_p - V_s$ in order to obtain v_o in Eq. (360), and then integrate Eqs. (365) to (367) to derive W_o, W_1, and W_2, each as a function of $V_p - V_s$.

3) For the particular geometry used, calculate $\rho_{e,+}$ and Λ from Eqs. (386) and (389), $\tilde{j}_e$ from Eq. (390), and $\tilde{j}_+$ from Eq. (391). Then obtain j_e and j_+ from Eq. (386).

4) Obtain n_s from Eq. (392) and V_s from Eq. (393) after n_s is substituted into its ln term. Knowing V_s and recalling that a value of $V_p - V_s$ has been adopted, we now have the correct value of V_p.

5) Redo the above for a whole range of $V_p - V_s$ values, and compute the total current $I = I_+ - I_e = A(j_+ - j_e)$ as a function of V_p.

3. RELATIONSHIP TO ANALYSES OF WAYMOUTH AND WILKINS AND KATRA

Waymouth's analysis is the simplest formulation for a combined free fall plus diffusion region. To obtain his results we have to make two simplifications. First, we adopt a Maxwellian distribution, so that for a species i

$$\tfrac{1}{4}\bar{v}_i = (kT_i/2\pi m_i)^{\frac{1}{2}}, \quad \tau = T_e/T_+, \quad D_i/\mu_i = kT_i/e_i \tag{394}$$

Also, $W_{oi} = \exp\left[-(V_p - V_s)/kT_i\right]$ for the retardation region, and $W_{oi} = 1$ for the acceleration region. Secondly, we have to set $W_1 = W_2 = 0$. Then, defining as he does

$$Q_e = \tfrac{1}{2}\rho_e s_p, \quad Q_+ = \tfrac{1}{2}\rho_+ s_p \quad \text{and} \quad Q = W_{oe}Q_e + W_{o+}Q_+ \tag{395}$$

we obtain from Eq. (389) $\Lambda = 1 + Q$. Also, Eqs. (390) to (393) reduce to

$$\frac{n_s}{n_o} = 1 - \frac{Q}{1+Q} = \frac{1}{1+Q}, \quad \frac{V_s}{kT_e} = -\left[1 - \frac{Q_e W_{oe}(1+\tau)}{\tau Q}\right] \ln\,(1+Q) \tag{396}$$

$$\tilde{j}_e = W_{oe}/(1+Q) \quad \text{and} \quad \tilde{j}_+ = W_{o+}/(1+Q) \tag{397}$$

For an acceleration region where $W_o = 1$, we have for the saturation current, I_{sat}, using Eq. (386), the result

$$\frac{I_{sat}}{A} = \frac{n_o e}{4(1/\bar{\nu} + Q/\bar{\nu}} \tag{398}$$

The two additive terms in the denomenator correspond, respectively, to the

usual Langmuir contribution and to the ambipolar collisional contribution, where $\bar{v}/Q$ defines the flow velocity. As another example, consider the case of a Maxwellian distribution, a constant mean free path ($D = \frac{1}{3} l_c \bar{v}$), a sphere ($s_p = 1$), and an electron retardation region with $W_{oe} = \exp[-(V_p - V_s)/kT_e]$ and $W_{o+} = 1$. Then,

$$\frac{Q}{r_p} = \frac{3\exp[-(V_p - V_s)kT_e]}{4l_{ce}(1+T_+/T_e)} + \frac{3}{4l_{c+}(1+T_e/T_+)} \tag{399}$$

This relation is given by Swift[11] (p. 229), where he uses $Y = Q/r_p$.

Swift implies that the assumptions in Waymouth are self-contradictory. On one hand, he is investigating the continuum limit where $l_c << r_p$, and, on the other hand, he wants f_o to remain isotropic up to the probe surface, in order for $W_1 = W_2 = 0$, which requires $l_c >> r_p$.

Wilkins and Katra attempt to improve the theory. They follow Waymouth, except that they adopt $W_1 = W_2 = W_o = W$, say. With this approximation, Eqs. (389) to (393) simplify thus:

$$\Lambda = (1 - \tfrac{1}{2} W_e)(1 - \tfrac{1}{2} W_+) + \tfrac{1}{4} W_e \rho_e s_p (1 - \tfrac{1}{2} W_+) + \tfrac{1}{4} W_+ \rho_+ s_p (1 - \tfrac{1}{2} W_e) \tag{400}$$

$$\frac{n_s}{n_o} = 1 - \frac{s_p}{2\Lambda}\left[\rho_e W_e (1 - \tfrac{1}{2} W_+) + \rho_+ W_+ (1 - \tfrac{1}{2} W_e)\right] \tag{401}$$

$$\frac{\mu_e V_s}{eD_e} = \left\{\frac{\tau\rho_+ W_+ (1 - \tfrac{1}{2} W_e) - \rho_e W_e (1 - \tfrac{1}{2} W_+)}{\tau[\rho_e W_e (1 - \tfrac{1}{2} W_+) + \rho_+ W_+ (1 - \tfrac{1}{2} W_e)]}\right\} \ln \frac{n_s}{n_o} \tag{402}$$

$$\tilde{j}_e = W_e (1 - \tfrac{1}{2} W_+)/\Lambda \quad \text{and} \quad \tilde{j}_+ = W_+ (1 - \tfrac{1}{2} W_e)/\Lambda \tag{403}$$

We note, however, that the assumption $W_1 = W_2 = W_o$ is incorrect according to the analysis in Section II. Our analysis here in Eqs. (365) and (367) would give the following expression, based on a Maxwellian distribution and a constant mean free path ($\nu_1 = v/l_c$),

$$W_o = \exp[-(V_p - V_s)/kT] \tag{404}$$

$$W_1 = W_2 = \left(1 + \frac{V_p - V_s}{kT}\right)\exp\left[-\left(\frac{V_p - V_s}{kT}\right)\right] - \sqrt{\pi}\left(\frac{V_p - V_s}{kT}\right)^{3/2}\left\{1 - \Phi\left[\left(\frac{V_p - V_s}{kT}\right)^{\frac{1}{2}}\right]\right\} \tag{405}$$

where Φ is the error function. Thus, W_o differs from W_1 and W_2, although W_1 is equal to W_2 for a Maxwellian distribution.

4. LIMITING CASES

Let us now go back to our generalized relations and look at several limiting cases.

Consider the limit of free electron diffusion, that is, when ambipolar effects become negligible. In Eqs. (389) to (393) we take the limits $\tau \gg 1$ and $\rho_e \gg \rho_+$ or $\tau \bar{v}_e D_+ > \bar{v}_+ D_e$ or $\tau > I_+ D_e / I_e D_+$. These inequalities were already mentioned in Eq. (336). Except for V_s and $\tilde{j}_+$, the relations now become independent of ion effects. We obtain $\Lambda = \Lambda_o(1 - \frac{1}{2} W_{2+})$, where

$$\Lambda_o = 1 - \tfrac{1}{2} W_{1e} + \tfrac{1}{2} W_{oe} \rho_e s_p \tag{406}$$

Also,

$$\frac{n_s}{n_o} = 1 - s_p \rho_e W_{oe}/\Lambda_o \tag{407}$$

$$\frac{\mu_e V_s}{eD_e} = \left\{\frac{\tau\rho_+ W_{o+}(1 - \frac{1}{2} W_{1e}) - \rho_e W_{oe}(1 - \frac{1}{2} W_{1+})}{\tau\rho_e W_{oe}(1 - \frac{1}{2} W_{2+})}\right\} \ln \frac{n_s}{n_o} \tag{408}$$

$$\tilde{j}_e = W_{oe}/\Lambda_o \tag{409}$$

and

$$\tilde{j}_+ = W_{o+}(1 - \tfrac{1}{2} W_{1e})/\Lambda + W_{oe}(W_{1+} - W_{2+})\rho_e/(2\rho_+ \tau\Lambda) \tag{410}$$

From Eqs. (386), (406), and (409), the total electron current when $\tau \gg 1$ can be written as

$$I_e = \tfrac{1}{4} An_o e \bar{v}_e W_{oe} \Big/ \left[1 + \frac{W_{oe} s_p \bar{Av}_e}{16\pi r_p D_e} - \tfrac{1}{2} W_{1e} \right] \tag{411}$$

From Eq. (365) and since $K_o = 2\pi e/m^2$, we note that

$$\tfrac{1}{4} n_o e \bar{v}_e W_{oe} = K_o \int_{V_p - V_s}^{\infty} f_o dU(U - V_p) \tag{412}$$

As mentioned following Eq. (381), under certain conditions one can associate the quantity $3As_p/(8\pi r_p) = \psi l_c = 3\psi D_e/\bar{v}_e$ with ψ given by Eqs. (331) to (333). Then we can write Eq. (411) as

$$I_e = \frac{AK_o \int_{V_p - V_s}^{\infty} f_o dU(U - V_p)}{1 + \frac{\psi}{2} W_{oe} - \frac{1}{2} W_{1e}} \tag{413}$$

This expression is strikingly similar to Eq. (350) in Section V. Here we use a moment approach whereas there a kinetic approach is adopted. Our basic assumption here (which is not used in Section V) is that $f_o^s/n_s = f_o/n_o$ is independent of position. The consequences appear as separate averaged terms over f_o in the various parts of Eq. (413), rather than as a single integral over f_o as in Eq. (350). Upon comparing the two expressions for I_e, we see that, if the two correction terms in the denomenator are omitted, the two I_e expressions become identical. The first correction term in Eq. (413) is our ψ effect associated with the differences between f_o^s and f_o. The second correction term is our ζ effect associated with f_{1r}^s, and, as seen in Eqs. (351) to (353), $\zeta = 1$ when $l_c \ll r_p$. The two correction terms are of opposite signs, as found previously in Section V. Although the moment approach is inferior in this limit, nonetheless the more general relations have successfully included the space charge electrostatic potential, a task which is exceedingly difficult with a kinetic approach.

Finally, we now adopt our generalized relations to the two situations of electron acceleration and ion retardation and the converse. In the first case we set $W_{oe} = W_{1e} = W_{2e} = 1$ (see Eq. (368)), and we obtain from Eqs. (389) to (393) the following results:

$$\Lambda = \tfrac{1}{2}\left[1 - \frac{W_{1+} + \tau W_{2+}}{2(1+\tau)}\right] + \tfrac{1}{4} W_{o+}\rho_+ s_p + \tfrac{1}{2}\rho_e s_p (1 - \tfrac{1}{2} W_{2+}) \tag{414}$$

$$\frac{n_s}{n_o} = 1 - \frac{s_p}{2\Lambda}\left[\rho_e(1 - \tfrac{1}{2} W_{2+}) + \tfrac{1}{2}\rho_+ W_{o+}\right] \tag{415}$$

$$\frac{\mu_e V_s}{eD_e} = \left\{\frac{\frac{1}{2}\tau\rho_+ W_{o+} - \rho_e(1 - \frac{1}{2}W_{1+})}{\tau\left[\rho_e(1 - \frac{1}{2}W_{2+}) + \frac{1}{2}\rho_+ W_{o+}\right]}\right\} \ln \frac{n_s}{n_o} \tag{416}$$

$$\tilde{j}_e = \left[1 - \frac{W_{1+} + \tau W_{2+}}{2(1+\tau)}\right]/\Lambda \tag{417}$$

and

$$\tilde{j}_+ = \left[\tfrac{1}{2} W_{o+} + \frac{1}{2(1+\tau)} \frac{\rho_e}{\rho_+}(W_{1+} - W_{2+})\right]/\Lambda \tag{418}$$

In the opposite limit, when electrons are retarded and ions are accelerated, we set $W_{o+} = W_{1+} = W_{2+} = 1$ and find the following results:

$$\Lambda = \tfrac{1}{2}\left[1 - \frac{W_{2e} + \tau W_{1e}}{2(1+\tau)}\right] + \tfrac{1}{4} W_{oe}\rho_e s_p + \tfrac{1}{2}\rho_+ s_p (1 - \tfrac{1}{2} W_{2e}) \tag{419}$$

$$\frac{n_s}{n_o} = 1 - \frac{s_p}{2\Lambda}\left[\tfrac{1}{2}\rho_e W_{oe} + \rho_+(1 - \tfrac{1}{2} W_{2e})\right] \tag{420}$$

$$\frac{\mu_e V_s}{eD_e} = \left\{\frac{\tau\rho_+(1 - \frac{1}{2} W_{1e}) - \frac{1}{2}\rho_e W_{oe}}{\tau\left[\frac{1}{2}\rho_e W_{oe} + \rho_+(1 - \frac{1}{2} W_{2e})\right]}\right\} \ln \frac{n_s}{n_o} \tag{421}$$

$$\tilde{j}_e = \left[\tfrac{1}{2} W_{oe} + \frac{\tau}{2(1+\tau)} \frac{\rho_+}{\rho_e}(W_{1e} - W_{2e})\right]/\Lambda \tag{422}$$

and

$$\tilde{j}_+ = \left[1 - \frac{W_{2e} + \tau W_{1e}}{2(1+\tau)}\right]/\Lambda \tag{423}$$

In both cases, the total current is given by

$$I = I_+ - I_e = A(j_+ - j_e) = \tfrac{1}{4} n_o e A(\bar{v}_+ \tilde{j}_+ - \bar{v}_e \tilde{j}_e) \qquad (424)$$

The above relations are thus appropriate to derive I-V characteristics in the continuum limit, $l_c \ll r_p$. They reduce to all known limits and generalize the works of previous authors in including the following effects: proper expressions or averages for W_1 and W_2 which are related to flow effects; generalized expressions even for W_o to non-Maxwellian distributions; allowance for any of three geometries, namely, plane, sphere, or cylinder; and an arbitrary energy dependence for the mean free path or collision frequency.

SECTION VII

DISCUSSION AND CONCLUSIONS

Electrostatic probe measurements of the electron velocity distribution function inside a plasma suitable for lasing action have become more and more important. They provide us with valuable information about the excitation mechanisms inside the medium and, hence, about ways of improving the laser efficiency. Measurements have been made with cylindrical probes for diagnostics to investigate the N_2 medium[32-39] both with and without CO_2 and the CO lasing medium[40]. The nitrogen plasma has also been studied with a plane probe[41].

An active electrical discharge, when used as a lasing medium, usually has an E/p value between 1 and 100 V/cm-torr, and the electric field, E, can be greater than 3 V/mm. In the CO_2-N_2 laser at low degrees of ionization, inelastic processes are decisive in shaping the electron distribution function, f, and coupling occurs between f and the molecular vibrational energy[36]. Direct electron impact excitation of vibrational levels plays an important role in the CO_2 laser. The region where the isotropic part of the distribution function, f_o, decreases sharply corresponds[37] to electron energies at which the elastic and inelastic electron scattering cross sections by molecules increase markedly. With probes, one can ascertain[36,39,40] the influence of different mixtures, pressure, current, gas flow, etc., on the form of f_o, on the number of fast electrons in the tail of f_o, on the average electron temperature, and on the electric field in the plasma. Probe measurements[35,36] also show that the laser action induces a pronounced depletion of electrons in the electron energy range around a few eV. Bletzinger and Garscadden[36] find essential agreement between their measured f_o functions and the calculated values of Nighan and Bennett[42] for CO_2 laser gas mixtures.

The interpretation of the Langmuir probe characteristics is largely complicated by the presence of the external E and by collisional effects. The field E causes f in the plasma to become both non-Maxwellian and anisotropic. In this report, we are concerned with the use of electrostatic probes to study the nonequilibrium aspects of active plasmas with a low degree of ionization. One of our aims is to provide information on deducing f from the probe current-voltage (I-V) characteristics.

There are three pressure regimes with differing theories in the study of electrostatic probes and the sheaths they create in a plasma. The regimes are characterized by the ratios of three basic physical lengths, namely the probe radius (r_p), the sheath thickness (λ_s) related to the Debye length, and the mean free path (l_c) of charged particles in the plasma.

In Sections II and III, the theory is based on the method of Langmuir and Mott-Smith[4]. A collisionless sheath is considered, subject to the conditions that l_c is greater than both r_p and λ_s and that the electric field at the sheath edge is predominantly that due to the discharge. Collisionless probe theory has been refined by many authors, for example, Bernstein and Rabinowitz[43] and Laframboise[44]. The refinements usually pertain to the acceleration region, and the methods usually assume the electrons to have a Maxwellian distribution and the ions to be either likewise or monoenergetic. For the electron retardation region from which the electron distribution function is deduced, the relations for the electron current given by all these theories agree, even for a general isotropic f_o. Most of our interest lies in the analysis of this region. We pursue the method of Langmuir and Mott-Smith, since it is the simplest approach, to

provide the corrections due to the potential drop (V_a) across the sheath in the presence of E and/or due to an anisotropic distribution function. We find that these correction terms depend on the probe geometry and on the ratio r_s/r_p, where r_s is the position of the sheath from the center of the probe. For a plane geometry, we obtain contributions, given in Eq. (134), from all three parts of the distribution function (viz., isotropic f_o, directional f_{1z}, and tensor f_{2zz} components) and additional corrections to each, given in Eqs. (294) to (297), when V_a is included. For a sphere, only the f_o term contributes if V_a is omitted (see Eq. (136)), and the f_{1z} and f_{2zz} contributions **appear only** for finite V_a (see Eqs. (300) to (303)). For a cylinder, f_o and f_{2zz} contribute if V_a is omitted (see Eq. (139)). However, f_{1z} contributes, and corrections appear in all the terms if V_a is included (see Eqs. (304) to (307)). Lukovnikov[7] has derived relations, including the f_o and f_{1z} contributions for a plane and cylindrical probe, which agree with our results. However, he didn't give the f_{2zz} and V_a corrections.

Certain relations require a knowledge of the sheath radius (r_s). When $V_a = 0$, the sheath radius appears as a separate parameter only in the accelerating region and even then only in the transition region from the space charge limited thin sheath ($r_s \approx r_p$) to the orbital limited thick sheath ($r_s >> r_p$). In either limit, the relations are independent of r_s, as can be seen from Eqs. (65) and (66) (where the second term only contributes when $r_s >> r_p$) for a sphere and from Eqs. (126) and (127) for a cylinder. Our orbital limited relations for a sphere and cylinder agree with Polychronopulos[6], who gives the integral over a general f_o in this limit. When V_a is included, we note that for a plane r_s appears only in the expression

for V_a, and the results are given in Eqs. (149) to (155). For the sphere and cylinder, it also appears in correction terms multiplying V_a. It thus appears that an approximate knowledge of the sheath radius is sufficient, since it is required only in certain transition regions and for correction terms. Our approximate expression for the sheath thickness is given in Eq. (308). It includes the Bohm sheath criterion and the effect of negative ions. We suggest that further effort be made to predict r_s from the solution of Poisson's equation and to include the changes in f_o from the sheath position to that in the plasma.

In this collisionless regime, we provide new relations to deduce all three components of the electron distribution function from the I-V characteristics. Because the cylindrical and spherical probes are insensitive to f_{1z} (except for V_a corrections), one contemplates the use of a plane probe or a spherical grid system. (The latter may, however, be too cumbersome and thus perturb the plasma in an unwanted fashion.) Without the V_a corrections, the response of a sphere could give f_o directly. However, the V_a corrections complicate the analysis, and, since a plane probe is required if f_{1z} is desired, it is simplest to use the plane probe to deduce f_o and f_{2zz} as well, rather than to insert multiple probes. When V_a is negligible, we find that three orientations of a one-sided plane probe are sufficient to deduce the three components of f. For stronger electric fields, five orientations of the probe are necessary. The relations for this new method of deducing the components of f are given in Eqs. (309) to (314). Lukovnikov[7], who provides the relations for the current response for given f_o and f_{1z}, does not solve the inverse problem to obtain f_o and f_{1z} from the current.

The three appendices cover the pressure (p) and E/p ranges of operation for such an one-sided plane probe, its construction and two computer programs for its use. Sample computer results are given in Section IV. These programs should be perfected to decrease the computer generated noise and to allieviate various other problems that are discussed in Section IV. Eventually, one may hope to provide real time Langmuir probe data reduced by a computer, as already done at ARL[45] for other systems. Our present programs allow us to diagnose by numerical means the anisotropy of a plasma with an imposed E from the data obtained by a plane probe in a very low pressure plasma.

An inherent problem in designing a plane probe is that it is difficult to construct a probe of disc radius r_p less than l_c, for pressures of the order of a torr, in order to satisfy the collisionless regime's requirement that $l_c > r_p$. We conclude that at these and higher pressures, probe theory has to include quasicollisional effects. If we were to choose a cylindrical probe and forego the measurement of f_{1z} due to E, then we could possibly design a sufficiently small probe radius to fall into the collisionless regime. In fact, Danilov et al[38] used two cylindrical probes of different r_p at pressures between 1 to 7 torr. They found that the finite probe size became noticeable even at $r_p/l_c \approx 0.1$ and that the distribution function was properly determined by the second derivative method only for very thin probes. With the larger probe, they obtained a significantly broadened f_o (with all f_o's normalized to the same maximum value). Self and Shih[46] have also observed collisional effects at pressures as low as 0.4 torr with a spherical probe. Quasicollisional theory thus seems to be a requirement for analyzing most measurements except those at quite low pressures.

In the quasicollisional regime where $r_p > l_c > \lambda_s$, usually corresponding to pressures of a few torr, the plasma sheath is a combination of collision free and collision dominated regions. It is still possible to use a kinetic approach in the analysis, as shown by Swift[26] and Lukovnikov and Novgorodov[27] for a spherical and cylindrical probe, respectively. These authors also show how one can derive by iteration the form of f_o from the second derivative of the current in the electron retarding region. In Section V, we extended these analyses, gave the result for a plane probe as well, and included the blocking action of the probe. This means that we include the f_{1r} radial component of the electron distribution. The value of f_{1r} is calculated from the diffusion of electrons in the quasicollisional part of the sheath. It is then used as an input function into the analyses given in Sections II and III for the current determined by f_o and $\underset{\sim}{f}_1$ at the collisionless sheath boundary, i.e., region of transition between the free fall and diffusion regions. The change in f_o from the plasma to this boundary due to diffusion is also calculated, somewhat as in the previous efforts[26,27] which included only this effect.

Two basic assumptions are made in Section V. The first is that the electron diffusion is free, which allows us to omit the space charge field and ion effects. This imposes the condition in Eq. (336) that the electron to ion temperature be very large. The second assumption is that, at the matching boundary, only f_{1r} due to diffusion contributes, whereas, in fact, f_{1z} and f_{2zz} due to the external electric field should be included, as we did in Sections II and III. We suggest that further efforts be directed towards these factors. To tackle the problem involving the space charge field, we require a solution of the ion dynamics. Also, including f_{1z} requires

a knowledge of the variation of each and coupling between f_{1r} and f_{1z} from the boundary to the outside plasma.

Our results on the quasicollisional sheath analysis are given in Eqs. (350) to (353), where the ζ factor represents the blocking action of the probe and the ψ factor is due to the variation of f_o or density from the boundary to the plasma. These relations agree with Swift[26] and Lukovnikov and Novgorodov[27] if we omit the ζ factor. The additional ζ factor is calculated with the proper multiplicative energy function H(U) obtained from the results in Section III. This H(U) function depends on the geometry and on the ratio of r_p/r_s, except when the ratio is either large or small. We find that the ζ factor is of the same order as the ψ factor when l_c is comparable to r_p. However, as l_c becomes small, the ζ factor is of lesser importance.

Attempts have been made by other authors to derive corrections similar to ours which account for the blocking action of the probe. For example, Wasserstrom et al[24] obtain an energy averaged factor for small V_p. They include the ion motion but assume equal electron and ion mean free paths and straight line trajectories between particle collisions, so that their results cannot be readily compared with ours.

Besides Wasserstrom et al[24], various other analyses, such as Chou et al[47], Bienkowski and Chang[48] and Su[49], have tried to derive moment relations from the Boltzmann transfer equation, both in the $l_c > r_p$ and $r_p > l_c$ regimes. Such analyses attempt to allow for the presence of the probe and how it influences the trajectories of the particles. However, every attempt at generalization introduces new approximations. Our analyses in Section VI are also such an attempt for $l_c < r_p$, and they are discussed below.

If $r_p > \lambda_s > l_c$, corresponding to pressures above 10 torr, the plasma density and potential in the vicinity of the probe are nonuniform due to diffusion and space charge effects, and collisions play an important role in determining the sheath profile. Kinetic approaches are difficult to pursue and one resorts to the moment equations. For this reason, the possibility of deducing f from I-V characteristics is uncertain in this regime. In Section VI, we calculate the probe current for given f_o and include the space charge potential and ambipolar diffusion effects. These effects influence the form of f_o, since f_o depends on the density. Sufficiently far from the probe, an ambipolar type of diffusion takes place in a sheath which is more or less quasineutral. The transition region between the collisionless and quasineutral sheaths is omitted in the analysis. Instead, a hybrid sheath is adopted, and the solutions for the two layers are matched at the boundary between them.

In obtaining the moment relations for the hybrid model, we have generalized the theories of Waymouth[28] and of Blue and Ingold[30] by deriving more accurate averages over the distribution function. However, in so doing, we had to adopt the commonly used approximation that the ratio of f_o to the density (n) at the boundary is the same as in the undisturbed plasma. This is valid for a Maxwellian f_o whose energy dependence does not change within the sheath, an assumption made in most analyses. We adopt the same concept for an arbitrary f_o. We generalize as well to include the blocking action of the probe and the anisotropic part of $\underset{\sim}{f}_1$, namely, f_{1r} due to radial flow near the probe, which was omitted by Waymouth[28]. Blue and Ingold[30], who included this effect, obtained a non-zero particle density at the probe surface and were able to recover a Boltzmann line for a Maxwellian f_o. Similarly, Wilkins and Katra[29] include the effects of the anisotropy.

However, the matching conditions at the collisionless boundary for f_{1r} used by these authors are not exact, whereas the matching equations used here are based on the correct relations derived in Section II for a thin collisionless sheath. Our final relations are given in Eqs. (414) to (424).

For a non-Maxwellian distribution function, the assumption that the ratio f_o/n is a function only of energy is, strictly speaking, incorrect. The function f_o is not necessarily a separable function of position and energy for all positions inside the sheath. One suggestion is to allow f_o to be the sum of two Maxwellians, each of which is separable in space and energy. However, even this supposition is not exact, since this decomposition may not apply within the sheath, even though it can reasonably be done within the bulk of the plasma. Further work along these lines will be useful. We also suggest that our method, presented in Section VI, be generalized to include the transition to the regime $l_c > r_p$, a task that should not be too difficult.

In comparing the moment theory, used here in hybrid form, with continuum theory in the collisional regime, one has to realize that the fluid equations, used in the latter approach, are obtained from the moment equations by letting l_c be infinitesimal and by ignoring the blocking effect of the probe. Consequently, it does not take care of the anisotropy of f near the probe surface. The equations in continuum theory, so derived, are inapplicable closer than a few mean free paths from the probe surface. It is assumed that l_c is so small that any particle in the sheath suffers enough collisions to "forget" about the existence of the probe. Essentially, this is equivalent to omitting the ζ, W_1, and W_2 factors in our theory, as Waymouth has done, and regarding the equations as valid up to the probe surface. Thus the continuum

theory can be regarded as the limit of the moment method for a negligible mean free path. Consequently, relations based on the moment method are superior provided they are tractable.

REFERENCES

1. Shkarofsky, I.P., Johnston, T.W. and Bachynski, M.P., The Particle Kinetics of Plasmas, Addison-Wesley Publ. Co., Reading, Mass., 1966, pp. 110-111.

2. Goldstein, H., Classical Mechanics, Addison-Wesley Publ. Co., Reading, Mass., 1950, pp. 107-109.

3. Symon, K.R., Mechanics, Addison-Wesley Publ. Co., Reading, Mass, 1964, p. 416.

4. Langmuir, I. and Mott-Smith, Jr., H., "Studies of Electric Discharges in Gases at Low Pressure, Part I", General Electric Review, Vol. 27, No. 7, pp. 449-455, July 1924. (Equations (31) and (46) to (48) are in error there but are corrected in the reprint given in the next reference.)

5. Suits, C.G., editor, The Collected Works of Irving Langmuir, Pergamon Press, N.Y., 1961, Vol. 4, pp. 32-35.

6. Polychronopulos, B., "Effects of Non-Maxwellian Electron Energy Distributions on the Orbital Limited Current-Voltage Characteristics of Cylindrical and Spherical Langmuir Probes Under Collisionless Conditions", Plasma Physics, Vol. 15, No. 1, pp. 37-48, January 1973.

7. Lukovnikov, A.I., "Probe Characteristics for an Anisotropic Energy Distribution", Zh. Tekh. Fiz., Vol. 43, No. 7, pp. 1478-1483, July 1973. (Translation: Sov. Phys. Tech. Phys., Vol. 18, No. 7, pp. 936-939, January 1974.)

8. Byrd, P.F. and Friedman, M.D., Handbook of Elliptic Integrals for Engineers and Physicists, Springer-Verlag, Berlin, 1954, pp. 121 (Eq. 256.06), 123 (Eq. 256.28) and 121 (Eq. 256.03).

9. Bohm, D., "Minimum Ionic Kinetic Energy for a Stable Sheath", in The Characteristics of Electrical Discharges in Magnetic Fields, Guthrie, A., and Wakerling, R.K., editors, McGraw Hill Publ. Co., N.Y., 1949, pp. 77-86.

10. Chen, F.F., "Electrical Probes", in Plasma Diagnostic Techniques, Huddlestone, R.H. and Leonard, S.L., editors, Academic Press, N.Y., 1965, pp. 113-200.

11. Swift, J.D. and Schwar, M.J.R., Electrical Probes for Plasma Diagnostics, Am. Elsevier Publ. Co., N.Y., 1969, pp. 131-135.

12. Boyd, R.L.F. and Thompson, J.B., "The Operation of Langmuir Probes in Electronegative Plasmas", Proc. Roy. Soc., Vol. A252, pp. 102-119, July 7, 1959.

13. Grard, R.J.L., "Interpretation of Impedance Probe Measurements in the Ionosphere", Stanford Electronics Laboratories, Tech. Report No. 2, Dec. 1965, pp. 13-29.

14. Langmuir, I., "The Effect of Space Charge and Initial Velocities on the Potential Distribution and Thermionic Current Between Parallel Plane Electrodes", Phys. Rev., Vol. 21, No. 4, pp. 419-435, April 1923. (Also in Ref. 5, Vol. 3)

15. Langmuir, I. and Blodgett, K.B., "Currents Limited by Space Charge Between Coaxial Cylinders", Phys. Rev., Vol. 22, Series 2, No. 4, pp. 347-356, Oct. 1923. (Also in Ref. 5, Vol. 3)

16. Langmuir, I. and Blodgett, K.B., "Currents Limited by Space Charge Between Concentric Spheres", Phys. Rev., Vol. 24, No. 1, pp. 49-59, July 1924. (Also in Ref. 5, Vol. 3.)

17. Nighan, L.N., "Electron Energy Distributions and Collision Rates in Electrically Excited N_2, CO and CO_2", Phys. Rev., Vol. A2, No. 5, pp. 1989-2000, Nov. 1970.

18. Bailey, W.F. and Long, W.H., "Electron Kinetic Processes in N_2 Discharges", presented at the 25th Gaseous Electronics Meeting, London, Ontario, Oct. 17-20, 1972.

19. Medicus, G., "Guarding Probes in Hot-Cathode Hg-Vapor Discharges", J. Appl. Phys., Vol. 37, No. 1, pp. 215-225, January 1966.

20. Boyd, R.L.F., "The Collection of Positive Ions by a Probe in an Electrical Discharge", Proc. Roy. Soc., Vol. A201, pp. 329-347, April 26, 1950.

21. Massey, H.S.W., Electronic and Ionic Impact Phenomena, Oxford Un. Press, London, 1969, Vol. II, p. 780.

22. Frost, L.S. and Phelps, A.V., "Rotational Excitation and Momentum Transfer Cross Sections for Electrons in H_2 and N_2 from Transport Coefficients", Phys. Rev., Vol. 127, No. 5, pp. 1621-1633, Sept. 1, 1962.

23. Long, W.H., Bailey, W.F. and Garscadden, A., "Negative Differential Conductivity in Molecular Gas-Rare Gas Mixtures: Nitrogen-Argon", presented at the Gaseous Electronics Meeting, Houston, Texas, Oct. 22-25, 1974.

24. Wasserstrom, E., Su, C.H. and Probstein, R.F., "Kinetic Theory Approach to Electrostatic Probes", Phys. Fluids, Vol. 8, No. 1, pp. 56-72, January 1965.

25. Johnston, T.W., "A Review of Collisional Probe Theory", RCA Limited Lab Report 7-801-82, Oct. 1969.

26. Swift, J.D., "Effects of Finite Probe Size in the Determination of Electron Energy Distribution Functions", Proc. Phys. Soc., Vol. 79, No. 4, pp. 697-716, April 1962.

27. Lukovnikov, A.I. and Novgorodov, M.Z., "On Distortion of Electron Energy Distribution Function Measured by a Cylindrical Probe", Krath. Soobsch. Fiz., No. 1, pp. 27-34, January 1971.

28. Waymouth, J.F., "Perturbation of a Plasma by a Probe", Phys. Fluids, Vol. 7, No. 11, pp. 1843-1854, November 1964.

29. Wilkins, D.R. and Katra, J.A., "Theory of Collision Dominated Langmuir Probes", Gen. Electric Co., Tech. Rep. AFAL-TR-67-327, Jan. 1968.

30. Blue, E., and Ingold, J.H., "Diffusion Theory for the Spherical Langmuir Probe", Plasma Physics, Vol. 10, No. 9, pp. 899-901, Sept. 1968.

31. Su, C.H. and Kiel, R.E., "Continuum Theory of Electrostatic Probes", Jour. Appl. Phys., Vol. 37, No. 13, pp. 4907-4910, December 1966.

32. Bletzinger, P. and Garscadden, A., "Influence of Xenon on CO_2 Laser Plasmas", Applied Physics Letters, Vol. 12, No. 9, pp. 289-291, May 1, 1968.

33. Bletzinger, P. and Garscadden, A., "Burning in the Electron Energy Distribution by Lasing Action in the CO_2-N_2-He Discharge", Phys. Letters, Vol. 29a, No. 5, pp. 265-266, May 19, 1969.

34. Garscadden, A. and Bletzinger, P., "Measurement of Electron Energy Distributions in CO_2 Laser Discharges", Ninth Int. Conf. on Phenomena in Ionized Gases, Bucharest, Rumania, Editura Akad. Repub. Soc. Romania, 1969, p. 250.

35. Garscadden, A. and Bletzinger, P., "Laser Perturbation Measurements in CO_2-N_2-He Discharges", Ninth Int. Conf. on Phenomena in Ionized Gases, Bucharest, Rumania, Editura Akad.Repub. Soc. Romania, 1969, p. 251.

36. Bletzinger, P. and Garscadden, A., "The CO_2 Laser Plasma", Proc. IEEE, Vol. 59, No. 4, pp. 675-679, April 1971.

37. Ivanov, Yu. A., Polak, L.S. and Slovetskii, D.I., "Electron Energy Distribution in a Glow Discharge in Molecular Gases", Teplofiz. Vys. Temp., Vol. 9, No. 6, pp. 1151-1158, Nov.-Dec. 1971. (Translation: High Temperature, Vol. 9, No. 6, pp. 1061-1067, June 1972.)

38. Danikov, V.V., Kruglyakov, E.P. and Shunko, Ye.V., "Cylindrical Probe in a Nitrogen Plasma from a Glow Discharge at Medium Pressures", Zh. Prikl. Mekh. i. Tekh. Fiz., No. 2, pp. 13-20, March-April 1973.

39. Novgordov, M.Z., Sviridov, A.G. and Sobolev, N.N., "Electron Energy Distribution in CO_2 Laser Discharges", IEEE J. Quant. Elect., Vol. QE-7, No. 11, pp. 508-512, Nov. 1971.

40. Novgordov, M.Z., Sviridov, A.G., Sobolev, N.N. and Shvarts, P., "Electron Energy in a CO Laser", Zh. Tekh. Fiz., Vol. 42, No. 10, pp. 2190-2197, Oct. 1972. (Translation: Sov. Phys. - Tech. Phys., Vol. 19, No. 10, pp. 1726-1730, April 1973.)

41. Garscadden, A. Bletzinger, P., Bailey, W.F. and Long, W.H., "Directional Probe Measurements in Molecular Gas Discharges", presented at the 26th Gaseous Electronics Meeting, Madison, Wis., Oct. 16-19, 1973. APS Bull., Series II, Vol. 19, No. 2, p. 146, Feb. 1974.

42. Nighan, W.L. and Bennett, J.M., "Electron Energy Distribution Functions and Vibrational Excitation Rates in CO_2 Laser Mixtures", Appl. Phys. Lett., Vol. 14, No. 8, pp. 240-243, April 15, 1969.

43. Bernstein, I.B. and Rabinowitz, I., "Theory of Electrostatic Probes in a Low Density Plasma", Phys. Fluids, Vol. 2, No. 2, pp. 112-121, March-April 1959.

44. Laframboise, J.G., "Theory of Spherical and Cylindrical Langmuir Probes in a Collisionless Maxwellian Plasma at Rest", Institute for Aerospace Studies, Univ. of Toronto, UTIAS Rep. No. 100, June 1966.

45. Corbin, J.C. Jr. and Curtis, J.A., "Real Time Langmuir Probe Data Reduction by a Minicomputer for a Collisionless Plasma", Aerospace Res. Labs. Report ARL-73-0114, Dec. 1973.

46. Self, S.A. and Shih, C.H., "Theory and Measurements for Ion Collection by a Spherical Probe in a Collisional Plasma", Phys. Fluids, Vol. 11, No. 7, pp. 1532-1545, July 1968.

47. Chou, Y.S., Talbot, L. and Willis, D.R., "Kinetic Theory of a Spherical Electrostatic Probe in a Stationary Plasma", Phys. Fluids, Vol. 9, No. 11, pp. 2150-2167, Nov. 1966.

48. Bienkowski, G.K. and Chang, K.W., "Asymptotic Theory of a Spherical Electrostatic Probe in a Stationary Weakly Ionized Plasma", Phys. Fluids, Vol. 11, No. 4, pp. 784-799, April 1968.

49. Su, C.H., "Kinetic Theory of a Highly Negative Langmuir Probe", Eightth Int. Conf. on Phenomena in Ionized Gases, Invited Papers, Vienna, Austria, Int. Atomic Energy Agency, Vienna, 1968, pp. 569-580.

50. Abramowitz, M. and Stegun, I.A., Handbook of Mathematical Functions, NBS Publ. Washington, D.C., 1964, Series 55, pp. 883, 914.

APPENDIX A

PARAMETER MAP

1. INTRODUCTION

In this appendix, we deduce (1) the parameter map for the validity of collisionless probe theory in an active discharge, with scaling conditions and plots relevant to nitrogen and (2) the minimum time for an I-V sweep. The effect of negative ions is covered in Section III.

There are many conditions that have to be obeyed for validity of collisionless probe theory. Some of these pertain to the dimensions of the probe and others pertain to the plasma and applied potentials. The latter criteria are considered here whereas the former will be considered in the next appendix. The limits for each of the three criteria for validity given below are drawn on a plot of E/p versus p/η for various V_p, where E is the electric field strength in the plasma, V_p is the potential applied to the probe, p is the pressure, and η is the ratio of electron density to neutral particle density. Such a plot has to be drawn for each gas or gas mixture. For illustration purposes we have done this for a nitrogen plasma.

2. PARAMETER MAP AND SCALING

Besides certain conditions on probe dimensions, to be given in Appendix B, the domain of validity of the present probe theory is determined by the following assumptions:

1) For the spherical harmonic expansion to be convergent[1], the electron drift velocity, v_d, must be smaller than the electron thermal energy, v_e. That is,

$$\frac{v_d}{v_e} \approx \frac{eE}{mv_e\nu_1} < 1$$

where E is the electric field in the plasma*, ν_1 is the momentum transfer collision frequency for electron-neutral collisions, and e and m are the electron charge and mass, respectively. However, since v_d varies non-linearly with E for strong electric fields and since v_e increases with E, it is more appropriate to use the experimentally and/or theoretically determined curves of v_d and v_e versus E/p to find the limits on the condition $v_d < v_e$.

2) For the sheath to be collisionless, the sheath thickness, λ_s, must be small compared to the electron mean free path, l_c:

$$\lambda_s < l_c$$

3) For the perturbation due to the external electric field E to be small around the probe, we must have

$$eE\lambda_s < V_p$$

where V_p is the magnitude of the (negative) probe potential with respect to plasma potential.

For a given gas temperature and ratio of electron to neutral densities, $\eta = n_e/N$, these assumptions impose limitations on the external electric field, E, and on the neutral pressure, p, and eventually on the probe voltage, V_p. We now discuss these limitations for each of the three conditions for the situation of a nitrogen gas at 300°K.

---

* This electric field E is the one we find in the probing region far from the electrodes. This means that for the experimental evaluation of E one must exclude the strong potential drops occurring near the electrodes, so that E is smaller than the potential difference between the electrodes divided by the length of the discharge.

Consider the first condition. A measure of v_d and $v_e \equiv (kT_e/m)^{\frac{1}{2}}$, or electron temperature, can be derived from experimental and theoretical curves (k is Boltzmann's constant). Figure 27 plots both v_d, v_e and the ratios $5v_d/v_e$ and $4v_d/v_e$ versus E/p from the experimental and calculated data given by Massey[21], Frost and Phelps,[22] and Nighan[17], as well as data by Long et al[23] of ARL. We note that v_d is equal to $v_e/5$ when $E/p \approx 35$. If we take $v_d = v_e/4$ as sufficient to satisfy the first condition, then the upper limit on E/p is about 88. Thus, this condition is usually satisfied for cases of concern in pure nitrogen.

The ratio of sheath thickness to Debye length, λ_D, is evaluated from Eq. (290). Adopting $V_e = V_{e1}$ for simplicity, we have

$$\frac{\lambda_s}{\lambda_D} = 2\left[\frac{1}{2}\left(1+\frac{2V_p}{V_e}\right)^{3/2} - \left(1+\frac{2V_p}{V_e}\right)\right]^{\frac{1}{2}}$$

with

$$\lambda_D(\eta p)^{\frac{1}{2}} = [1.717\times 10^{-11}\ T_e(eV)]^{\frac{1}{2}}\ \text{cm-torr}^{\frac{1}{2}}$$

and $V_e = kT_e/e = mv_e^2/e$. The ratio λ_s/λ_D is plotted in Figure 28. It is not valid for $V_p/V_e \leq 4$, but the graph has been extrapolated towards zero. Using the plot of v_e versus E/p in Figure 27, we evaluate V_e, $\lambda_D(\eta p)^{\frac{1}{2}}$, λ_s/λ_D, and finally $\lambda_s(\eta p)^{\frac{1}{2}}$. Plots of $\lambda_s(\eta p)^{\frac{1}{2}}$ versus E/p for various V_p values are given in Figure 29.

We can also calculate the mean free path, l_c, from the v_d and v_e data in Figure 27, based on the formula

$$l_c = \frac{3\pi}{8}\left(\frac{8kT}{\pi m}\right)^{\frac{1}{2}}\frac{m\sigma}{n_e e^2} = 3\left(\frac{\pi}{8}\right)^{\frac{1}{2}}\frac{m}{e}\ \frac{v_e v_d}{E}$$

where σ is the dc electrical conductivity. This equation, although derived (see p. 141 in Ref. 1) for a Maxwellian distribution function with a constant

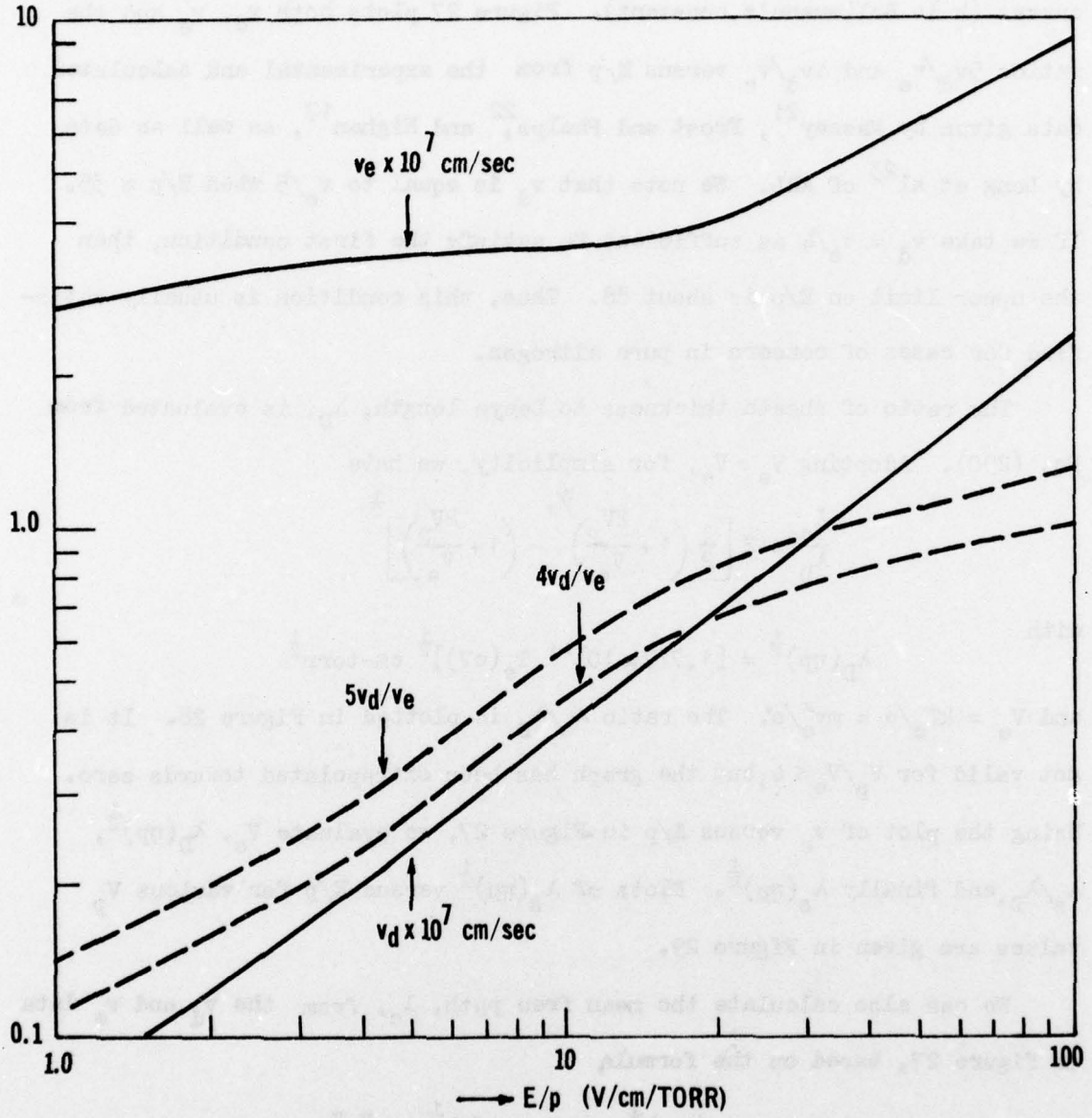

Figure 27. Drift Velocity, v_d, Thermal Velocity, v_e, and Ratios Versus E/p

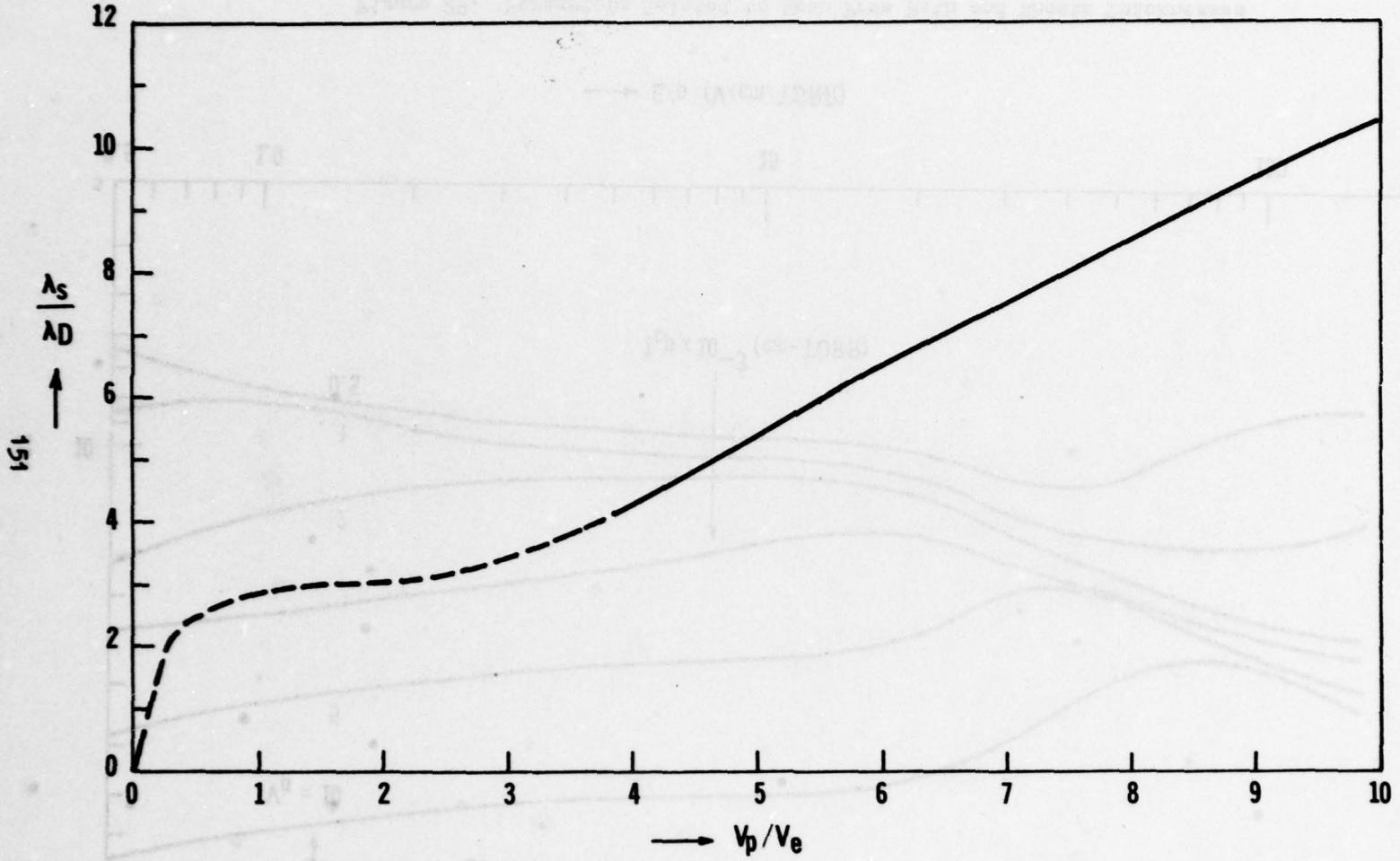

Figure 28. Ratio of Sheath Thickness to Debye Length Versus V_p/V_e

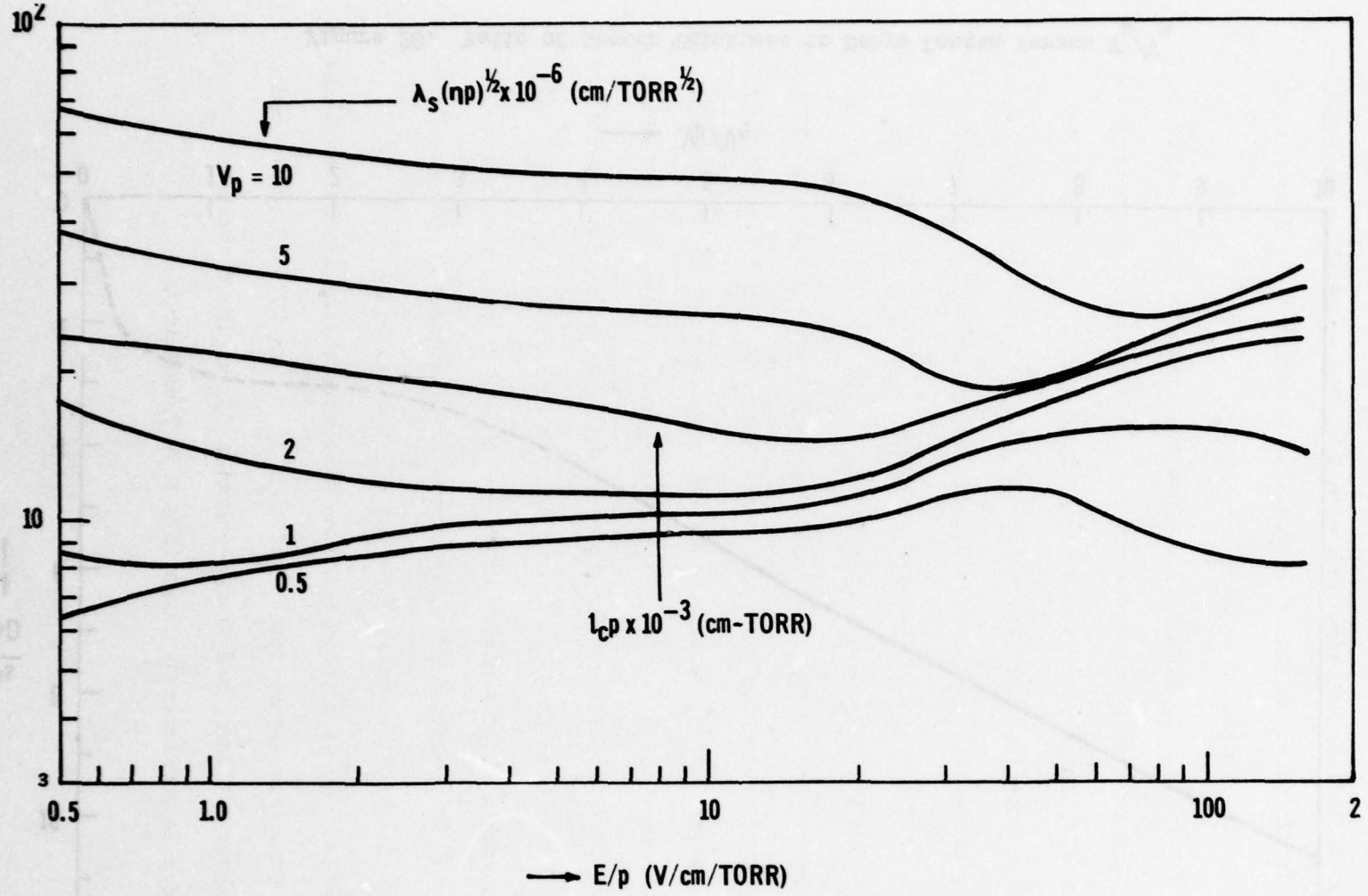

Figure 29. Parameters Related to Mean Free Path and Sheath Thicknesses for Various V_p Versus E/p

mean free path collisional model, is not too sensitive to the form of the distribution if l_c does not vary much with E/p. Figure 29 shows calculations of pl_c versus E/p based on this relation. As is evident, l_c does not vary appreciably in the indicated range of E/p or T_e.

Using the results in Figure 29, we can now evaluate the assumptions (2) and (3) and provide a parameter map for nitrogen. For assumption (1), we take $v_d = v_e/4$, which gives the horizontal line at E/p = 88 shown in Figure 30. We note that the evaluation of $(pl_c)^2/[\lambda_s(\eta p)^{\frac{1}{2}}]^2 = 1$ (or $l_c = \lambda_s$) for each E/p and each V_p value also depends on the ratio p/η. Thus in Figure 30 we show the $\lambda_s = l_c$ curves for various V_p versus E/p and p/η values. We also evaluate $E\lambda_s = V_p$ curves by equating $V_p^2/[(E/p)(\lambda_s(\eta p)^{\frac{1}{2}})]^2 = 1$ for various V_p versus E/p and p/η values, and these are also plotted in Figure 30.

Assumption (1) implies the requirement that E/p lies below the horizontal line. Assumption (2) imposes a maximum value for p/η for a given probe voltage. The maximum values for p are represented by the vertical curves for different probe voltages. For lower probe potentials, the restriction on p/η is less severe since the sheath becomes smaller and is less likely to be collisional. In the region under the oblique lines, assumption (3) is satisfied. The position of these curves also depends on the probe potential. The lowest V_p value is $V_p = 0.5\ kT_e/e = 0.5\ V_e$.

From Figure 30, it appears that the most severe limitations on plasma conditions come from assumption (2) at high V_p values ($V_p \geq 10$ volts) and pressures above 0.1 torr, and from assumption (3) at low V_p values ($V_p \leq 0.5$ Volts) if E/p is sufficiently large (E/p $\geq$ 70 V/cm-torr).

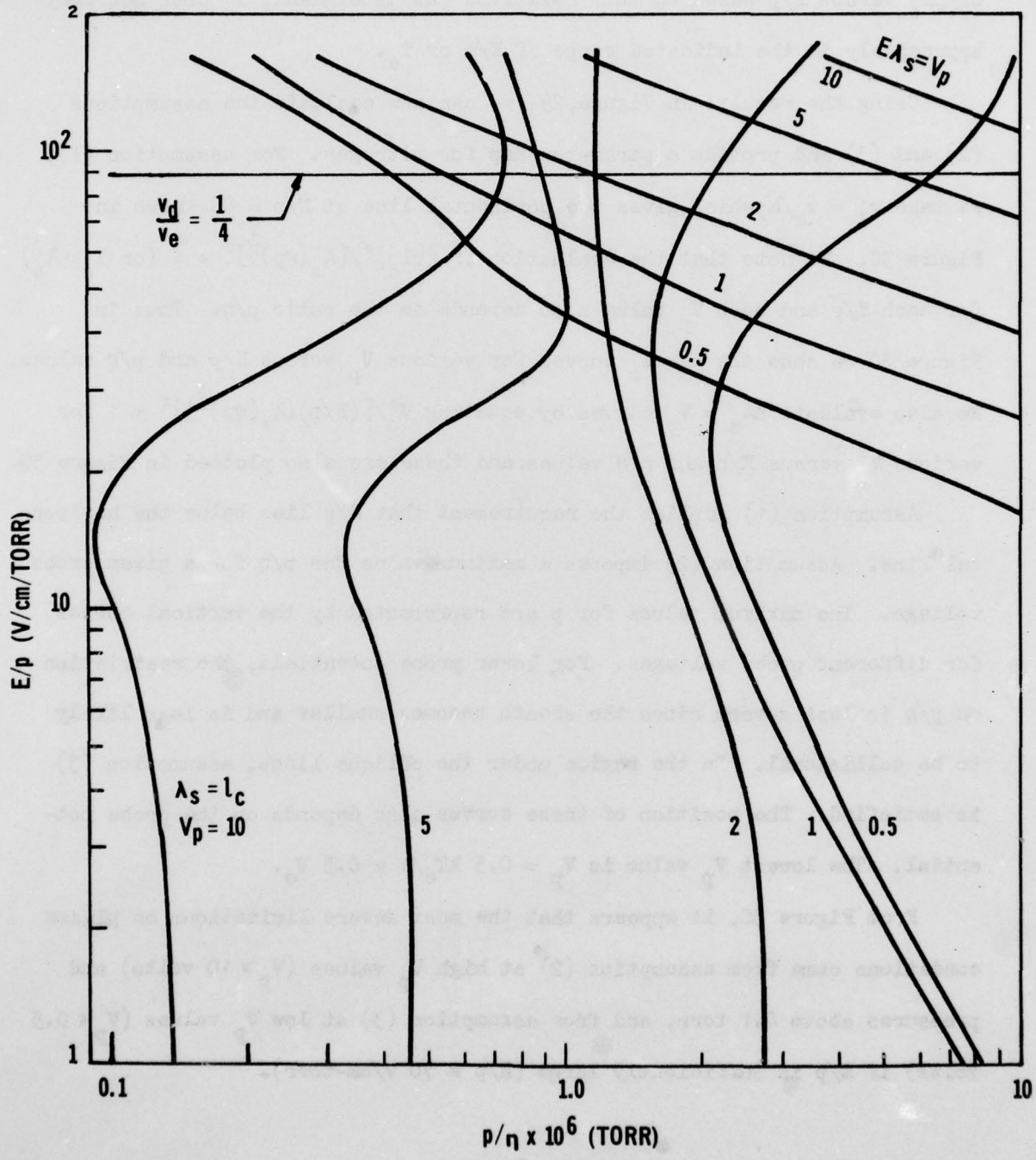

Figure 30. Parameter Map for Nitrogen Showing Various Limits on a E/p Versus p/η Plot

3. SWEEP FREQUENCY

The sweep frequency, f_s, of the probe voltage with time (t) must be small enough so that the slowest particles, namely the ions, will practically detect no time variation of potential when crossing the sheath. That is,

$$\frac{1}{V_p}\frac{dV_p}{dt} < \frac{v_+}{\lambda_s} \quad \text{or} \quad f_s \leq \frac{v_+}{\lambda_s}$$

where v_+ is the ion drift velocity at the sheath edge, approximately equal to $(kT_e/m_+)^{\frac{1}{2}}$. For λ_s = 1mm, kT_e/e = 1eV, and $m_+ = 4.65 \times 10^{-26}$ kg for N_2, we have

$$f_s < 1.86 \text{ MHz}$$

Thus, the sweep frequency, which is usually lower than this value, does not present any problem.

It is preferable to operate at frequencies below the ion plasma frequency as well. This imposes the condition that

$$f_s < (n_+ e^2/\varepsilon_o m_+)^{\frac{1}{2}}/2\pi$$

or $f_s < 2.7$ MHz if the ion density $n_+ = 4.5 \times 10^{15} m^{-3}$. This condition is thus also easy to satisfy.

APPENDIX B

DESIGN AND CONSTRUCTION OF A PLANE PROBE

1. DESIGN AND DIMENSIONS OF THE PLANE PROBE

The appropriate dimensions of the probe are determined mainly by the value of the tube radius R_t and the sheath thickness λ_s.

The tube radius R_t imposes a maximum value to the probe radius R_p. If the electron density varies radially as

$$n_e(r) \approx n_{eo} J_o(2.4\ r/R_t)$$

where n_{eo} is the electron density on the tube axis and J_o is the zero order Bessel function, then the probe radius R_p must be at most equal to $1/5\ R_t$ if we want a variation of density of less than 5% over the probe. For R_t = 1.25 cm and R_p = 0.75 mm or 2mm, the variation of density over the probe is about 0.5% or 4%, respectively.

Figure 31 indicates additional conditions that the plane probe has to satisfy. These are plotted on a V_p versus p diagram for three E/p or electron temperature values (0.78, 1.5, and 3eV) and for $\eta = n_e/N = 10^{-6}$. The conditions are (1) $l_c > \lambda_s$ in order for the sheath to be collisionless, a condition already discussed in Appendix A, (2) $2R_p > \lambda_s$, (3) $\lambda_s > \delta$, where δ is the gap between the central collecting disc and the surrounding guard ring if a guarded probe is used, and (4) $l_c > R_p$. The dashed curves are for a probe of radius 0.75 mm without a guard ring, and the solid curves are for a probe with R_p = 2mm, disc radius = r_p = 0.5 mm, and δ = 0.1 mm. The $\lambda_s = \delta$ curves apply only to the latter, whereas the $\lambda_s = l_c$ curves apply to both types of probes.

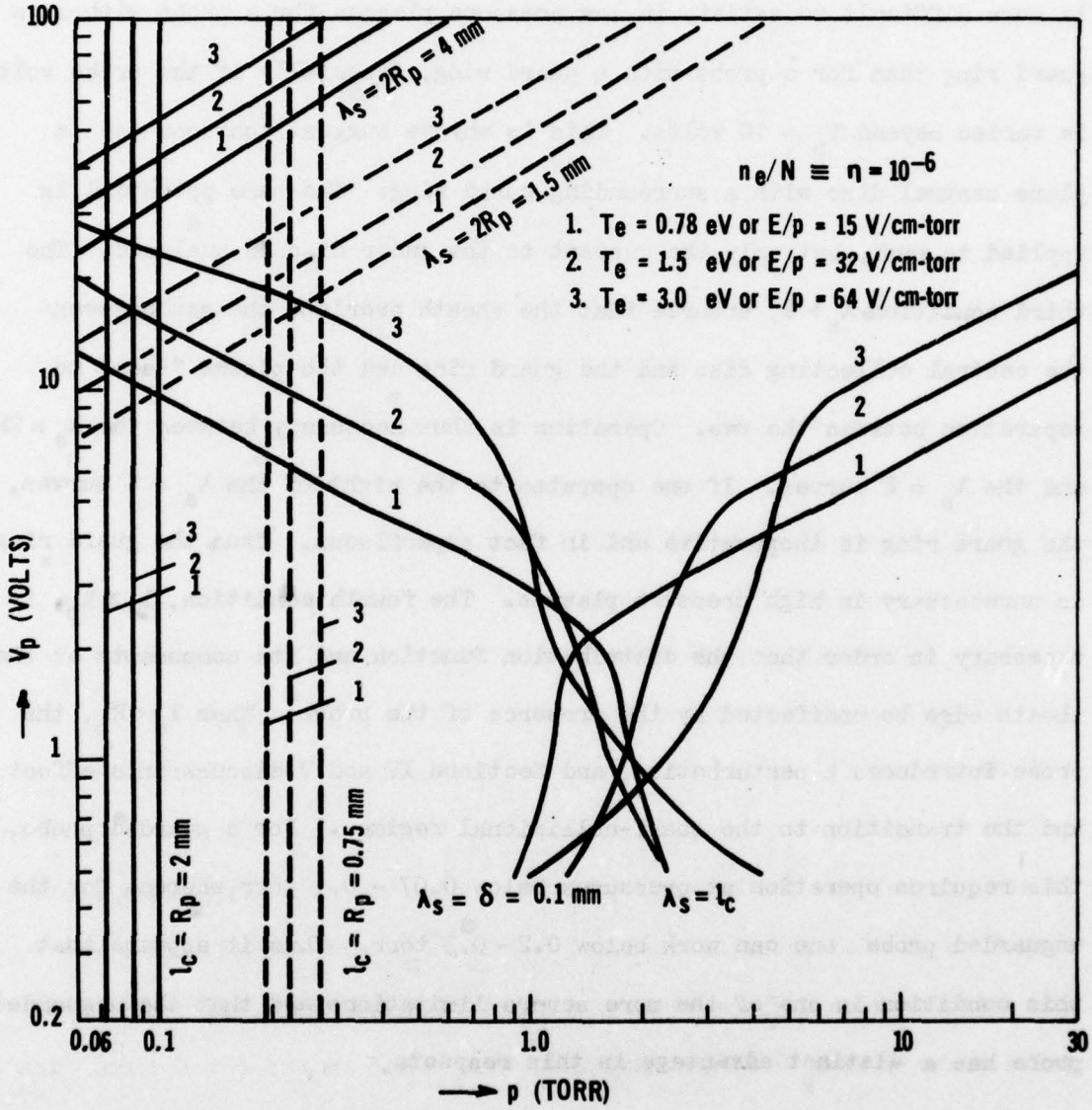

Figure 31. Various Limiting Conditions for a Plane Probe in Nitrogen Shown on a V_p Versus p Plot

The first condition requires operation at pressures to the left of the $\lambda_s = l_c$ curves. The second condition, $\lambda_s < 2R_p$, requires V_p and p values below the indicated curves. This condition is necessary in order for the edge effects of the plane probe to be negligible. As seen, this is more difficult to satisfy in low pressure plasmas for a probe without a guard ring than for a probe with a guard ring, especially if the probe voltage is varied beyond $V_p = 10$ volts. This is why we suggest that one use a plane central disc with a surrounding guard ring. The same potential is applied to each, but only the current to the inner disc is analyzed. The third condition, $\lambda_s > \delta$, ensures that the sheath overlaps the gap between the central collecting disc and the guard ring and the plasma "sees" no separation between the two. Operation is thus necessary between the $\lambda_s = 2R_p$ and the $\lambda_s = \delta$ curves. If one operates to the right of the $\lambda_s = \delta$ curves, the guard ring is inoperative and in fact superfluous. Thus, the guard ring is unnecessary in high pressure plasmas. The fourth condition, $l_c \geq R_p$, is necessary in order that the distribution function and its components at the sheath edge be unaffected by the presence of the probe. When $l_c < R_p$, the probe introduces a perturbation, and Sections IV and V discuss this effect and the transition to the quasi-collisional regime . For a guarded probe, this requires operation at pressures below 0.07 - 0.1 torr, whereas for the unguarded probe one can work below 0.2 - 0.3 torr. Thus it appears that this condition is one of the more severe limitations and that the unguarded probe has a distinct advantage in this respect.

In the next section, we provide details on the construction of the guarded probe. As compared to the unguarded probe, the guarded one is more difficult to fabricate, and an assembly drawing is useful.

2. METHOD USED FOR THE FABRICATION OF THE GUARD RING PROBE

An assembly drawing and a photograph are shown in Figures 32 and 33. This probe has been made to test the feasibility of the design.

The center of the probe has been cut with a diamond saw from a tungsten rod. According to Medicus[19], the center of the probe and the guard ring should be made of the same metal. Molybdenum rod was not available; tungsten has been substituted as only the mechanical difficulties of the construction were to be tested.

The guard ring has been cut from molybdenum foil. Tantalum has been tried and rejected because it deformed too easily at welding.

The ceramic washer has been cut with a diamond saw from a ceramic tube. The ceramic handle is made of a 10 cm ceramic tube of 2.8 mm O.D. This tube has four holes, two of which are used to insulate the .010" nickel connecting wires.

The .010 nickel connecting wires are spot welded to the center of the probe and to the guard ring. The four holes of the handle have been plugged with "TORR SEAL". ECCOCERAM SM-25 has been used to cover the back side of the probe and to secure the whole assembly to the ceramic handle. A thin ceramic coat of SM-25 is applied to the edge of the guard ring.

A slightly different version based on the above model has been constructed at ARL. An assembly drawing of the latter is shown in Figure 34. In addition, an unguarded probe of radius 0.75 mm has also been used at ARL. A major problem found with the first probe is the lack of a definitive break in the I-V characteristic, which is required to identify plasma potential. Another problem found with both probes is that the value of I/R_t^2, or current density in their particular discharge tube, could not be increased sufficiently to satisfy both the conditions that $l_c > \lambda_s$ and $R_p > \lambda_s$.

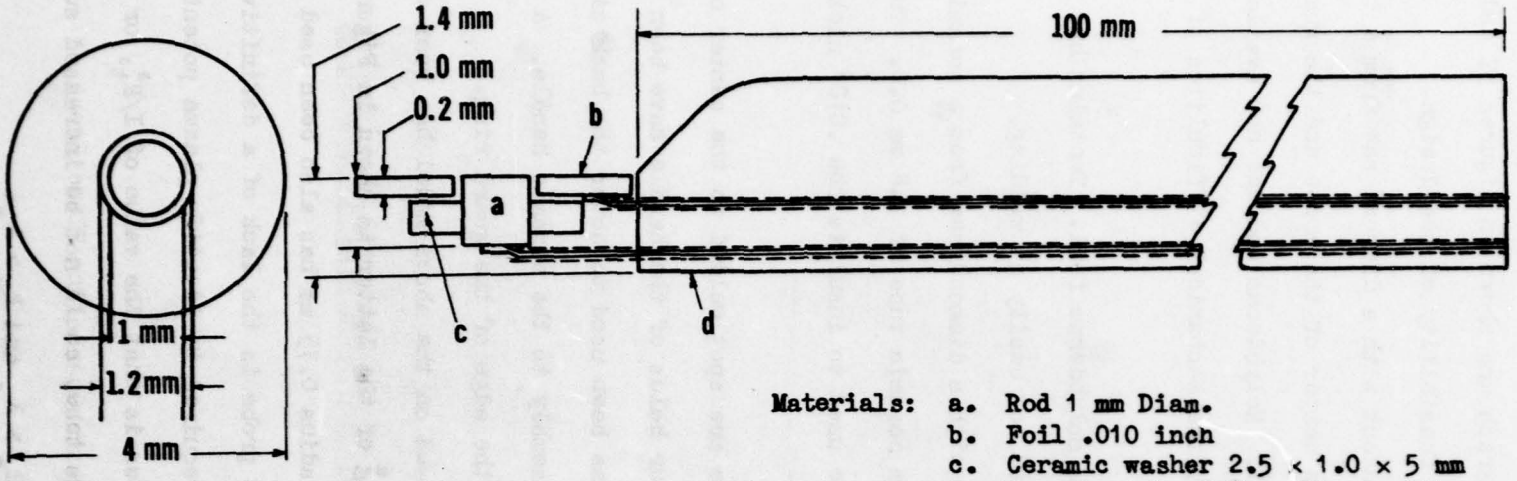

Materials:
a. Rod 1 mm Diam.
b. Foil .010 inch
c. Ceramic washer 2.5 x 1.0 x 5 mm
d. Ceramic tube 2.8 mm Diam. with 4 holes .6 mm

Items a. and b. should be made of the same material, Tungsten or Molybdenum.

The back side of the probe to be covered with Eccoceram SM-25 (Emerson & Cuming Inc.)

Figure 32. Assembly Drawing for a Plane Probe Plus Guard Ring

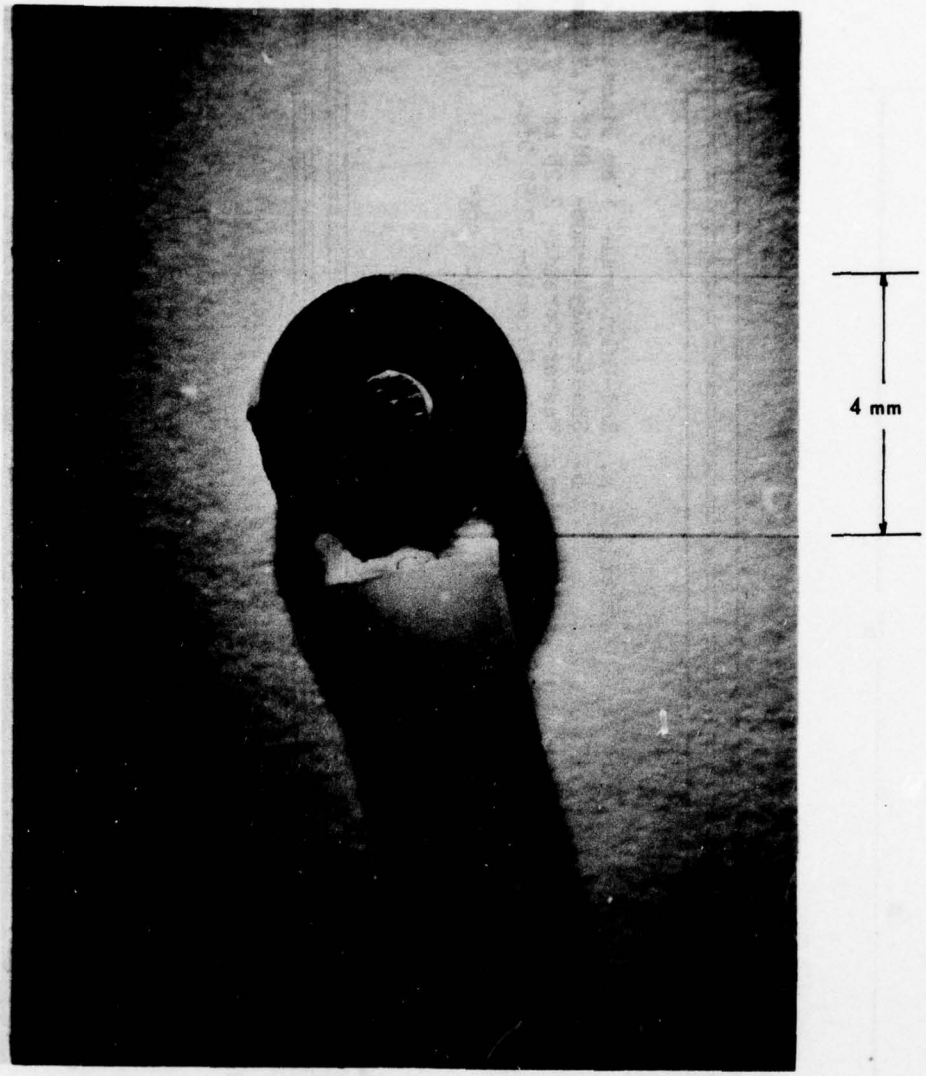

Figure 33. Photograph of the Guard Ring Plane Probe

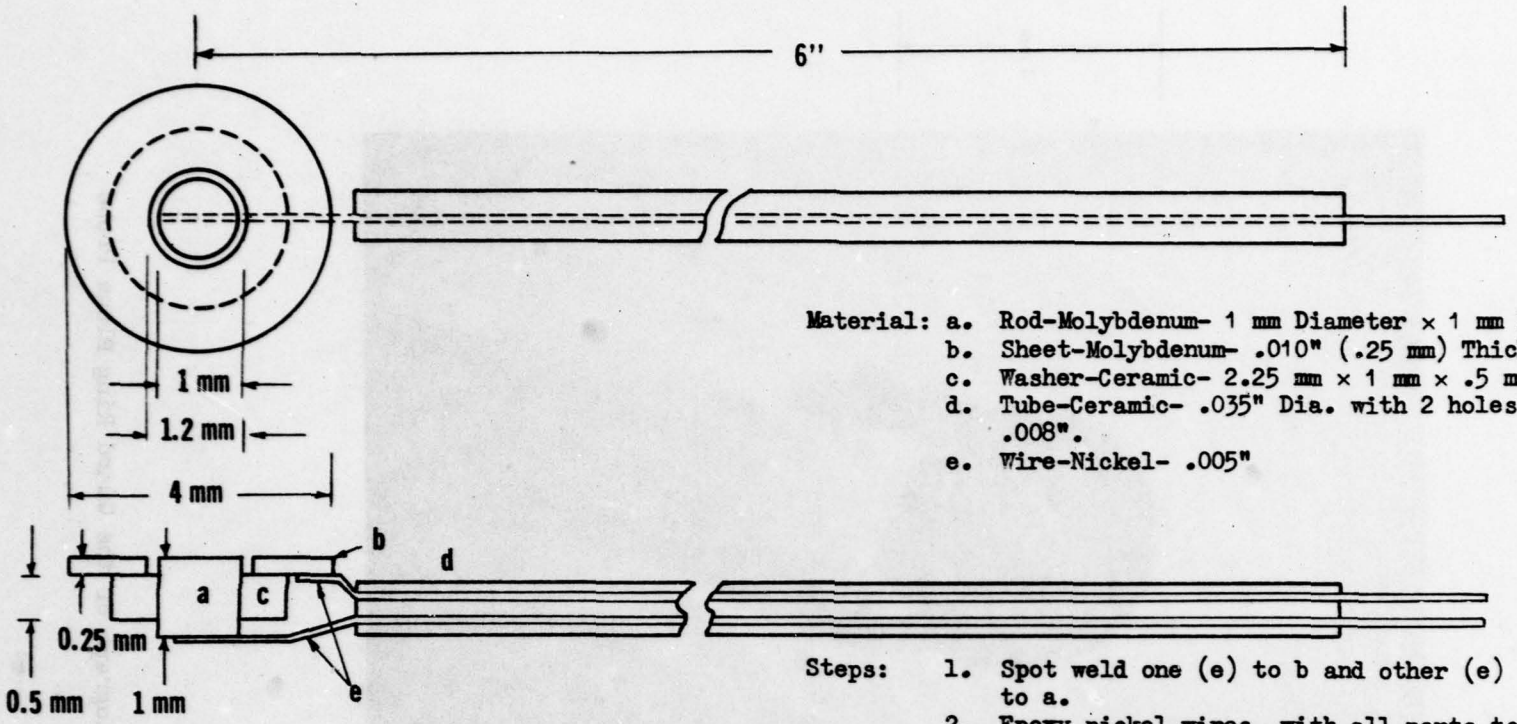

Material:
a. Rod-Molybdenum- 1 mm Diameter x 1 mm Lg.
b. Sheet-Molybdenum- .010" (.25 mm) Thick.
c. Washer-Ceramic- 2.25 mm x 1 mm x .5 mm.
d. Tube-Ceramic- .035" Dia. with 2 holes .008".
e. Wire-Nickel- .005"

Steps:
1. Spot weld one (e) to b and other (e) to a.
2. Epoxy nickel wires, with all parts together in an assembly and aligned, with Torr Seal. (Varian Associates, Vacuum Division). Epoxy wires Only to tube to form a vacuum seal.
3. After epoxy has hardened, cover back side of probe and edge of guard ring with Ceramabond 503 (AREMCO Products, Inc.) after aligning.

Figure 34. Assembly Drawing for the ARL Plane Probe Plus Guard Ring

APPENDIX C

COMPUTER PROGRAMS AND USER MANUALS

1. INTRODUCTION

Two computer programs are presented here for a plane probe. First we provide the program FTOJ for the calculation of the total current to the probe. It also gives, if desired, the electron current and the electron current density contributions from various parts of the electron velocity distribution function. The second program, JTOF, performs the inverse operation of calculating the components of the distribution function up to the second order of anisotropy from the current intercepted by a plane probe for five orientations. Both programs call the subroutines SUMT and SHEATH, which are used, respectively, for integration and for evaluating the sheath thickness. The second program JTOF calls the additional subroutine DER for differentiation, which in turn calls SE35 to smoothen the differentiated data. (Decks of all these programs were delivered to ARL.)

Below we outline the above programs. Also, the subroutines are discussed, except for SE35, which is a standard IBM subroutine. Printouts of all statements in both complete programs are given at the end in subsection 6.

2. PROGRAM FTOJ

a. Flow Chart

A flow chart for this program is given in Figure 35. As can be seen, the input instructions determine the number of regions for which the total current is calculated. These regions are the electron acceleration region and the electron retardation region, the latter based on exact theory (Eqs. (149) to (152)) and with the options of also being based on approximate

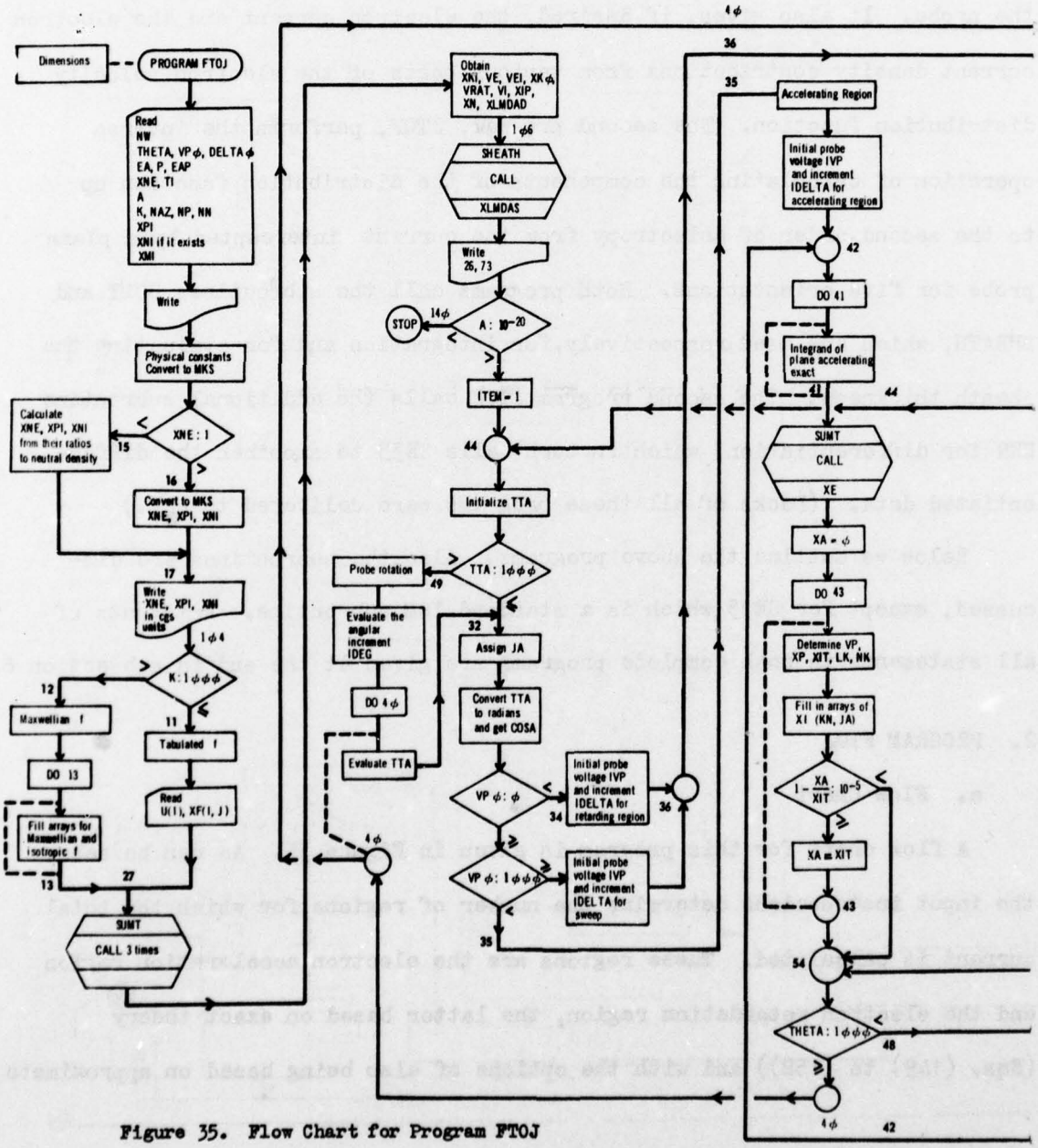

Figure 35. Flow Chart for Program FTOJ

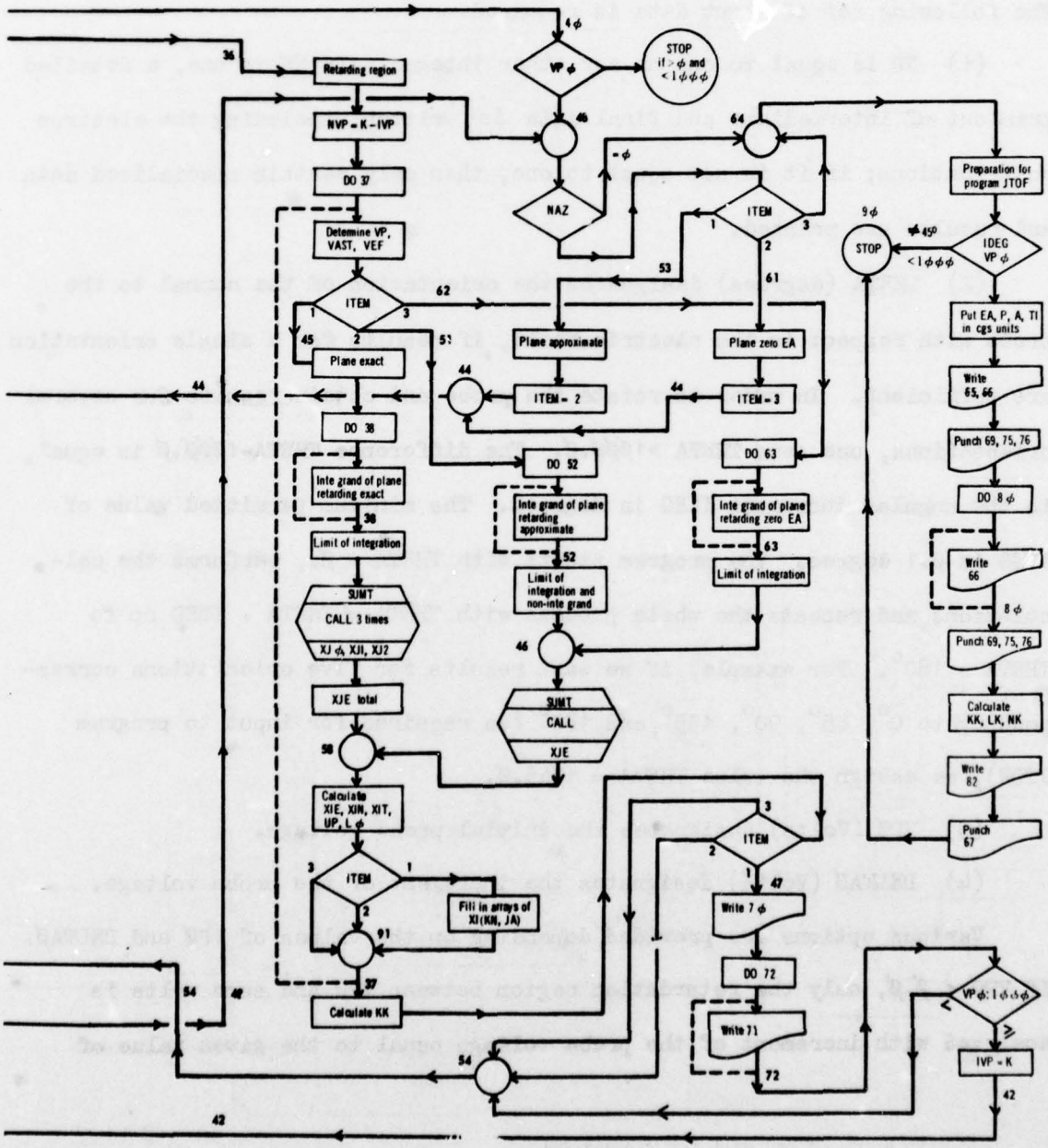
Retarding region
NVP = K - IVP
DO 37
Determine VP, VAST, VEF
ITEM
Plane exact
DO 38
Inte grand of plane retarding exact
Limit of integration
SUMT
CALL 3 times
XJ, XJI, XJ2
XJE total
Calculate XIE, XIN, XIT, UP, L
ITEM
Fill in arrays of XI(KN, JA)
Calculate KK
VP
STOP if > and < 1
NAZ
ITEM
Plane approximate
ITEM = 2
DO 52
Inte grand of plane retarding approximate
Limit of integration and non-inte grand
SUMT
CALL
XJE
Plane zero EA
ITEM = 3
DO 63
Inte grand of plane retarding zero EA
Limit of integration
ITEM
Write 7
DO 72
Write 71
VP: 1 to
IVP = K
Preparation for program JTOF
STOP
IDEG VP
Put EA, P, A, TI in cgs units
Write 65, 66
Punch 69, 75, 76
DO 8
Write 66
Punch 69, 75, 76
Calculate KK, LK, NK
Write 82
Punch 67

theory for $V_a << V_p$ (Eqs. (153) to (155)) or less approximate theory with $V_a = E = 0$ (Eq. (134)). The corresponding outputs are named "plane exact", "plane approximate", and "plane zero EA".

b. User's Manual

The procedures for the operation of this program are now provided. The following set of input data is required.

(1) NW is equal to one or any other integer. If NW is one, a detailed printout of intermediate and final data is written, including the electron contributions; if it is not equal to one, then only certain specialized data and results are printed.

(2) THETA (degrees) designates the orientation of the normal to the probe with respect to the electric field, if results for a single orientation are sufficient. In order to rotate the probe and obtain results for several orientations, one sets THETA >1ØØØ.Ø. The difference THETA-1ØØØ.Ø is equal to the angular increment IDEG in degrees. The minimum permitted value of IDEG is Ø.1 degree. The program starts with THETA = Ø., performs the calculations, and repeats the whole process with THETA = THETA + IDEG up to THETA ≥ 180°. For example, if we want results for five orientations corresponding to 0°, 45°, 90°, 135°, and 180° (as required for input to program JTOF), we assign the value THETA = 1Ø45.Ø.

(3) VPØ (Volts) designates the initial probe voltage.

(4) DELTAØ (Volts) designates the increment of the probe voltage.

Various options are provided, depending on the values of VPØ and DELTAØ. If VPØ < Ø.Ø, only the retardation region between VPØ and zero volts is analyzed with increment of the probe voltage equal to the given value of

DELTAØ. If VPØ is between zero and 1ØØØ.Ø, then only the accelerating region between zero and VPØ is analyzed with the same increment DELTAØ. The minimum permissable value of DELTAØ is Ø.1 volts. Program FTOJ allows for a sweep through the whole range of negative and positive probe voltages by setting VPØ > 1ØØØ.Ø. The difference VPØ-1ØØØ.Ø is set equal to the probe voltage increment DELTAØ, overriding the previously assigned value. The program sets the maximum probe voltage at the maximum value of the tabulated electron energy U(K), or, if a Maxwellian distribution is selected, it sets it at ten times the electron temperature $T_e \equiv VE$, in eV. The probe voltage varies from -U(K) to U(K) or from $-10\ T_e$ to $10\ T_e$ with the increment VPØ - 1ØØØ.Ø. However, the computer usually stops before the most positive potential is reached, since the instructions in the program ensure that, when two consecutive current values in the electron acceleration region differ by less than 10^{-3}%, no more calculations are done for this region. As an example, if 150 (determined by K in (11) below) electron energy values differing by Ø.1 volts are given, one sets VPØ = 1ØØØ.1 and DELTAØ = Ø.1, which will give a complete sweep, in Ø.1 volt steps, starting from -15.Ø volts through zero and into the positive voltage region.

(5) EA (V/cm) designates the external discharge electric field.

(6) P (torr) designates the neutral gas pressure.

(7) EAP (V/cm-torr) designates E/P.

Here we provide the option of assigning a value either to EA or to EAP, besides requiring a value for P. That is, the computer calculates EA if it is initially equated to zero and if P and EAP are given. Similarly, EAP is calculated if it is initially equated to zero and if P and EA are given.

(8) XNE designates the electron density in cm^{-3}, but, if XNE is between zero and one, it is interpreted as the ratio of electron to neutral density, η, instead of simply the electron density. In that case, the electron density is evaluated from η, p, and TI (see (9)) below, and XNE is redefined as the electron density. Furthermore, if XNE is between zero and one, the positive ion densities, XPI (see (15) below), and negative ion densities, XNI (see (16) below), are also interpreted as their ratios to neutral density.

(9) TI (^{o}K) designates the gas or ion temperature, T_g.

(10) A (mm^2) designates the area of the collecting part of the plane probe. If A = Ø.Ø, the program stops its execution. This option is provided to allow for possible extensions of the program to other geometries.

(11) K designates the number of values of the tabulated distribution function, f, if it is non-Maxwellian. K must be sufficiently less than 25Ø (say 24Ø as a maximum) to allow for the sum of positive and negative voltage values to be less than or equal to 25Ø. In order to insert a Maxwellian distribution function, one assigns a value of K > 1ØØØ, such that the electron temperature in eV is equal to VE = FLOAT (K - 1ØØØ)/1Ø. In this case, the program sets the first and second orders of anisotropy in f equal to zero and tabulates a Maxwellian form for f_o, so that it is not necessary to read in f_o. This option is seldom used (except for testing), since we are normally interested in a tabulated anisotropic f.

(12) NAZ is equal to zero or is non zero. If NAZ = Ø, only the "plane exact" results for the retardation region are calculated. If NAZ is non-zero, then the "plane approximate" and "plane zero EA" results are also calculated.

(13) NP designates the number of positive ion species. The value of NP must be less than or equal to five since up to five species only are allowed.

(14) NN designates the number of negative ion species and one must have $NN \leq 5$.

(15) XPI(I) values designate the positive ion densities (in cm^{-3}) multiplied by their respective ion charge numbers, but, if $\emptyset. < XNE < 1.$, then XPI(I) values designate the ratios of the above to neutral density. Up to five values of XPI(I) are allowed.

(16) XNI(I) values designate the negative ion densities (in cm^{-3}) multiplied by their respective charge numbers, and input values for these quantities are needed only if NN is nonzero. Also, if $\emptyset. < XNE < 1.$, then XNI(I) values designate the ratios of negative ion densities multiplied by respective charge numbers to the neutral density. Up to five values of XNI(I) are allowed. If $NN = \emptyset$, no input card is needed for XNI(I).

(17) XMI(I) values in atomic mass units designate the ion masses, starting from the positive ion species and following with the negative ion species. Up to ten values of XMI(I) are allowed.

(18) U(I) and F(I,J).

If the electron energy function is non-Maxwellian and given in tabulated form, the input requires data for U(I) and for F(I,1), F(I,2), and F(I,3). Here U(I), in eV, represents the electron energy, and, for each U(I), there are corresponding values of the zeroth, first, and second order of anisotropy of the electron distribution function, namely, F(I,1), F(I,2), and F(I,3), respectively. The maximum value of I is K. The zeroth order F(I,1) is normalized as in Eq. (315), and the other two components are normalized with respect

to it. The convention for F(I,2) in the input is that it represent $\underset{\sim}{f}_1$ in the cathode to anode direction, so that it is generally positive. The computer program alters its sign to correspond to our previous convention in our equations that the positive direction be from the anode to the cathode.

The output I-V characteristics are printed with the currents in amps and the voltage in volts. In addition, if VPØ > 1ØØØ.Ø and if THETA = 1Ø45.Ø or IDEG = 45°, then five I-V characteristics for the five orientations 0°, 45°, 90°, 135°, and 180° are printed and in addition punched onto cards for use as input data in the program JTOF. Three sets of cards are punched with respective significant digits in the current equal to 5, 4, and 3. This allows us to check on the sensitivity of the output of program JTOF to the accuracy of its input data. The present program FTOJ also punches out additional cards for use in program JTOF, namely, (1) EA and P, (2) A, (3) KK (the number of cards with negative voltage values), LK (with zero plus positive voltage), and MI (equal to zero when the total current is calculated), and (4) TI.

c. Symbols

A list of symbols is now provided.

A	: area of the plane probe
ARG	: $(V_p - V_a^*)/kT_g$
COSA	: $(3\cos^2\theta - 1)/2$
DELTAØ	: increment of the probe potential
E	: magnitude of the electron charge (e)
EA	: discharge electric field (E)
EAN	: E/N, ratio of electric field to neutral density in V-cm^2

EAP	: E/p, ratio of electric field to pressure in V/cm-torr
EPSØ	: permittivity of free space (ε_o)
F(I,J)	: electron velocity distribution function corresponding to f_o, f_{1z} and f_{2zz} for J = 1,2 and 3 respectively
G	: non-integrand part in the current density equations
I	: running variable
IDEG	: angular increment
IDELTA	: integer increment probe voltage
IP	: parameter used to write 40 output lines per page
ITEM	: parameter used for passing from one treatment to another: ITEM = 1 for "plane exact"; ITEM = 2 for "plane approximate"; ITEM = 3 for "plane zero EA"
IVP	: integer equal to one less than the designation of the largest voltage point for which the current is calculated
J	: running variable
JA	: variable used for designating currents evaluated for different orientations
K	: number of energy values U(I)
KK	: number of energy values initially; towards end it is changed to the number of negative voltage values in the calculated data
KN	: K - N + 1, a running variable
KP1	: KK + 1
L	: running variable
LK	: number of voltage values including zero and positive values in the calculated data
LØ	: L1-1, lower limit of integration in subroutine SUMT
L1	: integer designating the point after the lower limit of integration in subroutine SUMT

MI	: equal to zero when the total current values are used as input in program JTOF
M1	: equal to one
M2	: K - 1
N	: running variable
NAZ	: equal to one if only "plane exact" results are needed; nonzero if "plane approximate" and "plane zero EA" results are also desired
NK	: mainly used for KK + LK, or total number of voltage points (negative, zero and positive)
NM	: running variable
NN	: number of negative ions
NP	: number of positive ions
NT	: NP + NN
NVP	: K - IVP
NW	: equal to one if a detailed printout is desired; not equal to one if only specialized output data is wanted
N2	: equal to 2
P	: neutral gas pressure (p)
PI	: $\pi = 3.14159$
PREØ(I), PRE1(I), PRE2(I)	: integrand of "plane retarding exact" for the zeroth, first, and second order of anisotropy, respectively
PRNØ, PRN1, PRN2	: as above for "plane retarding approximate"
PRZØ, PRZ1, PRZ2	: as above for "plane retarding zero EA"
STP	: parameter equal to the inverse of the difference between two values of the tabulated electron energy
SUM	: value of the integral calculated by subroutine SUMT
THETA	: angular orientation of the probe if THETA < 1ØØØ.Ø
TI	: ion temperature (T_g)

TTA	: angular orientation of the probe (θ)
U(I)	: electron energy in eV
UP	: $-V_p$
VAST	: drop of the discharge electric field across the sheath (V_a^*)
VE	: electron temperature (V_e) in eV
VEF	: effective potential drop across the sheath ($V_p - V_a^*$) in eV
VE1	: the average electron energy (V_{e1}) in eV given in Eq. (278)
VI	: ion energy in eV at the sheath edge given by Eq.(280)
VP	: probe potential (V_p) in volts
VPØ	: initial probe potential
VRAT	: V_{e1}/kT_g
XA	: current in electron attraction region in initial approximation
XE	: electron contribution to the current in the electron attraction region
XF(I)	: function to be integrated by subroutine SUMT or for use in subroutine SHEATH
XFØ	: value of XF when its argument is zero
XI(KN,JA)	: XIT, or total current arrays for five orientations of the probe
XIE	: electron contribution to the current in the electron retardation region
XIN	: negative ion contribution to the current in the electron retardation region
XIP	: positive ion contribution to the current in the electron retardation region
XIT	: total current intercepted by the probe
XJE	: electron current density in the electron retardation region

XJØ(KN) : contribution to XJE arising from f_o

XJ1(KN) : contribution to XJE arising from f_{1z}

XJ2(KN) : contribution to XJE arising from f_{2zz}

XKØ : constant (K_o)

XK1 : normalization constant for the distribution functions

XLMDAD : Debye length (λ_D)

XLMDAS(I) : sheath thickness (λ_s)

XME : electron mass (m)

XMI(I) : ion masses

XMØ : atomic mass unit

XN : negative ion contribution to the current in the electron attraction region

XNE : electron density (n_e)

XNI(I) : negative ion density multiplied by the charge number

XNT : sum of XNI(I) over all species

XP : positive ion contribution to the current in the electron attraction region

XPI(I) : positive ion density multiplied by the charge number

XPT : sum of XPI(I) over all species

XVAST (KN) : V_a^* array for different V_p or λ_s

YF(I) : function to be integrated by subroutine SUMT

ZNE : XNE in cm^{-3}

ZNI(I) : XNI(I) in cm^{-3}

ZPI(I) : XPI(I) in cm^{-3}

ZPT : sum of ZPI(I) over all species

3. PROGRAM JTOF

a. Flow Chart

Figure 36 presents the flow chart for this program. Three sets of the components of the distribution function are deduced, based on three different approximations, namely, Eqs. (246) to (248), Eqs. (252) to (254), and Eqs. (255) to (257), respectively. These outputs are designated in the formulation by EA> 10^{-17}, 10^{-20} > EA> 10^{-17}, and EA = $\emptyset$. The first two outputs require I-V input characteristics for five orientations of the plane probe. For the last output, input results for three orientations of the probe are sufficient.

The program calculates a first approximation f_{01} for the zeroth order of the distribution function, f_o. This approximation is used to calculate the electron energy averages V_e, V_{e1}, the sheath thickness, λ_s, and the electron density, n_e. A second approximation for f_o is then evaluated from Eqs. (241) to (251). This is compared to f_{01} by evaluating the parameter ACCU defined as

$$\text{ACCU} = \int_o^\infty \left\{ \left[f_o(V_p) - f_{01}(V_p) \right]^2 V_p \right\}^{\frac{1}{2}} dV_p \Big/ \int_o^\infty f_o(V_p) V_p^{\frac{1}{2}} \, dV_p$$

If ACCU is less than 10^{-4}, f_o is an acceptable approximation. Otherwise, f_{01} is redefined equal to the second approximation, f_o, and the procedure is reiterated until ACCU is less than 10^{-4} or until the 100^{th} approximation for f_o is obtained. Usually less than ten iterations are sufficient for convergence.

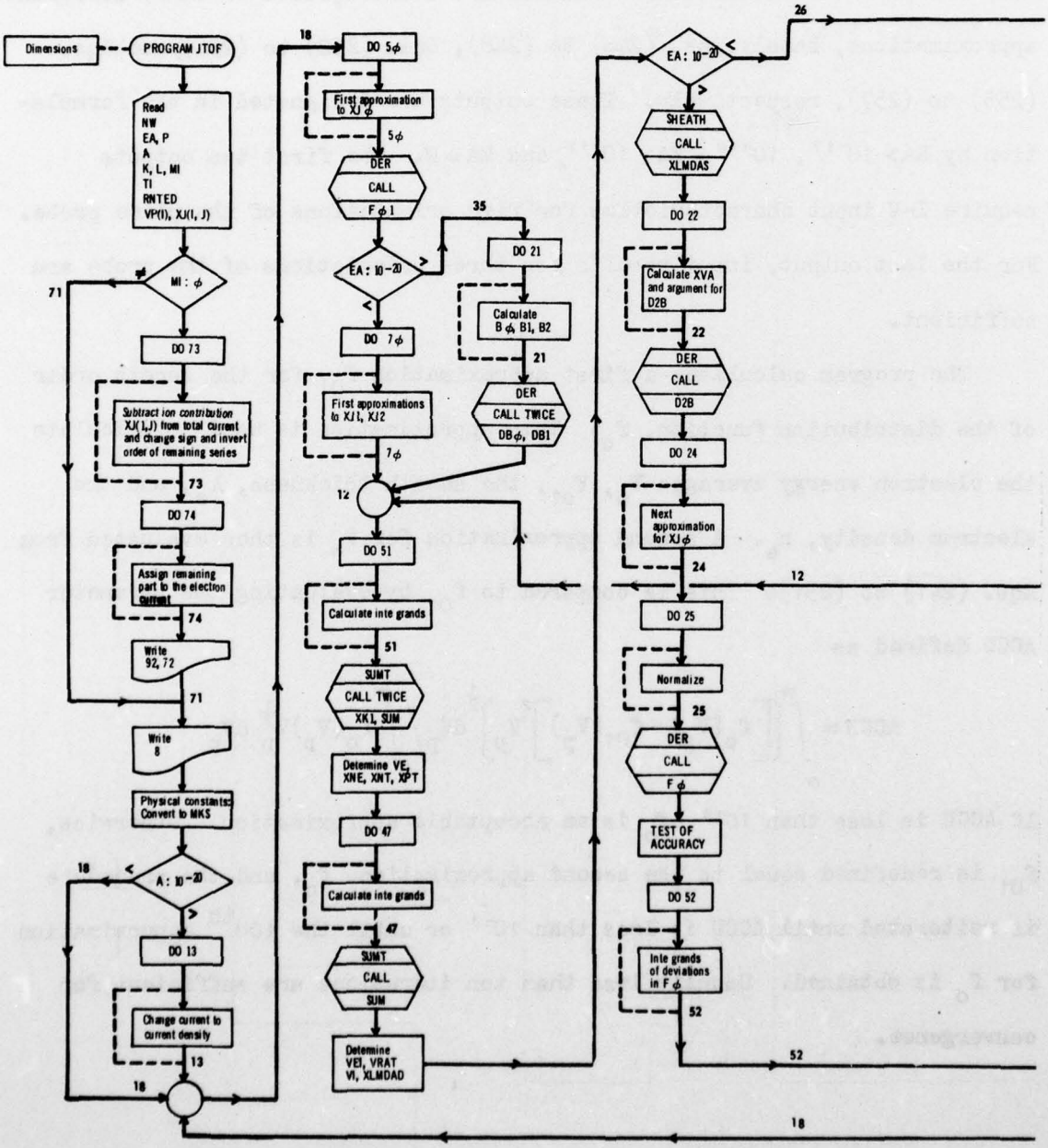

Figure 36. Flow Chart for Program JTOF

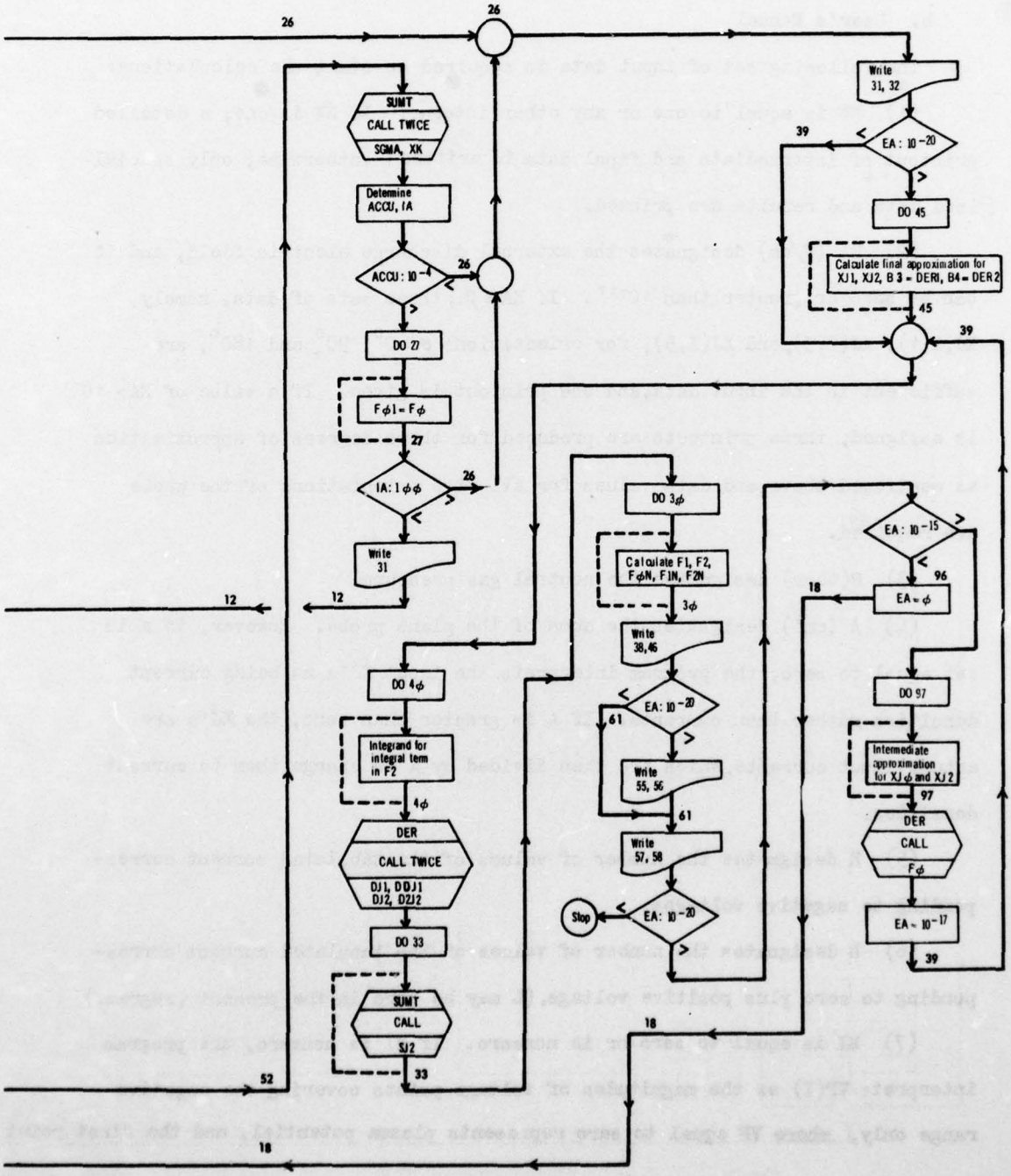
26
26
SUMT
CALL TWICE
SGMA, XK
Determine
ACCU, IA
ACCU: 10⁻⁴
26
DO 27
Fϕ1 = Fϕ
27
IA: 1ϕϕ
26
Write
31
12
12
DO 4ϕ
Integrand for
integral term
in F2
4ϕ
DER
CALL TWICE
DJ1, DDJ1
DJ2, DZJ2
DO 33
SUMT
CALL
SJ2
33
52
18
Write
31, 32
EA: 10⁻²⁰
39
DO 45
Calculate final approximation for
XJ1, XJ2, B3 = DER1, B4 = DER2
45
39
DO 3ϕ
Calculate F1, F2,
FϕN, F1N, F2N
3ϕ
Write
38, 46
EA: 10⁻²⁰
61
Write
55, 56
61
Write
57, 58
Stop
EA: 10⁻²⁰
18
EA: 10⁻¹⁵
96
EA = ϕ
DO 97
Intermediate
approximation
for XJϕ and XJ2
97
DER
CALL
Fϕ
EA ~ 10⁻¹⁷
39

b. User's Manual

The following set of input data is required to start the calculations:

(1) NW is equal to one or any other integer. If NW is one, a detailed printout of intermediate and final data is written; otherwise, only specialized data and results are printed.

(2) EA (V/cm) designates the external discharge electric field, and it can be zero or greater than 10^{-17}. If EA = $\emptyset$., three sets of data, namely, XJ(I,1), XJ(I,3), and XJ(I,5), for orientations $\theta = 0^{\circ}$, 90°, and 180°, are sufficient in the input data, and one printout is given. If a value of EA > 10^{-17} is assigned, three printouts are produced for three degrees of approximation as mentioned above, and data values for all five orientations of the probe are required.

(3) P(torr) designates the neutral gas pressure.

(4) A (mm^2) designates the area of the plane probe. However, if A is set equal to zero, the program interprets the input XJ's as being current densities rather than currents. If A is greater than zero, the XJ's are actual input currents, which are then divided by A to change them to current densities.

(5) K designates the number of values of the tabulated current corresponding to negative voltages.

(6) L designates the number of values of the tabulated current corresponding to zero plus positive voltage. (L may be zero in the present program.)

(7) MI is equal to zero or is nonzero. If MI is nonzero, the program interprets VP(I) as the magnitudes of voltage points covering the negative range only, where VP equal to zero represents plasma potential, and the first point

being the voltage increment beyond zero. Corresponding to these VP values, the XJ's are the magnitudes of the currents (or current densities if A = ∅.) due to the electrons only. If MI is equal to zero, the VP(I) values contain their sign and run over the range from most negative to positive in which VP equal to zero represents plasma potential. (The points VP ≥ ∅. may be omitted by setting L = ∅.) Also, the values of XJ contain their sign and include the ion contribution. The ion contribution is automatically subtracted from the XJ's, which are thereafter considered as electron currents (or current densities if A = ∅.). Presently, the read input data are based on MI = ∅.

(8) TI (^{o}K) designates the gas temperature.

(9) RNTED designates the ratio of the sum of negative ion density multiplied by charge number to the electron density.

(10) VP(I) in eV designates the set of equispaced voltage values. (See also (7) above.)

(11) XJ(I,J) values designate the sets of currents in amps (or current densities in amps/m^2 if A = ∅.) with J = 1 to 5, corresponding to $\theta = 0^{o}$, 45^{o}, 90^{o}, 135^{o}, and 180^{o}, and $\theta = 0^{o}$ is the anode to cathode direction. (See also (7) above.)

c. Symbols

The meaning of the various symbols is explained below.

A	: area of the plane probe
ACCU	: parameter used in the test of accuracy of f_o
BØ(I), B1(I), B2(I)	: mainly used for functions obtained from current densities (B_o, B_1, B_2 in Eqs. (241) to (243))
DBØ(I), DB1(I)	: mainly used for B_o', B_1' (see footnote*)

* The prime denotes the derivative with respect to V_p.

DDJ1(I) : j_1''

DER1(I),DER2(I) : first and second derivative of the function given in the output of subroutine DER. (At the end of the program, these symbols are also used for B_3 and B_4 in Eqs. (244) and (245).)

DJ1(I), DJ2(I) : j_1', j_2'

DV : voltage point just beyond the most positive input value

DVP : voltage difference between points

D2B(I) : $(V_a^e B_o')'$

D2J2(I) : j_2''

E : electron charge (e)

EA : discharge electric field (E)

EPSØ : permittivity of free space (ε_o)

FEØ(I),FE1(I), FE2(I) : exact values of f_o, f_{1z} and f_{2zz} deduced from the Boltzmann equation. These functions are not used in the present program but can be incorporated to evaluate their respective derivations from values deduced by this program.

FØ(I) : zeroth component of the electron distribution function (f_o)

FØN(I) : normalized value of f_o

FØ1(I) : first approximation to f_o, namely f_{o1}

F1(I), F2(I) : first and second components of the electron distribution function

F1N(I), F2N(I) : their normalized values

I : running variable

IA : number of passes in the test of accuracy

IP : parameter used to write 50 lines per page

J : running variable for orientation of the probe

K : number of values of the tabulated current for negative voltages

L : number of values of the tabulated current for zero plus positive voltages

M	: K-1
MI	: equal to zero if actual current values are read in; nonzero if electron current densities are read in
N	: running variable
NW	: equal to one if a detailed printout is desired; not equal to one if only specialized output is wanted
P	: neutral gas pressure (p)
PI	: $\pi = 3.14159$
RNTED	: ratio of summed negative ion densities (times respective charge numbers) to electron density
SGMA	: parameter used in the test of accuracy, equivalent to a rms difference between two successive approximations to f_o
SJ2(I)	: $\int_{V_p}^{\infty} [j_2(V_p)/V_p^{3/2}] dV_p$
SUM	: integrated result given by the output value in subroutine SUMT
TI	: neutral gas or ion temperature (T_g)
VE	: electron temperature (V_e) in eV
VE1	: the average electron energy (V_{e1}) in eV given in Eq. (278)
VI	: ion energy in eV at the sheath edge given by Eq. (280)
VRAT	: V_{e1}/kT_g
VP(I)	: probe voltage (V_p); also used for electron energy points
XF(I), XG(I), XH(I), XHØ	: functions used as inputs to subroutines DER and SUMT; XHØ is the zero energy value of the function XH
XJ(I,J)	: magnitude of the electron current for 5 orientations, J = 1 to 5, namely $\theta = 0^\circ$, 45°, 90°, 135° and 180° respectively
XJØ(I),XJ1(I), XJ2(I)	: j_o, j_1, j_2 (in Eqs. (246) to(248) and (252) to (257))

AD-A062 703 RCA LTD STE ANNE DE BELLEVUE (QUEBEC) RESEARCH AND D--ETC F/G 20/9
STUDY OF ELECTROSTATIC PROBES IN NONEQUILIBRIUM PLASMAS.(U)
JUN 75 I P SHKAROFSKY, A BONNIER F33615-73-C-4123

UNCLASSIFIED MNLD-75-TR-002 ARL-75-0228 NL

3 OF 3
AD
A062703

END
DATE
FILMED
3-79
DDC

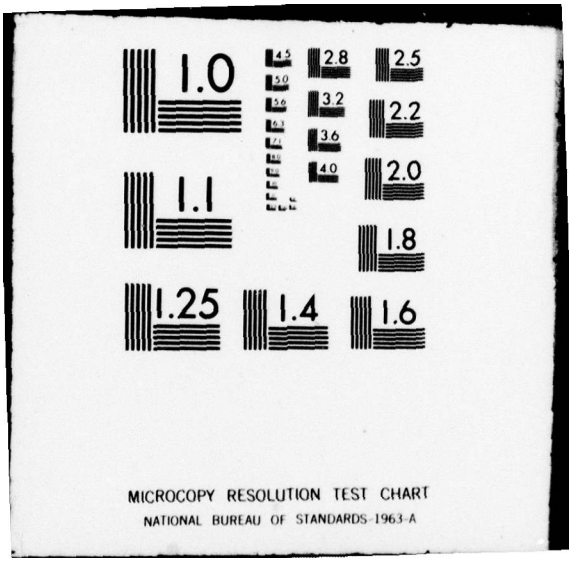
1.0
1.1
1.25
1.4
1.6
1.8
2.0
2.2
2.5
2.8
3.2
3.6
4.0
MICROCOPY RESOLUTION TEST CHART
NATIONAL BUREAU OF STANDARDS-1963-A

XK : parameter used in the test of accuracy equivalent to a normalization constant for f_o

XKØ : constant (K_o)

XK1 : normalization constant for the distribution functions

XLMDAD : Debye length (λ_D)

XLMDAS(I) : sheath thickness (λ_s)

XME : electron mass (m)

XNE : electron density (n_e)

XNT : sum over species of negative ion density times charge number

XPT : sum over species of positive ion density times charge number

XVA : V_a drop of the discharge electric field across the sheath

4. SUBROUTINE SHEATH

a. Flow Chart

This subroutine calculates an array of values of the sheath thickness XLMDAS(I), for a whole set of voltages equal to all the tabulated electron energies U(I). A flow chart is given in Figure 37. The relations used in calculating λ_s are given in Eqs. (286) to (288). The meaning of the input data required by the CALL statement is explained in the list of symbols below.

b. Symbols

A list of symbols appearing in this subroutine is given below.

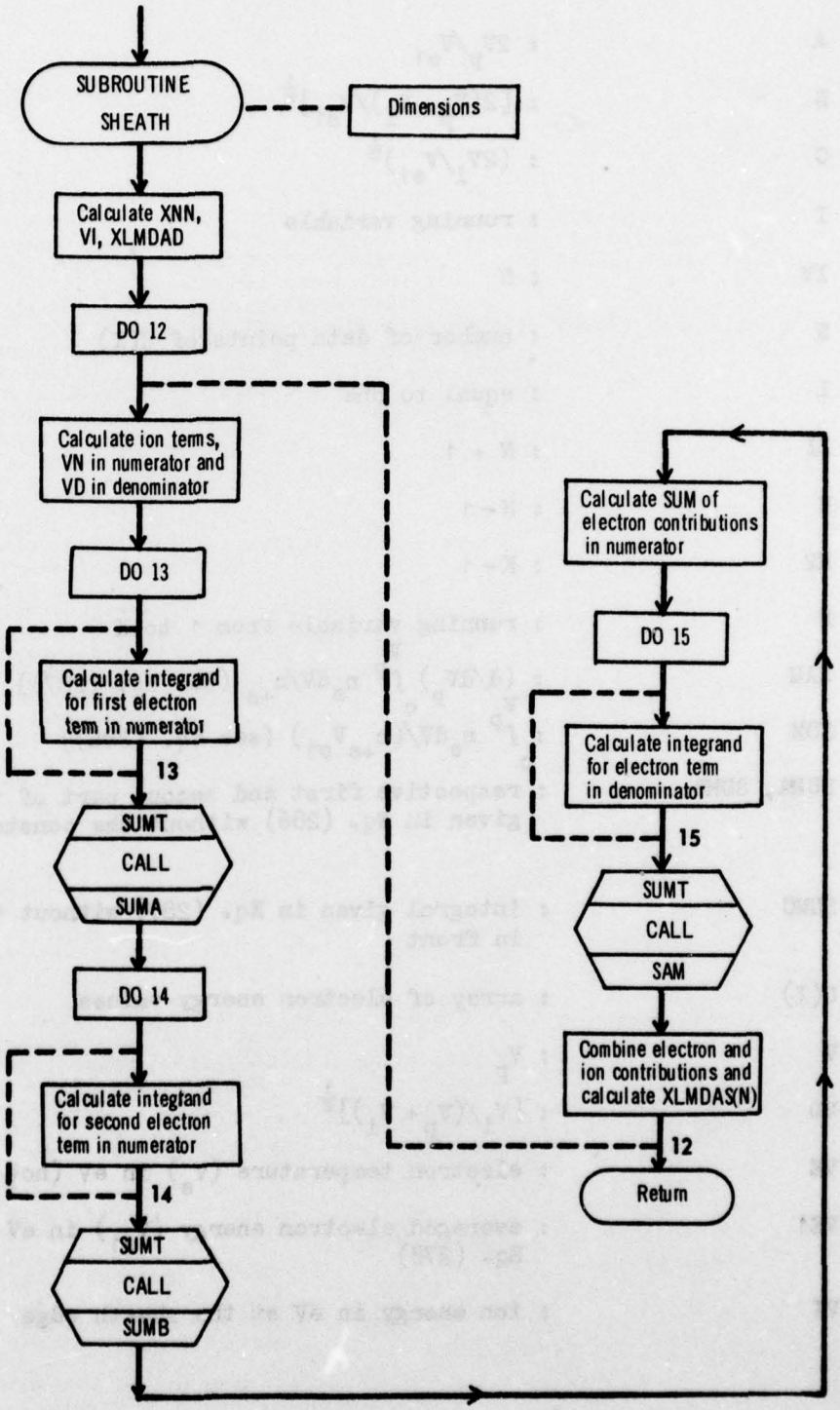

Figure 37. Flow Chart for Subroutine SHEATH

A	: $2V_p/V_{e1}$
B	: $[2(V_p + V_i)/V_{e1}]^{\frac{1}{2}}$
C	: $(2V_i/V_{e1})^{\frac{1}{2}}$
I	: running variable
IV	: N
K	: number of data points of U(I)
L	: equal to one
L1	: N + 1
M	: N - 1
M2	: K - 1
N	: running variable from 1 to K
SAM	: $(d/dV_p) \int_o^{V_p} n_e dV/n_{+s}$ (see Eq. (287))
SUM	: $\int_o^{V_p} n_e dV/(n_{+s} V_{e1})$ (see Eq. (286))
SUMA, SUMB	: respective first and second part of the integral given in Eq. (286) without the constant in front
SUMC	: integral given in Eq. (287) without the constant in front
U(I)	: array of electron energy values
V	: V_p
VD	: $[V_i/(V_p + V_i)]^{\frac{1}{2}}$
VE	: electron temperature (V_e) in eV (not used)
VE1	: averaged electron energy (V_{e1}) in eV given in Eq. (278)
VI	: ion energy in eV at the sheath edge

VN : $\left\{2[V_i(V_i + V_p)]^{\frac{1}{2}} - 2V_i\right\}/V_{e1}$

VRAT : ratio of V_{e1} to gas temperature in eV

V1 : $2V_i/V_{e1}$

XF(I) : array of f_o values for each energy value

XFØ : value of integrand at the lower limit

XK1 · normalizing constant for the distribution function

XLMDA : $(\varepsilon_o V_{e1}/n_{es}e^2)^{\frac{1}{2}}$ (see Eq. (289))

XLMDAD : $(\varepsilon_o V_{e1}/n_{+s}e^2)^{\frac{1}{2}}$

XLMDAS(I) : sheath thickness (λ_s)

XNE : electron density

XNN : $[n_{-s}kT_-/(n_{+s}V_{e1})]$ (see Eq. (288))

XPT : sum over species of positive ion density times charge number

Z(I) : function to be integrated by subroutine SUMT

5. SUBROUTINES SUMT AND DER

a. General Outline

Subroutines SUMT and DER perform, respectively, the integration and the differentiation of an input tabulated function f(x) with respect to the input variable x.

In both subroutines, the functional behaviour of function f around a certain point x is approximated by a parabola,

$$f(x) = c_1x^2 - c_2x + c_3$$

from which the first and second derivatives can be calculated as

$$f'(x) = 2c_1x - c_2$$

$$f''(x) = 2c_1$$

and the integral from a to b as

$$\int_a^b f(x)dx = \sum_{x=a+\Delta x}^{b} \left[\frac{1}{3} c_1(\Delta x)^3 - \frac{1}{2} c_2(\Delta x)^2 + c_3(\Delta x)\right]$$

where Δx is the difference between two successive values of x. The evaluation of parameters c_1, c_2, and c_3 are made from three successive points, namely, x_1, x_2, x_3, and the three corresponding values of f(x), namely, $f(x_1)$, $f(x_2)$, and $f(x_3)$:

$$c_1 = a_1 + a_2 + a_3$$

$$c_2 = (x_2 + x_3)a_1 + (x_1 + x_3)a_2 + (x_1 + x_2)a_3$$

$$c_3 = f(x_2) + (c_2 - c_1x_2)x_2$$

where

$$a_1 = \frac{f(x_1)}{(x_2 - x_1)(x_3 - x_1)}$$

$$a_2 = \frac{f(x_2)}{(x_2 - x_1)(x_2 - x_3)}$$

$$a_3 = \frac{f(x_3)}{(x_3 - x_1)(x_3 - x_2)}$$

From these definitions, one can see that the relation $f(x) = c_1x^2 - c_2x + c_3$ is indeed satisfied for all three points and in particular for the point x_2.

b. Subroutine SUMT

This subroutine integrates XF(U) from U(LI-1) to U(L2+1) and the value of the integral is SUM. A flow chart is given in Figure 38.

We first integrate from L = LI - 1 to LI using point LI + 1, then from LI to LI + 1 using point LI + 2, etc., until the next to final interval L2 - 1 to L2 using point L2 + 1. The final interval L2 to L2 + 1 is obtained by using the same c_1, c_2, and c_3 constants as in the interval L2-1 to L2.

The subroutine also allows for special cases of LI and L2, such as 0 or 1 or 2 values or differences between LI and L2 of 0 or 1 or 2.

The input data values required by the CALL statement are contained in the list of symbols given below. The following symbols appear in this subroutine.

A1,A2,A3	: parameters (a_1, a_2, a_3)
C1,C2,C3	: parameters (c_1, c_2, c_3)
L	: running variable
LA	: L2 + 1, designated upper limit of integration
LB	: L2 + 2
LI	: second designated x-point after lower limit of integration
L1	: = LI initially
L2	: designated x-point before upper limit of integration
SUM	: integral of the input function
SUM2	: integral of last interval L2 to L2 + 1
U(I)	: the tabulated x-argument values in eV
XF(I)	: the tabulated function, f(x), values

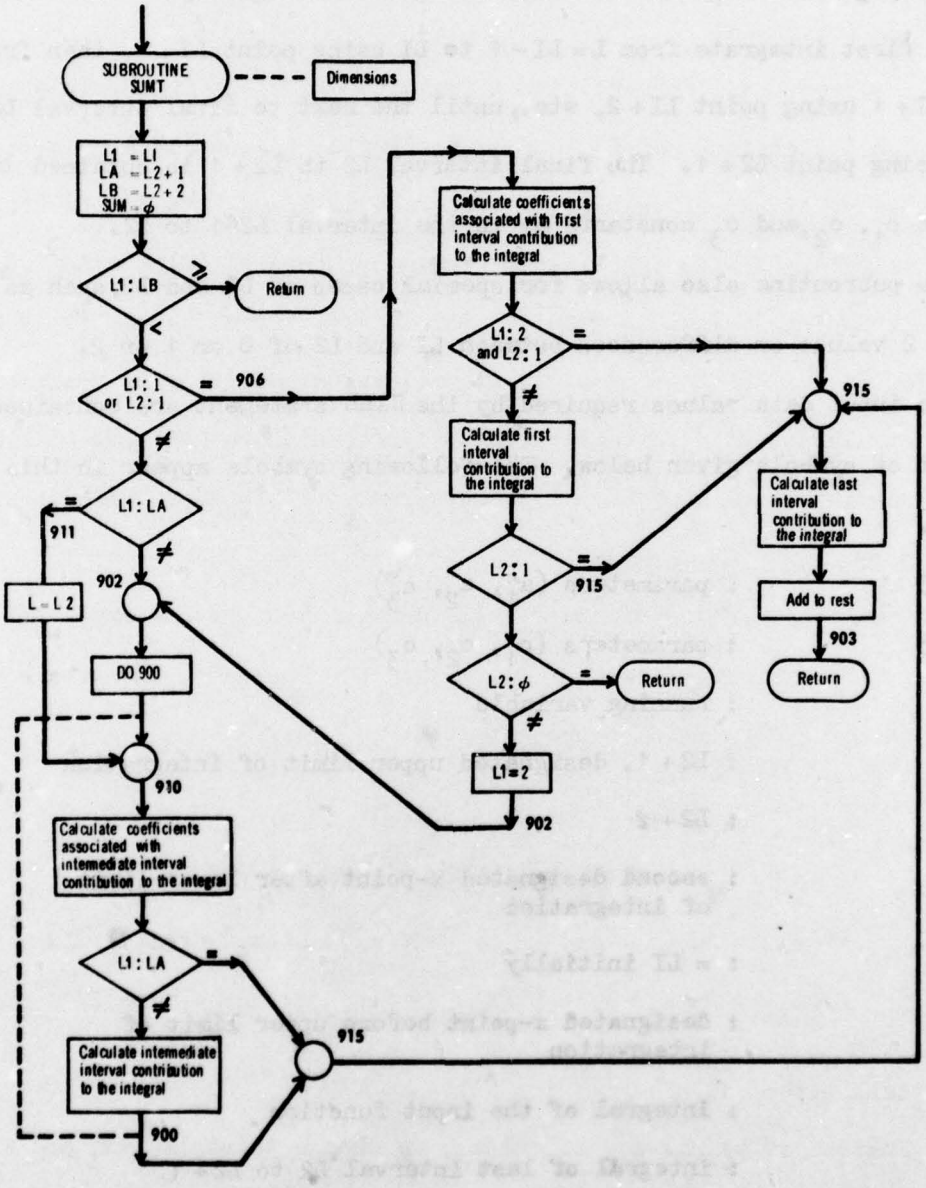

Figure 38. Flow Chart for Subroutine SUMT

XFØ	: value of XF for U = 0 or LI = 1, viz., f(x = 0), if integration starts from x equal to zero
XF1, XF2, XF3	: three successive values of the input function
X1, X2, X3	: three successive values of the input variable

c. Subroutine DER

This subroutine differentiates a function YF(VP) having K equispaced points of VP, starting from K = 1 to K = K. If IJ = 1, the output yields only the first derivative values DER1(VP), whereas, if IJ = 2, the second derviative values DER2(VP) are also calculated. In the process of calculating DER1, subroutine SE35 is called to smoothen the differentiated data. It is again called for the calculation of DER2. Sometimes no smoothing is desired, as in the calculation of f_o. Then one sets IJ = 4, and both DER1 and DER2 are calculated without calling SE35. A flow chart of this subroutine is given in Figure 39.

The methods used in calculating the derivatives are now explained. If Δx = VPD is the difference between equispaced x = VP points, then the equations in part (a) of this subsection reduce to

$$c_1 = [f(x_1) - 2f(x_2) + f(x_3)]/2(\Delta x)^2$$

$$c_2 = [f(x_1) - f(x_3)]/2\Delta x + [f(x_1) - 2f(x_2) + f(x_3)]x_2/(\Delta x)^2$$

$$f'(x_1) = 2c_1(x_2 - \Delta x) - c_2 = [-3f(x_1) + 4f(x_2) - f(x_3)]/2\Delta x$$

$$f'(x_i) = 2c_1 x_i - c_2 = [f(x_{i+1}) - f(x_{i-1})]/2\Delta x \quad (i \geq 2)$$

This we call method 1.

If instead of points x_1, x_2, and x_3, we choose points x_1, x_3, and x_5 for differentiation, then we have to change Δx to $2\Delta x$ and subscripts 2 and 3 to 3 and 5. We find

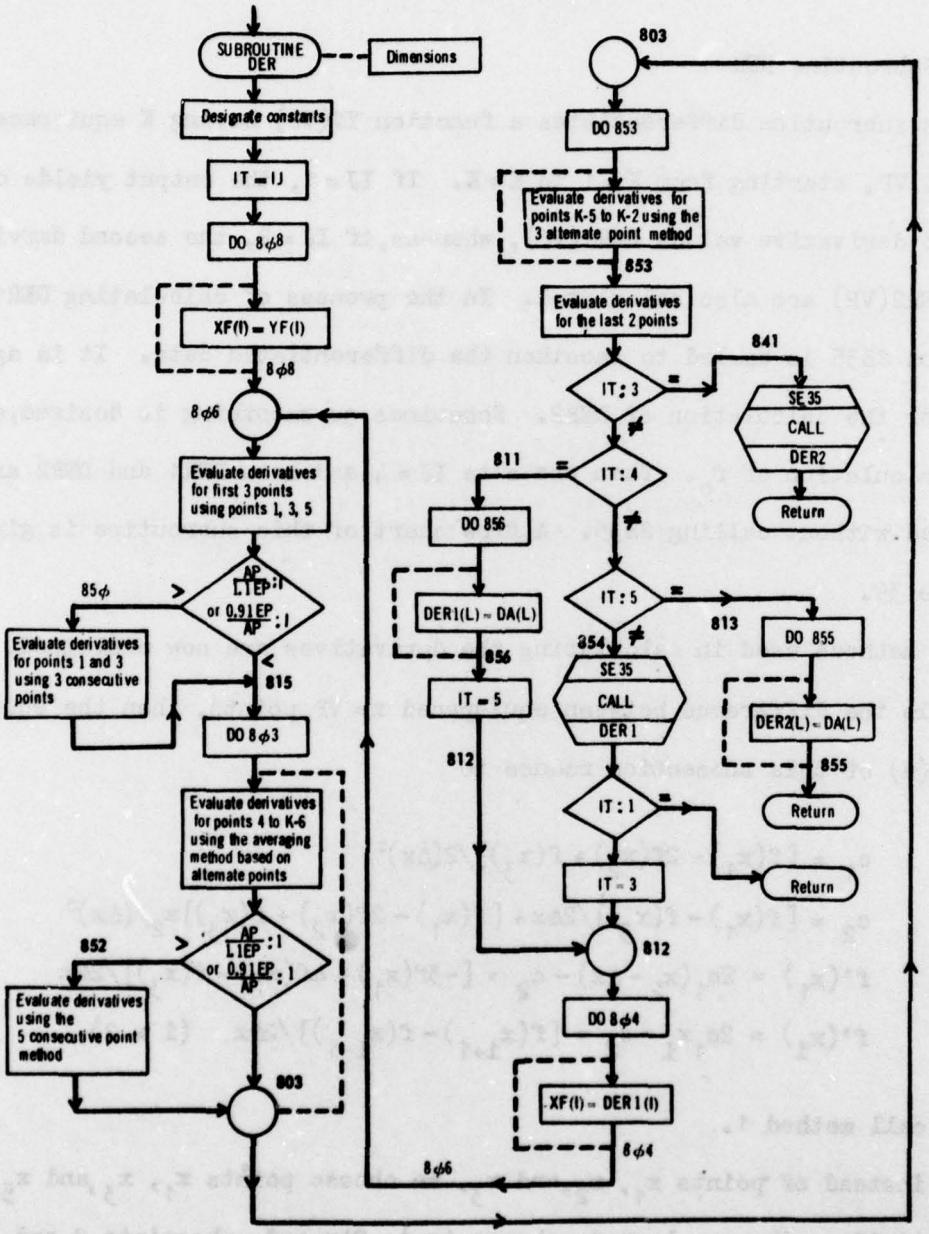

Figure 39. Flow Chart for Subroutine DER

$$f'(x_1) = 2c_1(x_3 - 2\Delta x) - c_2 = [-3f(x_1) + 4f(x_3) - f(x_5)]/4\Delta x$$

$$f'(x_2) = 2c_1(x_3 - \Delta x) - c_2 = [f(x_3) - f(x_1)]/2\Delta x$$

$$f'(x_i) = 2c_1 x_i - c_2 = [f(x_{i+2}) - f(x_{i-2})]/4\Delta x \quad (i \geq 3)$$

$$f'(x_4) = 2c_1(x_3 + \Delta x) - c_2 = [f(x_5) - f(x_3)]/2\Delta x$$

This is named method 2. For the first three initial points we use method 1 if the derivative is rapidly varying and method 2 if it varies slowly.

Consider point x_i and its derivative using three triplets, namely, (a) points x_{i-2}, x_i, and x_{i+2}, (b) x_{i-3}, x_{i-1}, and x_{i+1}, and (c) x_{i-1}, x_{i+1}, and x_{i+3}. Then one can obtain some "smoothing" by averaging the three values of $f'(x_i)$; thus,

$$f'(x_i) = \frac{1}{3} \cdot \frac{1}{4\Delta x}\left[f(x_{i+2}) - f(x_{i-2}) + 2f(x_{i+1}) - 2f(x_{i-1}) + 2f(x_{i+1}) - 2f(x_{i-1})\right]$$

$$= \left[f(x_{i+2}) + 4f(x_{i+1}) - 4f(x_{i-1}) - f(x_{i-2})\right] / 12\Delta x$$

We use this third method for $3 < i < K-6$ when $f'(x)$ varies slowly. When $f'(x)$ varies rapidly, we use a fourth method, namely, the 5 point method given in Abramowitz and Stegun[50], which yields

$$f'(x_i) = [-2f(x_{i+2}) + 16f(x_{i+1}) - 16f(x_{i-1}) + 2f(x_{i-2})]/24\Delta x$$

For the points K-5 to K-2 inclusive, we use the previous method 2. Finally, for K-1 and K, we adopt a straight line extension of $f(x)$ through points K-3 to K+2 so that

$$f(x_{K+1}) = 2f(x_{K-1}) - f(x_{K-3})$$

and $$f'(x_{K-1}) = [f(x_{K+1}) - f(x_{K-3})]/4\Delta x = [f(x_{K-1}) - f(x_{K-3})]/2\Delta x$$

Similarly, $$f'(x_K) = [f(x_K) - f(x_{K-2})]/2\Delta x$$

After the values of the first derivative are obtained, these are then used as the data to redo the calculation for the second derivative. The output yields the first derivative DER1 and, if asked for, the second derivative DER2. The input data values required by the CALL statement are explained below in the list of symbols.

Many different versions were tried for this subroutine, and the one given here was found thus far to be the best.

We list below the symbols appearing in this subroutine.

AP, EP	: the derivatives at two consecutive points which are compared to see how quickly the derivative is varying
DA(L)	: the derivative value at a given point
DER1(I)	: the first derivative set of values of the input function
DER2(I)	: the second derivative set of values of the input function
I	: running variable
IJ	: equal to one if only DER1 is required; equal to two if DER2 is also required; equal to four if both derivatives are wanted with no smoothing
IT	: = IJ initially
K	: number of data points for differentiation
KMM	: K-2
KM5	: K-5
KM6	: K-6
L	: running variable
VP(I)	: values of the tabulated x points in eV

VPD	: the value of Δx
XF(I)	: equated to YF initially, then later equated to DER1
YF(I)	: f(x) tabulated set of values
Z	: $(24\ \Delta x)^{-1}$
Z12	: $(2\ \Delta x)^{-1}$
Z2	: $(12\ \Delta x)^{-1}$
Z6	: $(4\ \Delta x)^{-1}$

6. PRINTOUT OF THE COMPLETE PROGRAMS

a. Program FTOJ and its Subroutines

```
      PROGRAM FTOJ (INPUT,OUTPUT,TAPE5,TAPE6,TAPE7)
      DIMENSION U(250),F(250,3),XLMDAS(250),XF(250),XI(250,5),
     CXVAST(250),PRE0(250),PRE1(250),PRE2(250),YF(250),
     CXJ0(250),XJ1(250),XJ2(250),XNI(5),XPI(5),XMI(10),ZNI(5),ZPI(5)
  5   READ(5,108) NW
  108 FORMAT(I1)
      READ(5,10)THETA,VP0,DELTA0,EA,P,EAP,XNE,TI,A,K,NA7,NP,NN
   10 FORMAT( 3F6.1/3F7.2/E9.3,F7.1/F6.3/4I4)
      KK=K
 10   NK=K
      IF(NP.GT.5) GO TO 141
      NT=NP+NN
      READ(5,7)(XPI(I),I=1,NP)
      IF(NN.EQ.0) GO TO 25
 15   IF(NN.GT.5) GO TO 141
      READ(5,7)(XNI(I),I=1,NN)
    7 FORMAT( 5E9.3)
   25 READ(5,77)(XMI(I),I=1,NT)
   77 FORMAT( 10F8.3)
 20   IF(EAP.LT.1.E-20) EAP=EA/P
      IF(EA.LT.1.E-20) EA=EAP*P
      EAN=EAP*TI*1.0358E-19
      WRITE(6,18)EA,P,EAP,EAN,A
   18 FORMAT(* EA=*,F5.2,*V/CM*,10X,*P=*,F6.2,*TORR*,10X,*E/P=*,F6.2,
 25  C*V/CM-TORR*,10X,*E/N=*,E11.4,*V-CM2*,10X,*A=*,F6.3,*MM2*)
      WRITE(6,2)(XMI(I),I=1,NT)
    2 FORMAT(* ATOMIC MASSES=*,10F8.3)
C
C CONSTANTS
 30   PI=3.14159
      E=1.602E-19
      EPS0=8.854E-12
      XME=9.1096E-31
      XM0=1.6606E-27
 35   IP=0
C
C RATIONALIZATION TO MKSA
      EA=EA*100.
      P=P*133.3
 40   A=A*1.E-6
      TI=TI*E/11604.
      DO 6 I=1,NT
    6 XMI(I)=XMI(I)*XM0
      IF(XNE-1.)15,15,16
 45   XNE=XNE*P/TI
      DO 5 I=1,NP
    5 XPI(I)=XPI(I)*P/TI
      IF(NN.EQ.0) GO TO 17
      DO 4 I=1,NN
 50   4 XNI(I)=XNI(I)*P/TI
      GO TO 17
   16 XNE=XNE*1.E6
      DO 3 I=1,NP
    3 XPI(I)=XPI(I)*1.E6
 55   IF(NN.EQ.0) GO TO 17
      DO 1 I=1,NN
    1 XNI(I)=XNI(I)*1.E6
```

```
   17 ZNE=XNE/1.E6
      ZPT=0.
      DO 100 I=1,NP
      ZPI(I)=XPI(I)*1.E-6
  100 ZPT=ZPI(I)+ZPT
      XPT=ZPT*1.E6
      XNT=XPT-XNE
      IF(NN.EQ.0) GO TO 102
      DO 101 I=1,NN
  101 ZNI(I)=XNI(I)*1.E-6
  102 WRITE(6,19)ZNE,(ZPI(I),I=1,NP)
   19 FORMAT(* NE=*,E12.4,5X,*POS.DENS.=*,5E12.4)
      IF(NN.EQ.0) GO TO 104
      WRITE(6,103) (ZNI(I),I=1,NN)
  103 FORMAT(* NEGATIVE DENS.=*,5E12.4)
  104 CONTINUE
C
C MAXWELLIAN OR TABULATED DISTRIBUTION
      IF(K-1000)11,11,12
   12 VE=FLOAT(K-1000)/10.
      K=10*(K-1000)
      IF(K.GT.250) GO TO 141
      DO 13 I=1,K
      U(I)=FLOAT(I)/10.
      F(I,1)=2./PI**.5/VE**1.5*EXP(-U(I)/VE)
      F(I,2)=0.
   13 F(I,3)=0.
      GO TO 27
   11 CONTINUE
      IF(K.GT.250) GO TO 141
      READ(5,14)(U(I),(F(I,J),J=1,3),I=1,K)
   14 FORMAT(1X,4E12.4)
      DO 150 I=1,K
  150 F(I,2)=-F(I,2)
   27 STP=1./(U(2)-U(1))
C
C CALCULATION OF XK1
      DO 20 I=1,K
   20 XF(I)=SQRT(U(I))*F(I,1)
      M1=1
      N2=2
      M2=K-1
      XF0=0.
      CALL SUMT(U,XF,M1,M2,XF0,XK1)
C
C CALCULATION OF VE
      DO 21 I=1,K
      YF(I)=F(I,1)/SQRT(U(I))
   21 XF(I)=SQRT(U(I)**3)*F(I,1)
      CALL SUMT(U,XF,M1,M2,XF0,SUM)
      VE=SUM*2./(XK1*3.)
      CALL SUMT(U,YF,N2,M2,XF0,SUM)
      SUM=SUM+F(1,1)*2.*SQRT(U(1))
      VE1=2.*XK1/SUM
      XK0=XNE*E*SQRT(E/XME/2.)/2./XK1
      VRAT=VE1*E/TI
      VI=.5*VE1*XPT/(XNE+XNT*VRAT)
```

```
      XIP=0.
      DO 105 I=1,NP
  105 XIP=XIP+A*E*XPI(I)*SQRT(2.*E*VI/XMI(I))
      XN=0.
      IF(NN.EQ.0)GO TO 106
      DO 107 I=1,NN
  107 XN=XN-A*E*XNI(I)*SQRT(TI/(2.*PI*XMI(NP+I)))
  106 CONTINUE
C
C CALCULATION OF XLMDAS(I)
      XLMDAD=SQRT(EPS0*VE1/(E*XNE))
      DO 22 I=1,K
   22 XF(I)=F(I,1)
      CALL SHEATH(U,XF,VI,VE1,VRAT,ANE,XPT,XK1,XLMDAD,K,XLMDAS,VF)
      WRITE(6,26)VF,VE1,XK1,VRAT,VI,XLMDAD
   26 FORMAT(* VF=*,F6.2,5X,*VE1=*,F6.2,5X,*XK1=*,E11.4,5X,*VRAT=*,F8.2,
     C5X,*VI=*,F6.2,5X,*XLMDAD=*,E11.4)
      WRITE(6,73) (XLMDAS(I),I=1,K)
   73 FORMAT( 10(2X,E11.4))
C
C
C PLANE EXACT
      IF(A.LT.1.E-20)GO TO 140
   30 IF(NW.EQ.1) WRITE(6,31)
   31 FORMAT(*0*,11HPLANE EXACT)
      ITEM=1
C
C ROTATE OR FIX
   44 TTA=THETA
      IF(TTA.GT.1000.) GO TO 49
   32 JA=INT((TTA+45.)/45.+.1)
      IF(NW.EQ.1)
     $WRITE(6,33)TTA,JA
   33 FORMAT(*0THETA=*,F6.1,5X,*JA=*,I4)
      TTA=TTA*PI/180.
      COSA=(3.*COS(TTA)**2-1.)/2.
      IF(VP0.LT.0.) GO TO 34
      IF(VP0.LT.1000.) GO TO 35
C
C RET SWEEP
      DELTA0=VP0-1000.
      IDELTA=INT(STP*DELTA0+.1)
      IVP=((K+1)/IDELTA)*IDELTA-1
      IF(IVP.EQ.K) IVP=IVP-IDELTA
      GO TO 36
C
C RET
   34 IVP=INT(-STP*VP0-.9)
      IDELTA=INT(STP*DELTA0+.1)
   36 NVP=K-IVP
      IF(NW.EQ.1)
     $WRITE(6,29)IDELTA,IVP,NVP
   29 FORMAT(* IDELTA=*,I4,5X,*IVP=*,I4,5X,*NVP=*,I4)
      IF(NW.EQ.1) WRITE(6,28)
   28 FORMAT(*0*,3X,*VP*,10X,*XIT*,10X,*XIE*,11X,*F0*,12X,*F1*,12X,*F2*,
     C8X,*VAST*,8X,*L0*)
      DO 37 N=NVP,K,IDELTA
```

```
      KN=K-N+1
      VP=FLOAT(KN)/STP
      VAST=EA*XLMDAS(KN)*COS(TTA)
175   XVAST(KN)=VAST
      VEF=VP-VAST
      IF(VEF.LT.0.)VEF=0.
      GO TO(45,51,62),ITEM
C
180   51 DO 52 I=1,K
      PRN0=XK0*(U(I)-VEF)*F(I,1)
      PRN1=XK0*(2./3.*U(I)*(1-(VP/U(I))**1.5)+VAST*SQRT(VP/U(I))-0.25*VA
     CST**2/SQRT(VP*U(I)))*F(I,2)*COS(TTA)
      PRN2=XK0*(0.25*(U(I)+2.*VP-3.*VP**2/U(I))+0.5*VAST*(3.*VP/U(I)-1.)
185   C-0.75*VAST**2/U(I))*F(I,3)*COSA
   52 YF(I)=PRN0-PRN1+PRN2
      G=0.5*XK0*VAST**2*(F(KN,1)-F(KN,2)*COS(TTA)+F(KN,3)*COSA)
      L1=KN+1
      GO TO 46
190   62 DO 63 I=1,K
      PRZ0=XK0*(U(I)-VP)*F(I,1)
      PRZ1=2./3.*XK0*U(I)*(1-(VP/U(I))**1.5)*F(I,2)*COS(TTA)
      PRZ2=0.25*XK0*(U(I)+2.*VP-3.*VP**2/U(I))*F(I,3)*COSA
   63 YF(I)=PRZ0-PRZ1+PRZ2
195   G=0.
      L1=KN+1
      GO TO 46
C
      45 DO 38 I=1,K
200   PRE0(I)=XK0*(U(I)-VEF)*F(I,1)
      PRE1(I)=2./3.*XK0*U(I)*(1.-(VEF/U(I))**1.5)*F(I,2)*COS(TTA)
      PRE2(I)=XK0/4.*(U(I)+2.*VEF-3.*VEF**2/U(I))*F(I,3)*COSA
   38 CONTINUE
      LJ=INT(VEF*STP+1.5)
205   IF(L1.GT.K)L1=K+1
      CALL SUMT(U,PRE0,L1,M2,XF0,SUM)
      XJ0(KN)=SUM
      CALL SUMT(U,PRE1,L1,M2,XF0,SUM)
      XJ1(KN)=SUM
210   CALL SUMT(U,PRE2,L1,M2,XF0,SUM)
      XJ2(KN)=SUM
      XJE=-XJ0(KN)+XJ1(KN)-XJ2(KN)
      GO TO 58
   46 CALL SUMT(U,YF,L1,M2,XF0,SUM)
215   XJE=-SUM-G
   58 CONTINUE
      XIE=A*XJE
      XIN=0.
      ARG=VEF*E/TI
220   IF((ARG.GT.100.).OR.(ARG.EQ.0.)) GO TO 74
      XIN=XN*EXP(-ARG)
   74 CONTINUE
      IF(ARG.EQ.0.) XIN=XN
      XIT=XIE+XIP+XIN
225   UP=-VP
      L0=L1-1
      IF(NW.EQ.1)
     $WRITE(6,39)UP,XIT,XIE,F(KN,1),F(KN,2),F(KN,3),XVAST(KN),L0
```

```
   39 FORMAT( F6.1,2X,2(2XE11.4),3(2XE12.4),2X,F7.4,6X,I4)
230      IF(IP.NE.39) GO TO 56
         IF(NW.EQ.1) WRITE(6,57)
   57 FORMAT(*1*)
         IP=-1
   56 IP=IP+1
235      GO TO(55,91,91),ITEM
   55 XI(KN,JA)=XIT
   91 CONTINUE
   37 CONTINUE
         KK=K-NVP+1
240      GO TO(47,54,54),ITEM
   47 IF(NW.EQ.1) WRITE(6,70)
   70 FORMAT(*0*,3X,*U*,11X,*XJ0*,10X,*XJ1*,10X,*XJ2*)
         DO 72 N=NVP,K,IDELTA
         I=K-N+1
245      IF(NW.EQ.1)
        $WRITE(6,71)U(I),XJ0(I),XJ1(I),XJ2(I)
   71 FORMAT( F6.1,2X,3(2XE11.4))
         IF(IP.NE.39)GO TO 72
         IF(NW.EQ.1) WRITE(6,57)
250      IP=-1
   72 IP=IP+1
         IF(VP0.LT.1000.) GO TO 54
C
C ACC
255      IVP=K
         GO TO 42
   35 IVP=INT(STP*VP0+.1)
         IDELTA=INT(STP*DELTA0+.1)
   42 IF(NW.EQ.1)
260     $WRITE(6,8)IDELTA,IVP
    8 FORMAT(*0ACCELERATING REGION,PLANE EXACT    IDELTA=*,I4,5X,*IVP=*,
        CI4,5X/*0*,3X,*VP*,10X,*XIT*)
         DO 41 I=1,K
   41 XF(I)=XK0*U(I)*(F(I,1)-2./3.*F(I,2)*COS(TTA)+0.25*F(I,3)*COSA)
265      CALL SUMT(U,XF,M1,M2,XF0,SUM)
         XE=-A*SUM
         XA=0.
         DO 43 N=1,IVP,IDELTA
         VP=FLOAT(N-1)/STP
270      XP=XIP*EXP(-VP*E/TI)
         XIT=XE+XP+XN
         LK=N
         NK=N+KK
         IF(NK.GT.250) GO TO 141
275      XI(NK,JA)=XIT
         IF(NW.EQ.1)
        $WRITE(6,39)VP,XIT
         IF(IP.NE.39) GO TO 59
         IF(NW.EQ.1) WRITE(6,57)
280      IP=-1
   59  IP=IP+1
         IF((1-XA/XIT).LT.1.E-5) GO TO 54
         XA=XIT
   43 CONTINUE
285    54 CONTINUE
```

```
      IF(NW.EQ.1)
     $WRITE(6,82)KK,LK,NK
   82 FORMAT(*0KK=*,I4,5X,*LK=*,I4,5X,*NK=*,I4)
      IF(THETA-1000.)48,40,40
   49 IDEG=INT(THETA-1000.+.1)
      IF(NW.EQ.1)
     $WRITE(6,9)IDEG
    9 FORMAT(* IDEG=*,I4)
      DO 40 NM=1,181,IDEG
      TTA=FLOAT(NM-1)
      GO TO 32
   40 CONTINUE
      IF((VP0.GT.0.0).AND.(VP0.LT.1.E3)) STOP
   48 IF(NAZ.EQ.0) GO TO 64
      GO TO(53,61,64),ITEM
C
C
C PLANE APPROXIMATE
   53 WRITE(6,50)
   50 FORMAT(*0*17HPLANE APPROXIMATE)
      ITEM=2
      GO TO 44
C PLANE ZERO EA
   61 WRITE(6,60)
   60 FORMAT(*0*13HPLANE ZERO EA)
      ITEM=3
      GO TO 44
   64 CONTINUE
C
C  PREPARATION FOR SUBROUTINE JTOF
      IF((IUEG.NE.45).OR.(VP0.LT.1000.)) GO TO 90
      EA=EA/100.
      P=P/133.3
      MI=0
      A=A*1.E6
      TI=TI*11604./E
      WRITE(6,65)
   65 FORMAT(*0*,9X*U*,5X,*XI(I,1)*,5X,*XI(I,2)*,5X,*XI(I,3)*,
     C5X,*XI(I,4)*,5X,*XI(I,5)*,11X,*F0*,10X,*F1*,10X,*F2*)
      DO 68 N=IDELTA,KK,IDELTA
      I=KK-N+IDELTA
      U(I)=-FLOAT(I)/STP
      WRITE(6,66)U(I),(XI(I,J),J=1,5),(F(I,L),L=1,3)
   66 FORMAT(* *,F12.2,5E12.4,5X,3E12.4)
      IF(IP.NE.39)GO TO 68
      WRITE(6,57)
      IP=-1
   68 IP=IP+1
      WRITE(7,69) (U(KK+IDELTA-I),(XI(KK+IDELTA-I,J),J=1,5),I=IDELTA,
     $   KK,IDELTA)
      WRITE(7,75) (U(KK+IDELTA-I),(XI(KK+IDELTA-I,J),J=1,5),I=IDELTA,
     $   KK,IDELTA)
      WRITE(7,76) (U(KK+IDELTA-I),(XI(KK+IDELTA-I,J),J=1,5),I=IDELTA,
     $   KK,IDELTA)
   69 FORMAT( F12.2,5E12.5)
   75 FORMAT( F12.2,5E12.4)
   76 FORMAT( F12.2,5E12.3)
```

```
      KP1=KK+1
      DO 80 I=KP1,NK,IDELTA
345   U(I)=FLOAT(I-KP1)/STP
      WRITE(6,66) U(I),(XI(I,J),J=1,5)
      IF(IP.NE.39) GO TO 80
      WRITE(6,57)
      IP=-1
350    80 IP=IP+1
      WRITE(7,69)(U(I),(XI(I,J),J=1,5),I=KP1,NK,IDELTA)
      WRITE(7,75)(U(I),(XI(I,J),J=1,5),I=KP1,NK,IDELTA)
      WRITE(7,76)(U(I),(XI(I,J),J=1,5),I=KP1,NK,IDELTA)
      KK=KK/IDELTA
355   LK=(LK-1)/IDELTA+1
      NK=KK+LK
      WRITE(6,82)KK,LK,NK
      WRITE(7,67)EA,P,A,KK,LK,MI,TI
    67 FORMAT( 2F7.2/F6.3/3I4/F7.1)
360   GO TO 90
   141 WRITE(6,142) NP,NN,K,NK
   142 FORMAT(* DECREASE NO.OF ENTRIES IN ONE OF NP=*,I4,5X,*NN=*,I4,5X,
     C*K=*,I4,5X,*NK=*,I4)
    90 CONTINUE
365 140 CONTINUE
      STOP
      END
```

```
      SUBROUTINE SHEATH(U,XF,VI,VE1,VRAT,XNE,XPT,XK1,XLMDA,K,XLMDAS,VE)
      DIMENSION U(250),XF(250),Z(250),XLMDAS(250)
      XNN=(XPT-XNE)/(XPT*VRAT)
      V1=2.*VI/VE1
    5 C=SQRT(V1)
      XF0=0.
      L=1
      M2=K-1
      XLMDAD=XLMDA *SQRT(XNE/XPT)
   10 DO 12 N=1,K
      V=U(N)
      A=2.*V/VE1
      B=SQRT(A+V1)
      VN=B*C-V1
   15 VD=C/B
      IV=N
      L1=IV+1
      M=IV-1
      DO 13 I=IV,K
   20 13 Z(I)=((U(I)-V)**1.5-U(I)**1.5-V**1.5)*XF(I)
      CALL SUMT(U,Z,L1,M2,XF0,SUMA)
      DO 14 I=1,IV
   14 Z(I)=(U(I)**1.5)*XF(I)
      CALL SUMT(U,Z,L,M,XF0,SUMB)
   25 SUM=(2.*SUMB-SUMA)*XNE/(3.*XPT*XK1*VE1)
      DO 15 I=IV,K
   15 Z(I)=(SQRT(U(I)-V)+SQRT(V))*XF(I)
      CALL SUMT(U,Z,L1,M2,XF0,SUMC)
      SAM=SUMC*XNE/(2.*XPT*XK1)
   30 17 XLMDAS(N)=XLMDAD*SQRT(2.*(VN-SUM-XNN))/(VD-SAM)
      12 CONTINUE
      RETURN
      END
```

```
      SUBROUTINE SUMT(U,XF,LI,L2,XF0,SUM)
      DIMENSION U(250),XF(250)
      L1=LI
      LA=L2+I
      LB=L2+2
      SUM=0.
      IF(L1.GE.LB)RETURN
      IF((L1.EQ.1).OR.(L2.EQ.1)) GO TO 906
      IF(L1.EQ.LA) GO TO 911
      GO TO 902
  906 X2=U(1)
      X3=U(2)
      XF2=XF(1)
      XF3=XF(2)
      A1=XF0/(X2*X3)
      A2=XF2/(X2*(X2-X3))
      A3=XF3/(X3*(X3-X2))
      C1=A1+A2+A3
      C2=(X2+X3)*A1+X3*A2+X2*A3
      C3=XF2+(C2-C1*X2)*X2
      IF((L1.EQ.2).AND.(L2.EQ.1)) GO TO 915
      SUM=C1*X2**3/3.-C2*X2*X2/2.+C3*X2
      IF(L2.EQ.1) GO TO 915
      IF(L2.EQ.0) RETURN
      L1=2
  902 DO 900 L=L1,L2
  910 X1=U(L-1)
      X2=U(L)
      X3=U(L+1)
      XF1=XF(L-1)
      XF2=XF(L)
      XF3=XF(L+1)
      A1=XF1/((X2-X1)*(X3-X1))
      A2=XF2/((X2-X1)*(X2-X3))
      A3=XF3/((X3-X1)*(X3-X2))
      C1=A1+A2+A3
      C2=(X2+X3)*A1+(X1+X3)*A2+(X1+X2)*A3
      C3=XF2+(C2-C1*X2)*X2
      IF(L1.EQ.LA) GO TO 915
  900 SUM=SUM+C1*(X2**3-X1**3)/3.-C2*(X2*X2-X1*X1)/2.+C3*(X2-X1)
  915 SUM2=C1*(X3**3-X2**3)/3.-C2*(X3*X3-X2*X2)/2.+C3*(X3-X2)
      SUM=SUM+SUM2
  903 RETURN
  911 L=L2
      GO TO 910
      END
```

b. Program JTOF and its Subroutines

```
      PROGRAM JTOF  (INPUT,OUTPUT,TAPE5,TAPE6)
      DIMENSION VP(250),XJ(250,5),F01(250),XLMDAS(250),
     CB0(250),B1(250),B2(250),DB0(250),FE0(250),FE1(250),FE2(250),
     CDB1(250),DB2(250),XJ0(250),XJ1(250),XJ2(250),DJ1(250),
     CDJ2(250),SJ2(250),F0(250),F1(250),F2(250),
     CDDJ1(250),D2J2(250),DER1(250),DER2(250),
     CXF(250),XG(250),XH(250),XVA(250),F0N(250),F1N(250),F2N(250)
      READ(5,108) NW
  108 FORMAT(I1)
      READ (5,10) EA,P,A,K,L,MI
   10 FORMAT( 2F7.2/F6.3/3I4)
      READ(5,11) TI
   11 FORMAT( F7.1)
      READ(5,109)RNTED
  109 FORMAT(E11.3)
      K=K+L
      READ(5,09)(VP(I),(XJ(I,J),J=1,5),I=1,K)
    9 FORMAT(F12.2,5E12.5)
      K=K-L
      DVP=VP(2)-VP(1)
      IF(MI.NE.0) GO TO 71
      DV=VP(K)+DVP
      DO 73 I=1,K
      N=K-I+1
      XVA(N)=DV-VP(I)
      B0(N)=-XJ(I,1)+XJ(1,1)
      B1(N)=-XJ(I,2)+XJ(1,2)
      B2(N)=-XJ(I,3)+XJ(1,3)
      DB0(N)=-XJ(I,4)+XJ(1,4)
   73 DB1(N)=-XJ(I,5)+XJ(1,5)
      DO 74 I=1,K
      VP(I)=XVA(I)
      XJ(I,1)=B0(I)
      XJ(I,2)=B1(I)
      XJ(I,3)=B2(I)
      XJ(I,4)=DB0(I)
   74 XJ(I,5)=DB1(I)
      WRITE(6,92)
   92 FORMAT(*1*,8X,*U*,10X,*XJ(1)*,9X,*XJ(2)*,9X,*XJ(3)*,9X,*XJ(4)*,9X,
     C*XJ(5)*)
      WRITE(6,72)(VP(I),(XJ(I,J),J=1,5),I=1,K)
   72 FORMAT( F12.2,5E14.5)
   71 CONTINUE
      WRITE(6,8) EA,P,A
    8 FORMAT(*0EA=*,F6.1,10X,*P=*,F7.2,10X,*A=*,F6.1)
C
C CONSTANTS
      PI=3.14159
      E=1.602E-19
      EPS0=8.854E-12
      XME=9.1096E-31
      IA=0
      IP=0
      XK0=2.*PI*E**3/XME**2
C
C RATIONALIZATION TO MKSA
      EA=EA*100.
```

```
      P=P*133.3
      A=A*1.E-6
      M=K-1
   59 IF(A.LT.1.E-20) GO TO 18
      DO 13 I=1,K
      DO 13 J=1,5
   13 XJ(I,J)=XJ(I,J)/A
C APPROXIMATED F0
   18 DO 50 I=1,K
      XJ0(I)=2./3.*XJ(I,3)+(XJ(I,1)+XJ(I,5))/6.
   50 XF(I)=XJ0(I)/XK0
      CALL DER(VP,XF,K,DER1,F01,4)
C
C DEDUCTION OF F FROM PLANE PROBE
      IF(EA.GT.1.E-20)GO TO 35
      DO 70 I=1,K
      XJ1(I)=(XJ(I,5)-XJ(I,1))/2.
      XJ1(I)=-XJ1(I)
      F0(I)=F01(I)
   70 XJ2(I)=(XJ(I,5)+XJ(I,1))/3.-2.*XJ(I,3)/3.
      GO TO 12
   35 DO 21 I=1,K
      B0(I)=XJ(I,3)
      B1(I)=2.**.5*(XJ(I,2)-XJ(I,4))-.5*(XJ(I,1)-XJ(I,5))
   21 B2(I)=2.*(XJ(I,2)+XJ(I,4))-3.*XJ(I,3)-.5*(XJ(I,1)+XJ(I,5))
      CALL DER(VP,B0,K,DB0,DER2,1)
      CALL DER(VP,B1,K,DB1,DER2,1)
C
C CALCULATION OF XK1,VE , XNE
   12 CONTINUE
      DO 51 I=1,K
      XF(I)=VP(I)**.5*F01(I)
   51 XG(I)=VP(I)**1.5*F01(I)
      CALL SUMT(VP,XF,1,M,0.,XK1)
      CALL SUMT(VP,XG,1,M,0.,SUM)
      VE=SUM*2./(XK1*3.)
      XNE=2.*XK1*PI*(2.*E/XME)**1.5
      XNT=XNE*RNTED
      XPT=XNE+XNT
      DO 47 I=1,K
   47 XF(I)=F01(I)/SQRT(VP(I))
      CALL SUMT(VP,XF,2,M,0.,SUM)
      SUM=SUM+F01(1)*2.*SQRT(VP(1))
      VE1=2.*XK1/SUM
      VRAT=11604.*VE1/TI
      VI=.5*VE1*XPT/(XNE+XNT*VRAT)
C
C CALCULATION OF XLMDAS(I)
   20 XLMDAD=SQRT(EPS0*VE1/(E*XNE))
      IF(EA.LT.1.E-20)GO TO 26
      CALL SHEATH(VP,F01,VI,VE1,VRAT,XNE,XPT,XK1,XLMDAD,K,XLMDAS,VE)
C
      DO 22 I=1,K
      XVA(I)=EA*XLMDAS(I)
      IF(VP(I).GT.XVA(I)) GO TO 22
      WRITE(6,91)VP(I),XVA(I)
   91 FORMAT(* U=*,F7.2,5X,*VA=*,E13.4)
```

```
      XVA(I)=VP(I)
   22 XF(I)=XVA(I)**2*DB0(I)
      CALL DER(VP,XF,K,D2B,DER2,1)
      DO 24 I=1,K
   24 XJ0(I)=B0(I)+B2(I)/3.+XVA(I)*DB1(I)/3.+D2B(I)/6.
   36 DO 25 I=1,K
   25 XF(I)=XJ0(I)/XK0
C
C CALCULATION OF F0(I)
      CALL DER(VP,XF,K,DER1,F0,4)
C
C TEST OF ACCURACY
   60 DO 52 I=1,K
      XF(I)= ABS(F0(I)-F01(I))*VP(I)**0.5
   52 XG(I)=VP(I)**.5*F0(I)
      CALL SUMT(VP,XF,1,M,0.,SGMA)
      CALL SUMT(VP,XG,1,M,0.,XK)
      ACCU=SGMA/XK
      IA=IA+1
      IF(ACCU.LT.1.E-4) GO TO 26
   23 DO 27 I=1,K
   27 F01(I)=F0(I)
      IF(IA.LE.100)  GO TO 29
      WRITE(6,28) ACCU
   28 FORMAT(* *26HF0 DOES NOT CONVERGE,ACCU=F8.4)
      GO TO 26
   29 WRITE(6,31)IA,ACCU,XK1,XNE,VE,VE1,VRAT,VI,XLMDAD
   31 FORMAT(* IA=*,I3,3X,*ACCU=*,F7.4,3X,*XK1=*,E11.4,3X,*XNE=*,E11.4,
     1 3X
     A*VE=*,F6.3,3X,*VE1=*,F6.3,3X,*VRAT=*,F8.2,3X,*VI=*,F6.3,3X,
     B*XLMDAD=*,E11.4)
      GO TO 12
C
C CALCULATION OF F1(I) + F2(I)
   26 WRITE(6,31)IA,ACCU,XK1,XNE,VE,VE1,VRAT,VI,XLMDAD
      WRITE(6,32) (XLMDAS(I),I=1,K)
   32 FORMAT ( 10(2X,E11.4))
      IF(EA.LT.1.E-20)GO TO 39
      DO 45 I=1,K
      DER1(I)=XJ(I,1)-XJ(I,5)-1.41421*(XJ(I,2)-XJ(I,4))
      DER2(I)=XJ(I,1)+XJ(I,5)-2.*(XJ(I,2)+XJ(I,4)-XJ(I,3))
      XJ1(I)=-B1(I)-XVA(I)*DB0(I)
      XJ1(I)=-XJ1(I)
   45 XJ2(I)=(2.*B2(I)+2.*XVA(I)*DB1(I)+D2B(I))/3.
   39 IF(NW.EQ.1) WRITE(6,37)
   37 FORMAT(*1*,9X,*U*,10X,*F0*,10X,*F1*,10X,*F2*,16X,*VA*)
      DO 40 I=1,K
   40 XH(I)=XJ2(I)/(VP(I)**1.5)
      CALL DER(VP,XJ1,K,DJ1,DDJ1,2)
      CALL DER(VP,XJ2,K,DJ2,D2J2,2)
      XH0=2.*XH(1)-XH(2)
      DO 33 I=1,K
      CALL SUMT(VP,XH,I+1,M,XH0,SUM)
   33 SJ2(I)=SUM
      IP=0
      DO 30 I=1,K
      F1(I)=(DDJ1(I)-.5*DJ1(I)/VP(I))/XK0
```

```
      F2(I)=(D2J2(I)-1.5/VP(I)*DJ2(I)+.75/VP(I)**2*XJ2(I)-3./(A.+VP(I)
     C**1.5)*SJ2(I))/XK0
      F0N(I)=F0(I)/XK1
      F1N(I)=F1(I)/XK1
      F2N(I)=F2(I)/XK1
      IF(NW.EQ.1)
     $WRITE(6,34) VP(I),F0(I),F1(I),F2(I),XVA(I)
   34 FORMAT(* *F12.2,3E12.4,5X,F12.2)
      IF(IP.LT.49)GO TO 41
      IF(NW.EQ.1)
     $WRITE(6,42)
   42 FORMAT(*1*)
      IP=-1
   41 IP=IP+1
   30 CONTINUE
   62 CONTINUE
      IP=0
      WRITE(6,38)
   38 FORMAT(*1*,7X,*U*,7X,*F0N*,9X,*F1N*,9X,*F2N*,9X,*VA*)
      DO 43 I=1,K
      WRITE(6,46)VP(I),F0N(I),F1N(I),F2N(I),XVA(I)
   46 FORMAT( F10.2,3E12.4,F12.2)
      IF(IP.LT.49)GO TO 44
      WRITE(6,42)
      IP=-1
   44 IP=IP+1
   43 CONTINUE
      IF(EA.LT.1.E-20)GO TO 61
      IF(NW.EQ.1)
     $WRITE(6,55)
   55 FORMAT(*1*,2X*B0*,10X*B1*,10X*B2*,10X*B3*,10X*B4*,10X*DB0*,9X,
     C*DB1*,9X,*D2B*,9X,*U*)
      IF(NW.EQ.1)
     $WRITE(6,56)(B0(I),B1(I),B2(I),DER1(I),DER2(I),DB0(I),DB1(I),D2B(I)
     C,VP(I),I=1,K)
   56 FORMAT( 9E12.4)
   61 IF(NW.EQ.1) WRITE(6,57)
   57 FORMAT(*1*,4X,*XJ0*,9X,*XJ1*,9X,*XJ2*,9X,*DJ1*,9X,*DJ2*,9X,*DDJ1*,
     CBX,*D2J2*,8X,*SJ2*,9X,*U*)
      IF(NW.EQ.1)
     $WRITE(6,58)(XJ0(I),XJ1(I),XJ2(I),DJ1(I),DJ2(I),DDJ1(I),D2J2(I),SJ2
     C(I),VP(I),I=1,K)
   58 FORMAT( 9E12.4)
      IF(EA.LT.1.E-20) STOP
      IF((EA.GT.1.E-20).AND.(EA.LT.1.E-15)) GO TO 96
      DO 97 I=1,K
      XJ0(I)=B0(I)+B2(I)/3.+XVA(I)*DB1(I)/3.
      XF(I)=XJ0(I)/XK0
   97 XJ2(I)=2.*B2(I)/3.+2.*XVA(I)*DB1(I)/3.
      CALL DER(VP,XF,K,XH,F0,4)
      EA=1.E-17
      GO TO 39
   96 EA=0.
      GO TO 18
      END
```

```
      SUBROUTINE SHEATH(U,XF,VI,VE1,VRAT,XNE,XPT,XK1,XLMDA,K,XLMDAS,VE
      DIMENSION U(250),XF(250),Z(250),XLMDAS(250)
      XNN=(XPT-XNE)/(XPT*VRAT)
      VI=2.*VI/VE1
      C=SQRT(V1)
      XF0=0.
      L=1
      M2=K-1
      XLMDAD=XLMDA *SQRT(XNE/XPT)
      DO 12 N=1,K
      V=U(N)
      A=2.*V/VE1
      B=SQRT(A+V1)
      VN=B*C-V1
      VO=C/B
      IV=N
      L1=IV+1
      M=IV-1
      DO 13 I=IV,K
   13 Z(I)=((U(I)-V)**1.5-U(I)**1.5-V**1.5)*XF(I)
      CALL SUMT(U,Z,L1,M2,XF0,SUMA)
      DO 14 I=1,IV
   14 Z(I)=(U(I)**1.5)*XF(I)
      CALL SUMT(U,Z,L,M,XF0,SUMB)
      SUM=(2.*SUMB-SUMA)*XNE/(3.*XPT*XK1*VE1)
      DO 15 I=IV,K
   15 Z(I)=(SQRT(U(I)-V)+SQRT(V))*XF(I)
      CALL SUMT(U,Z,L1,M2,XF0,SUMC)
      SAM=SUMC*XNE/(2.*XPT*XK1)
   17 XLMDAS(N)=XLMDAD*SQRT(2.*(VN-SUM-XNN))/(VO-SAM)
   12 CONTINUE
      RETURN
      END
```

```
      SUBROUTINE SUMT(U,XF,LI,L2,XF0,SUM)
      DIMENSION U(250),XF(250)
      L1=LI
      LA=L2+1
      LB=L2+2
      SUM=0.
      IF(L1.GE.LB)RETURN
      IF((L1.EQ.1).OR.(L2.EQ.1)) GO TO 906
      IF(L1.EQ.LA) GO TO 911
      GO TO 902
  906 X2=U(1)
      X3=U(2)
      XF2=XF(1)
      XF3=XF(2)
      A1=XF0/(X2*X3)
      A2=XF2/(X2*(X2-X3))
      A3=XF3/(X3*(X3-X2))
      C1=A1+A2+A3
      C2=(X2+X3)*A1+X3*A2+X2*A3
      C3=XF2+(C2-C1*X2)*X2
      IF((L1.EQ.2).AND.(L2.EQ.1)) GO TO 915
      SUM=C1*X2**3/3.-C2*X2*X2/2.+C3*X2
      IF(L2.EQ.1) GO TO 915
      IF(L2.EQ.0) RETURN
      L1=2
  902 DO 900 L=L1,L2
  910 X1=U(L-1)
      X2=U(L)
      X3=U(L+1)
      XF1=XF(L-1)
      XF2=XF(L)
      XF3=XF(L+1)
      A1=XF1/((X2-X1)*(X3-X1))
      A2=XF2/((X2-X1)*(X2-X3))
      A3=XF3/((X3-X1)*(X3-X2))
      C1=A1+A2+A3
      C2=(X2+X3)*A1+(X1+X3)*A2+(X1+X2)*A3
      C3=XF2+(C2-C1*X2)*X2
      IF(L1.EQ.LA) GO TO 915
  900 SUM=SUM+C1*(X2**3-X1**3)/3.-C2*(X2*X2-X1*X1)/2.+C3*(X2-X1)
  915 SUM2=C1*(X3**3-X2**3)/3.-C2*(X3*X3-X2*X2)/2.+C3*(X3-X2)
      SUM=SUM+SUM2
  903 RETURN
  911 L=L2
      GO TO 910
      END
```

```
      SUBROUTINE DER(VP,YF,K,DER1,DER2,IJ)
      DIMENSION VP(250),XF(250),DER1(250),DER2(250),YF(250),DA(250)
      KMM=K-2
      KM5=K-5
 5    KM6=K-6
      VPD=VP(2)-VP(1)
      Z=1./(24.*VPD)
      Z2=Z*2.
      Z6=Z*6.
10    Z12=Z*12.
      IT=IJ
      DO 808 I=1,K
  808 XF(I)=YF(I)
  806 DA(1)=(-3.*XF(1)+4.*XF(3)-XF(5))*Z6
15    DA(2)=(-XF(1)+XF(3))*Z12
      DA(3)=(-XF(1)+XF(5))*Z6
      EP=ABS(DA(1))
      AP=ABS(DA(2))
      IF((AP.GT.(1.1*EP)).OR.(AP.LT.(0.91*EP))) GO TO 850
20    GO TO 815
  850 DA(1)=(-3.*XF(1)+4.*XF(2)-XF(3))*Z12
      DA(3)=(-XF(2)+XF(4))*Z12
  815 DO 803 L=4,KM6
      DA(L)=(-XF(L-2)-4.*XF(L-1)+4.*XF(L+1)+XF(L+2))*Z2
25    EP=ABS(DA(L-1))
      AP=ABS(DA(L))
      IF((AP.GT.(1.1*EP)).OR.(AP.LT.(0.91*EP))) GO TO 852
      GO TO 803
  852 DA(L)=(2.*XF(L-2)-16.*XF(L-1)+16.*XF(L+1)-2.*XF(L+2))*Z
30    803 CONTINUE
      DO 853 L=KM5,KMM
  853 DA(L)=(-XF(L-2)+XF(L+2))*Z6
      DA(K-1)=(-XF(K-3)+XF(K-1))*Z12
      DA(K)=(-XF(K-2)+XF(K))*Z12
35    IF(IT.EQ.3) GO TO 841
      IF(IT.EQ.4)GO TO 811
      IF(IT.EQ.5)GO TO 813
      GO TO 854
  841 CALL SE35(DA,DER2,1,K)
40    RETURN
  854 CALL SE35(DA,DER1,1,K)
      IF (IT.EQ.1) RETURN
      IT=3
  812 DO 804 I=1,K
45    804 XF(I)=DER1(I)
      GO TO 806
  811 DO 856 L=1,K
  856 DER1(L)=DA(L)
      IT=5
50    GO TO 812
  813 DO 855 L=1,K
  855 DER2(L)=DA(L)
      RETURN
      END
```

```
      SUBROUTINE SE35(Y,Z,LI,K)
      DIMENSION Y(250),Z(250)
      L=K-LI-4
      IF(L.LE.0)RETURN
    5 L1=LI
      L2=LI+1
      L5=LI+4
      B=Y(L1)
      C=Y(L2)
   10 DO 3 I=L5,K
      A=B
      B=C
      C=Y(I-L2)
      D=C-B-Y(I-L1)
   15 D=D+D+C
      D=D+D+A+Y(I)
      IF(I-L5)2,2,3
    2 Z(L1)=A-.01428571*D
      Z(L2)=B+.05714286*D
   20 3 Z(I-L2)=C-.08571429*D
      Z(K-1)=Y(K-1)+.05714286*D
      Z(K)=Y(K)-.01428571*D
      RETURN
      END
```

LIST OF SYMBOLS

The symbols used in this report are given below with their interpretation in alphabetical form. Greek letters are treated towards the end. In many instances, the location of a symbol within the text is indicated instead of repeating here the equation for it.

a_1, a_2, a_3	coefficients in Appendix C.5
$a_1(U)$	function defined in Eq. (170) or (190)
$a_2(U)$	function defined in Eq. (175) or (193)
$a_3(U)$	function defined in Eq.(219)
A	area of the probe
A_r	area for current flow at position r within the sheath
A_r^s	area at the sheath position for current flow
b_1	variable defined in Eq. (171)
$b_2(U)$	function defined in Eq. (176) or (194)
$b_3(U)$	function defined in Eq. (220)
B_i (i = 0 to 4)	combinations of current densities for various orientations as given in Eqs. (241) to (245)
c_1, c_2, c_3	coefficients in Appendix C.5
c	coefficient in Eq. (146)
$c_2(U)$	function defined in Eq. (177)
$c_3(U)$	function defined in Eq. (221)
C_s	sheath capacitance
D, D_e, D_+	diffusion coefficient, for electrons and ions respectively
e	magnitude of the electron charge
E	electric field in the active discharge
E_p	electric field due to the probe voltage itself

f^*, f	energy distribution function in coordinate systems attached to the probe and to the plasma respectively
f_o^*, f_o	isotropic part of the distribution function
f_{o1}	approximate form for f_o
f_o^s	value of f_o at the collisionless sheath boundary
$(\delta f_o/\delta t)_c$	collisional term for f_o in the Boltzmann equation
$\underset{\sim}{f}_1^*$, $\underset{\sim}{f}_1$	directional part of the distribution function
f_{1x}, f_{1y}, f_{1z}, f_{1Z}^*	various components of above
f_{1r}, f_{1r}^s	radial component of $\underset{\sim}{f}_1$ and its value at the collisionless sheath boundary respectively
$\underset{\approx}{f}_2^*$, f_2	second order tensor part of the distribution function
f_{2ij}, f_{2xx}, f_{2yy}, f_{2zz}, f_{2ZZ}^*, etc.	various components of above
f_{1ms}^*	spherical harmonic components of the distribution function
f_s	voltage sweep frequency applied to the probe to derive experimentally the characteristic
$f(x)$	function in Appendix C.5
$F(\xi,k)$	incomplete elliptic integral of the first kind
$G(k)$, $G(\xi,k)$	respective complete and incomplete elliptic integrals of the second kind
$H(U)$	function given in Eqs. (338) to (344)
I, I_e, I_+	current to the probe (either total or of a species according to the context) and the electron and positive ion currents respectively
dI	element of the current to the probe in a certain electron energy range
I_o, I_1, I_2	various contributions to the current arising from the f_o, $\underset{\sim}{f}_1$ and $\underset{\approx}{f}_2$ parts of f
δI	current contribution to a surface element before integration over the probe surface

δI_o, δI_a, δI_b, δI_c	various contributions to δI
$\underset{\approx}{I}_2$	unit tensor
j, j_e, j_+, j_-	current density to the probe and the electron, positive and negative ion contributions respectively
j_Z	current density normal to the probe
j_{oZ}, j_{1Z}, j_{2Z}, j_{lZ}	contributions to the above from the f_o, f^*_{1Z}, f^*_{2ZZ} and lth tensor parts of f^*
$j_{\theta\phi}$, $j_{1\theta\phi}$, $j_{2\theta\phi}$, $j_{l\theta\phi}$	contributions to j, from total f, $\underset{\sim}{f}_1$, $\underset{\approx}{f}_2$ and l^{th} tensor part respectively, for a plane probe with normal orientation having Eulerian angles θ and ϕ
j_{1z}, j_{2z}	j_{1Z} and j_{2Z} with $\theta = 0$
j_{z-} , j_{z+}	difference and sum of two currents to both sides of a one-sided plane probe
j_o, j_1, j_2	contribution to j from f_o, $\underset{\sim}{f}_1$ and $\underset{\approx}{f}_2$ as given in Eqs. (238) to (240)
j_θ with $\theta = 2\pi, \pi/4, \pi/2, 3\pi/4$ and π	current densities to a plane probe for five orientations of the probe
$\tilde{j}_e$, $\tilde{j}_+$	electron and ion current densities normalized as in Eq. (386)
$J_o(r)$	zeroth order Bessel function
k	Boltzmann's constant
k_o	variable defined in Eq. (214)
k_1	variable defined following Eq. (217)
k_2	variable defined following Eq. (229)
k_3	variable defined following Eq. (224)
K_o	equal to $2\pi e/m^2$
K(k)	complete elliptic integral of the first kind
l_c, l_{ce}, l_{c+}	mean free path, for electrons and ions respectively
L	length of a cylindrical probe
m	electron mass

m_p or m_+	positive ion mass
n	charged particle density
n_e, n_+, n_-	electron and positive and negative ion densities respectively, the latter two summed over species after multiplication by the respective charge numbers
n_s, n_{es}, n_{+s}, n_{-s}	above at the collisionless sheath boundary
n_n, n_p	individual negative and positive ion densities respectively
n_{ns}, n_{ps}	above at the collisionless sheath boundary
n_o	charged particle density in the bulk of the plasma
n_{eo}	electron density in the bulk of the plasma
N	neutral gas particle density
p	gas pressure
P_l^m	associated Legendre harmonic function
P_l	Legendre polynomial
q	velocity squared parameter defined in Eq. (48)
q_p, q_s	respective values of q at the probe surface and at the sheath boundary
q_1	variable defined in Eq . (50) or (60)
Q, Q_e, Q_+	Waymouth's parameters defined in Eq. (395)
r	radial distance from the probe center
r_p	radius of the probe
r_s	distance of the sheath boundary from the center of the probe
R, R_θ, R_ϕ, R_{ij}	rotation matrix and various components, defined in Eqs. (27) to (30)
R_p	radius of a plane probe including its guard ring
R_t	radius of the plasma tube
s_p	parameter used in collisional theory. defined in Eqs. (378) to(380)

t	time
T	temperature
T_e, T_+, T_-, T_g	respective electron, positive and negative ions and gas temperatures
U	energy of the charged particle in joules
$\underset{\sim}{v}$, v	particle velocity and its speed
v_X, v_Y, v_Z	components of $\underset{\sim}{v}$ in the probe frame of reference
v_{Zp}, v_{Zs}	values of V_Z at the probe surface and at the collisionless sheath boundary
v_{Yp}, v_{Ys}	same for v_Y
v_e	$(kT_e/m)^{\frac{1}{2}}$, electron thermal velocity
v_+	$(kT_e/m_+)^{\frac{1}{2}}$, ion drift velocity at the sheath edge
$\bar{v}$, $\bar{v}_e$, $\bar{v}_+$	average speed as defined in Eq. (357) and the corresponding values for electrons and positive ions respectively
v_d	electron drift velocity
v_o	$(2V_p/m)^{\frac{1}{2}}$, $[2(V_p \mp V_a^*)/m]^{\frac{1}{2}}$ or $[2(V_p-V_s)/m]^{\frac{1}{2}}$ according to the context
v_V	$[2(V-V_s)/m]^{\frac{1}{2}}$
V	potential in joules
V_p	probe potential with respect to the collisionless sheath edge if V_s is not specifically written
V_s	potential at the collisionless sheath boundary
V_a^*, V_a	potential drop across the collisionless sheath due to the external discharge electric field for any orientation and for $\theta = 0$ respectively
V_i	ion directed energy at the collisionless sheath boundary
V_e	electron temperature in joules, kT_e, defined in Eq. (279)
V_{e1}	averaged electron energy in joules defined in Eq. (278)

W_o, W_1, W_2	averages over the distribution function defined in Eqs. (365) to (368)
W_{oe}, W_{1e}, W_{2e}	above for electrons
W_{o+}, W_{1+}, W_{2+}	above for positive ions
x, y, z, x', y', z' X,Y,Z	three respective coordinate system representations
x_1, x_2, x_3, Δx	variables used in Appendix C.5
x_c	variable defined after Eq. (292)
y	parameter defined in Eq. (83)
y_o, y_1	parameters defined after Eq. (93)
Z_p, Z_n	charge numbers for positive and negative ions respectively
α	azimuthal angle around a cylinder
α_o	coefficient defined in Eq. (214)
α_1	coefficient defined after Eq. (229)
β	$r_p^2/(r_s^2 - r_p^2)$
γ	$\beta v_o^2/v_i^2$ defined in Eq. (212) and after Eq. (229)
Γ	integral defined in Eq. (335)
$\delta(x)$	delta function
δ_{ij}	Kronecker function
δ	gap separation between the central disc probe and its guard ring
ε_o	permittivity of free space
ζ	parameter, defined in Eqs. (351) to (353), which depends on l_c/r_p
η	ratio of electron density to neutral gas density
θ	spatial angle defining the orientation from the z-axis of normal to the probe surface element.
θ_2	angle defined in Eq. (167)
θ_3	angle defined in Eq. (196)

θ	polar angle in velocity space
θ_o	angle defined in Eqs. (55) and (63)
θ_1	angle defined in Eqs. (2) and (78)
θ_a	acceptance angle for the spherical grid system
θ_V	angle defined after Eq. (267)
$\kappa_1 (1 = 1,2,3)$	coefficients defined in Eq. (131)
λ_s	sheath thickness
λ_D	Debye length defined in Eq. (289)
Λ	cross denomenator defined in Eq. (389)
Λ_o	denomenator defined in Eq. (406)
μ, μ_e, μ_+	mobility and corresponding values for electrons and positive ions respectively
ν_1, ν_2	collision frequencies appearing in Boltzmann's equation for $\underset{\sim}{f}_1$ and $\underset{\approx}{f}_2$
ξ	angle appearing in Eq. (123)
ξ_1	angle defined after Eq. (217)
π	3.14159
$\Pi(\alpha^2,k)$	complete elliptic integral of the third kind
ρ_e, ρ_+	parameters defined in Eq. (386)
σ	electrical conductivity of the plasma
Σ	summation sign
τ	a measure of electron to ion temperature defined in Eq. (376)
ϕ	azimuthal angle in configuration space
Φ	azimuthal angle in velocity space
Φ_o	angle defined in Eqs. (73) and (104)
$\Phi(x)$	error function
φ	space charge potential in volts
χ	angle appearing in Eq. (123)
ψ	function defined in Eqs. (331) to (333)

☆ U. S. GOVERNMENT PRINTING OFFICE: 1976 — 657-630/346